Universidade de Aveiro Departamento de Ciências Médicas
2017

Filipa de Sá Martins

Caracterização funcional de novos complexos da BRI2 e da BRI3

Functional characterization of novel BRI2 and BRI3 complexes

Universidade de Aveiro Departamento de Ciências Médicas
2017

Filipa de Sá Martins

Caracterização funcional de novos complexos da BRI2 e da BRI3

Functional characterization of novel BRI2 and BRI3 complexes

Tese apresentada à Universidade de Aveiro para cumprimento dos requisitos necessários à obtenção do grau de Doutor em Biomedicina, realizada sob a orientação científica da Professora Doutora Sandra Maria Tavares da Costa Rebelo, Professora Auxiliar Convidada do Departamento de Ciências Médicas da Universidade de Aveiro, e coorientação da Professora Doutora Odete Abreu Beirão da Cruz e Silva, Professora Auxiliar com Agregação do Departamento de Ciências Médicas da Universidade de Aveiro.

Este trabalho é financiado por Fundos Nacionais através da Fundação para a Ciência e Tecnologia (FCT), e do POPH/FSE no âmbito do III Quadro Comunitário de Apoio - Bolsa de Doutoramento SFRH/BD/81073/2011, pelo Instituto de Biomedicina – iBiMED (UID/BIM/04501/2013), e pelo projecto de reequipamento científico da FCT (REEQ/1023/BIO/2005).

Dedico este trabalho aos meus pais, e ao Tiago.

o júri

presidente

Professor Doutor Aníbal Guimarães da Costa
professor catedrático do Departamento de Engenharia Civil da Universidade de Aveiro

Professora Doutora Maria Paula Borges de Lemos Macedo
professora Catedrática Convidada do Departamento de Ciências Médicas da Universidade de Aveiro

Professor Doutor Carlos Jorge Alves Miranda Bandeira Duarte
professor Associado com Agregação da Faculdade de Ciências e Tecnologia da Universidade de Coimbra

Professor Doutor João Carlos Cruz Sousa
professor Associado da Escola de Ciências da Saúde da Universidade do Minho

Professora Doutora Sandra Maria Tavares da Costa Rebelo
professora Auxiliar Convidada do Departamento de Ciências Médicas da Universidade de Aveiro

agradecimentos

À minha orientadora, Sandra Rebelo, um agradecimento especial pela sua dedicação, motivação e companheirismo durante a realização deste trabalho.

À Professora Odete da Cruz e Silva, pela co-orientação e incentivo.

A todos os meus colegas do laboratório de Neurociências e Sinalização Celular. Em especial, à Rochinha, Oli, Roberto e Mariana, “meus companheiros de viagem” por todos os conhecimentos partilhados e acima de tudo pela amizade. À Pati, Lili, Regina, Serrano, Soraia e Hélder pelo companheirismo e acima de tudo pelos momentos de diversão.

Aos meus colegas do iBiMED, em particular à Joana Vieira, Maria Freitas, Juliana e Fábio por toda a ajuda disponiblizada durante a realização deste trabalho, que foi fundamental.

Aos meus amigos de londa data, Paulinho, Joana, Carlos, Fábio e Miguel pela verdadeira amizade, motivação e momentos de descontração.

À minha família pelo constante apoio e incentivo.

Aos meus pais por todos os ensinamentos e constante apoio. Ao Tiago pelo companheirismo e compreensão, e acima de tudo por acreditar sempre em mim. Foi o vosso amor incondicional que me permitiu superar esta etapa tão exigente.

palavras-chave

BRI2, BRI3, fosforilação de proteínas, proteina fosfatase 1, complexos proteicos, doenças neurodegenerativas

resumo

A BRI2 e a BRI3 são proteínas transmembranares de tipo II cujas funções fisiológicas ainda não se encontram bem caracterizadas. Duas mutações autossómicas dominantes no gene BRI2 estão na origem de duas formas de demência rara: Demência Familiar Britânica e Demência Familiar Dinamarquesa. Estas partilham características clinicas e neuropatológicas com a doença de Alzheimer, nomeadamente deposição de proteínas anormais no cérebro. Apesar de nunca ter sido associada a qualquer doença, a BRI3 está enriquecida no sistema nervoso central o que sugere que possa ter uma função neuronal.

Interações proteína-proteína têm adquirido uma importância crescente no estudo de funções de proteínas e vias de sinalização subjacentes. Neste trabalho, foram identificadas novas interações entre a BRI2 e a proteína fosfatase 1 (PP1), bem como entre a BRI3 com a PP1. A PP1 é a uma importante fosfatase serina/treonina presente em organismos eucariotas, onde se estima que seja capaz de catalisar a maioria dos eventos de defosforilação. Adicionalmente, determinámos a BRI2 e BRI3 como substratos da PP1, e identificámos os motivos RVxF presentes nos seus N-terminais como responsáveis pela ligação à PP1. A relevância fisiológica do complexo BRI2:PP1 foi investigada, e demonstrámos pela primeira vez que a fosforilação da BRI2, nomeadamente a defosforilação pela PP1, é um mecanismo de regulação do seu processamento proteolítico. Estabelecemos ainda uma relação entre os níveis de fosforilação da BRI2 com a diferenciação de processos neuronais, onde a fosforilação da proteína total parece estar envolvida no surgimento de processos neuronais, enquanto o fragmento N-terminal resultante do seu processamento parece estar relacionado com o elongamento e estabilização dos processos neuronais. No decorrer do trabalho, identificámos e caracterizámos os interactomas das proteínas BRI2 e BRI3 em cérebro, recorrendo a co-imunoprecipitações e identificação das proteínas por espectrometria de massa. Análise in silico do interactome da BRI2 reforçou os nossos resultados sugerindo um papel para esta proteína na diferenciação neuronal, e vários mecanismos subjacentes foram evidenciados. Adicionalmente, a análise dos interactomas localiza ambas proteínas na sinapse (pré e pós-sinapse). Esta evidência juntamente com a descoberta de interações com proteínas estruturais destes compartimentos celulares, nomeadamente a PSD-95, sugere um papel importante para ambas as proteínas em sinalização e transmissão sináptica. Assim, os nossos resultados compreendem informação importante para estudos futuros acerca da biologia das proteínas BRI2 e BRI3, e mecanismos celulares envolvidos, bem como na sua associação com o desenvolvimento de neuropatologias.

keywords

BRI2, BRI3, protein phoshorylation, protein phosphatase 1, protein complexes, neurodegenerative diseases

abstract

BRI2 and BRI3 are type II transmembrane protein family members whose physiological functions are poorly understood. Two different autosomal dominant mutations in the BRI2 gene are responsible for the development of two rare early-onset forms of dementia: Familial British and Familial Danish dementias that share clinical and neuropathological characteristics with Alzheimer´s disease, involving abnormal proteins' deposition in the brain. For BRI3 no disease association has been established so far, nevertheless, its enriched expression in the central nervous system strongly suggests a role for BRI3 in neuronal function.

Protein-protein interactions are becoming increasingly important in the study of protein function and underlying signaling pathways. In this work, both BRI2 and BRI3 were identified as novel protein phosphatase 1 (PP1) interacting proteins. PP1 is the major Ser/Thr protein phosphatase present in eukaryotic organisms, which catalyses the majority of protein dephosphorylation events. Moreover, we were able to determine BRI2 and BRI3 as PP1 substrates, which bind to the latter through an RVxF-like motif located in their N-terminal part. The physiological relevance of BRI2:PP1 complex was pursued, and we provide for the first time evidence suggesting that BRI2 phosphorylation, namely via PP1 dephosphorylation, is a regulatory mechanism for its proteolytic processing. Further, a correlation between BRI2 phosphorylation and neurite outgrowth was established. The phosphorylation of full-length protein seems to promote the emergence of neurites whereas the increased BRI2 N-terminal processing fragment plays a role in neurites' elongation and stabilization. Herein, we also identified and characterized the interactome of both BRI2 and BRI3 in the brain using co-immunoprecipitation followed by mass spectrometry analysis. *In silico* analysis of the BRI2 interactome strengthened our results suggesting a role in neuronal differentiation and some underlying mechanisms were pointed out. Moreover, interactomes' analysis suggested the presence of both BRI2 and BRI3 at synapses (pre- and post-synapse). This finding together with their ability to form complexes with structural constituents of these compartments, namely PSD-95 suggested an important role for both proteins in synaptic signaling and synaptic transmission.

Thus, our results provide valuable information for further studies on BRI2 and BRI3 biology, and potential underlying molecular mechanisms, as well as associations with neuropathologies.

This thesis is organized in four chapters (I, II, III and IV):

I. General Introduction and Aims, includes:

Published Book Chapter:

- **Martins F**, Serrano JB, Marafona AM, da Cruz E Silva OAB and Rebelo S (2017). Protein Phosphatase 1 (PP1). Editor: Choi S. *Encyclopedia of Signaling Molecules*. Springer. ISBN 978-1-4939-6799-5

II. Validation and Functional characterization of the BRI2:PP1 and BRI3:PP1 complexes, includes:

Published research paper:

- **Martins F**, Rebelo S, Santos M, Zita Cotrim C, da Cruz e Silva EF and da Cruz e Silva OCS (2016). BRI2 and BRI3 are functionally distinct phosphoproteins. *Cellular Signalling*, 28(1):130-44. doi: 10.1016/j.cellsig.2015.10.012

- **Martins F**, Serrano JB, Müller T, da Cruz e Silva OCS and Rebelo S (2017). BRI2 processing and its neuritogenic role are modulated by protein phosphatase 1 complexing. *Journal of Cellular Biochemistry*, in press. doi: 10.1002/jcb.25925

III. Identification of novel BRI2 and BRI3 protein interactors, includes:

Submitted research paper:

- **Martins F**, Müller T, Marafona AM, da Cruz e Silva OCS and Rebelo S (2017). Identification and characterization of the BRI2 interactome in the brain. (submitted to *Scientific Reports*)

Paper to be submitted:

- **Martins F**, Müller T, da Cruz e Silva OCS and Rebelo S (2017). The interactome of BRI3 reveals novel protein partners in brain tissue. (to be submitted)

IV. Discussion and Concluding Remarks

Table of contents

Table of Figures

Table of Tables

Abbreviations

ABP	Actin-binding protein
AD	Alzheimer´s Disease
ADAM10	'a disintegrin and metalloproteinase domain 10'
AICD	Amyloid precursor protein intracellular domain
AMPA	α-amino-3-hydroxy-5-methyl-4-isoxazolepropionic acid
APP	Amyloid precursor protein
Arg	Arginine
Asn	Asparagine
BACE1	β-amyloid protein converting enzyme 1
BDNF	Brain-derived neurotrophic factor
BMPs	Bone morphogenetic proteins
BRI2 ICD	BRI2 intracellular domain
BRI2 NTF	BRI2 N-terminal fragment
CAA	cerebral amyloid angiopathy
CaMKII	Calcium/calmodulin-dependent protein kinase II
CNS	Central nervous system
co-IP	Co-immunoprecipitation
CRMP-2	Collapsin-response mediator protein-2
Cys	Cysteine
DARPP-32	Dopamine and cAMP-regulated phosphoprotein
DB	Database
DCX	Doublecortin
DIV	Days *in vitro*
ECL	Enhanced chemiluminescence
ERK	Extracellular-signal-regulated kinase
FAK	Focal adhesion kinase
FBD	Familial British Dementia
FDD	Familial Danish Dementia
Glu	Glutamic acid
GO	Gene Ontology
GSK3	Glycogen synthase kinase 3
ITM2A	Integral membrane protein 2A
ITM2B	Integral membrane protein 2B
ITM2C	Integral membrane protein 2C
LAP1	Lamina-associated protein 1
LTD	Long-term depression
LTP	Long-term potentiation
Lys	Lysine
MAP	Microtubule-associated protein
MAPK	Mitogen-activated protein kinase
mAPP	Mature amyloid precursor protein
MARK	Microtubule Affinity-Regulating Kinase

MBP	Microtubule binding protein
mBRI2	Mature BRI2
MLCK	Ca^{2+}/calmodulin myosin light chain kinase
MLCP	Myosin light chain phosphatase
MS	Mass spectrometry
MT	Microtubule
MW	Molecular weight
MYPT1	Myosin phosphatase targeting subunit 1
NE	Nuclear envelope
NFT	Neurofibrillary tangles
NgCAM	Neuron-glia cell adhesion molecule
NGF	Nerve growth factor
NIPP1	Nuclear inhibitor of protein phosphatase 1
NMDA	N-methyl-D-aspartate
NT	Neurotrophin
NTF	N-terminal fragment
OA	Okadaic acid
PAK	p21-activated kinase
PI3K	Phosphatidylinositol-3 kinase
PIP	PP1 interacting protein
PIP3	Phosphatidylinositol (3,4,5)-triphosphate
PKB	Protein kinase B
PNUTS	Phosphatase 1 nuclear targeting subunit
PP	Protein phosphatase
PP1	Protein phosphatase 1
PP1-BM	Protein phosphatase 1 binding motif mutants
PP1c	Protein phosphatase 1 catalytic subunit
PPC	Proprotein convertases
PPI	Protein-protein interaction
PPMs	Metal-dependent protein phosphatases
PPPs	Phosphoprotein phosphatases
PSD	Postsynaptic density
PSD-95	Postsynaptic density protein 95
PSM	Peptide spectrum matches
PTEN	Phosphatase and tensin homolog
PTP	Protein tyrosine phosphatase
RA	Retinoic acid
RIP	Regulated intramembrane proteolysis
RNAPII	RNA polymerase II
ROCK	Rho-kinase
SAD	Synapse Amphid Defective
sAPPα	Secreted APP fragment derived from α-secretase APP processing
SCG10	Superior cervical ganglia neural-specific protein
Serine	

SPPL	Signal peptidase-like protease
Thr	Threonine
Tyr	Tyrosine
UPS	Ubiquitin-proteasome system
YTH	Yeast two-hybrid

CHAPTER I - GENERAL INTRODUCTION AND AIMS

I.1. Protein Phosphatase 1 (PP1)

Filipa Martins, Joana B. Serrano, Ana M. Marafona, Odete A. B. da Cruz e Silva and Sandra Rebelo

Neuroscience and Signaling Laboratory, Department of Medical Sciences, Institute of Biomedicine-iBiMED, University of Aveiro, Portugal

Corresponding author: Sandra Rebelo, Neuroscience and Signaling Laboratory, Department of Medical Sciences, Institute of Biomedicine-iBiMED, University of Aveiro, 3810-193 Aveiro, Portugal, Tel: +351-924406306, E-mail: srebelo@ua.pt

Martins F, Serrano JB, Marafona AM, da Cruz E Silva OAB and Rebelo S (2017). Protein Phosphatase 1 (PP1). Editor: Choi S. *Encyclopedia of Signaling Molecules*. Springer. ISBN 978-1-4939-6799-5

Synonyms:

Phosphoprotein phosphatase 1; Phosphoprotein phosphatase 1 catalytic subunit (PPP1C); Phophorylase phosphatase

I.1.1. Historical Background

Protein phosphatase 1 (PP1), also known as phosphorylase phosphatase, was first studied in 1943 by Cori and Green in the context of glycogen metabolism, as the enzyme responsible for the conversion of phosphorylase a to phosphorylase b (Cori and Green 1943). A decade later the discovery that this enzyme is in fact a phosphatase, together with the discovery of phosphorylase kinase by Fischer and Krebs in 1955, marked the beginning of the study of protein phosphorylation/dephosphorylation as a ubiquitous regulatory mechanism (Fischer and Krebs 1955). Research on PP1 further focused on the understanding of its enzymology and its role in glycogen metabolism. In fact, in the 1970s PP1 catalytic subunits (PP1c) was isolated from both liver and muscle (Brandt *et al*. 1975; Gratecos *et al*. 1977). Subsequent studies led to the discovery of PP1 inhibitors and targeting subunits, which are crucial aspects of PP1 biology. Namely, the role of the inhibitor proteins in regulating protein phosphatase activity; the role of targeting subunits that specifically target the PP1 catalytic subunit (PP1c) to specific subcellular locations; and the current view that PP1c exists in many holoenzyme forms (Cohen 1989). The concept of PP1 holoenzyme emerged and is comprised by the catalytic subunit with regulatory subunits. This concept was further supported by the finding that PP1 activity is generally associated with high molecular weight complexes (Killilea *et al*. 1979; Mellgren *et al*. 1979). However, the study of PP1 enzymology is still incomplete today. Over the last decade, PP1 has been implicated in many cellular processes, including, but not limited to, cell cycle control, apoptosis, transcription, adhesion, motility, metabolism, memory and HIV-1 viral transcription (reviewed in Cohen 2002).

I.1.2. Protein Phosphorylation and Protein Phosphatases

Reversible protein phosphorylation is one of the most common post-translational modifications in eukaryotic organisms and a key mechanism regulating the biological activity of several proteins. It involves either the addition of phosphate groups via the transfer of the terminal phosphate from ATP to the target residue of the protein by protein kinases (protein phosphorylation) or its removal by protein phosphatases (dephosphorylation) (Figure I.1). More than 70% of all eukaryotic proteins are regulated by protein phosphorylation occurring mainly at serine (Ser), threonine (Thr) and tyrosine (Tyr) residues (Barford *et al*. 1998).

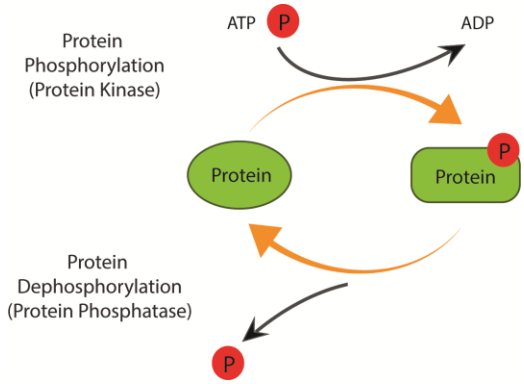

Figure I. 1 - Schematic representation of reversible protein phosphorylation. Protein kinases transfer a phosphate group from ATP to the target protein (protein phosphorylation), while protein phosphatases catalyze the hydrolysis of the phosphate group from the target protein (protein dephosphorylation).

Based on structural conservation and mechanism of action of their catalytic subunit, protein phosphatases can be classified in four distinct superfamilies'. The protein tyrosine phosphatase (PTP) superfamily comprises the classical and non-classical protein tyrosine phosphatases. In addition, the dual-specificity protein phosphatases that dephosphorylate both Tyr and Ser/Thr residues are also included in this superfamily. Beyond protein substrates, some PTPs can also dephosphorylate non-protein substrates namely phospholipids, RNA and glycogen. The HAD superfamily of hydrolases comprises some protein serine/threonine/tyrosine phosphatases. The metal-dependent protein phosphatase (PPM) superfamily is mainly composed by monomeric protein Ser/Thr phosphatases that are activated by divalent cations. Finally, the phosphoprotein phosphatase (PPP) superfamily which also exclusively dephosphorylates Ser and Thr residues (Boens *et al*. 2013).

I.1.3. Phosphoprotein phosphatase (PPP) superfamily

PPP family includes PP1, PP2A, PP3 (also known as calcineurin or PP2B), PP4, PP5, PP6 and PP7. PPPs comprise a structurally related catalytic core domain that is conserved among species and an identical catalytic mechanism (Barford et al. 1998; Shi 2009). The remarkable degree of evolutionary conservation of these enzymes is associated with their essential role in the regulation of important cellular processes (Honkanen and Golden 2002). Several biochemical studies have indicated that PPPs catalyze more than 90% of all dephosphorylation events in eukaryotic cells, mainly performed by PP1 and PP2A. Moreover, the functional diversity achieved by PPP family is achieved by the existence of several isoforms for each catalytic subunit of each protein phosphatase. Of note, there are two genes coding for the PP2A isoforms, PP2Aα and PP2Aβ (PPP2CA and PPP2CB,

respectively) that share 97% identity and are highly conserved (Honkanen and Golden 2002). PP3 comprises 3 isoforms (PP3α, PP3β and PP3γ) that share more than 80% identity in their primary amino acid sequence and are coded by 3 distinct genes (PPP3CA, PPP3CB and PPP3CC, respectively). Each gene, in turn, undergoes alternative splicing to each give rise to three alternatively spliced isoforms (reviewed in Korrodi-Gregório et al. 2014). Concerning PP4 and PP6 they are structurally related to PP2A and are predicted to share around 65% and 57% identity respectively, at the amino acid sequence level when compared to PP2A. PP6 has 3 different isoforms derived by alternative splicing of the PPP6C gene. Of note PP5 and PP7 belong to this family since they contain the catalytic subunit common to the other family members. However, they have different N- and C-termini that are implicated in the targeting and regulation of enzymatic activity. PP5 is coded by one single gene (PPP5C) resulting in 2 isoforms, while PP7, also named protein phosphatase with EF-hand calcium-binding domain (PPEF) is coded by two genes (PPEF1 and PPEF2) resulting in 4 isoforms (reviewed in Korrodi-Gregório et al. 2014). PP1 has four isoforms: PP1α, PP1β/δ, PP1γ1 and PP1γ2 that are discussed in detail in the next section. Overall, several functions have been ascribed to PPP family members and those should not be exclusively attributed to the different catalytic subunits, their binding to regulatory proteins should also be considered (reviewed in da Cruz e Silva et al. 2004).

I.1.3.1. Protein phosphatase 1 (PP1)

PP1 is a major protein phosphatase present in eukaryotic organisms and is expected to catalyze the majority of protein dephosphorylation events (Bollen *et al*. 2010; Heroes *et al*. 2013). Interestingly, eukaryotic genomes contain multiple genes encoding PP1 isoforms with an exception for *Saccharomyces cerevisiae* that only contains one gene coding for PP1. PP1 isoforms are about 70% identical in the central region being mainly different at the N- and C-terminal sequences. Interestingly, PP1 has been indicated as one of the most conserved eukaryotic proteins. PP1 sequences are highly conserved among species, as is the case of *Giardia lamblia* which expresses a PP1 isoform very similar to the mammalian form. Altogether these results suggest that PP1 might have similar functions in different organisms (Ceulemans and Bollen 2004; Lin *et al*. 1999). In mammals, PP1c is encoded by 3 separate genes *PPP1CA*, *PPP1CB* and *PPP1CC*, which originate PP1α, PP1β/δ and PP1γ, respectively (Figure I.2). Of note, alternative splicing events on each of the transcripts give rise to 3 PP1α isoforms, 2 PP1β/δ isoforms (both with the same coding sequence) and 2 PP1γ isoforms (Figure I.2). Particularly interesting is the case of *PPP1CC* gene that suffers tissue-specific splicing, giving rise to PP1γ1 isoform that is ubiquitous expressed and a testis-enriched and sperm-specific, PP1γ2 (Figure I.2C). The main difference between these two PP1γ isoforms resides in the C-terminus (reviewed in Fardilha *et al*. 2010).

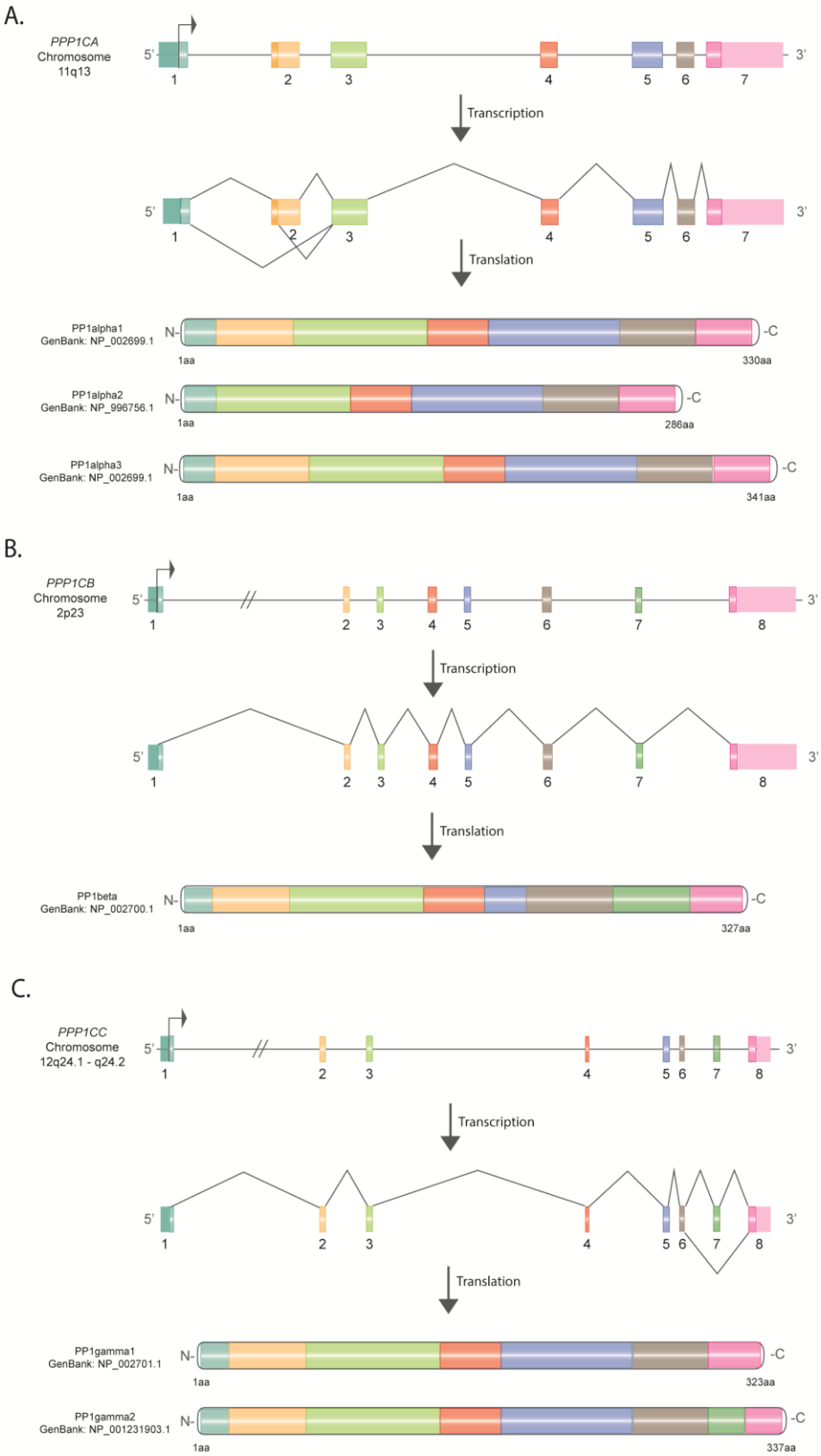

Figure I. 2 - Structure of the human PPP1C genes, and respective mRNAs and proteins. A- The human PPP1CA, located at chromosome position 11q13 contains 7 exons. Human PPP1CA transcripts variants differ only by an alternative splicing of exon 2 in transcript variant 2 or by an alternative in-frame splice site at the 5' end of exon2 in transcript variant 3. Human PP1α isoform 2 and 3 has the same N- and C-termini as isoform 1, however isoform 2 lacks an internal region

and isoform 3 is longer compared to isoform 1. **B**- The human PPP1CB, located at chromosome position 2p23 contains 8 exons. **C**- The human PPP1CC, located at chromosome position 12q24.1-q24.2 contains 8 exons. Human PPP1CC transcript variant 2 is generated by alternative splicing of exon 7, which results in a longer testis-enriched and sperm-specific PP1γ2 isoform with a distinct C-terminus compared to isoform 1. Coding exons are represented by a white line running across the boxes while non-coding sequences in exons are represented by opaque boxes. The in-frame ATG codons are indicated by arrows.

PP1 holoenzymes are essentially composed of a highly conserved PP1 catalytic subunit (PP1c) that is associated with one or two variable regulatory subunits (also known as PP1 regulatory subunit, PP1R or PP1 interacting protein, PIP). The PIPs interact with PP1c through well characterized PP1 docking motifs. So far, about ten distinct PP1 docking motifs were described, but certainly, more will be identified in a near future. These include RVxF, SILK, MyPhoNe, SpiDoC, RNYF, IDoHA, BiSTriP, AnkCap, NiHiP and the apoptotic signature (Boens *et al*. 2013; Ayllón *et al*. 2000) (Table I.1). Of note is that some of the binding motifs are often found in only one of the known PIPs, while others have been identified in several PIPs. For example, IDoHA motif only exists in inhibitor-2, while the RVxF motif is found in about 90% of all identified PIPs. Additionally, some PP1 binding motifs are isoform-specific and thereby specific holoenzymes are formed with only one PP1 isoform. The AnkCap motif consists of ankyrin repeats that bind especially to PP1β/δ (Terrak et al. 2004). Moreover, most PIPs contain several PP1 docking motifs in order to form a unique and stable complex with PP1 (Boens *et al*. 2013).

Table I. 1- PP1 docking motifs. PP1 docking motifs are presented, as well as, the specific sequence, the function, and other known characteristics. aa, amino acid; ND, not determined.

PP1 docking motif	Consensus sequence	Function	Other characteristics	References
RVxF	[RK]-X(0,1)-[VI]-{P}-[FW] X(0,1) is any aa, present or absent; {P} represents any aa except P.	PP1 anchoring	-Binds to a hydrophobic groove of the PP1c, which is opposite to the catalytic site -Binding through this motif does not affect PP1 conformation and activity	(Egloff *et al*. 1997; Wakula *et al*. 2003)
SILK	[GS –I–L–[RK]	PP1 anchoring	- Binds to a hydrophobic groove of the PP1c, which is opposite to the catalytic site -N-terminally positioned to RVxF motif -Binding through this motif does not affect PP1 conformation	(reviewed in Hendrickx *et al*. 2009; and in Bollen *et al*. 2010)
MyPhone	R–X–X–Q-[VIL]-[KR]–X-[YW] X is any aa.	Substrate selection	-binds to a shallow hydrophobic cleft of PP1 -N-terminally positioned to RVxF motif	(reviewed in Bollen *et al*. 2010)
SpiDoC	8-residue motif	Substrate selection	-binds to the C-terminal groove of PP1	(reviewed in Heroes *et al*. 2013; and in Boens *et al*. 2013)
RNYF	R–N–Y-F	--	- the binding sequence of the motif on PP1c is ND	(Llanos *et al*. 2011)
IDoHA	α-helix structure	Inhibition	-prevents access to the active site of PP1 by binding the hydrophobic and acidic grooves of PP1	(reviewed in Heroes *et al*. 2013)
BiSTriP	Leucine-rich repeats	--	- binds to the triangular region of PP1 delineated by helices α4-6	(reviewed in Ceulemans and Bollen 2004a)
AnkCap	8 ankyrin repeats	Substrate selection	- enclose the C-terminus of PP1β	(reviewed in Heroes *et al*. 2013)
NiHip	α-helix structure	--	- binds to the PP1 bottom surface	(reviewed in Boens *et al*. 2013)
Apoptotic signature	F-X-X-[KR]-X-[KR] X is any aa.	--	- the binding sequence of the motif on PP1c is ND -the motif is found in several proteins involved in the control of cell survival pathways	(Godet *et al*. 2010)

MyPhone, Myosin Phosphatase N-terminal Element; SpiDoC, Spinophilin Docking site for the C-terminal groove; IDoHA, Inhibitor-2 Docking site for the Hydrophobic and Acidic grooves; BiSTriP, Bipartide docking site of the leucine-rich repeat protein SDS22 interacting with a Triangular region that is delineated by helices α_{4-6} of PP1; AnkCap, Ankyrin repeat Cap; NiHip, NIPP1 Helix that interacts with PP1.

To date, more than 200 PIPs are known and many more will certainly be identified in the future. PIPs confer specificity to PP1c by targeting it to a specific subcellular compartment, modulating its specificity, inhibiting its catalytic activity, or serving as substrates. According to this, PIPs can be categorized as targeting subunits, substrate-specifier subunits (s-s subunits), inhibitory subunits and

substrates (Figure I.3) (reviewed in Bollen *et al*. 2009; in Bollen *et al*. 2010; and in Rebelo *et al*. 2015). However, for most PIPs, the physiological relevance of their binding to PP1 is not known.

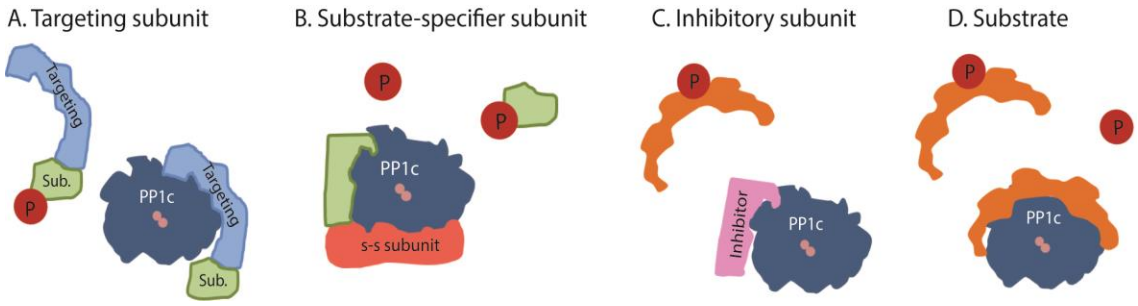

Figure I. 3 - **Schematic representation of the PP1 holoenzyme structure.** The protein phosphatase 1 catalytic subunit (PP1c) interacts with regulatory subunits that can be targeting proteins (**A**), substrate-specifiers (**B**), inhibitors of the catalytic activity (**C**) or substrates (**D**).

Some specific PP1 binding proteins target PP1 to either a specific subcellular compartment or to a protein complex. For example, spinophilin directs PP1 to dendritic spines in the brain, near to potential substrates, mediating the regulation of PP1 synaptic function (Allen *et al*. 1997). Additionally, other PP1 complexes have been identified, as is the case of APP:Fe65:PP1, where Fe65 is the scaffolding protein responsible for the bridging between PP1 and the Alzheimer's amyloid precursor protein (APP), being the latter dephosphorylated, apparently by PP1 (Rebelo *et al*. 2013). Phosphatase 1 nuclear targeting subunit (PNUTS) is a PP1 targeting subunit and recently the C-terminal domain (CTD) of RNAPII was described as the first substrate of the PNUTS:PP1 complex. Many substrates that directly associate with PP1c are enzymes that are activated by dephosphorylation, as is the case for focal adhesion kinase, E3 ubiquitin ligase and caspase 2 (reviewed in Bollen *et al*. 2010). Some substrates are dephosphorylated specifically on a single residue, whereas others are dephosphorylated on multiple residues. Recently, Lamina-associated protein 1 (LAP1), BRI2 and BRI3 were added to the list of PP1 substrates (Santos *et al*. 2013; Martins *et al*. 2016a). Some PIPS are substrate specifiers since they enhance PP1 activity towards PP1 substrates, as is the case of myosin phosphatase targeting subunit 1 (MYPT1). Interaction of the later protein with PP1 not only promotes the dephosphorylation of the myosin regulatory light chain but also decreases PP1 activity towards other substrates. PP1 inhibitors, are capable of blocking the PP1 active site and inhibit the dephosphorylation of all substrates. Inhibitor-1, DARPP-32 (dopamine and cAMP-regulated phosphoprotein), inhibitor-2 and inhibitor-3 are potent PP1c inhibitors (reviewed in Bollen *et al*. 2010; and in Ceulemans and Bollen 2004a).

I.1.3.1.1. PP1 isoforms expression

All three PP1 isoforms (PP1α, PP1β and PP1γ1) are ubiquitously expressed in mammalian tissues, PP1α is particularly enriched in brain and heart, PP1β in the brain, small intestine, muscle and lung and PP1γ1 in the brain, heart and skeletal muscle. Regarding PP1γ2 it is now well accepted that is highly enriched in testis, presenting only low expression in brain (Aoyama *et al*. 2011; da Cruz e Silva *et al*. 1995; Lüss *et al*. 2000; Ouimet *et al*. 1995; Strack *et al*. 1999) (Table I.2). All PP1 isoforms are differentially distributed in the brain and PP1α and PP1γ1 isoforms present the highest expression levels. From all brain tissues, PP1α and PP1γ1 were found to be greatly expressed in the striatum (da Cruz e Silva *et al*. 1995) (Table I.2). PP1γ2 is homogeneously expressed in most forebrain regions but particularly enriched in the striatum. However, lower levels were observed in hindbrain and cerebellum. PP1β levels were quite similar in all forebrain regions analyzed and lower in the hindbrain and cerebellum (Strack *et al*. 1999) (Table I.2). Using i*n situ* hybridization it was established that PP1α, PP1β and PP1γ1 genes were widely expressed throughout the rat brain. Broad cortical distribution was observed, but their mRNAs were particularly abundant in hippocampus and cerebellum. All three PP1 isoforms were found in the striatum, however, a lower signal was observed for PP1β compared to PP1α and PP1γ. From the three PP1 isoforms, only PP1β and PP1γ1 presented significant expression levels in the midbrain (da Cruz e Silva *et al*. 1995). Further, using RT-PCR and Northern blot techniques it was shown that all three PP1 isoforms are expressed in human muscular tissues (heart and skeletal muscle). The expression levels of PP1α, PP1β and PP1γ were higher in right ventricles than in right atria (Lüss *et al*. 2000) (Table I.2). Additional microarray studies using failing human hearts revealed that PP1α and PP1γ mRNAs were downregulated, while the mRNA for PP1β was upregulated in end-stage of dilated cardiomyopathy (Paul and Jozef 2004).

Table I. 2 - Tissue expression and subcellular distribution of the PP1 isoforms PP1 isoforms' tissue expression, as well as subcellular localization is presented.

Gene name	PP1 catalytic isoform	Tissue expression	Subcellular localization	References
PPP1CA	**PP1α**	Ubiquitous; enriched in brain and heart	- Cytoplasm (centrosomes) and nucleus (nuclear matrix and nucleoplasm) - During mitosis is in the centrosomes and kinetochores - In neurons is localized at dendritic spines, perikaryal cytoplasm and nucleus - Present in spermatozoa	da Cruz e Silva *et al*. 1995; Aoyama *et al*. 2011; Lüss *et al*. 2000; Ouimet *et al*. 1995; Strack *et al*. 1999; Korrodi-Gregório *et al*. 2014; Trinkle-Mulcahy *et al*. 2003; Santos *et al*. 2012
PPP1CB	**PP1β**	Ubiquitous; enriched in brain, small intestine, muscle and lung	- Cytoplasm and nucleus (nucleoplasm and nucleolus) - During mitosis is associated with chromosomes - In neurons is localized in cell soma and associated with microtubules - In spermatozoa is in sperm head and tail	da Cruz e Silva *et al*. 1995; Aoyama *et al*. 2011; Korrodi-Gregório *et al*. 2014; Strack *et al*. 1999; Trinkle-Mulcahy *et al*. 2003
PPP1CC	**PP1γ1**	Ubiquitous; enriched in brain, heart and skeletal muscle	- Cytoplasm and nucleus (nucleolus) - During mitosis is in the kinetochores and associated with chromatin - In neurons is localized in dendritic spines, pre-synaptic terminals and associated with actin cytoskeleton	da Cruz e Silva *et al*. 1995; Ouimet *et al*. 1995; Trinkle-Mulcahy *et al*. 2003; Santos *et al*. 2012; Strack *et al*. 1999
	PP1γ2	Highly enriched in testis; low levels of expression in brain	- In spermatozoa, is present in the posterior region and equatorial segment of sperm head and more predominantly at the tail	da Cruz e Silva *et al*. 1995; Fardilha *et al*. 2011; Korrodi-Gregório *et al*. 2014

I.1.3.1.2. PP1 isoforms cellular and subcellular localization

Interestingly, all PP1 isoforms are present in all mammalian cells analyzed but their localization within those cells is surprisingly different and specific. During interphase, all PP1 isoforms are present both in cytoplasm and nucleus (Table I.2). Within the nucleus PP1α is found associated with the nuclear matrix, PP1β localizes to non-nucleolar whole chromatin and PP1γ1 concentrates in nucleoli in association with RNA. Further, using the transient expression of PP1 fused with fluorescent proteins (FP) it was established that FP-PP1α is mainly found in a diffuse nucleoplasmic pool and largely excluded from the nucleolus. PP1γ accumulates predominantly in the nucleolus and PP1β is found in both nucleoplasm and nucleolus but its accumulation in the nucleolus is different to that observed for PP1γ (Trinkle-Mulcahy et al., 2003). Furthermore, it is known that PP1 plays a key role in mitosis where PP1 isoforms are differentially targeted to specific subcellular structures (Table I.2). Essentially during mitosis PP1α and PP1γ are distributed throughout the cell excluding the chromosomal area and are also in the mitotic spindle and mid-body. PP1α is also localized to the

centrosome, and PP1β strongly associates with chromosomes (Santos *et al*. 2012; Andreassen *et al*. 1998; Trinkle-Mulcahy *et al*. 2003). Given that PP1α and PP1γ1 isoforms were found particularly enriched in medium-sized spiny neurons of the striatum (da Cruz e Silva *et al*. 1995) the subcellular localization of those isoforms in neuronal cells is of particular interest (see Table I.2). Furthermore, the PP1γ2 isoform is highly enriched in testis where it is localized at the cytoplasm and nucleus of secondary spermatocytes, round spermatids, as well as elongating spermatids, and testicular and epididymal spermatozoa (Table I.2). However, all PP1 isoforms are expressed in mammalian testis where PP1γ1 is mainly observed in the cytoplasm of interstitial cells, spermatogonia and preleptotene spermatocytes, and PP1α in the cytoplasm of Leydig and peritubular cells, spermatogonia, and preleptotene spermatocytes (Table I.2). In spermatozoa, only PP1α, PP1β and PP1γ2 were present, being the latter more abundant and present in sperm head and more predominantly at the tail (Fardilha *et al*. 2011; Korrodi-Gregório *et al*. 2014) (Table I.2).

I.1.4. PP1 function

PP1 has been associated with a variety of cellular functions including glycogen metabolism, transcription, protein synthesis, cell cycle, meiosis, and apoptosis. It is known that when nutrients are abundant PP1 stimulates glycogen synthesis and also enables the return to the basal state of protein synthesis, recycling the transcription factors. PP1 is also important for regulating nuclear events, particularly transcription and mRNA processing and cell cycle (interphase and mitosis) through association with specific nuclear regulatory proteins (Figure I.4) (reviewed in Rebelo *et al*. 2015). Additionally, PP1 can promote apoptosis when cells are subjected to DNA damage. PP1 has also been involved in additional cellular processes namely neurotransmission, neurite outgrowth, synapse formation (reviewed in Ceulemans and Bollen 2004; and in Cohen 2002) and spermatogenesis and sperm motility (reviewed in Han *et al*.; in Fardilha *et al*. 2011; and in Silva *et al*. 2014) (Fig. I.4).

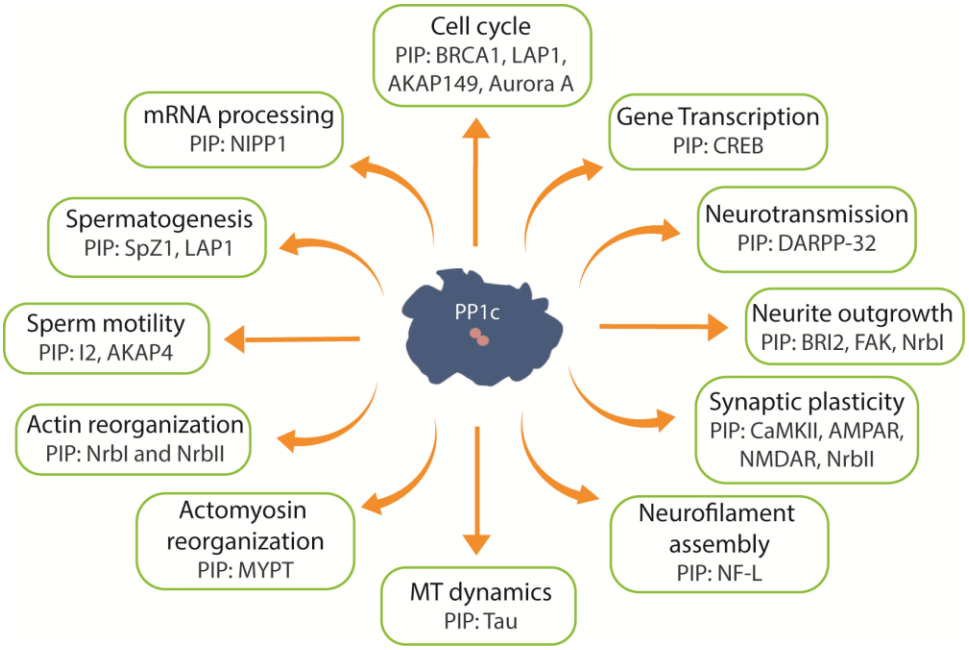

Figure I. 4 - Diagram of PP1 functions. Examples of PIPs, which together with PP1c have been associated with a variety of cellular functions. PIP, PP1 interacting protein; NrbI, neurabin-I; NrBII, neurabin-II.

I.1.4.1. PP1 function in the nucleus

Protein phosphorylation is a crucial regulatory mechanism involved in key nuclear events, namely gene transcription, mRNA processing, cell survival and cell cycle (reviewed in Rebelo *et al*. 2015). PP1, is enriched in the nucleus, and its localization is highly dynamic and changes throughout mitosis. The nuclear PP1 binding proteins associated with transcription include PNUTS, RNAPII CTD, HDAC1, CREB, Hox11, HCF1, MEF2, SARP1, SARP2, PITK and hnRNP K. From these, the transcription factor CREB mediates the expression of cAMP-induced genes. Moreover, when it is dephosphorylated at Ser133 by PP1, the c-AMP gene transcription is attenuated (reviewed in Rebelo *et al*. 2015).

Several reports have already suggested that PP1 activity is required for pre-mRNA splicing. Indeed, PNUTS and nuclear inhibitor of protein phosphatase 1 (NIPP1), the most abundant nuclear PIPs, bind to RNA and are involved in the regulation of pre-mRNA splicing. For example, PNUTS was shown to inhibit the phosphatase activity of PP1γ and PP1α *in vitro*, and anchors PP1 to specific RNA-associated complexes. Moreover, PNUTS interacts with RNA polymerase II (RNAPII) at active sites of transcription. PNUTS:PP1 holoenzyme is capable of enhancing the dephosphorylation of RNAPII C-terminal domain which suggests that this complex is also important for gene transcription regulation (reviewed in Rebelo *et al*. 2015).

The following list of nuclear PIPS are the ones involved in mRNA processing, specifically NIPP1, CDC5L, SAP155, P54nrb, PSF, Tra2-beta1 and SIPP1. From these proteins NIPP1 has a

nucleoplasmic distribution and also accumulates in nuclear speckles where it binds to pre-mRNA splicing factors. Further, NIPP mediates the interaction between PP1 and CDC5L (a regulator of pre-RNA splicing). It has been suggested that CDC5L and PP1:NIPP1 complex may be involved in the splice reaction and in the spliceosome disassembly (reviewed in Rebelo *et al*. 2015).

A role for PP1 in controlling cell cycle progression is supported by the existence of multiple substrates for PP1 in all phases of the cell cycle and by the evidence supporting that PP1 is targeted to some mitotic structures such as chromosomes, centrosomes and spindle apparatus. In fact, some PP1 complexes are involved in the regulation of numerous cellular architecture changes namely chromosome condensation, nuclear envelope disassembly, spindle formation and chromosome segregation (reviewed in Rebelo *et al*. 2015). PP1 is also suggested to be involved in centrosome maturation (G2 phase), a process characterized by recruitment of γ-tubulin and other proteins that function as nucleation sites for microtubules, by dephosphorylating and activating BRCA1 protein. PP1 controls the entry into mitosis by regulating the activity of mitotic kinases. Indeed, activation of Cdk1, by Cdc25B and Cdc25C dephosphorylation, in association with the cyclins is a key molecular indicator for entry into mitosis. Interestingly, Cdc25 activation is achieved by dephosphorylation mediated by PP1, further resulting in the activation of Cdk1 and consequently in the transition between G2/M phase (reviewed in Rebelo *et al*. 2015).

PP1 may prevent premature splitting of centrosomes, by inactivating some kinases involved in this process, namely Aurora A and Nek2A (reviewed in Rebelo *et al*. 2015). Moreover, after the proper separation of centrosomes, they should be correctly positioned near the outer nuclear membrane. Nuclear envelope (NE) proteins, namely LAP1 and emerin, are crucial in this process. However, LAP1 is not only crucial for centrosome positioning near the NE, but also its depletion results in a decrease of mitotic cells and in the levels of acetylated α-tubulin and lamin B1. In addition, LAP1 activity is regulated by PP1 dephosphorylation at residues Ser306 and Ser310 (Santos *et al*. 2014b; Santos *et al*. 2014a).

Additionally, PP1 activity is involved in the maintenance of microtubules-kinetochores attachment and spindle assembly checkpoint (SAC) which are crucial for accurate chromosome separation. For example, PP1 stabilizes correct microtubule-kinetochore attachment during metaphase by reversing the activity of Aurora B, a kinase that phosphorylates numerous proteins involved in the destabilization of microtubules-kinetochores binding. Protein phosphatases, namely PP1, are required for the mitotic exit which is characterized by mitotic spindle breakdown, chromosome decondensation, and reassembly of interphase structures such as the NE. For example, PP1 and its regulatory subunit, Repo-man (recruits PP1 to chromatin at anaphase), are required for chromosome decondensation. At the end of mitosis, PP1/Repo-man complex is responsible for histone H3 dephosphorylation that seems to be correlated with chromosome decondensation. Furthermore, PP1

is involved in nuclear envelope reassembly by dephosphorylating lamin-B, a component of the nuclear lamina that is phosphorylated at the onset of mitosis leading to nuclear lamina disassembly. At the end of mitosis, PP1 is targeted to lamin-B by AKAP149 resulting in reassembly of the nuclear lamina (reviewed in Rebelo *et al*. 2015). Given the presence of PP1γ in the cleavage furrow and spindle zone at the end of mitosis and in the center of the midbody during cytokinesis, it has been suggested that PP1 may have a role in cytokinesis regulation, however, the precise mode of action remains elusive (reviewed in Rebelo *et al*. 2015).

I.1.4.2. PP1 regulation of neuronal functions

Protein phosphorylation plays an important and critical role in many aspects of neuronal function, namely in neurotransmission, synaptic plasticity, and neurite outgrowth. In fact, dopamine-regulated signaling pathways involving the DARPP-32 and PP1 in the brain, are well documented (reviewed in Greengard *et al*. 1999). Briefly, the neurotransmitter dopamine has an excitatory effect on striatonigral neurons expressing D1 receptors, and causes activation of PKA and phosphorylation of DARPP-32 on Thr34, leading to PP1 inhibition. In a sharp contrast, striatopallidal neurons expressing D2 receptors are inhibited by dopamine, restoring PP1 activity by inhibiting PKA or by mediating the dephosphorylation of DARPP-32 by the Ca^{2+}/calmodulin-dependent PP2B. Other neurotransmitters could also affect the DARP-32/PP1 pathway. For instance, glutamate binding to N-methyl-D-aspartate (NMDA) receptors, stimulates DARPP-32 dephosphorylation by PP2B due to the Ca^{2+} influx. In contrast, the activation of adenosine A2 receptors activates PKA leading to DARPP-32 phosphorylation and inhibition of PP1c (reviewed in Greengard *et al*. 1999).

Of particular relevance, PP1 has been identified as a key regulator of synaptic plasticity in both long-term depression (LTD) and long-term potentiation (LTP). PP1 is activated during LTD, whereas inhibition of PP1 has been suggested to take place during LTP (Blitzer *et al*. 1998; Mulkey *et al*. 1994). In fact, LTD-inducing stimuli promote the targeting of PP1 to dendritic spines, where it can dephosphorylate specific substrates, such as calcium/calmodulin-dependent protein kinase II (CaMKII), α-amino-3-hydroxy-5-methyl-4-isoxazolepropionic acid (AMPA) and NMDA receptors (Mulkey *et al*. 1994). On the other hand, LTP-inducing stimuli lead to cAMP-dependent phosphorylation of the inhibitor-1 resulting in decreased PP1 activity. Consequently, an increase in the phosphorylation level of CaMKII at Thr286 is observed and also an increase in its activity, which phosphorylates the AMPA receptor subunits and potentiates synaptic current (Soderling and Derkach 2000). PP1 also binds yotiao, a protein member of the AKAP family. Yotiao functions as a scaffold protein that attaches PP1 and PKA to NMDA receptors to regulate channel activity (Westphal *et al*. 1999).

Protein phosphorylation also plays a dynamic role in regulating the extension and branching of neurites in growing neurons in response to specific guidance cues. Indeed, PP1, alongside with PP2A, were reported to have a role in the neurite structure. Inhibition of PP1 and PP2A in cultured hippocampal neurons leads to decrease number and length of neurites and synapse loss (Malchiodi-Albedi *et al*. 1997). Additionally, another study showed that general inhibition of all PP1 isoforms in hippocampal neurons, using lower concentrations of tautomycin, reduced neuritis length and branching. Further, it was suggested that PP1 is responsible for the focal adhesion kinase (FAK) targeting, during growth cone advance and adhesion, in the earlier stages of outgrowth. Indeed, PP1 could stimulate FAK activity promoting actin polymerization and growth cone movement (Monroe and Heathcote 2013).

Recently it was demonstrated that BRI2 protein is a novel PP1 substrate. It was shown that the interaction is mediated through a RVxF motif, specifically ^{3}RVTF^{6}. By using BRI2 PP1 binding motif mutant constructs, where the BRI2:PP1 interaction is diminished (Myc-BRI2 KVTA) or abolished (Myc-BRI2 KATA), it was possible to observe a dramatic increase in BRI2 phosphorylation levels. Moreover, when BRI2:PP1 interaction was abolished a phenotype consistent with neurite outgrowth and neuronal differentiation was observed (Martins *et al*. 2016a; Martins *et al*. 2016b).

I.1.4.3. PP1 in cytoskeletal organization

Cytoskeleton organization and dynamics is controlled by signaling pathways that clearly involve protein phosphorylation, namely PP1 and some of its regulatory subunits. Two families of PP1 regulatory subunits, neurabins and MYPTs, are involved in actin and actomyosin reorganization.

Neurabin-I and spinophilin (also called neurabin-II) in response to physiological signals, are able to target signaling proteins, such as PP1, to the actin cytoskeleton in order to control cell morphology. Neurabin-I is a neural-specific actin-binding protein highly enriched in both dendritic spines and growth cones and its expression is important to support neurite formation (McAvoy *et al*. 1999; Oliver *et al*. 2002). In fact, neurabin-I targets PP1 to actin-rich structures, such as postsynaptic density to promote the formation of filopodia as well as the maturation of dendritic spines, suggesting a significant role in spine morphogenesis. Additionally, PP1/Neurabin-I complex regulates the trafficking of AMPA receptors to the synaptic membrane and therefore modulates synaptic transmission (Hu *et al*. 2006). Neurabin-I is phosphorylated near the PP1-binding motif at Ser461 by PKA which results in a dramatic reduction of PP1 affinity (Oliver *et al*. 2002). Spinophilin is a ubiquitously expressed actin-binding protein that targets PP1 to the dendritic spine compartment, where it associates with the actin-rich cytoskeletal structure known as the postsynaptic density (PSD) (Ragusa *et al*. 2011). In the PSD, the complex PP1:spinophilin regulates actin cytoskeleton

organization and spine density by targeting PP1 to several substrates in dendritic spines (such as AMPA and NMDA receptors), controlling their phosphorylation (Feng *et al*. 2000; Ragusa *et al*. 2011). Blocking the spinophilin:PP1 complex formation prevents PP1-mediated dephosphorylation of the AMPA receptors, decreasing the rundown of AMPA currents and increasing the latter's activity (Yan *et al*. 1999). Spinophilin knockout mice exhibited a marked increase in spine density during development and altered filopodia formation, suggesting it functions as a negative regulator of spine morphogenesis. PKA also phosphorylates spinophilin but at Ser94 residue reducing its interaction with F-actin, displacing spinophilin from the PSD to the cytosol, which may ultimately serve to control PP1-mediated changes in the actin cytoskeleton or PP1 anchoring to receptors (Hsieh-Wilson *et al*. 2003).

Protein phosphorylation of myosin II regulatory light chain subunit (myosin II LC) regulates the contraction of actomyosin fibers which are responsible for several cellular functions, namely smooth muscle contraction, cell shape change and cell motility. Phosphorylation of myosin II LC relieves their inhibitory action on the contraction of actomyosin fibers, whereas its dephosphorylation favors the relaxation of those fibers (Ceulemans and Bollen 2004). Briefly, the phosphorylation of myosin II LC enables the interaction of myosin II with actin filaments converting the chemical energy of ATP into mechanical force or movement. Several kinases are responsible for myosin II LC phosphorylation, nonetheless, the most predominant is the Ca^{2+}/calmodulin myosin light chain kinase (MLCK). On the other hand, dephosphorylation of myosin II LC is catalyzed by a myosin light chain phosphatases (MLCP) that is composed by PP1β in complex with a myosin phosphatase targeting (MYPT) subunit. Therefore, MYPTs are PIPs that confers substrate specificity and subcellular localization to PP1β. MYPT subunit family consists of 5 different members, MYPT1, MYPT2, protein phosphatase 1 myosin binding subunit of 85 kDa (MBS85), MYPT3 and the TGF-β1-inhibited, membrane-associated protein (TIMAP) (Grassie ME et al 2011), which possess different expression patterns. MYPT1 is ubiquitously expressed but highly enriched in smooth muscle cells where it is involved in contraction. Briefly, smooth muscle contraction is activated by a raise of the cytosolic Ca^{2+} concentration which results in the activation of MLCK mediated by calmodulin. Further, MLCK phosphorylates myosin II LC at Ser19 promoting the interaction of myosin II with actin resulting in the generation of a contractile force. Once this stimulus has stopped, cytosolic Ca^{2+} concentration returns to its basal levels and the myosin II LC is dephosphorylated by the MLCP. Therefore, actin and myosin II dissociates allowing for the relaxation of the muscle (Grassie *et al*. 2011; reviewed in Ceulemans and Bollen 2004). In addition, the phosphorylation of myosin II LC is responsible for the formation of stress fibers that connect focal adhesions thus regulating cell shape, migration and adhesion (Xia *et al*. 2005). MYPT2 is expressed in striated muscles and in the brain, and both cardiac and skeletal muscle MLCPs consist of MYPT2 in complex with PP1β. However, in

the striated muscle contraction, the phosphorylation of myosin II LC is not a requirement but affects the speed and force of contraction (Grassie *et al*. 2011; reviewed in Ceulemans and Bollen 2004). At the postsynaptic density PP1 also binds to NF-L, a major component of the intermediate filament network in neurons. NF-L targets PP1 to neuronal membranes and cytoskeleton. Additionally, NF-L:PP1 complex seems to control NF-L phosphorylation levels as well as other neurofilament proteins, thus regulating the neurofilament assembly (Terry-Lorenzo *et al*. 2000). Moreover, PP1 is associated with microtubule network organization and dynamics, namely by association with tau protein, a neuronal microtubule-associated protein (MAP). In fact, tau is a PP1 substrate and its dephosphorylation enhances its association with microtubules promoting their stability (Gong *et al*. 1994; Liao *et al*. 1998).

I.1.4.4. PP1 in spermatogenesis and sperm motility

PP1 has been shown to be expressed in testis and/or in spermatozoa, suggesting an important role in spermatogenesis and spermatozoa physiology (reviewed in Han *et al*. 2007; in Fardilha *et al*. 2011; and in Silva *et al*. 2014). Indeed, *Ppp1cc* null male mice were shown to be infertile due to defective spermatogenesis and increased apoptosis of germ cells, leading to the absence of epididymal spermatozoa (reviewed in Han *et al*. 2007). Remarkably, some PIPs, namely testis/sperm-specific PIPs, have been identified. These include, for instance, the spermatogenic zip protein 1 (Spz1), a member of the basic helix-loop-helix family of transcription factors that specifically interact with PP1γ2. Remarkably, Spz1 overexpression and PP1γ loss in the testis show similar phenotypes, namely increased apoptosis and spermatogenic cycle arrest, suggesting a functional association for both proteins (reviewed in Han *et al*. 2007). Recently, LAP1 was, for the first time, associated with the spermatogenesis. LAP1 was found expressed during nuclear elongation in spermiogenesis and was located at the centriolar pole of spermatids. LAP1 was found expressed during nuclear elongation in spermiogenesis and was located at the centriolar pole of spermatids. In addition, PP1γ2 staining shares an extraordinary similar pattern to that observed for LAP1, due to their homogenous distribution in the cytoplasm at the posterior pole. Given that LAP1 and PP1 interact, and also that both proteins have important roles in mitosis, regulating MT dynamics, there is an additional putative significance for this complex in the spermatid elongation process (Serrano *et al*. 2016).

As mentioned before, in sperm, PP1γ2 is present along the entire flagellum including the mid-piece, consistent with a role in sperm motility, but it is also found in the posterior and equatorial regions of the head, suggesting a role in the acrosome reaction. Several proteins have been implicated in the regulation of PP1γ2 activity during sperm maturation: inhibitor-2, sds22, inhibitor-3, 14-3-3 and AKAPs (Fardilha *et al*. 2011). Inhibitor-2 forms a stable complex with PP1, where PP1 is inactive. However, when inhibitor-2 is phosphorylated by GSK3, its inhibitory effect is relieved and PP1

becomes active. Thus, it is proposed that in the first segments of the epididymis the sperm is immotile because the PP1γ2:inhibitor-2 complex is activated by GSK3. In the last segment of the epididymis, the complex is inactive triggering sperm motility (Silva *et al*. 2014). AKAP4 is a major fibrous sheath protein located in the principal piece of spermatozoa that recruits PKA and facilitates local phosphorylation to regulate flagellum function (Han *et al*. 2007). In *Akap4* knockout mice, spermatozoa lack motility and are infertile. Remarkably, the activity and phosphorylation of PP1γ2 is significantly altered, suggesting a functional relationship between PP1 and AKAP4 in sperm motility (Han *et al*. 2007; Silva *et al*. 2014)

I.1.5. Summary

The major post-translational modification in eukaryotes is reversible protein phosphorylation, a key mechanism for signal transduction. Protein phosphatase 1 (PP1) is a ubiquitous serine/threonine phosphatase that belongs to the phosphoprotein phosphatase (PPP) superfamily and is responsible for about one-third of all the dephosphorylations that occur in the eukaryotic cell. In mammals, three PP1 isoforms (PP1α, PP1β/δ and PP1γ) exist that are coded by three different genes (*PPP1CA*, *PPP1CB and PPP1CC*, respectively). The *PPP1CC* gene undergoes tissue-specific splicing, giving rise to a ubiquitously expressed isoform, PP1γ1, and a testis-enriched and sperm-specific isoform, PP1γ2. The PP1 isoforms are expressed in virtually all tissues but exhibit different tissue expression and subcellular localization. Since its discovery, several roles have been attributed to PP1 in the regulation of several cellular functions, such as glycogen metabolism. In the nucleus, PP1 is involved in gene transcription, mRNA processing, cell survival and cell cycle regulation. Moreover, PP1 is important in cytoskeleton organization and regulates many aspects associated with neurotransmission, synaptic plasticity, neurite outgrowth, and spermatogenesis and sperm motility. This versatility of PP1 is determined by the binding of its catalytic subunit (PP1c) to different regulatory subunits, also known as PP1 interacting proteins (PIPs). PIPs are essential regulators that modulate PP1 cellular localization, substrate specificity and also activity. The binding of PIPs to PP1 is mediated by conserved PP1 binding motifs and about 10 have already been described. To date, more than 200 PIPs were identified and in near the future several more will certainly be found, increasing the number of cellular processes involving PP1.

I.2. BRI gene family

The BRI gene family comprises three members, *BRI1/ITM2A, BRI2/ITM2B and BRI3/ITM2C*, which encode three integral type II transmembrane glycoproteins: BRI1, BRI2 and BRI3, respectively. Homology searches of expressed sequence tag (EST) databases indicate that the three genes exists in humans, rat, mouse, chimpanzee, monkey, cow, chicken, rabbit, pig and horse, and also in non-vertebrate animals, including flies and worms. The three genes are highly homologues in mouse and humans, with similar genomic organization. In fact, mouse BRI3 protein shares 92.9% amino acid sequence identity with the human protein. Together, these observations suggest that the BRI genes are part of an evolutionarily conserved gene family (Vidal *et al*. 2001; Rostagno *et al*. 2005). Several studies were carried out, and each of the human BRI gene family members were mapped by fluorescence in situ hybridization (FISH) to different human chromosomes: *BRI1* gene is located in chromosome X (position Xq13.3 – Xq21.2; Pittois *et al*. 1999), *BRI2* in the long arm of chromosome 13 (position 13q14.3; Pittois *et al*. 1998; Vidal *et al*. 1999) and *BRI3* in chromosome 2 (position 2q37; Vidal *et al*. 2001). Their genomic organization in humans is similar and consists of six exons and five introns for *BRI1* and *BRI2* genes, and seven exons and six introns for *BRI3* gene. The first intron is remarkably longer in comparison with the others and may contain regulatory sequences important for transcription (Pittois *et al*. 1999; Vidal *et al*. 2001; Rostagno *et al*. 2005).

The *Bri1* cDNA was first isolated from a cDNA library of organ cultures from prenatal mouse mandibular condyles (Deleersnijder *et al*. 1996). Database searches revealed that in human two alternatively spliced variants encoding different isoforms have been found for this gene: transcript variant 1 (GeneBank: NM_004867.4) and transcript variant 2 (GeneBank: NM_001171581.1). Transcript variant 1 represents the longest transcript and is identical to the first human BRI1 sequence reported in 1999 (Pittois *et al*. 1999). The transcript variant 2 results from the alternative splicing of exon 2. The complete *Bri2* cDNA was isolated from a cDNA library of the osteogenic stromal cell line MN7 and the cDNA sequence of the human homolog (*BRI2*) was assembled using data from available human ESTs (Pittois *et al*. 1998). Database searches identified only one transcript (GenBank: NM_021999.4) that corresponds to the identified human BRI2 sequence. In a previous study, two mRNAs transcripts of BRI2 of 2.0 kb and 1.6 kb were identified by Northern blot analysis, however, only one specific DNA fragment was observed. So, the two mRNA transcripts may represent alternatively spliced or different polyadenylated isoforms (Vidal *et al*. 2004). *Bri3* cDNA was first cloned from a 13.5-day mouse embryonic library in 2001 (Choi *et al*. 2001). Four alternative transcripts were identified using database searches: transcript variant 1 (GenBank: NM_030926.5) that represents the longest transcript; transcript variant 2 (GenBank: NM_001012516.2) that lacks the exon 4; transcript variant 3 (GenBank: NM_001012514.2) that lacks the exon 4; and transcript variant 4 (GenBank: NM_001287240.1) that differs in its 5' UTR and initiates translation from a

downstream start codon, compared to variant 1. Transcript variant 1 represents the longest and corresponds to the first human BRI3 sequence reported (Vidal *et al*. 2001).

As mentioned above these three genes encode BRI1, BRI2 and BRI3 proteins that present 27% of amino acid identity (Figure I.5), being the pattern of expression quite different across the tissues. The members of this family possess an intracellular N-terminus, a single pass transmembrane domain, and an extracellular C-terminus. The three members also contain a furin cleavage site at the C-terminus and a BRICHOS domain (Tai *et al*. 2014).

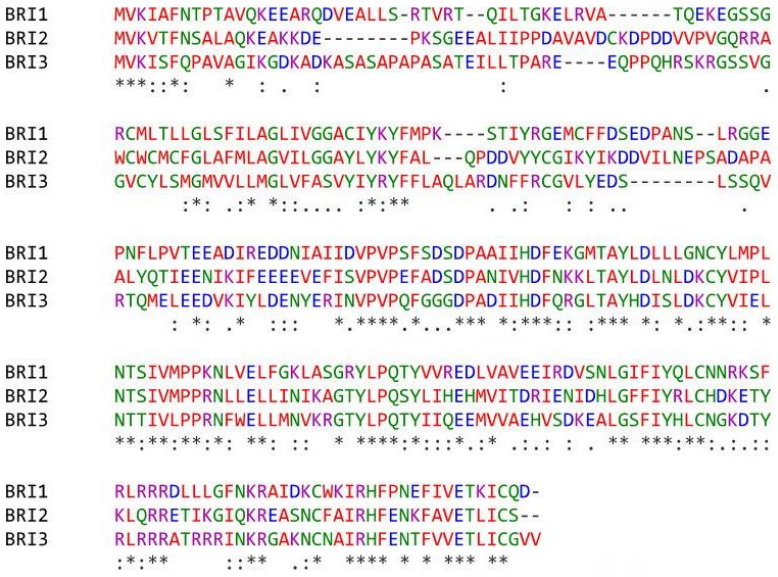

Figure I. 5 - Amino acid sequence alignment of the three BRI proteins. BRI1 has 263 amino acids, BRI2 has 266 amino acids and BRI3 has 267 amino acids. The alignment was obtained using the bioinformatic tool clustal omega (http://www.ebi.ac.uk/Tools/msa/clustalo). (*) indicates amino acid identity, (:) indicates conservative amino acid change - between groups of strongly similar properties, (.) indicates semi-conservative amino acid change - between groups of weakly similar properties.

The BRICHOS domain contains approximately 100 aa residues and is present in several proteins associated with dementia, chondrosarcoma, respiratory distress, and stomach cancer. The proteins that contain BRICHOS domain are predicted to be type II transmembrane or secretory proteins and have in common a complex post-translational processing. Its precise function is unknown, however, some roles have been proposed and include: targeting of the protein to the secretory pathway; chaperone-like function, preventing misfolding and peptide aggregation; and assisting the proper folding and processing of the proproteins (Sánchez-Pulido *et al*. 2002).

I.2.1. BRI1 protein

The human BRI1, also denominated as ITM2A or E25A, is a 263-residue protein with a calculated molecular weight (MW) of 29.7 kDa and theoretical isoelectric point (pI) of 5.62 (Deleersnijder *et al*. 1996; Pittois *et al*. 1999). BRI1 contains a cytosolic N-terminal domain (1-53-aa) followed by a single transmembrane domain (54-74 aa) and a luminal C-terminal of 189 aa which contains the BRICHOS domain (133-227 aa) (Figure I.6).

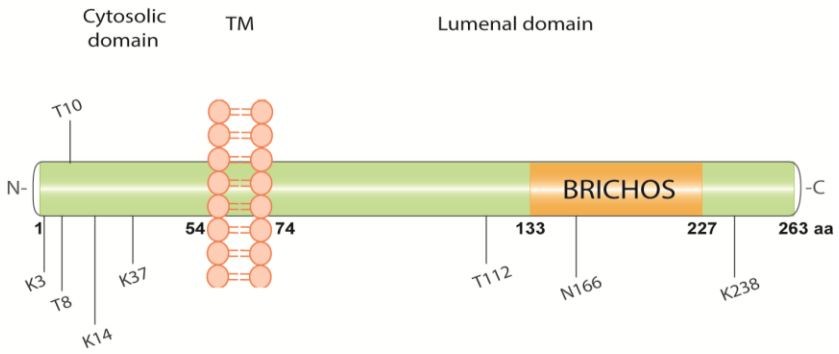

Figure I. 6 - Schematic representation of human BRI1 protein and its domains. Human BRI1 has a short N-terminal cytosolic domain, a long C-terminal luminal domain, one transmembrane domain (TM) and one BRICHOS domain. BRI1 can be phosphorylated at threonine (T) residues and each residue phosphorylated is indicated. BRI1 can also be modified by ubiquitination (K) and N-glycosylation (N) at the sites indicated.

BRI1 is expressed in several mesenchymal tissues, and was found to be most abundantly expressed in chondro- and osteogenic tissues: postnatal mandibular condyle, bone trabecula of mature bones, tooth germs and hair follicles, and strong expression in neonatal calvaria, paws, tail and skin (Deleersnijder *et al*. 1996; Pittois *et al*. 1999). BRI1 is also highly expressed in skeletal muscle, thymus and brain (Van den Plas and Merregaert 2004b; Van den Plas and Merregaert 2004a; Kirchner and Bevan 1999). Few studies have so far addressed the subcellular localization of BRI1. In a murine thymoma cell line, BRI1 appears to localize in large cytoplasmic vesicles, in the Golgi apparatus and also in the plasma membrane (Kirchner and Bevan 1999). In human uterine endometrial stoma sarcoma cells was also observed in the nuclei (Kihara *et al*. 2014).

A putative furin cleavage site is present on BRI1 but it remains unknown whether cleavage occurs. Moreover, for BRI1 are suggested some post-translational modifications that may regulate its cellular location and physiological function. Bioinformatic analysis suggests one putative N-glycosylation site at Asn166 (Choi *et al*. 2001). More recently, by using high-throughput techniques three phosphorylation sites (Thr8, Thr10 and Thr112; Mertins *et al*. 2013; Weber *et al*. 2012) and four ubiquitination sites (Lys3, Lys14, Lys37 and Lys238) (Figure I.6) (Mertins *et al*. 2013; Kim *et al*. 2011a; Udeshi *et al*. 2012) were identified, however its physiological relevance was not pursued.

I.2.1.1. BRI1 physiological function and associated proteins

The cellular function of BRI1 is so far not characterized. However, some data suggests a possible involvement of BRI1 in cell differentiation during chondrogenesis, odontogenesis and myogenesis (Pittois *et al*. 1999; Van den Plas and Merregaert 2004b; Van den Plas and Merregaert 2004a; Kirchner and Bevan 1999; Kihara *et al*. 2014). BRI1 was found to interact with ameloblastin, homeobox protein MOX-2 and GTPase KRas which corroborates the involvement of BRI1 in the previously suggested functions (Table I.1). Recently it was described that BRI1 expression is regulated by PAX3, a transcriptional factor important for muscle and neural development in vertebrates (Lagha *et al*. 2013).

In addition, a study by Kirchner *et al* revealed that BRI1 expression is enhanced during thymocyte selection and T-cell activation causing CD8 downregulation when overexpressed in CD4/CD8 double-positive thymocytes (Kirchner and Bevan 1999). Given this and the fact that BRI1 expression is also regulated by GATA3, a T cell-specific transcription factor, BRI1 may also be involved in T-cell development (Tai *et al*. 2014). BRI1 expression was also found to be dependent on the PKA-CREB pathway, and by interacting and interfering with the function of vacuolar ATPase, negatively regulates autophagic flux (Namkoong *et al*. 2015).

Furthermore, a recent report suggests a role for BRI1 as a cell cycle regulator, as its expression induces G2/M cell cycle arrest, being down-regulated during ovarian carcinogenesis (Nguyen *et al*. 2016). This potential role for BRI1 is strengthened by the recently described interaction between BRI1 and Polyubiquitin-C, a protein involved in several processes namely in the G2/M transition of the cell cycle (Table I.3).

Table I. 3 - List of the identified BRI1 interacting proteins. Information about the identified BRI1 interactors, as well as, the experimental evidence supporting the interactions.

Interactor	Description	Experimental evidence	References
Ambn	Ameloblastin	Two-hybrid	(Wang *et al*. 2005)
RNF2	E3 ubiquitin-protein ligase RING2	Co-IP and affinity chromatography-MS	(Cao *et al*. 2014)
UBC	Polyubiquitin-C	affinity chromatography-MS	(Udeshi *et al*. 2012; Kim *et al*. 2011)
MEOX2	Homeobox protein MOX-2	Two-hybrid	(Rolland *et al*. 2014)
KRAS	GTPase KRas	Genetic interference	(Luo *et al*. 2009)

Co-IP, co-immunoprecipitation; MS, mass spectrometry.

I.2.2. BRI2 protein

BRI2, also denominated as ITM2B or E25B, is a type II transmembrane protein with 266 aa, a calculated MW of 30.3 kDa and theoretical pI of 4.86. However, the apparent MW of the BRI2 protein (42-44 kDa) is higher than predicted from the number and composition of amino acids, suggesting that it suffers post-translational modifications. It contains nine cysteine residues and is highly rich in leucine (9.02%) and isoleucine (9.02%) (Vidal *et al*. 2000; Vidal *et al*. 1999). BRI2 also contains a cytosolic N-terminal domain (1-54 aa) followed by a single transmembrane domain (55-75 aa) and a luminal C-terminal of 191-aa which contains the BRICHOS domain (137-231 aa) (Figure I.7).

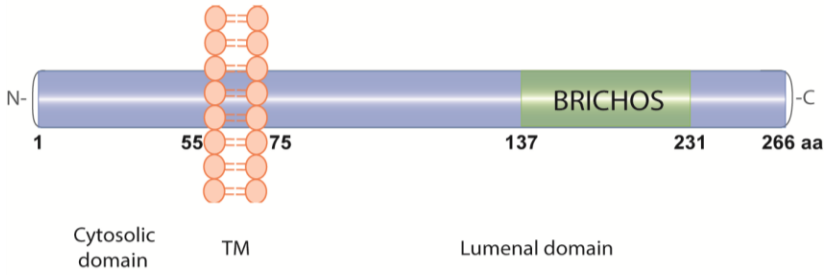

Figure I. 7 - Schematic representation of human BRI2 protein and its domains. Human BRI2 has a short N-terminal cytosolic domain, a long C-terminal luminal domain, one transmembrane domain (TM) and one BRICHOS domain.

BRI2 is a ubiquitously expressed protein; mRNA transcripts are found to be highly expressed in the brain, placenta, pancreas, and kidney and presents lower expression levels in heart, lung, liver and skeletal muscle. In the brain, analysis of different regions detected predominantly the longer transcript in the cerebellum, spinal cord, subthalamic nucleus, substantia nigra, and hippocampus. However, lower expression levels were also detected in the cerebral cortex, amygdala, and thalamus (Vidal *et al*. 1999). *In situ* hybridization studies demonstrated that within the brain, BRI2 mRNA is distributed in different cellular populations: neurons, astrocytes, and microglial cells as well as in smooth muscle and cerebral endothelial cells (Rostagno *et al*. 2005). Further immunohistochemistry studies in postmortem human brain tissues, detected BRI2 as fine granules in the neuronal cytoplasm, as well as in proximal dendrites and axons. In CA3 and CA4 pyramidal neurons of the hippocampus and Purkinje cells of the cerebellar cortex, the BRI2 staining is particularly intense (Akiyama *et al*. 2004). Additionally, BRI2 was detected in some pathological structures such as globular dystrophic neurites in senile plaques in Alzheimer´s disease. Regarding the subcellular localization, BRI2 is mainly localized in the endoplasmic reticulum (ER), Golgi apparatus, plasma membrane and cytoplasmic vesicles (Choi *et al*. 2004).

I.2.2.1. BRI2 processing

BRI2 undergoes regulated intramembrane proteolysis (RIP) in the cis- or medial-Golgi resulting in the formation of several secreted peptides (Choi *et al*. 2004). RIP describes the processing of several transmembrane proteins by an ectodomain shedding followed by an intramembrane cleavage. This processing is mainly involved in cellular signaling events and in the removal and degradation of membrane-retained fragments that are produced by the initial shedding event (Martin *et al*. 2008). First, in its extracellular region, BRI2 is cleaved between Arg243 and Glu244 to release a secreted C-terminal 23-residue peptide (3KDa; Figure I.8). The amino acid sequence that flanks this cleavage site (QKR243/E244A) is a consensus sequence required for processing by proprotein convertases (PPC). Several PPC's including furin, paired basic amino acid cleaving enzyme 4 (PACE4), lymphoma proprotein convertase (LPC) and proprotein convertase 5/6 (PC 5/6) are capable of processing BRI2. Of these BRI2 cleaving enzymes, furin appears to be the most effective (Choi *et al*. 2004; Kim *et al*. 1999). However, furin activity is mainly detected in the trans-Golgi and the BRI2 processing occurs in the *cis*- or *medial*-Golgi (Choi *et al*. 2004), and so it remains unclear whether furin is the main BRI2-cleavage enzyme. The function of the released 23-aa peptide remains undisclosed however some reports suggest that the peptide may act as signal peptide, since the deletion of the C-terminal peptide leads to BRI2 retention in ER and consequently inefficient transport to the cell surface (Matsuda *et al*. 2011a).

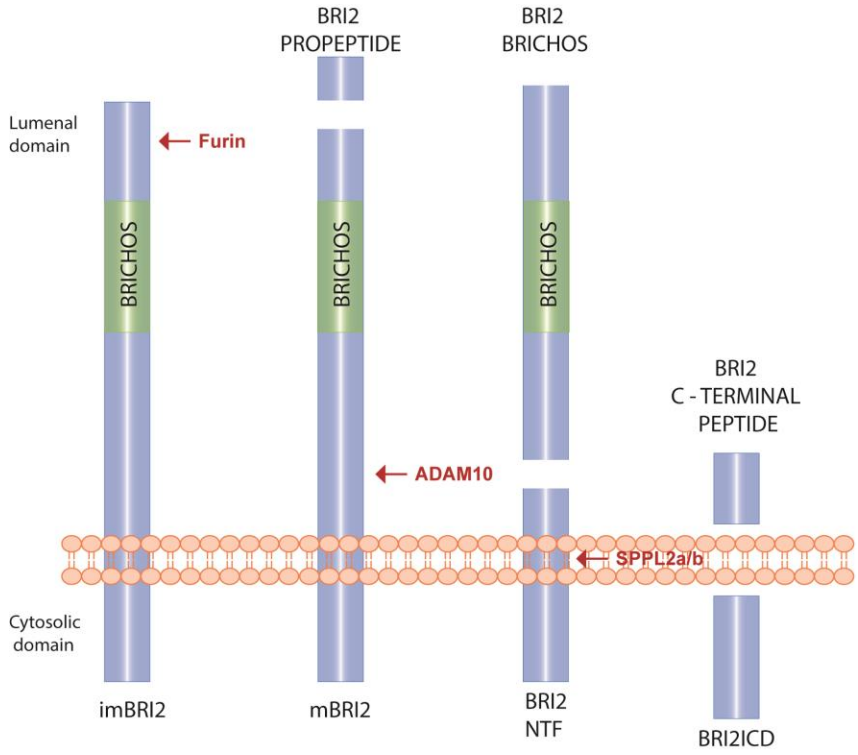

Figure I. 8 - Schematic representation of BRI2 processing. BRI2 (immature BRI2 – imBRI2) is cleaved by a proprotein convertase, namely furin, to release a secreted C-terminal 23-residue peptide (BRI2 propeptide). The remaining membrane-bound N-terminal fragment is the mature form of BRI2 (mBRI2). BRI2 undergoes an additional cleavage in its ectodomain exerted by ADAM-10 which results in the secretion of a soluble peptide containing the BRICHOS domain (BRI2 BRICHOS) and in a membrane-bound N-terminal fragment (BRI2 NTF). The NTF is subsequently subjected to intramembrane proteolysis cleavage by the SPPL2/b, generating a small, secreted, BRI2 C-terminal peptide and an intracellular domain (BRI2ICD).

The remaining membrane-bound N-terminal fragment is the mature form of BRI2 that undergoes an additional cleavage in its ectodomain exerted by 'a disintegrin and metalloproteinase domain 10' (ADAM-10) (Figure I.8) (Choi *et al*. 2004). ADAM10 is a α-secretase that cleaves several other transmembrane proteins, including APP, Notch-1 and N- and E-cadherin (Tsachaki *et al*. 2008). The precise cleavage site of ADAM10 in BRI2 remains unidentified, however, it is predicted to occur between amino acids 76 and 170 (Choi *et al*. 2004). ADAM10 processing of BRI2 results in secretion of a soluble peptide containing the BRICHOS domain (25KDa) and in a membrane-bound N-terminal fragment (NTF; 22KDa) (Figure I.8). The secretion of the complete BRICHOS domain suggests a physiological function for this peptide. However, this function remains unclear. The NTF is subsequently subjected to intramembrane proteolysis cleavage by the signal peptidase-like proteases (SPPLs) SPPL2a and SPPL2b, generating a small, secreted, BRI2 C-terminal domain and an intracellular domain (BRI2ICD; 10KDa) (Figure I.8). SPPL2a/b are members of the family of intramembrane-cleaving aspartyl proteases of the GXGD-type that efficiently processes its substrates if their transmembrane domains adopt a β-strand-like conformation (Martin *et al*. 2008; Martin *et al*.

2009). A recent study suggests that a single glycine in the BRI2 transmembrane domain (Gly60) is a determinant of the secondary structure of the BRI2 transmembrane domain in lipid vesicles since it is essential for the destabilization of its α-helical structure and consequently for the cleavage efficiency of BRI2 by SPPL2a/b. Interestingly, BRI2 shedding by ADAM10 significantly facilitates the intramembrane cleavage by SPPL2a/b (Fluhrer *et al*. 2012). It was recently described that BRI2ICD can translocate to the nucleus following its proteolytic liberation suggesting a particular function for this fragment in signal transduction and transcriptional regulation as it has been described for the APP ICD (AICD) and Notch1 ICD (NICD) (Rebelo *et al*. 2013; Mentrup *et al*. 2015; Artavanis-Tsakonas *et al*. 1999). Therefore, further research on BRI2 processing and its fragments may lead to new insights into the physiological role of BRI2. Of note, BRI2 processing by ADAM10 and SPPL2a/b seems to occur independently from furin processing (Martin *et al*. 2008).

I.2.2.2. BRI2 post-translational modifications

Moreover, during the maturation process in the cis-medial Golgi, BRI2 suffers post-translational modifications, such as glycosylation and phosphorylation, leading to various forms of BRI2 that may have different cellular locations and physiological functions (Akiyama *et al*. 2004; Lashley *et al*. 2008; Del Campo and Teunissen 2014; Tsachaki *et al*. 2011). Several studies demonstrated that BRI2 is N-glycosylated at Asn170 (Figure I.9). In fact, by using an N-glycosylation mutant (mutation of Asn170 to Ala) it was possible to conclude that N-glycosylation is essential for the proper trafficking of BRI2 through the secretory pathway to the cell surface (Tsachaki *et al*. 2011). Surprisingly, this mutation did not affect the proteolytic processing of BRI2 by furin or ADAM10 which suggests that cleavage by ADAM10 can also take place intracellularly. Interestingly, was described an interaction for BRI2 protein with the brain-specific membrane-anchored protein TMEM59L (Table I.2), a protein that modulates O- and N-glycosylation occurring during the Golgi maturation of APP (Ullrich *et al*. 2010). Therefore, it is possible that TMEM59L is also able to modulate the described N-glycosylation of BRI2 protein and this deserve further elucidation.

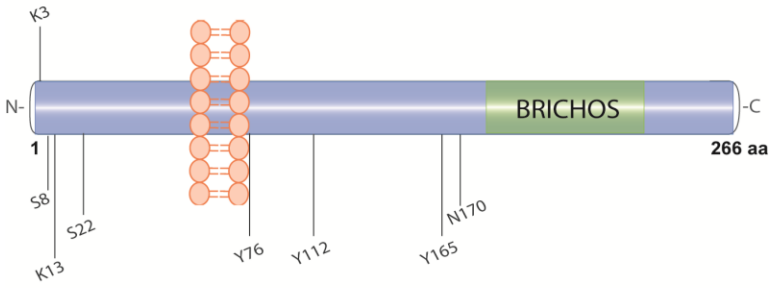

Figure I. 9 - Human BRI2 post-translational modifications. BRI2 can be phosphorylated at numerous serine (S) and tyrosine (Y) residues, and each residue phosphorylated is indicated. BRI2 can also be modified by N-glycosylation (N) and ubiquitination (K) at the sites indicated.

Additionally, bioinformatic analysis of the BRI2 sequence, suggests several putative phosphorylation sites, being only confirmed five phosphoresidues by high-throughput studies: Ser8, Ser22, Tyr76, Tyr112 and Tyr165 (Figure I.9) (Demirkan *et al*. 2011; Sharma *et al*. 2014a; Wilhelm *et al*. 2014). However, the physiological relevance of BRI2 phosphorylation remains unknown. Moreover, BRI2 was found to be post-translationally modified by ubiquitination at the residues Lys3 and Lys13 (Figure I.9) (Udeshi *et al*. 2012; Shi *et al*. 2011). Ubiquitination is an important regulatory mechanism for various cellular processes, including protein degradation, cell cycle and division, DNA repair, transcriptional regulation, differentiation and development, morphogenesis of neuronal networks, modulation of cell surface receptors, regulation of the immune and inflammatory responses, as well as for controlling stability and localization of proteins (Ciechanover 1994; Glickman and Ciechanover 2002).

I.2.2.3. BRI2 physiological function and associated proteins

The precise biological function of BRI2 remains elusive, however, given some hints proposed by previous studies, some BRI2 functions have been suggested. Besides, given the broad distribution, it is plausible to assume that BRI2 presents a wide-ranging function.

The distribution of BRI2 within proximal dendrites and axons, as well as cell bodies, and its presence in some neuropathological structures suggests that BRI2 could be transported in nerve terminals and that it may have a role at the nerve terminals (Akiyama *et al*. 2004). In fact, it was demonstrated that BRI2 overexpression in human neuronal cells induces neurites elongation, indicating that BRI2 could be involved in neurite outgrowth (Choi *et al*. 2004). The already described interactions of BRI2 with the RYK receptor-like tyrosine kinase, Semaphorin-6A, heparan sulfate 6-O-sulfotransferase 1,

adhesion molecule with Ig-like domain 1 and leucine-rich repeat and fibronectin type-III domain-containing protein 3 also supports the putative role BRI2 on neuronal differentiation and neurite growth (Table I.4; Berndt *et al*. 2011; Huttlin *et al*. 2015).

BRI2 has a Bcl-2 homology-3 (BH-3) domain encoded in exon 2 characteristic of pro-apoptotic proteins of the Bcl-2 family. Interestingly, a short splice variant of BRI2 that lacks exon 1 seems to be up-regulated in a murine T cell line before the induction of apoptosis, suggesting that BRI2 could participate in the apoptotic pathway. Indeed, overexpression of the short variant of BRI2 in IL-2 stimulated T cells and also in COS-7 cells induces apoptosis. The BH-3 domain mutation of this BRI2 variant abolished the ability of BRI2 to induce apoptosis, suggesting an important role for this domain in the BRI2 apoptotic activities. Moreover, BRI2 pro-apoptotic functions seem to be associated with the activation of a mitochondrial apoptotic pathway leading to cytochrome *c* release, and with caspase 3 and caspase 9 activation (Fleischer *et al*. 2002).

Interestingly, the *BRI2* gene is located in the chromosome segment 13q14 and the loss of heterozygosity (LOH) on chromosome arm 13q14.2-q14.3 is frequently observed in prostate tumors, ovarian carcinoma, head and neck squamous cell carcinoma and in pituitary tumors. In fact, by using a real-time quantitative RT-PCR assay, BRI2 expression was found to be significantly reduced in sporadic prostate tumors with a correlation with cancer stage and grade. Besides a positive association between the decreased BRI2 expression and LOH at 13q14.2 was described. Therefore, BRI2 has been suggested as a candidate to act as a tumor suppressor gene (Latil *et al*. 2003). Additionally, was already established an interaction for BRI2 with CREB3, an important signaling protein also involved in tumor suppression (Table I.4; Yu *et al*. 2011; Hein *et al*. 2015).

Further studies demonstrated that BRI2 forms homodimers held by disulfide bonds, and the extracellular cysteine located at position 89 is involved. The BRI2 dimers seem to be formed in the ER and transferred to the cell membrane. Several transmembrane proteins that act as receptors form dimers at the cell surface, and thus it is possible to assume that BRI2 could act as a receptor or is a part of a receptor complex and participates in signal transduction pathways (Tsachaki *et al*. 2010).

Additionally, a yeast two-hybrid screen using a human brain cDNA library as bait allowed the identification of proteins that interact with Alzheimer's amyloid Precursor Protein (APP). This study identified BRI2 protein as novel APP binding protein (Table I.4; Fotinopoulou *et al*. 2005). The aa 648-719 of APP_{751} and the aa 46-106 of BRI2, both inclusive of the full transmembrane domains, are responsible for the interaction. Therefore, it is possible that both proteins interact when are expressed on the same cell membrane, by forming a molecular complex, rather than on adjacent cells as receptor/ligand (Matsuda *et al*. 2005; Fotinopoulou *et al*. 2005). BRI2 interacts with both APP_{751} and APP_{695} isoforms, suggesting that the interaction is not APP isoform-dependent (Fotinopoulou *et al*. 2005). Besides, only the mature forms of both BRI2 and APP interacts, and the interaction occurs at

the cell surface and in endocytic compartments (Matsuda *et al*. 2011a). BRI2-APP interaction is suggested to be a regulatory mechanism of APP processing that inhibits Aβ production (Matsuda *et al*. 2005). In the amyloidogenic pathway that produces Aβ, APP is firstly cleaved by β-secretase (β-secretase β-amyloid protein converting enzyme 1, BACE1) to release a secreted fragment (sAPPβ) and to produce a membrane-bound C-terminal fragment. This fragment is subsequently subjected to regulated intramembrane proteolysis by γ-secretase to release extracellularly Aβ and intracellularly AICD. Matsuda and colleagues suggested that functionally BRI2 restrict docking of γ-secretase to APP and by masking the α- and β-secretase cleavage rather than affecting the secretase activity (Matsuda *et al*. 2008). However, a recent study demonstrates that in fact, BRI2 also interacts with BACE1 promoting its lysosomal degradation and also reducing its expression levels (Table I.4; Tsachaki *et al*. 2013). Besides a role in the processing of APP, BRI2 may also inhibit Aβ aggregation and several mechanisms have been proposed. Kim and colleagues demonstrated that the 23 aa C-terminal peptide released by furin processing inhibits Aβ aggregation *in vitro* (Kim *et al*. 2008). Another study revealed that a BRI2 fragment (90-236 aa) that contains the BRICHOS domain also binds to Aβ peptide inhibiting its aggregation and fibril formation (Peng *et al*. 2010). More recently, it was reported that transgenic expression of the BRI2 BRICHOS domain in the *Drosophila* central nervous system efficiently inhibited Aβ42 toxicity (Poska *et al*. 2016). Furthermore, it was shown that BRI2 promotes Aβ degradation by increasing the levels of the secreted insulin-degrading enzyme (IDE), a metalloprotease that cleaves insulin and other peptide substrates (Kilger *et al*. 2011).

Finally, was described an association between BRI2 and ADAM7, a member of the ADAM family that is specifically expressed in the epididymis. ADAM7/BRI2 complexes are present in membrane lipid rafts or microdomains at the sperm surface, and the formation of this complex is promoted during sperm capacitation suggesting a role for BRI2 in sperm functions and fertilization (Han *et al*. 2011).Several other proteins were found to interact with BRI2 that may uncover potentially functions for BRI2 (Table I.4).

Table I. 4 – List of the identified BRI2 interacting proteins. Information about the identified BRI2 interactors, as well as, the experimental evidence supporting the interactions.

Interactor	Description	Experimental evidence	References
APP	Amyloid beta A4 protein	Two-hybrid Co-IP	(Matsuda *et al*. 2005; Fotinopoulou *et al*. 2005)
BCL2	Apoptosis regulator Bcl-2 (protein phosphatase 1, regulatory subunit 50)	Co-IP	(Fleischer *et al*. 2002)
BACE1	β-secretase β-amyloid protein converting enzyme 1	Co-IP	(Tsachaki *et al*. 2013)
UBC	Polyubiquitin-C	Affinity Capture-MS	(Danielsen *et al*. 2011; Shi *et al*. 2011; Wagner *et al*. 2011; Kim *et al*. 2011; Oshikawa *et al*. 2012; Udeshi *et al*. 2012; Emanuele *et al*. 2011; Povlsen *et al*. 2012; Renaudin *et al*. 2014)
RYK	RYK receptor-like tyrosine kinase	Affinity Capture-MS	(Berndt *et al*. 2011)
CREB3	Cyclic AMP-responsive element-binding protein 3	Two-hybrid; Affinity Capture-MS	(Yu *et al*. 2011; Hein *et al*. 2015)
SEMA6A	Semaphorin-6A	Affinity Capture-MS	(Huttlin *et al*. 2015)
GLG1	Cysteine-rich fibroblast growth factor receptor	Affinity Capture-MS	(Huttlin *et al*. 2015)
PGAP1	Post-GPI attachment to proteins factor 1	Affinity Capture-MS	(Huttlin *et al*. 2015)
CACNA2D1	Dihydropyridine-sensitive L-type, calcium channel alpha-2/delta subunit	Affinity Capture-MS	(Huttlin *et al*. 2015)
HS6ST1	Heparan sulfate 6-O-sulfotransferase 1	Affinity Capture-MS	(Huttlin *et al*. 2015)
TGFBR3	Transforming growth factor beta receptor type 3	Affinity Capture-MS	(Huttlin *et al*. 2015)
AMIGO1	Adhesion molecule with Ig-like domain 1	Affinity Capture-MS	(Huttlin *et al*. 2015)
KIAA1467	Uncharacterized protein KIAA1467	Affinity Capture-MS	(Huttlin *et al*. 2015)
LRFN3	Leucine-rich repeat and fibronectin type-III domain-containing protein 3	Affinity Capture-MS	(Huttlin *et al*. 2015)
TMEM219	Insulin-like growth factor binding protein-3 receptor	Affinity Capture-MS	(Huttlin *et al*. 2015)
B4GALNT1	UDP-N-acetyl-alpha-D-galactosamine:(N-acetylneuraminyl)-galactosylglucosylceramide N-acetylgalactosaminyltransferase (GalNAc-T)	Affinity Capture-MS	(Huttlin *et al*. 2015)
CHST12	Carbohydrate (chondroitin 4) sulfotransferase 12	Affinity Capture-MS	(Huttlin *et al*. 2015)
UBR1	Ubiquitin protein ligase E3 component n-recognin 1	Affinity Capture-MS	(Huttlin *et al*. 2015)
HLA-A	HLA class I histocompatibility antigen, A-1 alpha chain	Affinity Capture-MS	(Huttlin *et al*. 2015)
MR1	Bajor histocompatibility complex class I-related gene protein	Affinity Capture-MS	(Huttlin *et al*. 2015)
ATF6B	cAMP response element-binding protein-related protein	Affinity Capture-MS	(Huttlin *et al*. 2015)
SEMA4F	Semaphorin-4F	Affinity Capture-MS	(Huttlin *et al*. 2015)

BTN2A2	Butyrophilin, subfamily 2, member A2	Affinity Capture-MS	(Huttlin *et al*. 2015)
TMEM59L	Brain-specific membrane-anchored protein (C19orf4)	Affinity Capture-MS	(Huttlin *et al*. 2015)
UL25	Virion-packaging protein UL25	Two-hybrid	(Zhang *et al*. 2011)
CSF1	Macrophage colony-stimulating factor 1	Pull-down	(Cross *et al*. 2005)
ADAM7	Desintegrin and metalloproteinase domain-containing protein 7	Affinity Capture-MS	(Han *et al*. 2011)
SPPL2B	Signal peptide peptidase-like 2B	Co-IP	(Martin *et al*. 2008)
SPPL2A	Signal peptide peptidase-like 2A	Co-IP	(Martin *et al*. 2008)
FCGRT	IgG receptor FcRn large subunit p51	Affinity Capture-MS	(Huttlin *et al*. 2015)
NEK2	Serine/threonine-protein kinase Nek2	Affinity Capture-MS	(Hein *et al*. 2015)
SHOC2	Leucine-rich repeat protein SHOC-2	Affinity Capture-MS	(Hein *et al*. 2015)
KIF18A	Kinesin-like protein KIF18A	Affinity Capture-MS	(Hein *et al*. 2015)
UNK	RING finger protein unkempt homolog	Affinity Capture-RNA	(Murn *et al*. 2015)
TMEM17	Transmembrane protein 17	Proximity Label-MS	(Gupta *et al*. 2015)
NAALADL2	Inactive N-acetylated-alpha-linked acidic dipeptidase-like protein 2	Two-hybrid	(Rolland *et al*. 2014)
SYNE4	Nesprin-4	Two-hybrid	(Rolland *et al*. 2014)
CCDC155	Protein KASH5	Two-hybrid	(Rolland *et al*. 2014)
DCBLD2	Discoidin, CUB and LCCL domain-containing protein 2	Affinity Capture-MS	(Huttlin *et al*. 2015)
LMO2	Rhombotin-2	Two-hybrid	(Sincennes *et al*. 2016)
RPL31	60S ribosomal protein L31	Two-hybrid	(Bell *et al*. 2009)
HNF1A	Hepatocyte nuclear factor 1-alpha	Cross-linking study	(Odom *et al*. 2004)
ENV	Envelope glycoprotein gp160	Affinity Capture-MS	(Jäger *et al*. 2011)

Co-IP, co-immunoprecipitation; MS, mass spectrometry.

I.2.2.4. BRI2 associated diseases

Familial British and Danish dementias (FBD and FDD, respectively), two rare early-onset forms of dementia, are associated with different autosomal dominant mutations in the *BRI2* gene (*ITM2B)*. These diseases share several clinical symptoms such as progressive cognitive impairment, cerebellar ataxia, and spasticity (Tsachaki *et al*. 2008). FBD was first described in 1933 by Worster-Drought and the age of onset is in the fourth and fifth decade of life (Worster-Drought *et al*. 1933; Mead *et al*. 2000; Plant *et al*. 1990). The majority of affected patients succumb in the sixth decade of life. Clinical symptoms include progressive dementia, spastic tetraparesis and cerebellar ataxia (Plant *et al*. 1990; Mead *et al*. 2000). Neuropathological studies of FBD revealed the presence of pre-amyloid (non-fibrillar) and amyloid parenchymal lesions in the brain (primarily localized to the hippocampus

and cerebellum), extensive cerebral amyloid angiopathy (CAA) and intraneuronal formation of neurofibrillary tangles (NFT) within the limbic regions (Plant *et al*. 1990; Revesz *et al*. 1999). FDD was first identified in 1970 by Stromgren and collaborators in a Danish kindred and clinically is characterized by the development and progression of cataracts during the second decade of life (Strömgren *et al*. 1970; Vidal *et al*. 2000). Later on the patients develop deafness, cerebellar ataxia, paranoid psychosis and progressive dementia. The majority of patients succumb within the fifth or sixth decade of life (Strömgren *et al*. 1970; Vidal *et al*. 2000). Neuropathological lesions in FDD patients are closely similar to those found in FBD, however in FDD was found Aβ deposition and co-deposition with the Danish amyloid in all patients with FDD, and parenchymal compact plaques are absent (Holton *et al*. 2002; Vidal *et al*. 2000). In addition, activation of the proinflammatory complement system, which are among the features characteristic of AD, have also been associated with FBD and FDD (Rostagno *et al*. 2005). In FBD, a point mutation in the stop codon of the *BRI2* gene generates a longer open reading frame, resulting in the production of a longer 277 residues BRI2 precursor protein (ABriPP) (Figure I.10) (Ghiso *et al*. 2000). In FDD, there is a 10 nucleotide duplication insertion (TTTAATTTGT) between codons 265 and 266, resulting in the production of a mutated BRI2 precursor protein (ADanPP) that is also 11 amino acids longer (Figure I.10) (Vidal *et al*. 2000).

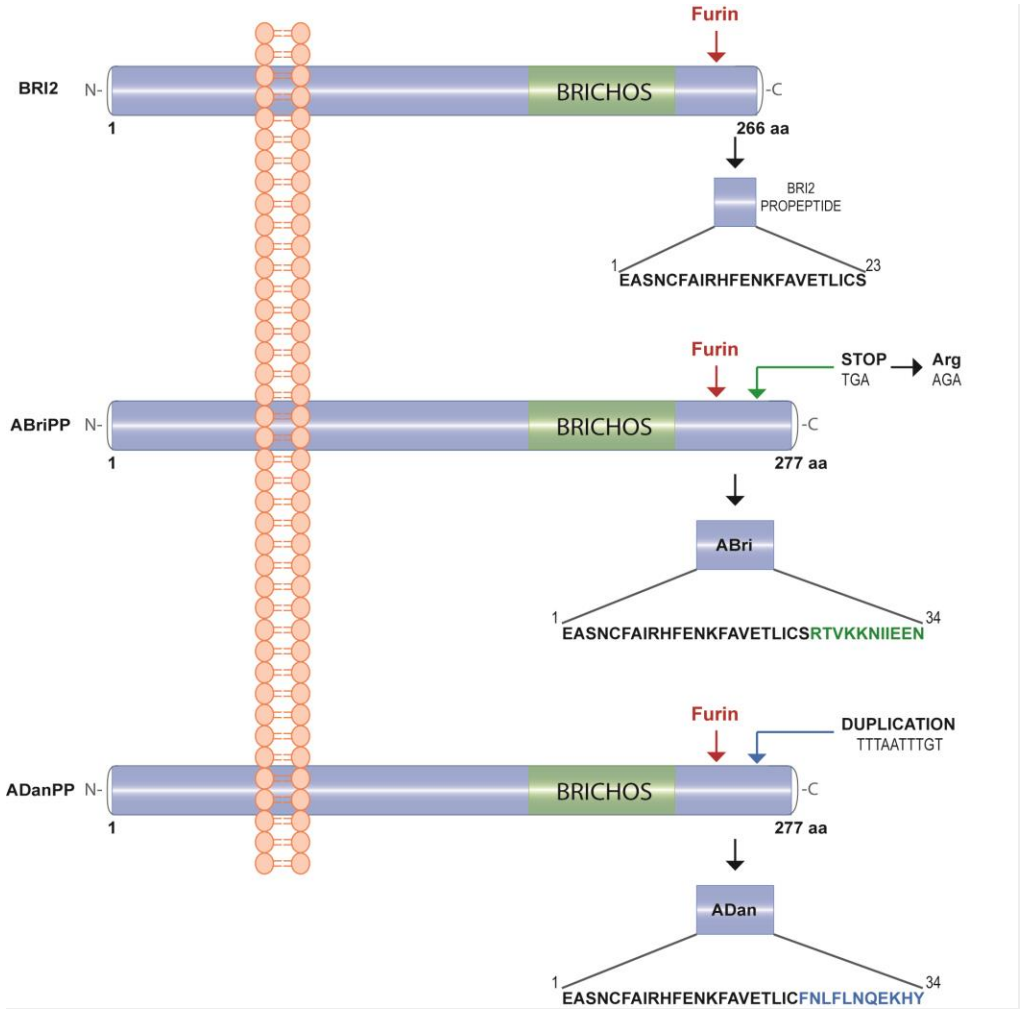

Figure I. 10 - Schematic representation of the BRI2 protein and its mutated forms, ABriPP and ADanPP, and the amyloid peptides in patients affected with FBD and FDD. The BRI2 gene encodes a type II transmembrane protein with 266 amino acids, BRI2. In FBD, a point mutation at codon 267 in BRI2 gene (Stop →Arg) originate a longer precursor protein, ABriPP, with 277 amino acids. Furin proteolytically processes ABriPP generating the ABri peptide (34 amino acids long) which composes the amyloid deposits in FBD. In FDD, a ten nucleotide duplication (TTTAATTTGT) after codon 265 in BRI2 gene originate a longer precursor protein, ADanPP, with 277 amino acids. Furin proteolytically processes ADanPP generating the ADan peptide (34 amino acids long) which composes the amyloid deposits in FDD. Although originated by different genetic defects in the BRI gene, both mutated precursors have 277 amino acids. Both amyloids (ABri and ADan) have an identical N-terminal amino acid sequence (first 22 amino acids) and a completely different C-terminal sequence (last 12 amino acids). FBD, familial British dementia; FDD, familial Danish dementia; aa, amino acid.

Mutated BRI2 proteins undergo furin-like proteolytic processing at the same site as wild-type BRI2 which results in the release of the 34-aa C-terminal secreted peptides (4KDa), ABri and ADan, in the case of FBD and FDD, respectively (Figure I.10). In fact, it was reported that the expression of the mutant BRI2 proteins in a neuronal cell line, produced more peptide than those transfected with the wild type, indicating that the C-terminal extension enhances PCs proteolysis (Choi *et al*. 2004). On the contrary, a more recent study reported that the cleavage of BRI2 by PCs is more efficient for the

wild-type BRI2 than for mutant BRI2 (both FBD and FDD mutants) since the mutant sequences may interfere both with the proper folding of BRI2 and the enzymatic activity of PCs. In turn, the reduced processing observed for mutant precursor proteins leads to its intracellular accumulation in the Golgi of neurons and glial cells (Garringer *et al*. 2017).

ABri and ADan are identical in the 22 N-terminal aa but differ in their additional 12 C-terminal aa, and in contrast with the normally secreted peptide, shows a high tendency to oligomerize and aggregate (Figure I.10) (Kim *et al*. 1999). Moreover, these peptides were identified in the insoluble amyloid deposits, and as soluble monomeric forms in the plasma of patients with FBD and FDD (Vidal *et al*. 1999; Vidal *et al*. 2000; Ghiso *et al*. 2001; Tomidokoro *et al*. 2005). Both ABri and ADan peptides contain two cysteine residues in their sequence (Cys248 and Cys265) that were shown to form an intramolecular disulfide bond, and thus they can exist in an oxidized or reduced form (El-Agnaf *et al*. 2004; Gibson *et al*. 2004). ABri seems to be more toxic in oxidized forms, aggregating in soluble oligomers (El-Agnaf *et al*. 2004). However, ADan forms soluble oligomers in both oxidized and reduced state, being the latter more neurotoxic (Gibson *et al*. 2004). Therefore, soluble oligomers, rather than highly fibrillized peptides seems to be implicated in the neurodegeneration process in FBD and FDD, as already has been suggested for AD (Rostagno and Ghiso 2008). In addition, *in vitro* studies determined that both ABri and ADan peptides are able to activate the complement cascade at levels compared to those observed in AD (Bradt *et al*. 1998).

Moreover, the analysis of genetically congruous with human cases mouse models of the FBD and FDD (FBD_{KI} and FDD_{KI} mice, respectively) shows reduced expression of mature BRI2 levels in both cases (Tamayev *et al*. 2010a; Tamayev *et al*. 2010b), and in the FDD_{KI} mice was found accumulation of mature BRI2 in dystrophic neurites (Garringer *et al*. 2017). Of note, in human FBD brains was also detected a significant reduction of mature BRI2 levels (Tamayev *et al*. 2010a). Besides, BRI2 haploinsufficient ($BRI2^{+/-}$) mice exhibit similar synaptic and memory deficits, and in FDD_{KI} mice the expression of wt BRI2 in the forebrain prevented the memory deficits. Hence, it is possible that both FBD and FDD are caused by loss of BRI2 function rather than amyloidosis or tauopathy as previously suggested (Tamayev *et al*. 2010a; Tamayev *et al*. 2010b). Noteworthy, in FDD_{KI} mice the APP fragments resulting from its processing are significantly increased, and BRI2:APP interaction is significantly reduced in synaptic membranes (Tamayev *et al*. 2011; Matsuda *et al*. 2011b). In FBD_{KI} mice brains there is no alterations in the APP processing, however APP haploinsufficiency ($FBD_{KI}/APP^{+/-}$), as well as inhibition of β-processing of APP prevents the associated memory and synaptic impairments (Tamayev and D'Adamio 2012). Additionally, Aph1B/C (a component of the γ-secretase complex) deletion, which resulted in increased β-CTF but decreased Aβ production in FDD_{KI} mice ($FDD_{KI}/Aph1BC^{-/-}$), does not rescue the memory deficits as would have been expected if Aβ played a pathogenic role in FDD_{KI} mice. In fact, the FDD mutation and the $Aph1BC^{-/-}$ deletion

cause similar behavioral deficits in spatial memory and appear to have a small additive negative effect. These observations are consistent with a pathological role of β-CTF, which is increased in FDD_{KI} mice due to increased production and in *Aph1BC*$^{-/-}$ mice due to reduced turnover. Therefore, given the nature of the functional interaction of BRI2 and APP it is also plausible to assume that the pathogenesis of synaptic and memory deficits in FDD, as well as in FBD, is mediated by the toxic APP metabolites.

BRI2 was also found to be deposited in the hippocampus of early stages of AD cases, and clearly associated with Aβ plaques. By using western blot analysis it was also possible to detect increased levels of unprocessed BRI2 in the brain of AD patients, as well as decreased furin and ADAM10 levels and increased SPPl2b levels (Figure I.11). Therefore, it is possible that an alternative processing of BRI2 leads to the secretion of BRI2 ectodomain, which aggregates and deposits (Figure I.2.7). Besides the BRI2 binding to APP was lost in brain homogenates of AD patients. Indeed, processing of BRI2 into mature BRI2 and its transport along the secretory pathway are required to generate a functional APP processing inhibitor. Thus, BRI2 abnormal accumulation and subcellular localization of BRI2 may prevent the formation of the BRI2-APP complex formation leading to an increase in the APP processing and Aβ production (Figure I.11). On the other hand, the deposits of BRI2 containing the BRICHOS domain also affects its inhibitory function in the aggregation and fibrillation of the Aβ peptide (Figure I.11) (Peng *et al*. 2010; Willander *et al*. 2012; Del Campo *et al*. 2014).

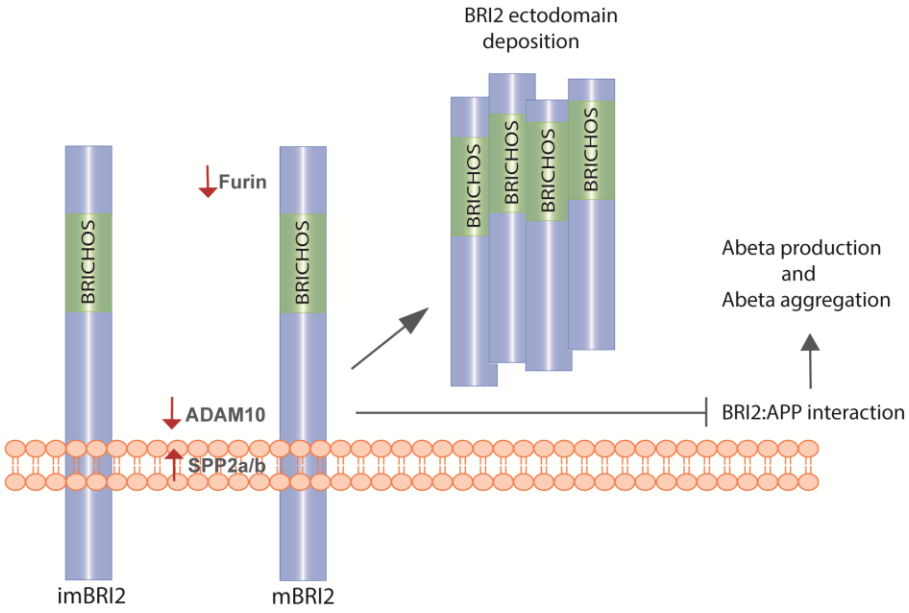

Figure I. 11 - Schematic representation of the proposed role for BRI2 deposition in Alzheimer´s disease. Reduced cleavage of BRI2 by furin and ADAM10 and the increase of BRI2 processing by SPPL2b leads to the release of the whole BRI2 ectodomain. BRI2 ectodomain has high aggregation propensities and therefore its release may lead to accumulation

and deposition of BRI2. BRI2 deposits lead to a loss of BRI2 function and impair the formation of BRI2:APP complexes and the subsequent inhibition of Abeta (Aβ) production and aggregation. APP, amyloid precursor protein (adapted from Del Campo et al. 2014).

Besides the loss of function of BRI2, the accumulation of BRI2 ectodomain may also lead to a gain of toxic function and have a negative impact on cell homeostasis. In human neuroblastoma cells, recombinant BRI2 ectodomain was shown to induce apoptosis by increasing the levels of proapoptotic protein Bax, decreasing the levels of antiapoptotic protein Bcl-2, and increasing the activity of caspase 3 and 9. In addition, the BRI2 ectodomain leads to tau truncation at D421, that has already been observed in AD and seems to be involved in the formation of NFT, a neuropathological hallmark of AD (Del Campo *et al*. 2015). Thereby, BRI2 may also be involved in the AD pathogenesis and its understanding may open new insights in the development of new therapies. Recently, a report by Baron et al identifies BRI2 as a target of BCL6 repression in human lymphomas (Baron *et al*. 2015). BCL6 is a crucial transcriptional repressor involved in the pathogenesis of some human lymphomas and binds to a consensus binding site within the first intron of BRI2. Knockdown of BCL6 in a B lymphoma cell line significantly increases the levels of endogenous BRI2. Besides, it was reported an inverse relationship between BCL6 and BRI2 protein levels in B- and T- cell human lymphomas studied by immunohistochemistry (Baron *et al*. 2015). Therefore, the dysfunction of BRI2 and its regulators may be relevant for the pathogenesis of lymphomas and may provide insights for the development of new molecular targeted therapies.

I.2.3. BRI3 protein

BRI3, is a protein composed of 267 aa, with a MW of 30 kDa and a pI of 8.47 (Vidal *et al*. 2001). Contains a cytosolic N-terminal domain (1-54 aa) followed by a single transmembrane domain (55-75 aa), and a luminal C-terminal of 192-aa which contains the BRICHOS domain (136-230) (Figure I.12). It is mainly expressed in the brain with the highest levels of expression in cerebral cortex, medulla oblongata, amygdala, hippocampus, thalamus, striatum, caudate nucleus and spinal cord (Vidal *et al*. 2001; Choi *et al*. 2001). BRI3 is also expressed in plasmocytoid dendritic cells, granulocytes, appendix, bone marrow, fetal liver and to a lesser extent in spleen, lymph nodes and thymus (Rissoan *et al*. 2002). Subcellularly, BRI3 is mainly localized in the perinuclear region of cytoplasm, Golgi apparatus and plasma membrane (Gong *et al*. 2008; Martin *et al*. 2008).

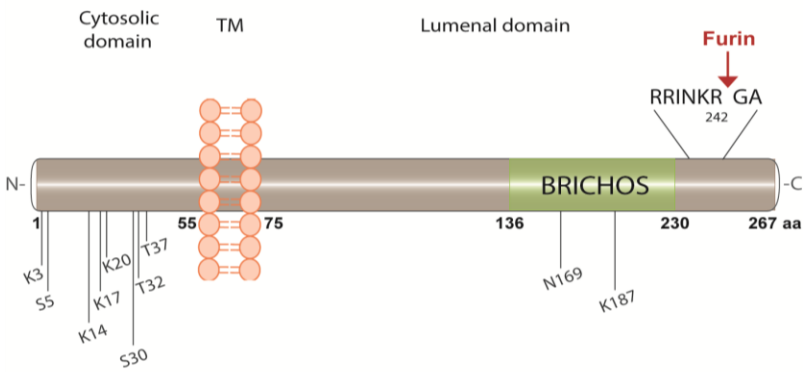

Figure I. 12 - Schematic representation of human BRI3 protein and its domains. Human BRI3 has a short N-terminal cytosolic domain, a long C-terminal luminal domain, one transmembrane domain (TM) and one BRICHOS domain. Human BRI3 is processed at Arg242 by furin resulting in the secretion of a C-terminal 4KDa peptide. BRI3 can be phosphorylated in the cytosolic domain at two serine (S) and two threonine (T) residues. Each residue phosphorylated is indicated. BRI3 can also be modified by ubiquitination (K) and N-glycosylation (N) at the sites indicated.

BRI3 protein is also processed by furin and to a lesser extent by other members of the pro-protein convertase family at Arg242, within the sequence RRINKR^{242}GA. This processing within the BRI2 ectodomain results in the secretion of a C-terminal 4KDa fragment (Figure I.12) (Martin *et al*. 2009; Wickham *et al*. 2005). The furin processing occurs in the TGN (Trans-Golgi network) or post-TGN compartments, where furin is active, generating N- and C-terminal polypeptides that might be disulfide linked (Wickham *et al*. 2005). However, although BRI3 is highly homologous to BRI2, it seems that it fails to undergo shedding by ADAM-10 as well as intramembrane proteolysis by SPPL2a/b (Martin *et al*. 2009).

The sequence of BRI3 predicts a single site of N-glycosylation at Asn169 and several phosphorylation sites being four already identified (Ser5, Ser30, Thr32 and Thr37) (Vidal *et al*. 2001; Gauci *et al*. 2009; Stuart *et al*. 2015; Sharma *et al*. 2014b; Mertins *et al*. 2013). Additionally, BRI3 is post-translationally modified by ubiquitination at Lys3, Lys14, Lys17, Lys20 and Lys187 (Figure I.12) (Mertins *et al*. 2013; Danielsen *et al*. 2011; Kim *et al*. 2011a; Wagner *et al*. 2011).

I.2.3.1. BRI3 physiological function and associated diseases

BRI3 biological function remains to be fully elucidated, although it has been suggested that it may be involved in neuronal differentiation (Gong *et al*. 2008). In a yeast two-hybrid screen stathmin-2, a neuron-specific microtubule-destabilizing protein was identified as a novel BRI3 interacting protein (Table I.5). In addition, overexpression of stathmin-2 seems to significantly enhance neurite outgrowth in NGF-treated PC12 cells, while the BRI3 overexpression slightly decreases neurite outgrowth. However, the overexpression of both proteins strongly attenuates stathmin-2 induced

microtubule disassembly and the outgrowth of neurites. Therefore, it is possible to assume that BRI3 may inhibit neurite outgrowth through interaction with stathmin-2 by decreasing dynamic instability of microtubules caused by stathmin-2 (Gong *et al*. 2008). The suggested interaction of BRI3 with the tyrosine-protein kinase RYK (Table I.5), a protein involved in neuron differentiation and neurite outgrowth, also strengthened a role for BRI3 in above-mentioned processes (Berndt *et al*. 2011). Besides, a recent report demonstrated that BRI3 knockdown in rat hippocampal neurons significantly decreased neuronal cell survival and induced neuronal cell apoptosis (Yang *et al*. 2015). Therefore, BRI3 may also be involved in neuronal survival and cell death.

Moreover, as BRI2, BRI3 also binds to APP being considered a negative regulator of Aβ production (Table I.3; Matsuda *et al*. 2009). BRI3 inhibits APP processing by masking the access of APP to α- and β-secretases, but is a poor inhibitor of γ-secretase processing (Matsuda *et al*. 2009). As described above, the BRI2 23 aa C-terminal peptide released by furin and a fragment that contains the BRICHOS domain also affects Aβ aggregation and deposition, however for BRI3 similar function remains to be elucidated. Additionally, as it was already described for BRI2, BRI3 also interacts with BACE1 (Table I.3). The functional relevance of this interaction is not addressed, however, it is clear that BRI3 does not regulate BACE1 processing of APP (Wickham *et al*. 2005). It is possible that this interaction may assist in the mutual folding and/or targeting of these proteins.

Table I. 5 - List of the identified BRI3 interacting proteins. Information about the identified BRI2 interactors, as well as, the experimental evidence supporting the interactions.

Interactor	Description	Experimental evidence	References
BACE1	β-secretase β-amyloid protein converting enzyme 1	Two-hybrid Co-IP	(Wickham *et al*. 2005)
STT3A	Dolichyl-diphosphooligosaccharide--protein glycosyltransferase subunit STT3A	Two-hybrid	(Stelzl *et al*. 2005)
MTNR1B	Melatonin receptor type 1B	Tandem affinity purification	(Daulat *et al*. 2007)
FURIN	Furin	Two-hybrid	(Wickham *et al*. 2005)
RNF7	RING-box protein 2	Two-hybrid	(Rual *et al*. 2005)
RYK	Tyrosine-protein kinase RYK	Affinity chromatography - MS	(Berndt *et al*. 2011)
LLGL2	Lethal(2) giant larvae protein homolog 2	Peptide array	(Arbuckle *et al*. 2010)
POLR2F	DNA-directed RNA polymerases I, II, and III subunit RPABC2	Co-IP	(Freaney *et al*. 2013)
UBC	Polyubiquitin-C	Affinity chromatography - MS	(Danielsen *et al*. 2011; Kim *et al*. 2011; Wagner *et al*. 2011; Emanuele *et al*. 2011;

Interactor	Description	Experimental evidence	References
			Povlsen *et al*. 2012; Udeshi *et al*. 2012)
EGR1	Early growth response protein 1	Co-IP	(Arora *et al*. 2008)
DLG4	Disks large homolog 4		(Arbuckle *et al*. 2010)
CUL7	Cullin-7	Affinity chromatography - MS	(Hanson *et al*. 2014)
MVB12B	Multivesicular body subunit 12B	Affinity chromatography - MS	(Huttlin *et al*. 2015)
STMN2	Stathmin-2	Two-hybrid Co-IP	(Gong *et al*. 2008)
APP	Amyloid beta A4 protein	Two-hybrid Co-IP	(Matsuda *et al*. 2009)
TMEM216	Transmembrane protein 216	proximity-dependent biotin identification	(Gupta *et al*. 2015)
TMEM17	Transmembrane protein 17	proximity-dependent biotin identification	(Gupta *et al*. 2015)

Co-IP, co-immunoprecipitation; MS, mass spectrometry.

I.2.3.2. BRI3 associated diseases

Contrary to BRI2, no similar mutation of the stop codon or any form of mutation has yet been reported for BRI3. However, a polymorphism (A→G) of *BRI3* (rs3111754) was associated with the prevalence of subarachnoid hemorrhage in Japanese individuals, and thus may be beneficial in the assessment of the genetic risk for subarachnoid hemorrhage (Yoshida *et al*. 2010). A recent studied demonstrated that miR-323, which has been reported to be upregulated in ischemia/reperfusion brain injury, promotes apoptosis and suppresses survival. miR-323 could bind to BRI3 and suppress its expression in a post-transcriptional manner. Therefore, it is possible that miR-323 regulate ischemia/reperfusion-induced cell death via targeting BRI3 (Yang *et al*. 2015).

As mentioned before, BRI3 contains a BRICHOS domain which is found in a variety of proteins implicated in dementia, respiratory distress, and cancer (Sánchez-Pulido *et al*. 2002). Therefore, further studies are necessary to assess the involvement of BRI3 in any of these diseases.

I.3. Neuronal differentiation

Neurons are highly polarized cells with two type of processes molecularly and functionally distinct which emerge out of the soma: a single long and thin axon and multiple dendrites that are relatively short with a tapered morphology (Fukata *et al*. 2002; Dotti *et al*. 1988). In fact, is the polarization of axon and dendrites that underlie the ability of neurons to integrate and transmit information in the brain. Dendrites primary function is to receive information from other neurons that is processed and integrated at the level of soma, whereas axons conduct information away from the soma to the presynaptic terminals onto target cells (Barnes and Polleux 2009; Dotti *et al*. 1988).

However, at the onset of neuronal differentiation, the structure of the neurons is quite distinct from the polarized morphology above described. Neurons arise from terminal mitotic cell divisions in disperse regions of the nervous system presenting a simple spheroid shape. Before differentiate, the immature neuron or its precursor commonly migrates from its birthplace and settles in some other specific locations, and neuritogenesis occurs as neurites start to emerge out of the soma. During migration, neuronal polarization takes place as the initial sprouting of neurites occur and is followed by the polarized emergence of a leading and trailing processes, becoming the axon or the dendrite, respectively. This is the case for some neuronal subpopulations undergoing long-range migration as cerebellar granule neurons, and cortical and hippocampal pyramidal neurons (Rakic 1971; Komuro *et al*. 2001; Noctor *et al*. 2004). However, in other neuronal populations, as is the case of retinal ganglion cells and bipolar cells in the developing vertebrate retina, neurons can inherit their polarity directly from the apico-basal polarity of their progenitors (Hinds and Hinds 1978; Morgan *et al*. 2006; Zolessi *et al*. 2006). Dissociated neuronal culture systems have been extensively used to study the mechanisms of neuronal polarization. In fact, using cultured rodent hippocampal neurons Dotti *et al* (Dotti *et al*. 1988) described for the first time that neurons undergo a stereotypical development divided into five consecutive stages, in a similar manner to their *in vivo* development. The events range from cells bearing immature neurites in stage 1, to functionally differentiated neurons harboring dendritic spines and synapses, in stage 5 (Figure I.13). During stage 1 the initially spherical neurons begin extending broad circumferential lamellipodia and filopodia protrusions around the periphery of the cell (Figure I.13). In stage 2 lamellipodia and stable filopodia form growth cone and begin extending forming multiple neurites (neuritogenesis) (Figure I.13). At stage 3 the initial symmetry breaking event starts as one of the minor neurites elongates at a faster rate to become the axon (Figure I.13). Stage 4 comprehends the growth and arborization of the remaining processes developing into dendrites (Figure I.13). Neurons then mature and form dendritic spines and functional synaptic connections (stage 5) (Dotti *et al*. 1988) (Figure I.13).

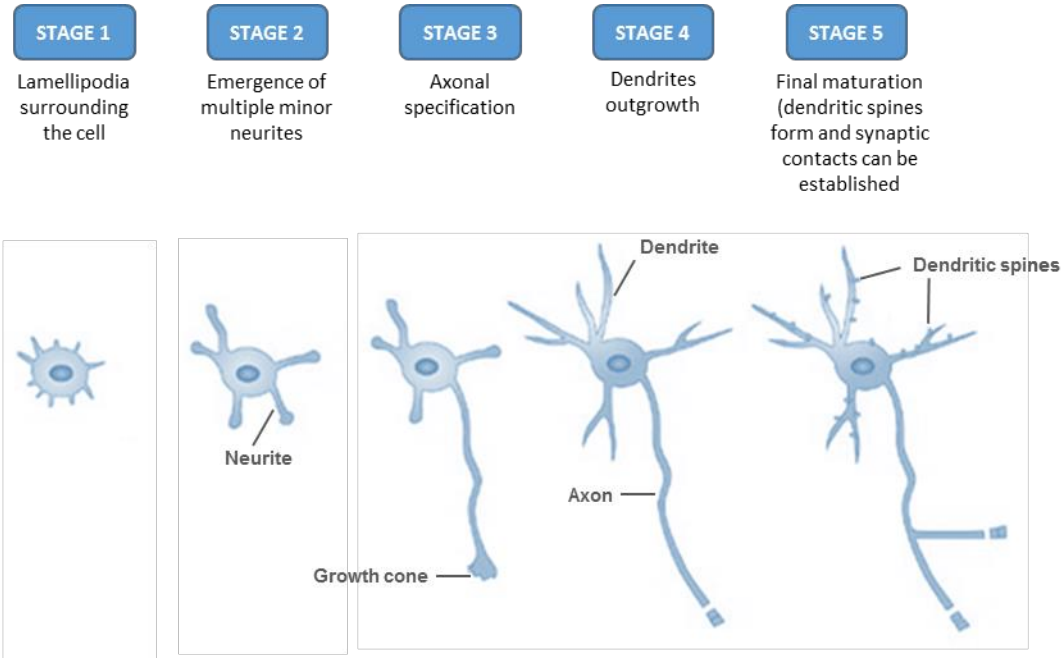

Figure I. 13 - Developmental stages of neuronal polarization in cultured rodent embryonic hippocampal neurons. Hippocampal neurons transform from round cells bearing lamellipodia (Stage 1) into multipolar cells (Stage 2). One neurite enlarges its growth cone and extends rapidly to become the axon (Stage 3). The remaining shorter neurites will develop into dendrites (Stage 4). This is followed by functional maturation and formation of dendritic spines and synapses (Stage 5) (Adapted from Arimura and Kaibuchi 2007).

I.3.1. Cytoskeletal dynamics in neuritogenesis

Several studies on neurite outgrowth mechanisms have emphasized the crucial roles of cytoskeletal dynamics in the process of neurite elongation. In fact, the establishment and maintenance of neuronal polarity is coordinated by rearrangements of the cytoskeletal architecture, namely filamentous (F)-actin and microtubules (MTs). Neuritogenesis depends on the highly motile tip of the neurite, the growth cone, which has the ability to sense extracellular guidance cues transducing these signals to the cytoskeleton. The cytoskeletal structure of the growth cone is divided into two cytoplasmic domains; the central domain (C-domain) which contains organelles and a core of microtubules, and the peripheral domain (P-domain) consisting of membrane protrusions containing F-actin (Figure I.14). These protrusions take the form of F-actin tapered finger-like projections, called filopodia, and veil-like sheets of branched actin, the lamellipodia (Mattson 1999; da Silva and Dotti 2002; Tahirovic and Bradke 2009) (Figure I.14). During neuronal polarization, the growth cone of the future axon constantly undergoes dynamic changes in its structure, whereas the future dendrites, quiescent at that moment, have a static growth cone and retains a rigid actin cytoskeleton (Tahirovic and Bradke 2009). Briefly, axon outgrowth results from the transformation of the distal C-domain of the growth cone into a stable neurite shaft, while the actual growth cone advances at the same time. This elongation process progress through three stages that repeat successively: protrusion, engorgement,

and consolidation. During protrusion, F-actin polymerization in the P-domain drives membrane protrusions at the edges of the growth cone as either filopodia or lamellipodia (Figure I.14). Further, microtubule-driven transport of membranous organelles and vesicles into the growth cone occurs during the engorgement phase. Finally, in the consolidation phase, actin polymerization and the protrusion are suppressed, microtubules become progressively more bundled developing the nascent neurite cylindrical shaft. Is the coordination of these three steps that determines neurite extension.

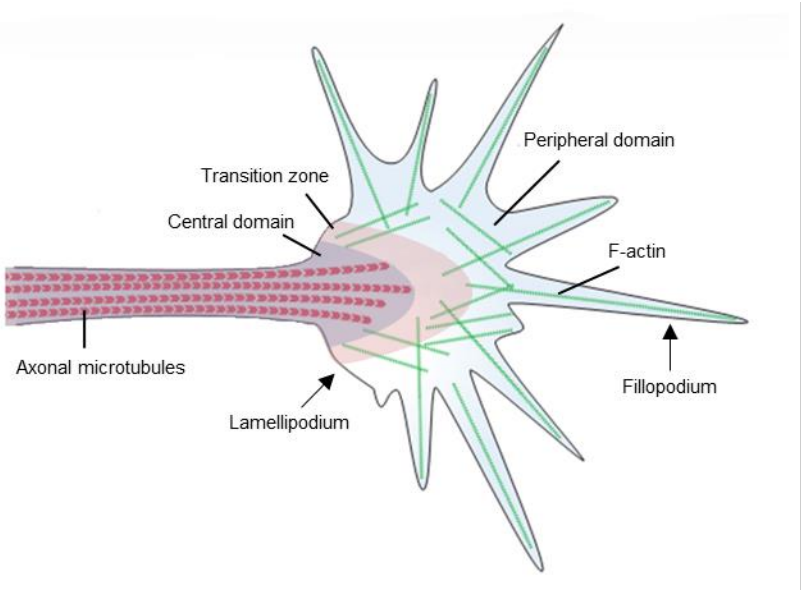

Figure I. 14 - Growth cone cytoskeletal structure. The peripheral (P) domain contains long, bundled actin filaments (F-actin bundles; green) which form the filopodia, as well as mesh-like branched F-actin networks, which give structure to lamellipodia-like veils. The central (C) domain encloses stable, bundled Microtubules that enter the growth cone from the axon shaft, in addition to numerous organelles, vesicles and central actin bundles. Finally, the transition (T) zone sits is the interface between the P and C domains (Adapted from Tahirovic and Bradke 2009).

I.3.1.1. Actin dynamics

Actin exists in a balance of ATP-bound monomeric, globular actin (G-actin) and helical actin filaments (F-actin) which are polar polymers composed of a barbed end, where the actin monomer addition occurs, and a pointed end where dissociation of actin monomers occur (Witte and Bradke 2008). As already mentioned, actin polymerization occurs preferentially at the leading edge of the growth where actin filaments drive the protrusion of lamellipodia and filopodia. In fact, filopodia is mainly composed of F-actin bundles with their barbed-end towards the leading edge, whereas lamellipodia contain randomly oriented F-actin networks between the filopodia (Tojima and Ito 2004). These actin structures in the peripheral growth cone are highly dynamic and in constant remodeling to direct the movement of the growth cone. Another feature of actin dynamics is the actin retrograde flow from the leading edge toward the center of the growth cone powered by myosin motors. Is the balance between actin polymerization rate and retrograde flow that regulates growth

cone protrusion. Therefore, it is clear that growth cone motility and guidance, and consequently axon growth is modulated by actin dynamics and organization which in turn are regulated by a diversity of actin-binding proteins (ABP), namely actin nucleating, severing, branching, and bundling proteins (Tahirovic and Bradke 2009). Several ABPs promote actin polymerization at the leading edge of the protrusions, namely profilin, Arp2/3 complex and ADF/cofilin. Profilin, a G-actin-binding protein, allows G-actin to bind F-actin barbed-end thus supporting polymerization (Dominguez 2009). Arp2/3 complex is involved in the nucleation of new filaments as a branch on the side of existing F-actin (Pollard and Beltzner 2002). Actin severing proteins as ADF/cofilin, which are abundant in neuronal growth cones, enhances F-actin severing and actin subunit dissociation at the pointed-end. ADF/cofilin accelerates F-actin disassembly at the pointed ends which increase the actin monomers able to re-associate with the barbed ends (Bamburg 1999). Furthermore, WAVE (Wiscott-Aldrich syndrome protein [WASP]-family verprolin-homologues protein) protein which is localized to lamellipodia, is able to regulate actin polymerization through Arp2/3 or profiling, promoting axon growth. Monomer binding to the barbed ends of filaments is also regulated by capping proteins. Therefore, capping proteins such as CapZ, by binding to the barbed ends of actin filaments block the access of monomers, halts actin polymerization and reduces F-actin length. On the other hand, barbed-end binding proteins such as Ena/VASP proteins, localized to tips of lamellipodia and filopodia, accelerate actin polymerization by interacting with profilin:G-actin complexes and promoting the transfer of G-actin monomers from profilin to the barbed end. Moreover, Ena/VASP proteins exhibit anti-capping activity, by which they protect actin filaments from capping proteins (Tahirovic and Bradke 2009).

In addition to proteins that regulate directly the actin kinetics, other ABPs affects actin architecture and dynamic by cross-linking actin filaments and therefore help to determine the arrangement of actin filaments into networks. For instance, fascin is an F-actin bundling protein which cross-links and stabilizes actin filaments given rise to parallel/unipolar F-actin bundles (Sasaki *et al*. 2002; Aratyn *et al*. 2007). It is suggested that fascin is crucial for the maintenance of filopodia and normal growth cone morphology (Cohan *et al*. 2001). Spectrins links F-actin cytoskeleton to numerous proteins in the cell membrane to form a multiunit structural element which organizes the protein network underlying the plasma membrane (Garbe *et al*. 2007; Hülsmeier *et al*. 2007).

I.3.1.2. Microtubule dynamics

Microtubules are cylindrical polar polymers composed of a plus end, where occur dimer addition and dissociation, and a minus end where can occur dimer dissociation. In neurons, the minus end of microtubules is often stabilized and its dynamics rest mainly on the polymerization and depolymerization at the plus end (Flynn 2013). Neurite microtubules show increased stability with

neuronal polarization which can be achieved by stabilization of existing microtubules, increased polymerization, reduced microtubule destabilization and microtubule bundling. Several microtubule binding proteins (MBP) affects microtubule dynamics and organization which can be divided into five classes: (1) microtubule-stabilizing proteins, including the structural microtubule-associated proteins (MAPs), (2) plus-end tracking proteins (+TIPs), (3) microtubule destabilizing proteins, (4) microtubule motor proteins, and (5) microtubule severing proteins (Tahirovic and Bradke 2009; Flynn 2013; Dent *et al*. 2011). Structural MAPs usually act to stabilize microtubule structure and consists of two distinct and unrelated families highly expressed in neurons: type I (Map1a/Map1b) and type II (Map2/tau) (Flynn 2013). The most abundant neuronal MAPS, Map1b, Map2 and tau are differentially distributed in axons and dendrites and have distinct mechanisms to affect microtubule stability. Map1b has been shown to be involved in axon guidance, and both Map2 and tau are particularly important for neurite formation. Map2 is particularly important in the earliest phases of neurite formation given that its suppression in cerebellar neurons affects the extension of neurites, whereas tau suppression only affects axon elongation (Caceres and Kosik 1990; Caceres *et al*. 1992). In addition, a particular role for Map2c, a juvenile isoform that is downregulated after the early stages of neuronal development, in neuronal development and neurite outgrowth was also highlighted. Map2c mediates neurite formation not only due to its microtubule-stabilizing activity which facilitates the extension of bundled microtubule, but also due to its ability to bind F-actin and alter actin dynamics (Dehmelt and Halpain 2004). Another important microtubule stabilizing protein with implications in neuritogenesis is doublecortin (DCX). DCX is found preferentially near the plus ends of the microtubules and promotes stability, assembly and nucleation of microtubules. During neuritogenesis, DCX activation by dephosphorylation mediated by a PP1-spinophilin pathway, promotes the consolidation of the growth cone into the elongating neurite shaft by facilitating the bundling of microtubules (Reiner 2013; Bielas *et al*. 2007). Microtubule destabilizing proteins such as stathmin, superior cervical ganglia neural-specific (SCG10), and SCG10-like protein (SCLIP) has also been pointed has having a role in neuronal polarity, and prevents polymerization by (1) sequestering free tubulin heterodimers and preventing its association with microtubules plus end or by (2) associating with tubulin on microtubule plus ends (Grenningloh *et al*. 2004; Wittmann *et al*. 2004). The stathmin/SCG10 family of proteins are highly expressed in developing neurons and its expression and activity are important for neurite outgrowth. For instance, stathmin/SCG10 family of proteins are negatively regulated by phosphorylation which in turn regulates its microtubule destabilizing activity promoting microtubule polymerization which is necessary for axon specification (Tahirovic and Bradke 2009; Manna *et al*. 2006).

Microtubule elongation is favored by proteins that bind free tubulin heterodimers and increase polymerization, as for example the collapsin-response mediator protein-2 (CRMP-2), or by +TIPs,

as adenomatous polyposis coli (APC), End-binding protein 1 (EB1) and End-binding protein 3 (EB3), which stabilize the dynamic plus-end. For instance, CRMP-2 binds to free tubulin subunits and promotes their capacity to bind microtubules. During neuronal differentiation, CRMP-2 accumulates in one neurite before the morphological polarization, which further becomes the axon (Tahirovic and Bradke 2009).

Besides its well-known role in transporting material either anterogradely (kinesins) or retrogradely (dynein), microtubule motor proteins also have an important role in microtubule stability. The kinesin 13 family, namely Kif2A, which is enriched in growth cones, has the ability to destabilize microtubules at their plus ends. Finally, two main microtubule severing proteins expressed in neurons, katanin and spastin, are also important for microtubule dynamics during neuritogenesis. In fact, when katanin and spastin are overexpressed the axon/neurite outgrowth is diminished due to increased severing of microtubules (Conde and Cáceres 2009).

In addition, microtubule dynamics during neuritogenesis might also be modulated by post-translational modifications (detyrosination, glutamylation, glycylation, phosphorylation and acetylation) of the tubulin heterodimers which can affect the dynamic properties of microtubules and also the binding of structural MBPs. Acetylation is one prominent modification in microtubules which occurs in stable microtubules in neurons, and for instance, may affect the binding of microtubule motor proteins (Flynn 2013).

I.3.2. Membrane protein trafficking in neuronal polarization

The plasma membrane of neurons can be divided into the soma-dendritic and the axonal domains, which perform distinct functions. This functional specialization is generated by sorting and anchoring mechanisms that guarantee the correct delivery and retention of specific membrane proteins. Hence, polarized membrane protein trafficking in neurons is necessary for both the establishment and the maintenance of neuronal polarity (Fukata et al. 2002). Axonal and dendritic membrane proteins are synthesized in the rough endoplasmic reticulum and undergo post-translational modification in the Golgi complex. Proteins could be sorted to axon or dendrite by at least three mechanisms: (1) the direct transport of the proteins in a polarized manner from the trans-Golgi network to the appropriate membrane; (2) the non-polarized transport of proteins within the cell, followed by selective retrieval by endocytosis from the incorrect domain and degradation; (3) the sort of proteins in the trans-Golgi network and traffic to axon or dendrite domains, which are subsequently endocytosed and resorted in endosomes, followed by polarized delivery (transcytosis) (Fukata *et al*. 2002; Lasiecka and Winckler 2011).

Briefly, the polarized delivery of proteins to the plasma membrane involves budding, transport, and fusion that is orchestrated by a complex set of trafficking proteins. Vesicle budding is mediated by a set of coat proteins which are recruited to the membrane from the cytosol, including cargo adaptors. Cargo adaptors recognize and bind to transmembrane cargo proteins containing sorting motifs and concentrate them in the forming bud, and to other proteins that induce membrane curvature and bud fission (Guo *et al*. 2014; Bentley and Banker 2016). Selective vesicle transport along to either axon or dendrites is mediated by kinesin and dyneins which translocate along microtubules. It is the unique distribution of microtubules in neurons that underlies significant differences in protein trafficking of axonal and dendritic proteins: in axons, the microtubules are oriented with the plus-ends toward, whereas in dendrites may have the plus or minus ends outwardly directed. Therefore, it is proposed that the dendritic targeting of cargoes is governed by the minus-end microtubules allowing dynein-dependent sorting, while axonal targeting is facilitated by kinesin-dependent sorting governed by the oriented plus-end microtubules (Maeder *et al*. 2014). These motor proteins normally do not bind directly to vesicles being linked by adaptor proteins (Akhmanova and Hammer 2010). Lastly, fusion is initiated by tethering proteins that form a complex, linking the vesicle to its target membrane. Subsequent formation of a SNARE (N-ethylmaleimide-sensitive factor attachment protein receptor) complex drives the fusion of the lipid bilayers of the vesicle and target membrane, which allows the incorporation of vesicle cargo proteins into the target membrane (Bentley and Banker 2016).

I.3.3. Local protein translation and degradation regulates neuronal polarization

Local protein translation and degradation are key mechanisms that could locally regulate proteins involved in the establishment of neuronal polarization. The presence of mRNA and the translation machinery in developing axon and dendrites suggests an important role for local protein translation in axon and dendrite specification. In fact, the target of specific mRNAs to specific neuronal domains promotes a rapid change in the local proteome via local translation. Therefore, local protein translation links extrinsic signals to particular cellular responses and can mediate stimulus-driven adaptive responses. For instance, in axons, it is well established the impact of local translation in axon specification, growth and guidance (Polleux and Snider 2010). In isolated retinal growth cones it was demonstrated that when translation is inhibited, they lose the ability to respond to the guidance cues, namely semaphorin 3A and netrin-1. Therefore, local translation occurring in growing axons seems to be implicated in mediating the responses to guidance signals (Campbell and Holt 2001). Remarkably, the most frequently identified embryonic mRNAs are those encoding cytoskeletal or cytoskeletal binding proteins such as actin, tau and ADF (Piper and Holt 2004).

Furthermore, the local regulation of protein expression by degradation mediated by the ubiquitin-proteasome system (UPS) was shown to have a crucial role in the regulation of neuronal development

and differentiation, namely in the formation and maintenance of neuronal polarity (Polleux and Snider 2010). In fact, several proteins critical for neuronal polarity, such as the serine/threonine kinase Akt undergo selective degradation. Akt is important for axon growth and maintenance, and in neurites that develop into axons its protein levels are stable, however in neurites that differentiate into dendrites are reduced in an ubiquitin-dependent manner. Therefore, the regulated local protein degradation of Akt by the UPS seems to be a requirement for neuronal polarization (Yan *et al*. 2006). Further understanding regarding the upstream regulatory signals responsible for the spatially limited local protein degradation is crucial.

I.3.4. Importance of extracellular cues for neuronal differentiation

Several families of extracellular cues have been suggested to be involved in the polarized emergence of axon and dendrites (Polleux and Snider 2010). This asymmetric neurite outgrowth requires the ability of postmitotic neurons to sense gradients of extracellular cues which lead to the asymmetric activation of intracellular signaling cascades converging on axon and dendrites formation. There are several extracellular signals acting through distinct receptors existing in the growth cone, converging on cytoskeletal arrangements and thereby the direction of axonal elongation (Hall and Lalli 2010). Candidate proteins that have been shown to influence axonal and dendritic development include mainly neurotrophins, other growth factors, bone morphogenetic proteins (BMPs) and morphogens such as retinoic acid, semaphorins, netrins, extracellular matrix proteins and neurotransmitters.

Neurotrophins are an important family of neurotrophic factors comprised by the nerve growth factor (NGF), the brain-derived neurotrophic factor (BDNF), the neurotrophin-3 (NT-3) and NT-4, which have been proposed as extracellular regulators of neuronal polarization by enhancing axon growth (Yuen *et al*.). Neurotrophins mediate their functions by selectively binding to two types of cell surface receptors, the Trk tyrosine kinase receptors and the p75 neurotrophin receptor (p75NTR), a member of the TNF receptor superfamily (Dechant and Barde 2002). Remarkably, Trk receptors transmit positive signals whereas p75NTR transmit both positive and negative signals, and the two neurotrophin receptors exist in a paradoxical relationship as can either augment or oppose each other (Yuen *et al*.; Kaplan and Miller 2000; Zagrebelsky *et al*. 2005). Overall, neurotrophins increase the dendritic complexity of pyramidal neurons by increasing total dendritic length, the number of branchpoints, and/or the number of primary dendrites (Whitford *et al*. 2002). In addition, other growth factors have been shown to be involved in neuronal polarization: (1) the basic fibroblast growth factor (bFGF), which accelerates the outgrowth of axons and dendrites in hippocampal neurons; (2) and the insulin-like growth factor-1 (IGF-1) that functions as a neurotrophic factor regulating neurite growth in developing brain and affects dendritic growth and branching of post-natal layer 2 cortical neurons (Whitford *et al*. 2002).

BMPs are multifunctional growth factors belonging to the transforming growth factor β (TGFβ) superfamily, all of which transduce signals by binding type I and type II Ser/Thr kinases receptors (BMPRI and BMPRII). BMP signaling plays an important role in neuronal differentiation, namely in the regulation of the number, length, and branching of neurites (Benavente *et al*. 2012). For instance, it was demonstrated that BMP7 activates c-Jun N-terminal kinase (JNK) which induces microtubule stabilization and thus rearrangement of the cytoskeletal network to promote dendrite outgrowth (Podkowa *et al*. 2010).

Retinoic acid (RA) is a potent morphogen capable of inducing neurite outgrowth. RA works by binding directly to nuclear transcription factors, which include the retinoic acid receptors (RARs) and the retinoid X receptors (RXRs), to influence gene expression (Ross *et al*. 2000).

Semaphorins constitute a large family of secreted proteins, transmembrane proteins or membrane-bound proteins that act as guidance signals for axons and dendrites during neuronal differentiation through their interactions with the plexin and neuropilin receptor family (Fiore and Püschel 2003; Hall and Lalli 2010). Remarkably, secreted semaphorin 3A (Sema3A) regulates the asymmetric growth of neurons either by acting as a chemorepellant for axons or as a chemoattractant for dendrites (Polleux and Snider 2010). On the other hand, semaphorin 7A (Sema7A) seems to be only involved in axon outgrowth promotion. Interestingly, sema7A signaling is not mediated by plexins or neuropilins, but instead seems to be mediated by its binding to integrins which activate MAPKs and focal adhesion kinases (FAK) and culminates with alterations in actin dynamics (Guan and Rao 2003). Netrins are a family of extracellular proteins acting through binding to receptors which include deleted in colorectal cancer (DCC), the DCC paralogue neogenin, the UNC-5 homologues UNC5A-D, and Down syndrome cell adhesion molecule (DSCAM), and function as axon guidance cues during neural development (Sun *et al*. 2011). They act as chemoattractants for some cell types and chemorepellents for others. Netrin-mediated axon chemoattraction is mediated by DCC signaling, which activates several signal transduction molecules and ultimately leads to rearrangement of the actin cytoskeleton and process extension, namely mitogen-activated protein (MAP) kinases, Rac1 and cdc42. The signaling mechanisms for netrin-mediated chemorepulsion are less well understood than those underlying chemoattraction, although appear to be mediated by UNC5, alone or in complex with DCC (Sun *et al*. 2011; Guan and Rao 2003). Additionally, netrins can also promote axon outgrowth by activating the nuclear factor of activated T cell (NFAT) which is mediated by DCC signaling (Guan and Rao 2003).

Several extracellular matrix proteins and adhesion molecules, such as laminin and neuron-glia cell adhesion molecule (NgCAM) influence neurite outgrowth and axon elongation (Esch *et al*. 2000). In fact, in dissociated cultures of both cortical and hippocampal pyramidal neurons, plated on striped substrates coated with laminin or NgCAM, the first immature neurite contacting the boundary

between two stripes of either laminin or NgCAM becomes the axon. In addition, neurotransmitters may also regulate the axon and neurite outgrowth during neuronal differentiation. For instance, in cultured embryonic hippocampal neurons, glutamate suppresses dendrite elongation whereas axon elongation is unaffected. On the other hand, the activation of GABA receptors can counteract the inhibiting effects of glutamate on dendritic elongation (Mattson 1999).

I.3.5. Signaling pathways involved in neuronal differentiation

The events that lead to neuronal differentiation and polarization are controlled by signaling molecules that have established roles on cytoskeletal arrangements and protein trafficking converging on axon and dendrites formation (Arimura and Kaibuchi 2005). Therefore the extracellular cues acting through distinct receptors existing in the growth cone are able to activate several intracellular signaling pathways closely associated to growth cone reorientation, and some are discussed in the next sections.

I.3.5.1. Rho- and Ras-family of small GTPases

Rho- and Ras-family of small GTPases are members of the Ras superfamily of small GTPases and have been reported as important regulators of axon specification and growth (Colicelli 2004; Arimura and Kaibuchi 2007). These proteins function as molecular switches that interact with downstream effectors to induce cellular responses in their GTP-bound active state, and are inactive in their GDP-bound state. The small GTPases exhibit high-affinity binding for GDP and GTP, however, possess low intrinsic GTP hydrolysis and GDP/GTP exchange activities. These conversions are controlled by two main classes of regulatory proteins: GTPase-exchange factors (GEFs) and GTPase-activating proteins (GAPs). GEFs promote the exchange of GDP for GTP promoting the formation of the active GTP-bound form, whereas GAPs increase the intrinsic GTPase activity promoting the formation of the inactive GDP-bound form (Barnes and Polleux 2009; Hall and Lalli 2010). At least 20 members of the Rho-family of small GTPases have been identified, Cdc42, Rac1 and RhoA being the most extensively characterized. This family of small GTPases are key regulators of actin reorganization. Rac1 and Cdc42 are positive regulators of neurite outgrowth through the promotion of lamellipodia and filopodia formation in growth cones, whereas RhoA acts as a negative regulator of neurite extension promoting actin stress fiber formation and focal adhesion assembly. So, it has been hypothesized that polarity inducing signals switch Rac/Cdc42 to their GTP-bound active states in the future axon, whereas Rho remains in its GDP-bound inactive state. In parallel, the other growth cones remain with GDP-bound inactive Cdc42/Rac, where the relatively high content of GTP-bound active Rho inhibit those neurites elongation (Hall and Lalli 2010).

In developing neurons, Cdc42 regulates actin dynamics through the effectors N-WASP and p21-activated kinase (PAK). N-WASP is an important Cdc42 effector during neurite extension promoting actin polymerization through the Arp2/3 complex (Figure I.15) (Hall and Lalli 2010). The PAK pathway signals to the actin cytoskeleton via cofilin and seems to be critical for axon formation (Ng and Luo 2004). In addition, in cdc42 knockout mice, where an axon specification defect is observed, the phosphorylation levels of cofilin (inactive form) were found increased. The phosphorylation of cofilin is achieved by LIM kinase (LIMK) whose activity is regulated by PAK (Figure I.15) (Garvalov *et al*. 2007).

Rac is a positive regulator of axon growth modulating actin cytoskeleton dynamics through its two main effectors, PAK and WASP-family verprolin-homologous protein (WAVE) (Figure I.15) (Tahirovic and Bradke 2009). In addition, Rac acts on microtubule dynamics to promote axon formation. Briefly, the Rac-specific GEF, dedicator of cytokinesis 7 (DOCK7) by regulating Rac activity mediate the phosphorylation and inhibition of the microtubule destabilizer stathmin in the nascent axon (Figure I.15) (Watabe-Uchida *et al*. 2006). Besides, two other Rac-specific GEFs, T-lymphoma and metastasis 1 protein (TIAM1) and TIAM1-like exchange factor (TIAM2), have been associated with neuronal polarity by regulating actin reorganization (Arimura and Kaibuchi 2007).

Rho primary action is to induce actin cytoskeleton rearrangements but also modulates local dynamics of microtubules (MTs). The best-characterized RhoA effectors are Rho-kinase (ROCK) and the mammalian Diaphanous formin (mDia). RhoA/ROCK signaling negatively regulate the early steps of axon outgrowth. For instance, ROCK is able to increase MLC phosphorylation either by phosphorylating it directly or by phosphorylating the myosin-binding subunit of myosin phosphatase impeding it of dephosphorylating MLC. As result myosin II is activated enhancing actomyosin contractility which promotes neurite retraction (Figure I.15) (Narumiya *et al*. 2009). Moreover, Rho-mediated neurite retraction can be achieved by phosphorylation and consequently activation of LIM kinase by ROCK which in turn phosphorylates and inactivates cofilin (Figure I.15) (Maekawa *et al*. 1999). Regarding, the Rho-mDia pathway it has been shown that mDia catalyzes actin nucleation and polymerization but is also able to stabilize microtubules through association with the microtubule end capping protein complex EB1/APC (Figure I.15) (Bartolini *et al*. 2008).

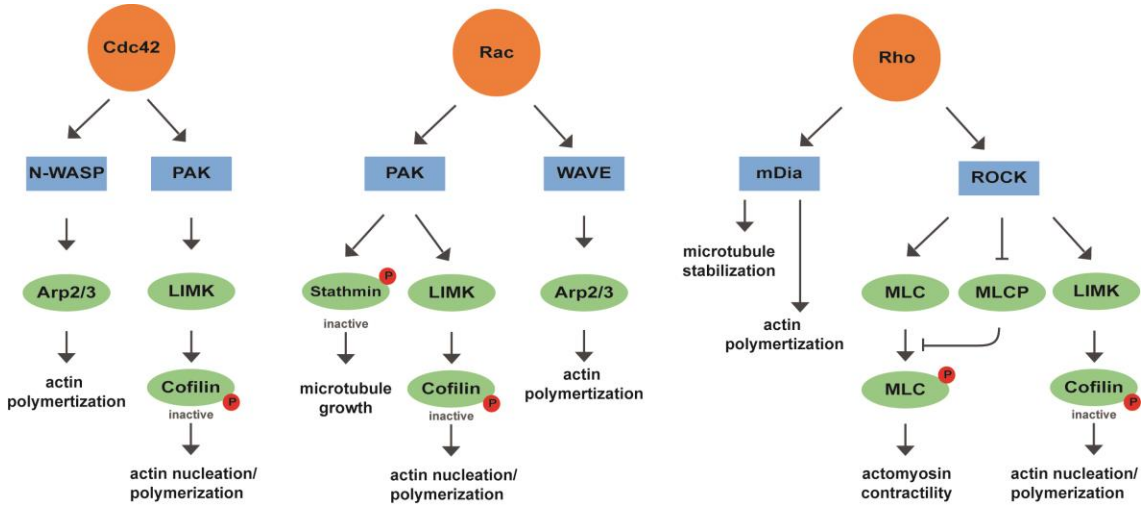

Figure I. 15 - Signal transduction pathways downstream of the Rho GTPases in the regulation of cytoskeletal dynamics. Arp, actin-regulated protein; LIMK, LIM kinase; mDia, a mammalian homologue of the Drosophila diaphanous protein; MLC, myosin light chain; MLCP, MLC phosphatase; PAK, p21 activated kinase; ROCK, Rho kinase; WASP, Wiskott-Aldrich syndrome protein; WAVE, WASP family verprolin-homologous protein; p, phosphorylated.

Finally, for the Ras family of small GTPases, a crucial role in the establishment and maintenance of neuronal differentiation have also been reported. In brief, Ras functions upstream of the phosphatidylinositol-3 kinase (PI3K) and the mitogen-activated protein kinase (MAPK) pathways (Arimura and Kaibuchi 2007; Barnes and Polleux 2009).

I.3.5.2. PI3K/Akt pathway

Several evidences support a role for PI3K signaling pathway in the establishment of neuronal polarity. PIK3 activity results in the generation of phosphatidylinositol (3,4,5)-triphosphate (PIP3) which is able to activate signaling molecules and several regulators of actin and microtubule dynamics at the cell membrane. During neuronal differentiation, PI3K activity and PIP3 were found concentrated at the distal region and growth cone of one of the immature neurites in stage 2 of differentiation, which is crucial for axonal specification and elongation. In fact, the pharmacological inhibition of PI3K activity in cultured hippocampal neurons prevents axon formation (Shi *et al*. 2003; Ménager *et al*. 2004). Different extracellular cues, namely neurotrophins, modulate axonal growth behavior through activation of the PI3K signaling pathway. One of the best characterized downstream mediators of PI3K signaling in neuronal differentiation is the protein kinase Akt, also called protein kinase B (PKB). PI3K activation recruits Akt from the cytosol to the membrane where it is activated by dual phosphorylation at Thr308 and Ser473 by phosphoinositide-dependent kinase

1 (PKD1) and phosphoinositide-dependent kinase 2 (PKD2), respectively. In addition, integrin-linked kinase (ILK) is also able to phosphorylate Akt at Ser473. This activated forms of Akt are enriched in the growth cones of polarized neurons, and phosphorylates GSK3β on Ser9, inactivating it. Therefore, it was shown that as Akt localizes to the tips of the axons in hippocampal neurons the inactive GSK3β is also circumscribed to the tips of growing axons (Alessi *et al*. 1997; Burgering and Coffer 1995; Shi *et al*. 2003). In addition, it has been suggested that the described asymmetric distribution of Akt is regulated by localized protein degradation since the inhibition of the ubiquitin-proteasome system induces multiple axons along with symmetric Akt distribution (Guo and Zhong 2006).

I.3.5.3. PTEN

The phosphatase and tensin homolog (PTEN) is a dual-specificity protein phosphatase (Myers *et al*. 1997) and a PIP phosphatase (Maehama and Dixon 1998). PTEN and PI3K have opposing effects on PIP3 levels since it is able to dephosphorylate PIP3 generating PIP2, and consequently have opposing effects in the establishment of neuronal polarity (Barnes and Polleux 2009; Polleux and Snider 2010). In fact, overexpression of PTEN blocks axon formation whereas the knockdown of PTEN induces multiple axon formation (Jiang and Rao 2005; Shi *et al*. 2003).

I.3.5.4. LKB1-SAD/MARK pathway

Serine/threonine kinase LKB1, the mammalian counterpart of the *C. elegans* Par-4 protein, has a key role in axon formation during neuronal polarization by acting on its downstream effectors Synapse Amphid Defective (SAD) and Microtubule Affinity-Regulating Kinase (MARK) kinases. In fact, the conditional deletion of *Lkb1* in mouse forebrain or the down-regulation of LKB1 expression by siRNA in rat cortical progenitors abolished axon formation *in vivo*. LKB1 activity in axon formation requires its association with the pseudokinase Strad and phosphorylation at Ser431 by PKA and ribosomal protein S6 kinase (p90RSK), which activates it. The LKB1 phosphorylated at Ser431 is predominantly found accumulated in only one neurite of undifferentiated neurons (Barnes *et al*. 2007; Shelly *et al*. 2007). In addition, the overexpression of a mutated LKB1 (S431A) with serine to alanine mutation at this site impaired axon formation both in vitro and in vivo, presumably by interfering with the association of STRAD or other proteins important for LKB1 function (Shelly *et al*. 2007). Once activated, LKB1 phosphorylates and activates the kinases SAD-A/B and MARK1-4 (Kishi 2005; Chen *et al*. 2006). Both SAD and MARK kinases phosphorylate several MAPS, including MAP2, MAP4, and tau, reducing their microtubule binding affinity which results in microtubule destabilization (Polleux and Snider 2010).

I.3.5.5. GSK3

GSK3 (glycogen synthase kinase 3) is a serine/threonine kinase with described functions in the regulation of multiple cellular processes. There are two isoforms, GSK3α and GSK3β, encoded by two different genes, which presents 85% of amino acid identity (Woodgett 1990). GSK3 has the particularity of being constitutively active, and its inactivation is achieved following its phosphorylation at Ser9 in GSK3β or Ser21 in GSK3α by upstream regulators in response to stimuli. Therefore, several signaling pathways regulate GSK3 activity and emerging evidences points to GSK3 as an essential regulator of several neurodevelopmental processes, namely neurogenesis, neuronal migration, neuronal polarization and axon growth and guidance (Frame and Cohen 2001; Cross *et al*. 1995; Hur and Zhou 2010). Remarkably, GSK3 signaling exhibits crosstalk with other signaling pathways involved in neuronal polarization, including PI3K/Akt, Rho-GTPases, Par3/6, and PKA-LKB1. Therefore GSK3 acts an important mediator in the control and maintenance of neuronal polarization by transducing upstream signaling, and several kinases including Akt, ILK and atypical PKC (aPKC) are reported to be involved in its dephosphorylation (Barnes and Polleux 2009). In fact, the decreased activity of GSK3 seems to be required for neuronal polarization. Studies in rat hippocampal neurons show that the expression of constitutively active GSK3β (GSK3β-S9A) impaired axon formation, whereas the global inhibition of GSK3 by pharmacological inhibitors, a peptide inhibitor, and shRNAs induces the formation of multiple axons. Furthermore, it was shown that the inactive form of GSK3β is located at the tip of each neurite before polarization, however when neurons begin to polarize phospho-GSK3β becomes concentrated at the axonal tip. Together these results suggest that localized inactivation of GSK3β at the nascent axon is crucial for polarization (Jiang et al. 2005; Shi et al. 2004; Yoshimura et al. 2005).

Several MBPs involved in neuronal polarization are GSK3 substrates, namely APC, CRMP-2, which localizes to axon tips, and the microtubule-associated proteins MAP1B and tau (Polleux and Snider 2010). The function of these MBPs is to promote microtubule assembly and stability, and its phosphorylation by GSK3 abolishes their ability to interact with microtubules. For instance, CRMP2 which is enriched in the tip of the nascent axon, is regulated by GSK3, such that phosphorylated CRMP2 displays decreased binding affinity for tubulin. Overexpression of CRMP2 induce the formation of multiple axons, whereas it's knocking down antagonizes the multiple axon formation induced by GSK3 inactivation, which indicates that the CRMP2 acts downstream of GSK3 inactivation (Yoshimura et al. 2005). Therefore, GSK3 signaling regulates neuronal polarization by controlling cytoskeletal reorganization, in particular, microtubule dynamics.

Moreover, GSK3 signaling is also involved in the polarized transport of proteins and membrane, local protein translation, and local protein degradation, which are key processes for the maintenance of the polarized axon extension (Kim *et al*. 2011b).

I.3.5.6. Raf/MEK/ERK pathway

Several evidences suggest a role for Raf/mitogen-activated protein kinase (MEK)/extracellular-signal-regulated kinase (ERK), downstream effectors of Ras, in axon growth formation mediated by neurotrophic factors (Markus *et al*. 2002; Zhou and Snider 2006). Briefly, Ras is able to recruit Raf to the cell membrane where it becomes activated. Then the activation of Raf phosphorylates and activates MEK, a dual-specificity kinase. MEK further phosphorylates and activates ERK that translocates to the nucleus and phosphorylates several targets, including transcription factors and several microtubule-associated proteins (Polleux and Snider 2010).

I.3.5.7. Calcium-mediated signalling

Calcium-mediated signaling is also involved in the regulation of neuronal differentiation, contributing to the regulation of axonal growth and guidance, and dendritic growth and arborization (Rosenberg and Spitzer 2011).

Briefly, spatiotemporal patterns of calcium transients activate calcium-binding proteins that transduce the signals and impact growth cone motility and neurite elongation by regulating cytoskeletal dynamics. For example, Ca^{2+} regulates proteins that are involved in the actin filaments dynamics; Ca^{2+} is able to activate the protein gelsolin, which then cleaves actin filaments (Furukawa *et al*. 1997).

The Ca^{2+}/calmodulin-dependent serine–threonine phosphatase, calcineurin has also been implicated in promoting neurite outgrowth. In fact, it was shown that in Xenopus cultured neurons the suppression of calcineurin with pharmacological inhibitors, in the presence of extracellular Ca^{2+} but not in its absence, results in an increase in neurite extension. The expression of an autoinhibitory domain of calcineurin in the presence of Ca^{2+} waves also increases neurite extension, whereas expression of a constitutively active form of calcineurin in the absence of Ca^{2+}waves retards neurite growth. Moreover, it was shown that Ca^{2+} waves act via calcineurin to dephosphorylate GAP-43 protein resulting in a destabilization of actin filaments which affects neurite extension (Lautermilch and Spitzer 2000).

Another well characterized Ca^{2+}-binding protein is calmodulin (CaM), which functions as an intracellular Ca^{2+} sensor, associating with a wide-range of targets to elicit diverse signaling cascades, as is the case for Ca^{2+}/CaM-dependent protein kinases (CaMKs). CaMKII is unique for its ability to autophosphorylate and seems to function in both growth cone turning and branching. For instance, the activation of CaMKII by Ca^{2+}/CaM could promote microtubules depolymerization by phosphorylating tau protein (Mattson 1999).

Supporting all these findings, in vivo imaging studies have provided direct evidence for a negative relationship between the frequency of spontaneous Ca^{2+} transients and the rate of axon outgrowth (Polleux and Snider 2010).

References

Akhmanova A., Hammer J. A. (2010) Linking molecular motors to membrane cargo. *Curr. Opin. Cell Biol.* **22**, 479–487.

Akiyama H., Kondo H., Arai T., Ikeda K., Kato M., Iseki E., Schwab C., McGeer P. L. (2004) Expression of BRI, the normal precursor of the amyloid protein of familial British dementia, in human brain. *Acta Neuropathol.* **107**, 53–8.

Alessi D. R., Deak M., Casamayor A., Caudwell F. B., Morrice N., Norman D. G., Gaffney P., et al. (1997) 3-Phosphoinositide-dependent protein kinase-1 (PDK1): structural and functional homology with the Drosophila DSTPK61 kinase. *Curr. Biol.* **7**, 776–89.

Allen P. B., Ouimet C. C., Greengard P. (1997) Spinophilin, a novel protein phosphatase 1 binding protein localized to dendritic spines. *Proc. Natl. Acad. Sci. U. S. A.* **94**, 9956–61.

Andreassen P. R., Lacroix F. B., Villa-Moruzzi E., Margolis R. L. (1998) Differential subcellular localization of protein phosphatase-1 alpha, gamma1, and delta isoforms during both interphase and mitosis in mammalian cells. *J. Cell Biol.* **141**, 1207–15.

Aoyama H., Ikeda Y., Miyazaki Y., Yoshimura K., Nishino S., Yamamoto T., Yano M., Inui M., Aoki H., Matsuzaki M. (2011) Isoform-specific roles of protein phosphatase 1 catalytic subunits in sarcoplasmic reticulum-mediated Ca(2+) cycling. *Cardiovasc. Res.* **89**, 79–88.

Aratyn Y. S., Schaus T. E., Taylor E. W., Borisy G. G. (2007) Intrinsic Dynamic Behavior of Fascin in Filopodia. *Mol. Biol. Cell* **18**, 3928–3940.

Arbuckle M. I., Komiyama N. H., Delaney A., Coba M., Garry E. M., Rosie R., Allchorne A. J., et al. (2010) The SH3 domain of postsynaptic density 95 mediates inflammatory pain through phosphatidylinositol-3-kinase recruitment. *EMBO Rep.* **11**, 473–8.

Arimura N., Kaibuchi K. (2005) Key Regulators in Neuronal Polarity. *Neuron* **48**, 881–884.

Arimura N., Kaibuchi K. (2007) Neuronal polarity: from extracellular signals to intracellular mechanisms. *Nat. Rev. Neurosci.* **8**, 194–205.

Arora S., Wang Y., Jia Z., Vardar-Sengul S., Munawar A., Doctor K. S., Birrer M., McClelland M., Adamson E., Mercola D. (2008) Egr1 regulates the coordinated expression of numerous EGF receptor target genes as identified by ChIP-on-chip. *Genome Biol.* **9**, R166.

Artavanis-Tsakonas S., Rand M. D., Lake R. J. (1999) Notch signaling: cell fate control and signal integration in development. *Science* **284**, 770–6.

Ayllón V., Martínez-A C., García A., Cayla X., Rebollo A. (2000) Protein phosphatase 1alpha is a Ras-activated Bad phosphatase that regulates interleukin-2 deprivation-induced apoptosis. *EMBO J.* **19**, 2237–46.

Bamburg J. R. (1999) Proteins of the ADF/Cofilin Family: Essential Regulators of Actin Dynamics. *Annu. Rev. Cell Dev. Biol.* **15**, 185–230.

Baron B. W., Baron R. M., Baron J. M. (2015) The ITM2B (BRI2) gene is a target of BCL6 repression: Implications for lymphomas and neurodegenerative diseases. *Biochim. Biophys. Acta* **1852**, 742–8.

Barford D., Das A. K., Egloff M. P. (1998) The structure and mechanism of protein phosphatases: insights into catalysis and regulation. *Annu. Rev. Biophys. Biomol. Struct.* **27**, 133–64.

Barnes A. P., Lilley B. N., Pan Y. A., Plummer L. J., Powell A. W., Raines A. N., Sanes J. R., Polleux F. (2007) LKB1 and SAD Kinases Define a Pathway Required for the Polarization of Cortical Neurons. *Cell* **129**, 549–563.

Barnes A. P., Polleux F. (2009) Establishment of axon-dendrite polarity in developing neurons. *Annu. Rev. Neurosci.* **32**, 347–81.

Bartolini F., Moseley J. B., Schmoranzer J., Cassimeris L., Goode B. L., Gundersen G. G. (2008) The formin mDia2 stabilizes microtubules independently of its actin nucleation activity. *J. Cell Biol.* **181**, 523–536.

Bell R., Hubbard A., Chettier R., Chen D., Miller J. P., Kapahi P., Tarnopolsky M., Sahasrabuhde S., Melov S., Hughes R. E. (2009) A human protein interaction network shows conservation of aging processes between human and invertebrate species. *PLoS Genet.* **5**, e1000414.

Benavente F., Pinto C., Parada M., Henríquez J. P., Osses N. (2012) Bone morphogenetic protein 2 inhibits neurite outgrowth of motor neuron-like NSC-34 cells and up-regulates its type II receptor. *J. Neurochem.* **122**, 594–604.

Bentley M., Banker G. (2016) The cellular mechanisms that maintain neuronal polarity. *Nat. Rev. Neurosci.* **17**, 611–622.

Berndt J. D., Aoyagi A., Yang P., Anastas J. N., Tang L., Moon R. T. (2011) Mindbomb 1, an E3 ubiquitin ligase, forms a complex with RYK to activate Wnt/β-catenin signaling. *J. Cell Biol.* **194**, 737–50.

Bielas S. L., Serneo F. F., Chechlacz M., Deerinck T. J., Perkins G. A., Allen P. B., Ellisman M. H., Gleeson J. G. (2007) Spinophilin Facilitates Dephosphorylation of Doublecortin by PP1 to Mediate Microtubule Bundling at the Axonal Wrist. *Cell* **129**, 579–591.

Blitzer R. D., Connor J. H., Brown G. P., Wong T., Shenolikar S., Iyengar R., Landau E. M. (1998) Gating of CaMKII by cAMP-regulated protein phosphatase activity during LTP. *Science* **280**, 1940–2.

Boens S., Szekér K., Eynde A. Van, Bollen M. (2013) Interactor-guided dephosphorylation by protein phosphatase-1. *Methods Mol. Biol.* **1053**, 271–81.

Bollen M., Gerlich D. W., Lesage B. (2009) Mitotic phosphatases: from entry guards to exit guides. *Trends Cell Biol.* **19**, 531–41.

Bollen M., Peti W., Ragusa M. J., Beullens M. (2010) The extended PP1 toolkit: designed to create specificity. *Trends Biochem. Sci.* **35**, 450–8.

Bradt B. M., Kolb W. P., Cooper N. R. (1998) Complement-dependent proinflammatory properties of the Alzheimer's disease beta-peptide. *J. Exp. Med.* **188**, 431–8.

Brandt H., Capulong Z. L., Lee E. Y. (1975) Purification and properties of rabbit liver phosphorylase phosphatase. *J. Biol. Chem.* **250**, 8038–44.

Burgering B. M. T., Coffer P. J. (1995) Protein kinase B (c-Akt) in phosphatidylinositol-3-OH kinase signal transduction. *Nature* **376**, 599–602.

Caceres A., Kosik K. S. (1990) Inhibition of neurite polarity by tau antisense oligonucleotides in primary cerebellar neurons. *Nature* **343**, 461–463.

Caceres A., Mautino J., Kosik K. S. (1992) Suppression of MAP2 in cultured cerebellar macroneurons inhibits minor neurite formation. *Neuron* **9**, 607–18.

Campbell D. S., Holt C. E. (2001) Chemotropic responses of retinal growth cones mediated by rapid local protein synthesis and degradation. *Neuron* **32**, 1013–26.

Campo M. Del, Hoozemans J. J. M., Dekkers L.-L., Rozemuller A. J., Korth C., Müller-Schiffmann A., Scheltens P., et al. (2014) BRI2-BRICHOS is increased in human amyloid plaques in early stages of Alzheimer's disease. *Neurobiol. Aging* **35**, 1596–604.

Campo M. Del, Oliveira C. R., Scheper W., Zwart R., Korth C., Müller-Schiffmann A., Kostallas G., et al. (2015) BRI2 ectodomain affects Aβ42 fibrillation and tau truncation in human neuroblastoma cells. *Cell. Mol. Life Sci.* **72**, 1599–611.

Campo M. Del, Teunissen C. E. (2014) Role of BRI2 in Dementia. *J. Alzheimers. Dis.* **40**, 481–94.

Cao Q., Wang X., Zhao M., Yang R., Malik R., Qiao Y., Poliakov A., et al. (2014) The central role of EED in the orchestration of polycomb group complexes. *Nat. Commun.* **5**, 3127.

Ceulemans H., Bollen M. (2004) Functional diversity of protein phosphatase-1, a cellular economizer and reset button. *Physiol. Rev.* **84**, 1–39.

Chen Y. M., Wang Q. J., Hu H. S., Yu P. C., Zhu J., Drewes G., Piwnica-Worms H., Luo Z. G. (2006) Microtubule affinity-regulating kinase 2 functions downstream of the PAR-3/PAR-6/atypical PKC complex in regulating hippocampal neuronal polarity. *Proc. Natl. Acad. Sci. U. S. A.* **103**, 8534–9.

Choi S.-I., Vidal R., Frangione B., Levy E. (2004) Axonal transport of British and Danish amyloid peptides via secretory vesicles. *FASEB J.* **18**, 373–5.

Choi S. C., Kim J., Kim T. H., Cho S. Y., Park S. S., Kim K. D., Lee S. H. (2001) Cloning and characterization of a type II integral transmembrane protein gene, Itm2c, that is highly expressed in the mouse brain. *Mol. Cells* **12**, 391–7.

Ciechanover A. (1994) The ubiquitin-proteasome proteolytic pathway. *Cell* **79**, 13–21.

Cohan C. S., Welnhofer E. A., Zhao L., Matsumura F., Yamashiro S. (2001) Role of the actin bundling protein fascin in growth cone morphogenesis: Localization in filopodia and lamellipodia. *Cell Motil. Cytoskeleton* **48**, 109–120.

Cohen P. (1989) The structure and regulation of protein phosphatases. *Annu. Rev. Biochem.* **58**, 453–508.

Cohen P. T. W. (2002) Protein phosphatase 1 - targeted in many directions. *J. Cell Sci.* **115**, 241–256.

Colicelli J. (2004) Human RAS Superfamily Proteins and Related GTPases. *Sci. Signal.* **2004**.

Conde C., Cáceres A. (2009) Microtubule assembly, organization and dynamics in axons and dendrites. *Nat. Rev. Neurosci.* **10**, 319–32.

Cori G., Green A. (1943) Crystalline muscle phosphorylase II. Prosthetic Group. *J Biol Chem* **151**, 31–38.

Cross D. A. E., Alessi D. R., Cohen P., Andjelkovich M., Hemmings B. A. (1995) Inhibition of glycogen synthase kinase-3 by insulin mediated by protein kinase B. *Nature* **378**, 785–789.

Cross M., Nguyen T., Bogdanoska V., Reynolds E., Hamilton J. A. (2005) A proteomics strategy for the enrichment of receptor-associated complexes. *Proteomics* **5**, 4754–63.

Cruz e Silva E. F. da, Fox C. A., Ouimet C. C., Gustafson E., Watson S. J., Greengard P. (1995) Differential expression of protein phosphatase 1 isoforms in mammalian brain. *J. Neurosci.* **15**, 3375–89.

Cruz e Silva O. A. B. da, Fardilha M., Henriques A. G., Rebelo S., Vieira S., Cruz e Silva E. F. da (2004) Signal transduction therapeutics: relevance for Alzheimer's disease. *J. Mol. Neurosci.* **23**, 123–42.

Danielsen J. M. R., Sylvestersen K. B., Bekker-Jensen S., Szklarczyk D., Poulsen J. W., Horn H., Jensen L. J., Mailand N., Nielsen M. L. (2011) Mass spectrometric analysis of lysine ubiquitylation reveals promiscuity at site level. *Mol. Cell. Proteomics* **10**, M110.003590.

Daulat A. M., Maurice P., Froment C., Guillaume J.-L., Broussard C., Monsarrat B., Delagrange P., Jockers R. (2007) Purification and identification of G protein-coupled receptor protein complexes under native conditions. *Mol. Cell. Proteomics* **6**, 835–44.

Dechant G., Barde Y.-A. (2002) The neurotrophin receptor p75NTR: novel functions and implications for diseases of the nervous system. *Nat. Neurosci.* **5**, 1131–1136.

Dehmelt L., Halpain S. (2004) The MAP2/Tau family of microtubule-associated proteins. *Genome Biol.* **6**, 204.

Deleersnijder W., Hong G., Cortvrindt R., Poirier C., Tylzanowski P., Pittois K., Marck E. Van, Merregaert J. (1996) Isolation of markers for chondro-osteogenic differentiation using cDNA library subtraction. Molecular cloning and characterization of a gene belonging to a novel multigene family of integral membrane proteins. *J. Biol. Chem.* **271**, 19475–82.

Demirkan G., Yu K., Boylan J. M., Salomon A. R., Gruppuso P. A. (2011) Phosphoproteomic profiling of in vivo signaling in liver by the mammalian target of rapamycin complex 1 (mTORC1). *PLoS One* **6**, e21729.

Dent E. W., Merriam E. B., Hu X. (2011) The dynamic cytoskeleton: backbone of dendritic spine plasticity. *Curr. Opin. Neurobiol.* **21**, 175–181.

Dominguez R. (2009) Actin filament nucleation and elongation factors – structure–function relationships. *Crit. Rev. Biochem. Mol. Biol.* **44**, 351–366.

Dotti C. G., Sullivan C. A., Banker G. A. (1988) The establishment of polarity by hippocampal neurons in culture. *J. Neurosci.* **8**, 1454–68.

Egloff M. P., Johnson D. F., Moorhead G., Cohen P. T., Cohen P., Barford D. (1997) Structural basis for the recognition of regulatory subunits by the catalytic subunit of protein phosphatase 1. *EMBO J.* **16**, 1876–87.

El-Agnaf O., Gibson G., Lee M., Wright A., Austen B. M. (2004) Properties of neurotoxic peptides related to the Bri gene. *Protein Pept. Lett.* **11**, 207–12.

Emanuele M. J., Elia A. E. H., Xu Q., Thoma C. R., Izhar L., Leng Y., Guo A., et al. (2011) Global identification of modular cullin-RING ligase substrates. *Cell* **147**, 459–74.

Esch T., Lemmon V., Banker G. (2000) Differential effects of NgCAM and N-cadherin on the development of axons and dendrites by cultured hippocampal neurons. *J. Neurocytol.* **29**, 215–23.

Fardilha M., Esteves S. L. C., Korrodi-Gregório L., Cruz e Silva O. A. B. da, Cruz e Silva F. F. da (2010) The physiological relevance of protein phosphatase 1 and its interacting proteins to health and disease. *Curr. Med. Chem.* **17**, 3996–4017.

Fardilha M., Esteves S. L. C., Korrodi-Gregório L., Pelech S., Cruz E Silva O. A. B. da, Cruz E Silva E. da (2011) Protein phosphatase 1 complexes modulate sperm motility and present novel targets for male infertility. *Mol. Hum. Reprod.* **17**, 466–77.

Feng J., Yan Z., Ferreira A., Tomizawa K., Liauw J. A., Zhuo M., Allen P. B., Ouimet C. C., Greengard P. (2000) Spinophilin regulates the formation and function of dendritic spines. *Proc. Natl. Acad. Sci. U. S. A.* **97**, 9287–92.

Fiore R., Püschel A. W. (2003) The function of semaphorins during nervous system development. *Front. Biosci.* **8**, s484-99.

Fischer E., Krebs E. (1955) Conversion of phosphorylase b to phosphorylase a in muscle extracts. *J. Biol. Chem.* **216**, 121–32.

Fleischer A., Ayllón V., Dumoutier L., Renauld J.-C., Rebollo A. (2002) Proapoptotic activity of ITM2B(s), a BH3-only protein induced upon IL-2-deprivation which interacts with Bcl-2. *Oncogene* **21**, 3181–9.

Fluhrer R., Martin L., Klier B., Haug-Kröper M., Grammer G., Nuscher B., Haass C. (2012) The α-helical content of the transmembrane domain of the British dementia protein-2 (Bri2) determines its processing by signal peptide peptidase-like 2b (SPPL2b). *J. Biol. Chem.* **287**, 5156–63.

Flynn K. C. (2013) The cytoskeleton and neurite initiation. *Bioarchitecture* **3**, 86–109.

Fotinopoulou A., Tsachaki M., Vlavaki M., Poulopoulos A., Rostagno A., Frangione B., Ghiso J., Efthimiopoulos S. (2005) BRI2 interacts with amyloid precursor protein (APP) and regulates amyloid beta (Abeta) production. *J. Biol. Chem.* **280**, 30768–72.

Frame S., Cohen P. (2001) GSK3 takes centre stage more than 20 years after its discovery. *Biochem. J.* **359**, 1–16.

Freaney J. E., Kim R., Mandhana R., Horvath C. M. (2013) Extensive cooperation of immune master regulators IRF3 and NFκB in RNA Pol II recruitment and pause release in human innate antiviral transcription. *Cell Rep.* **4**, 959–73.

Fukata Y., Kimura T., Kaibuchi K. (2002) Axon specification in hippocampal neurons. *Neurosci. Res.* **43**, 305–15.

Furukawa K., Fu W., Li Y., Witke W., Kwiatkowski D. J., Mattson M. P. (1997) The actin-severing protein gelsolin modulates calcium channel and NMDA receptor activities and vulnerability to excitotoxicity in hippocampal neurons. *J. Neurosci.* **17**, 8178–86.

Garbe D. S., Das A., Dubreuil R. R., Bashaw G. J. (2007) -Spectrin functions independently of Ankyrin to regulate the establishment and maintenance of axon connections in the Drosophila embryonic CNS.

Development **134**, 273–284.

Garringer H. J., Sammeta N., Oblak A., Ghetti B., Vidal R. (2017) Amyloid and intracellular accumulation of BRI2. *Neurobiol. Aging* **52**, 90–97.

Garvalov B. K., Flynn K. C., Neukirchen D., Meyn L., Teusch N., Wu X., Brakebusch C., Bamburg J. R., Bradke F. (2007) Cdc42 Regulates Cofilin during the Establishment of Neuronal Polarity. *J. Neurosci.* **27**, 13117–13129.

Gauci S., Helbig A. O., Slijper M., Krijgsveld J., Heck A. J. R., Mohammed S. (2009) Lys-N and trypsin cover complementary parts of the phosphoproteome in a refined SCX-based approach. *Anal. Chem.* **81**, 4493–501.

Ghiso J. A., Holton J., Miravalle L., Calero M., Lashley T., Vidal R., Houlden H., et al. (2001) Systemic amyloid deposits in familial British dementia. *J. Biol. Chem.* **276**, 43909–14.

Ghiso J., Vidal R., Rostagno A., Mead S., Révész T., Plant G., Frangione B. (2000) A newly formed amyloidogenic fragment due to a stop codon mutation causes familial British dementia. *Ann. N. Y. Acad. Sci.* **903**, 129–37.

Gibson G., Gunasekera N., Lee M., Lelyveld V., El-Agnaf O. M. A., Wright A., Austen B. (2004) Oligomerization and neurotoxicity of the amyloid ADan peptide implicated in familial Danish dementia. *J. Neurochem.* **88**, 281–90.

Glickman M. H., Ciechanover A. (2002) The ubiquitin-proteasome proteolytic pathway: destruction for the sake of construction. *Physiol. Rev.* **82**, 373–428.

Godet A. N., Guergnon J., Maire V., Croset A., Garcia A. (2010) The combinatorial PP1-binding consensus Motif (R/K)x((0,1))V/IxFxx(R/K)x(R/K) is a new apoptotic signature. *PLoS One* **5**, e9981.

Gong C.-X., Grundke-Iqbal I., Damuni Z., Iqbal K. (1994) Dephosphorylation of microtubule-associated protein tau by protein phosphatase-1 and -2C and its implication in Alzheimer disease. *FEBS Lett.* **341**, 94–98.

Gong Y., Wu J., Qiang H., Liu B., Chi Z., Chen T., Yin B., Peng X., Yuan J. (2008) BRI3 associates with SCG10 and attenuates NGF-induced neurite outgrowth in PC12 cells. *BMB Rep.* **41**, 287–93.

Grassie M. E., Moffat L. D., Walsh M. P., MacDonald J. A. (2011) The myosin phosphatase targeting protein (MYPT) family: a regulated mechanism for achieving substrate specificity of the catalytic subunit of protein phosphatase type 1δ. *Arch. Biochem. Biophys.* **510**, 147–59.

Gratecos D., Detwiler T. C., Hurd S., Fischer E. H. (1977) Rabbit muscle phosphorylase phosphatase. 1. Purification and chemical properties. *Biochemistry* **16**, 4812–7.

Greengard P., Allen P. B., Nairn A. C. (1999) Beyond the dopamine receptor: the DARPP-32/protein phosphatase-1 cascade. *Neuron* **23**, 435–47.

Grenningloh G., Soehrman S., Bondallaz P., Ruchti E., Cadas H. (2004) Role of the microtubule destabilizing proteins SCG10 and stathmin in neuronal growth. *J. Neurobiol.* **58**, 60–69.

Guan K.-L., Rao Y. (2003) Signalling mechanisms mediating neuronal responses to guidance cues. *Nat. Rev. Neurosci.* **4**, 941–956.

Guo H.-F., Zhong Y. (2006) Requirement of Akt to Mediate Long-Term Synaptic Depression in Drosophila. *J. Neurosci.* **26**, 4004–4014.

Guo Y., Sirkis D. W., Schekman R. (2014) Protein Sorting at the *trans* -Golgi Network. *Annu. Rev. Cell Dev. Biol.* **30**, 169–206.

Gupta G. D., Coyaud É., Gonçalves J., Mojarad B. A., Liu Y., Wu Q., Gheiratmand L., et al. (2015) A Dynamic Protein Interaction Landscape of the Human Centrosome-Cilium Interface. *Cell* **163**, 1484–99.

Hall A., Lalli G. (2010) Rho and Ras GTPases in Axon Growth, Guidance, and Branching. *Cold Spring Harb. Perspect. Biol.* **2**, a001818–a001818.

Han C., Park I., Lee B., Jin S., Choi H., Kwon J. T., Kwon Y., Kim D. H., Park Z. Y., Cho C. (2011) Identification of heat shock protein 5, calnexin and integral membrane protein 2B as Adam7-interacting membrane proteins in mouse sperm. *J. Cell. Physiol.* **226**, 1186–95.

Han Y., Haines C. J., Feng H. L. (2007) Role(s) of the serine/threonine protein phosphatase 1 on mammalian sperm motility. *Arch. Androl.* **53**, 169–77.

Hanson D., Stevens A., Murray P. G., Black G. C. M., Clayton P. E. (2014) Identifying biological pathways that underlie primordial short stature using network analysis. *J. Mol. Endocrinol.* **52**, 333–44.

Hein M. Y., Hubner N. C., Poser I., Cox J., Nagaraj N., Toyoda Y., Gak I. A., et al. (2015) A human interactome in three quantitative dimensions organized by stoichiometries and abundances. *Cell* **163**, 712–23.

Hendrickx A., Beullens M., Ceulemans H., Abt T. Den, Eynde A. Van, Nicolaescu E., Lesage B., Bollen M. (2009) *Docking Motif-Guided Mapping of the Interactome of Protein Phosphatase-1*.

Heroes E., Lesage B., Görnemann J., Beullens M., Meervelt L. Van, Bollen M. (2013) The PP1 binding code: a molecular-lego strategy that governs specificity. *FEBS J.* **280**, 584–95.

Hinds J. W., Hinds P. L. (1978) Early development of amacrine cells in the mouse retina: An electron microscopic, serial section analysis. *J. Comp. Neurol.* **179**, 277–300.

Holton J. L., Lashley T., Ghiso J., Braendgaard H., Vidal R., Guerin C. J., Gibb G., et al. (2002) Familial Danish dementia: a novel form of cerebral amyloidosis associated with deposition of both amyloid-Dan and amyloid-beta. *J. Neuropathol. Exp. Neurol.* **61**, 254–67.

Honkanen R. E., Golden T. (2002) Regulators of serine/threonine protein phosphatases at the dawn of a clinical era? *Curr. Med. Chem.* **9**, 2055–75.

Hsieh-Wilson L. C., Benfenati F., Snyder G. L., Allen P. B., Nairn A. C., Greengard P. (2003) Phosphorylation of spinophilin modulates its interaction with actin filaments. *J. Biol. Chem.* **278**, 1186–94.

Hu X. D., Huang Q., Roadcap D. W., Shenolikar S. S., Xia H. (2006) Actin-associated neurabin-protein phosphatase-1 complex regulates hippocampal plasticity. *J. Neurochem.* **98**, 1841–51.

Hülsmeier J., Pielage J., Rickert C., Technau G. M., Klämbt C., Stork T. (2007) Distinct functions of α-Spectrin and β-Spectrin during axonal pathfinding. *Development* **134**.

Hur E.-M., Zhou F.-Q. (2010) GSK3 signalling in neural development. *Nat. Rev. Neurosci.* **11**, 539–51.

Huttlin E. L., Ting L., Bruckner R. J., Gebreab F., Gygi M. P., Szpyt J., Tam S., et al. (2015) The BioPlex Network: A Systematic Exploration of the Human Interactome. *Cell* **162**, 425–40.

Jäger S., Cimermancic P., Gulbahce N., Johnson J. R., McGovern K. E., Clarke S. C., Shales M., et al. (2011) Global landscape of HIV-human protein complexes. *Nature* **481**, 365–70.

Jiang H., Guo W., Liang X., Rao Y. (2005) Both the Establishment and the Maintenance of Neuronal Polarity Require Active Mechanisms. *Cell* **120**, 123–135.

Jiang H., Rao Y. (2005) Axon formation: fate versus growth. *Nat. Neurosci.* **8**, 544–546.

Kaplan D. R., Miller F. D. (2000) Neurotrophin signal transduction in the nervous system. *Curr. Opin. Neurobiol.* **10**, 381–91.

Kihara M., Kiyoshima T., Nagata K., Wada H., Fujiwara H., Hasegawa K., Someya H., Takahashi I., Sakai H. (2014) Itm2a expression in the developing mouse first lower molar, and the subcellular localization of Itm2a in mouse dental epithelial cells. *PLoS One* **9**, e103928.

Kilger E., Buehler A., Woelfing H., Kumar S., Kaeser S. A., Nagarathinam A., Walter J., Jucker M., Coomaraswamy J. (2011) BRI2 protein regulates β-amyloid degradation by increasing levels of secreted insulin-degrading enzyme (IDE). *J. Biol. Chem.* **286**, 37446–57.

Killilea S. D., Mellgren R. L., Aylward J. H., Metieh M. E., Lee E. Y. (1979) Liver protein phosphatases: studies of the presumptive native forms of phosphorylase phosphatase activity in liver extracts and their

dissociation to a catalytic subunit of Mr 35,000. *Arch. Biochem. Biophys.* **193**, 130–9.

Kim J., Miller V. M., Levites Y., West K. J., Zwizinski C. W., Moore B. D., Troendle F. J., et al. (2008) BRI2 (ITM2b) inhibits Abeta deposition in vivo. *J. Neurosci.* **28**, 6030–6.

Kim S. H., Wang R., Gordon D. J., Bass J., Steiner D. F., Lynn D. G., Thinakaran G., Meredith S. C., Sisodia S. S. (1999) Furin mediates enhanced production of fibrillogenic ABri peptides in familial British dementia. *Nat. Neurosci.* **2**, 984–8.

Kim W., Bennett E. J., Huttlin E. L., Guo A., Li J., Possemato A., Sowa M. E., et al. (2011a) Systematic and quantitative assessment of the ubiquitin-modified proteome. *Mol. Cell* **44**, 325–40.

Kim Y. T., Hur E.-M., Snider W. D., Zhou F.-Q. (2011b) Role of GSK3 Signaling in Neuronal Morphogenesis. *Front. Mol. Neurosci.* **4**, 48.

Kirchner J., Bevan M. J. (1999) ITM2A is induced during thymocyte selection and T cell activation and causes downregulation of CD8 when overexpressed in CD4(+)CD8(+) double positive thymocytes. *J. Exp. Med.* **190**, 217–28.

Kishi M. (2005) Mammalian SAD Kinases Are Required for Neuronal Polarization. *Science (80-.).* **307**, 929–932.

Komuro H., Yacubova E., Yacubova E., Rakic P. (2001) Mode and tempo of tangential cell migration in the cerebellar external granular layer. *J. Neurosci.* **21**, 527–40.

Korrodi-Gregório L., Esteves S. L. C., Fardilha M. (2014) Protein phosphatase 1 catalytic isoforms: specificity toward interacting proteins. *Transl. Res.* **164**, 366–91.

Lagha M., Mayeuf-Louchart A., Chang T., Montarras D., Rocancourt D., Zalc A., Kormish J., Zaret K. S., Buckingham M. E., Relaix F. (2013) Itm2a is a Pax3 target gene, expressed at sites of skeletal muscle formation in vivo. *PLoS One* **8**, e63143.

Lashley T., Revesz T., Plant G., Bandopadhyay R., Lees A. J., Frangione B., Wood N. W., et al. (2008) Expression of BRI2 mRNA and protein in normal human brain and familial British dementia: its relevance to the pathogenesis of disease. *Neuropathol. Appl. Neurobiol.* **34**, 492–505.

Lasiecka Z. M., Winckler B. (2011) Mechanisms of polarized membrane trafficking in neurons — Focusing in on endosomes. *Mol. Cell. Neurosci.* **48**, 278–287.

Latil A., Chêne L., Mangin P., Fournier G., Berthon P., Cussenot O. (2003) Extensive analysis of the 13q14 region in human prostate tumors: DNA analysis and quantitative expression of genes lying in the interval of deletion. *Prostate* **57**, 39–50.

Lautermilch N. J., Spitzer N. C. (2000) Regulation of Calcineurin by Growth Cone Calcium Waves Controls Neurite Extension. *J. Neurosci.* **20**.

Liao H., Li Y., Brautigan D. L., Gundersen G. G. (1998) Protein phosphatase 1 is targeted to microtubules by the microtubule-associated protein Tau. *J. Biol. Chem.* **273**, 21901–8.

Lin Q., Buckler E. S., Muse S. V, Walker J. C. (1999) Molecular evolution of type 1 serine/threonine protein phosphatases. *Mol. Phylogenet. Evol.* **12**, 57–66.

Llanos S., Royer C., Lu M., Bergamaschi D., Lee W. H., Lu X. (2011) Inhibitory member of the apoptosis-stimulating proteins of the p53 family (iASPP) interacts with protein phosphatase 1 via a noncanonical binding motif. *J. Biol. Chem.* **286**, 43039–44.

Luo J., Emanuele M. J., Li D., Creighton C. J., Schlabach M. R., Westbrook T. F., Wong K.-K., Elledge S. J. (2009) A genome-wide RNAi screen identifies multiple synthetic lethal interactions with the Ras oncogene. *Cell* **137**, 835–48.

Lüss H., Klein-Wiele O., Bokník P., Herzig S., Knapp J., Linck B., Müller F. U., et al. (2000) Regional expression of protein phosphatase type 1 and 2A catalytic subunit isoforms in the human heart. *J. Mol. Cell. Cardiol.* **32**, 2349–59.

Maeder C. I., Shen K., Hoogenraad C. C. (2014) Axon and dendritic trafficking. *Curr. Opin. Neurobiol.* **27**, 165–170.

Maehama T., Dixon J. E. (1998) The tumor suppressor, PTEN/MMAC1, dephosphorylates the lipid second messenger, phosphatidylinositol 3,4,5-trisphosphate. *J. Biol. Chem.* **273**, 13375–8.

Maekawa M., Ishizaki T., Boku S., Watanabe N., Fujita A., Iwamatsu A., Obinata T., Ohashi K., Mizuno K., Narumiya S. (1999) Signaling from Rho to the actin cytoskeleton through protein kinases ROCK and LIM-kinase. *Science* **285**, 895–8.

Malchiodi-Albedi F., Petrucci T. C., Picconi B., Iosi F., Falchi M. (1997) Protein phosphatase inhibitors induce modification of synapse structure and tau hyperphosphorylation in cultured rat hippocampal neurons. *J. Neurosci. Res.* **48**, 425–38.

Manna T., Thrower D., Miller H. P., Curmi P., Wilson L. (2006) Stathmin Strongly Increases the Minus End Catastrophe Frequency and Induces Rapid Treadmilling of Bovine Brain Microtubules at Steady State in Vitro. *J. Biol. Chem.* **281**, 2071–2078.

Markus A., Patel T. D., Snider W. D. (2002) Neurotrophic factors and axonal growth. *Curr. Opin. Neurobiol.* **12**, 523–31.

Martin L., Fluhrer R., Haass C. (2009) Substrate requirements for SPPL2b-dependent regulated intramembrane proteolysis. *J. Biol. Chem.* **284**, 5662–70.

Martin L., Fluhrer R., Reiss K., Kremmer E., Saftig P., Haass C. (2008) Regulated intramembrane proteolysis of Bri2 (Itm2b) by ADAM10 and SPPL2a/SPPL2b. *J. Biol. Chem.* **283**, 1644–52.

Martins F., Rebelo S., Santos M., Cotrim C. Z., Cruz E Silva E. F. da, Cruz E Silva O. A. B. da (2016) BRI2 and BRI3 are functionally distinct phosphoproteins. *Cell. Signal.* **28**, 130–44.

Martins F., Serrano J., Muller T., Cruz e Silva O. da, Rebelo S. (2017) BRI2 processing and its neuritogenic role are modulated by protein phosphatase 1 complexing. *J. Cell. Biochem.* **in press**.

Matsuda S., Giliberto L., Matsuda Y., Davies P., McGowan E., Pickford F., Ghiso J., Frangione B., D'Adamio L. (2005) The familial dementia BRI2 gene binds the Alzheimer gene amyloid-beta precursor protein and inhibits amyloid-beta production. *J. Biol. Chem.* **280**, 28912–6.

Matsuda S., Giliberto L., Matsuda Y., McGowan E. M., D'Adamio L. (2008) BRI2 inhibits amyloid beta-peptide precursor protein processing by interfering with the docking of secretases to the substrate. *J. Neurosci.* **28**, 8668–76.

Matsuda S., Matsuda Y., D'Adamio L. (2009) BRI3 inhibits amyloid precursor protein processing in a mechanistically distinct manner from its homologue dementia gene BRI2. *J. Biol. Chem.* **284**, 15815–25.

Matsuda S., Matsuda Y., Snapp E. L., D'Adamio L. (2011a) Maturation of BRI2 generates a specific inhibitor that reduces APP processing at the plasma membrane and in endocytic vesicles. *Neurobiol. Aging* **32**, 1400–8.

Matsuda S., Tamayev R., D'Adamio L. (2011b) Increased AβPP processing in familial Danish dementia patients. *J. Alzheimers. Dis.* **27**, 385–91.

Mattson M. P. (1999) Establishment and plasticity of neuronal polarity. *J. Neurosci. Res.* **57**, 577–89.

McAvoy T., Allen P. B., Obaishi H., Nakanishi H., Takai Y., Greengard P., Nairn A. C., Hemmings H. C. (1999) Regulation of neurabin I interaction with protein phosphatase 1 by phosphorylation. *Biochemistry* **38**, 12943–9.

Mead S., James-Galton M., Revesz T., Doshi R. B., Harwood G., Pan E. L., Ghiso J., Frangione B., Plant G. (2000) Familial British dementia with amyloid angiopathy: early clinical, neuropsychological and imaging findings. *Brain*, 975–91.

Mellgren R. L., Aylward J. H., Killilea S. D., Lee E. Y. (1979) The activation and dissociation of a native high

molecular weight form of rabbit skeletal muscle phosphorylase phosphatase by endogenous CA2+-dependent proteases. *J. Biol. Chem.* **254**, 648–52.

Ménager C., Arimura N., Fukata Y., Kaibuchi K. (2004) PIP3 is involved in neuronal polarization and axon formation. *J. Neurochem.* **89**, 109–118.

Mentrup T., Häsler R., Fluhrer R., Saftig P., Schröder B. (2015) A Cell-Based Assay Reveals Nuclear Translocation of Intracellular Domains Released by SPPL Proteases. *Traffic* **16**, 871–92.

Mertins P., Qiao J. W., Patel J., Udeshi N. D., Clauser K. R., Mani D. R., Burgess M. W., Gillette M. A., Jaffe J. D., Carr S. A. (2013) Integrated proteomic analysis of post-translational modifications by serial enrichment. *Nat. Methods* **10**, 634–7.

Monroe J. D., Heathcote R. D. (2013) Protein phosphatases regulate the growth of developing neurites. *Int. J. Dev. Neurosci.* **31**, 250–7.

Morgan J. L., Dhingra A., Vardi N., Wong R. O. L. (2006) Axons and dendrites originate from neuroepithelial-like processes of retinal bipolar cells. *Nat. Neurosci.* **9**, 85–92.

Mulkey R. M., Endo S., Shenolikar S., Malenka R. C. (1994) Involvement of a calcineurin/inhibitor-1 phosphatase cascade in hippocampal long-term depression. *Nature* **369**, 486–8.

Myers M. P., Stolarov J. P., Eng C., Li J., Wang S. I., Wigler M. H., Parsons R., Tonks N. K. (1997) P-TEN, the tumor suppressor from human chromosome 10q23, is a dual-specificity phosphatase. *Proc. Natl. Acad. Sci. U. S. A.* **94**, 9052–7.

Namkoong S., Lee K. Il, Lee J. I., Park R., Lee E.-J., Jang I.-S., Park J. (2015) The integral membrane protein ITM2A, a transcriptional target of PKA-CREB, regulates autophagic flux via interaction with the vacuolar ATPase. *Autophagy* **11**, 756–768.

Narumiya S., Tanji M., Ishizaki T. (2009) Rho signaling, ROCK and mDia1, in transformation, metastasis and invasion. *Cancer Metastasis Rev.* **28**, 65–76.

Ng J., Luo L. (2004) Rho GTPases Regulate Axon Growth through Convergent and Divergent Signaling Pathways. *Neuron* **44**, 779–793.

Nguyen T. M. H., Shin I.-W., Lee T. J., Park J., Kim J. H., Park M. S., Lee E.-J. (2016) Loss of ITM2A, a novel tumor suppressor of ovarian cancer through G2/M cell cycle arrest, is a poor prognostic factor of epithelial ovarian cancer. *Gynecol. Oncol.* **140**, 545–553.

Noctor S. C., Martínez-Cerdeño V., Ivic L., Kriegstein A. R. (2004) Cortical neurons arise in symmetric and asymmetric division zones and migrate through specific phases. *Nat. Neurosci.* **7**, 136–44.

Odom D. T., Zizlsperger N., Gordon D. B., Bell G. W., Rinaldi N. J., Murray H. L., Volkert T. L., et al. (2004) Control of pancreas and liver gene expression by HNF transcription factors. *Science* **303**, 1378–81.

Oliver C. J., Terry-Lorenzo R. T., Elliott E., Bloomer W. A. C., Li S., Brautigan D. L., Colbran R. J., Shenolikar S. (2002) Targeting protein phosphatase 1 (PP1) to the actin cytoskeleton: the neurabin I/PP1 complex regulates cell morphology. *Mol. Cell. Biol.* **22**, 4690–701.

Oshikawa K., Matsumoto M., Oyamada K., Nakayama K. I. (2012) Proteome-wide identification of ubiquitylation sites by conjugation of engineered lysine-less ubiquitin. *J. Proteome Res.* **11**, 796–807.

Ouimet C. C., Cruz e Silva E. F. da, Greengard P. (1995) The alpha and gamma 1 isoforms of protein phosphatase 1 are highly and specifically concentrated in dendritic spines. *Proc. Natl. Acad. Sci. U. S. A.* **92**, 3396–400.

Paul A., Jozef B. (2004) Human Cardiac Tissues, Control and Diseased. *http://cardiogenomics.med.harvard.edu/home, 2004*.

Peng S., Fitzen M., Jörnvall H., Johansson J. (2010) The extracellular domain of Bri2 (ITM2B) binds the ABri peptide (1-23) and amyloid beta-peptide (Abeta1-40): Implications for Bri2 effects on processing of amyloid precursor protein and Abeta aggregation. *Biochem. Biophys. Res. Commun.* **393**, 356–61.

Piper M., Holt C. (2004) RNA translation in axons. *Annu. Rev. Cell Dev. Biol.* **20**, 505–23.

Pittois K., Deleersnijder W., Merregaert J. (1998) cDNA sequence analysis, chromosomal assignment and expression pattern of the gene coding for integral membrane protein 2B. *Gene* **217**, 141–9.

Pittois K., Wauters J., Bossuyt P., Deleersnijder W., Merregaert J. (1999) Genomic organization and chromosomal localization of the Itm2a gene. *Mamm. Genome* **10**, 54–6.

Plant G. T., Révész T., Barnard R. O., Harding A. E., Gautier-Smith P. C. (1990) Familial cerebral amyloid angiopathy with nonneuritic amyloid plaque formation. *Brain*, 721–47.

Plas D. Van den, Merregaert J. (2004a) Constitutive overexpression of the integral membrane protein Itm2A enhances myogenic differentiation of C2C12 cells. *Cell Biol. Int.* **28**, 199–207.

Plas D. Van den, Merregaert J. (2004b) In vitro studies on Itm2a reveal its involvement in early stages of the chondrogenic differentiation pathway. *Biol. Cell* **96**, 463–70.

Podkowa M., Zhao X., Chow C.-W., Coffey E. T., Davis R. J., Attisano L. (2010) Microtubule stabilization by bone morphogenetic protein receptor-mediated scaffolding of c-Jun N-terminal kinase promotes dendrite formation. *Mol. Cell. Biol.* **30**, 2241–50.

Pollard T. D., Beltzner C. C. (2002) Structure and function of the Arp2/3 complex. *Curr. Opin. Struct. Biol.* **12**, 768–74.

Polleux F., Snider W. (2010) Initiating and Growing an Axon. *Cold Spring Harb. Perspect. Biol.* **2**, a001925–a001925.

Poska H., Haslbeck M., Kurudenkandy F. R., Hermansson E., Chen G., Kostallas G., Abelein A., et al. (2016) Dementia-related Bri2 BRICHOS is a versatile molecular chaperone that efficiently inhibits A 42 toxicity in Drosophila. *Biochem. J.* **473**, 3683–3704.

Povlsen L. K., Beli P., Wagner S. A., Poulsen S. L., Sylvestersen K. B., Poulsen J. W., Nielsen M. L., Bekker-Jensen S., Mailand N., Choudhary C. (2012) Systems-wide analysis of ubiquitylation dynamics reveals a key role for PAF15 ubiquitylation in DNA-damage bypass. *Nat. Cell Biol.* **14**, 1089–98.

Ragusa M. J., Allaire M., Nairn A. C., Page R., Peti W. (2011) Flexibility in the PP1:spinophilin holoenzyme. *FEBS Lett.* **585**, 36–40.

Rakic P. (1971) Neuron-glia relationship during granule cell migration in developing cerebellar cortex. A Golgi and electronmicroscopic study in Macacus Rhesus. *J. Comp. Neurol.* **141**, 283–312.

Rebelo S., Domingues S. C., Santos M., Fardilha M., Esteves S. L. C., Vieira S. I., Vintém A. P. B., Wu W., Cruz E Silva E. F. da, Cruz E Silva O. A. B. da (2013) Identification of a novel complex AβPP:Fe65:PP1 that regulates AβPP Thr668 phosphorylation levels. *J. Alzheimers. Dis.* **35**, 761–75.

Rebelo S., Santos M., Martins F., Cruz E Silva E. F. da, Cruz E Silva O. A. B. da (2015) Protein Phosphatase 1 is a key player in nuclear events. *Cell. Signal.* **27**, 2589–98.

Reiner O. (2013) LIS1 and DCX: Implications for Brain Development and Human Disease in Relation to Microtubules. *Scientifica (Cairo).* **2013**, 1–17.

Renaudin X., Guervilly J.-H., Aoufouchi S., Rosselli F. (2014) Proteomic analysis reveals a FANCA-modulated neddylation pathway involved in CXCR5 membrane targeting and cell mobility. *J. Cell Sci.* **127**, 3546–54.

Revesz T., Holton J. L., Doshi B., Anderton B. H., Scaravilli F., Plant G. T. (1999) Cytoskeletal pathology in familial cerebral amyloid angiopathy (British type) with non-neuritic amyloid plaque formation. *Acta Neuropathol.* **97**, 170–6.

Rissoan M.-C., Duhen T., Bridon J.-M., Bendriss-Vermare N., Péronne C., Saint Vis B. de, Brière F., Bates E. E. M. (2002) Subtractive hybridization reveals the expression of immunoglobulin-like transcript 7, Eph-B1, granzyme B, and 3 novel transcripts in human plasmacytoid dendritic cells. *Blood* **100**, 3295–303.

Rolland T., Taşan M., Charloteaux B., Pevzner S. J., Zhong Q., Sahni N., Yi S., et al. (2014) A proteome-scale

map of the human interactome network. *Cell* **159**, 1212–26.

Rosenberg S. S., Spitzer N. C. (2011) Calcium Signaling in Neuronal Development. *Cold Spring Harb. Perspect. Biol.* **3**, a004259–a004259.

Ross S. A., McCaffery P. J., Drager U. C., Luca L. M. De (2000) Retinoids in embryonal development. *Physiol. Rev.* **80**, 1021–54.

Rostagno A., Ghiso J. (2008) Preamyloid lesions and cerebrovascular deposits in the mechanism of dementia: lessons from non-beta-amyloid cerebral amyloidosis. *Neurodegener. Dis.* **5**, 173–5.

Rostagno A., Tomidokoro Y., Lashley T., Ng D., Plant G., Holton J., Frangione B., Revesz T., Ghiso J. (2005) Chromosome 13 dementias. *Cell. Mol. Life Sci.* **62**, 1814–25.

Rual J.-F., Venkatesan K., Hao T., Hirozane-Kishikawa T., Dricot A., Li N., Berriz G. F., et al. (2005) Towards a proteome-scale map of the human protein-protein interaction network. *Nature* **437**, 1173–8.

Sánchez-Pulido L., Devos D., Valencia A. (2002) BRICHOS: a conserved domain in proteins associated with dementia, respiratory distress and cancer. *Trends Biochem. Sci.* **27**, 329–32.

Santos M., Costa P., Martins F., Cruz E Silva E. F. da, Cruz E Silva O. A. B. da, Rebelo S. (2015) LAP1 is a crucial protein for the maintenance of the nuclear envelope structure and cell cycle progression. *Mol. Cell. Biochem.* **399**, 143–53.

Santos M., Domingues S. C., Costa P., Muller T., Galozzi S., Marcus K., Cruz E Silva E. F. da, Cruz E Silva O. A. da, Rebelo S. (2014) Identification of a Novel Human LAP1 Isoform That Is Regulated by Protein Phosphorylation. *PLoS One* **9**, e113732.

Santos M., Rebelo S., Cruz E Silva O. A. B. Da, Cruz E Silva E. F. Da (2012) Immunolocalization of PPP1C Isoforms in SH-SY5Y Cells during the Cell Cycle. *Microsc* **18(S5)**, 41–42.

Santos M., Rebelo S., Kleeff P. J. M. Van, Kim C. E., Dauer W. T., Fardilha M., Cruz E Silva O. A. da, Cruz E Silva E. F. da (2013) The nuclear envelope protein, LAP1B, is a novel protein phosphatase 1 substrate. *PLoS One* **8**, e76788.

Sasaki Y., Hayashi K., Shirao T., Ishikawa R., Kohama K. (2002) Inhibition by Drebrin of the Actin-Bundling Activity of Brain Fascin, a Protein Localized in Filopodia of Growth Cones. *J. Neurochem.* **66**, 980–988.

Serrano J., Martins F., Sousa J., VanPelt A., Rebelo S., Cruz e Silva O. da (2016) The distribution of LAP1 and associated proteins throughout spermatogenesis. *Reprod. Fertil. Dev.* (**submitted**.

Sharma K., D'Souza R. C. J., Tyanova S., Schaab C., Wiśniewski J. R., Cox J., Mann M. (2014a) Ultradeep Human Phosphoproteome Reveals a Distinct Regulatory Nature of Tyr and Ser/Thr-Based Signaling. *Cell Rep.* **8**, 1583–94.

Sharma K., D'Souza R. C. J., Tyanova S., Schaab C., Wiśniewski J. R., Cox J., Mann M. (2014b) Ultradeep human phosphoproteome reveals a distinct regulatory nature of Tyr and Ser/Thr-based signaling. *Cell Rep.* **8**, 1583–94.

Shelly M., Cancedda L., Heilshorn S., Sumbre G., Poo M. (2007) LKB1/STRAD Promotes Axon Initiation During Neuronal Polarization. *Cell* **129**, 565–577.

Shi S.-H., Cheng T., Jan L. Y., Jan Y.-N. (2004) APC and GSK-3β Are Involved in mPar3 Targeting to the Nascent Axon and Establishment of Neuronal Polarity. *Curr. Biol.* **14**, 2025–2032.

Shi S.-H., Jan L. Y., Jan Y.-N., Adams A. E., Johnson D. I., Longnecker R. M., Sloat B. F., et al. (2003) Hippocampal neuronal polarity specified by spatially localized mPar3/mPar6 and PI 3-kinase activity. *Cell* **112**, 63–75.

Shi Y. (2009) Serine/threonine phosphatases: mechanism through structure. *Cell* **139**, 468–84.

Shi Y., Chan D. W., Jung S. Y., Malovannaya A., Wang Y., Qin J. (2011) A data set of human endogenous protein ubiquitination sites. *Mol. Cell. Proteomics* **10**, M110.002089.

Silva J. S. da, Dotti C. G. (2002) Breaking the neuronal sphere: regulation of the actin cytoskeleton in neuritogenesis. *Nat. Rev. Neurosci.* **3**, 694–704.

Silva J. V, Freitas M. J., Fardilha M. (2014) Phosphoprotein phosphatase 1 complexes in spermatogenesis. *Curr. Mol. Pharmacol.* **7**, 136–46.

Sincennes M.-C., Humbert M., Grondin B., Lisi V., Veiga D. F. T., Haman A., Cazaux C., et al. (2016) The LMO2 oncogene regulates DNA replication in hematopoietic cells. *Proc. Natl. Acad. Sci. U. S. A.* **113**, 1393–8.

Soderling T. R., Derkach V. A. (2000) Postsynaptic protein phosphorylation and LTP. *Trends Neurosci.* **23**, 75–80.

Stelzl U., Worm U., Lalowski M., Haenig C., Brembeck F. H., Goehler H., Stroedicke M., et al. (2005) A human protein-protein interaction network: a resource for annotating the proteome. *Cell* **122**, 957–68.

Strack S., Kini S., Ebner F. F., Wadzinski B. E., Colbran R. J. (1999) Differential cellular and subcellular localization of protein phosphatase 1 isoforms in brain. *J. Comp. Neurol.* **413**, 373–84.

Strömgren E., Dalby A., Dalby M. A., Ranheim B. (1970) Cataract, deafness, cerebellar ataxia, psychosis and dementia--a new syndrome. *Acta Neurol. Scand.* **46**, Suppl 43:261+.

Stuart S. A., Houel S., Lee T., Wang N., Old W. M., Ahn N. G. (2015) A Phosphoproteomic Comparison of B-RAFV600E and MKK1/2 Inhibitors in Melanoma Cells. *Mol. Cell. Proteomics* **14**, 1599–615.

Sun K. L. W., Correia J. P., Kennedy T. E. (2011) Netrins: versatile extracellular cues with diverse functions. *Development* **138**, 2153–2169.

Tahirovic S., Bradke F. (2009) Neuronal Polarity. *Cold Spring Harb. Perspect. Biol.* **1**, a001644–a001644.

Tai T.-S., Pai S.-Y., Ho I.-C. (2014) Itm2a, a target gene of GATA-3, plays a minimal role in regulating the development and function of T cells. *PLoS One* **9**, e96535.

Tamayev R., D'Adamio L. (2012) Inhibition of γ-secretase worsens memory deficits in a genetically congruous mouse model of Danish dementia. *Mol. Neurodegener.* **7**, 19.

Tamayev R., Giliberto L., Li W., d'Abramo C., Arancio O., Vidal R., D'Adamio L. (2010a) Memory deficits due to familial British dementia BRI2 mutation are caused by loss of BRI2 function rather than amyloidosis. *J. Neurosci.* **30**, 14915–24.

Tamayev R., Matsuda S., Fà M., Arancio O., D'Adamio L. (2010b) Danish dementia mice suggest that loss of function and not the amyloid cascade causes synaptic plasticity and memory deficits. *Proc. Natl. Acad. Sci. U. S. A.* **107**, 20822–7.

Tamayev R., Matsuda S., Giliberto L., Arancio O., D'Adamio L. (2011) APP heterozygosity averts memory deficit in knockin mice expressing the Danish dementia BRI2 mutant. *EMBO J.* **30**, 2501–9.

Terrak M., Kerff F., Langsetmo K., Tao T., Dominguez R. (2004) Structural basis of protein phosphatase 1 regulation. *Nature* **429**, 780–4.

Terry-Lorenzo R. T., Inoue M., Connor J. H., Haystead T. A., Armbruster B. N., Gupta R. P., Oliver C. J., Shenolikar S. (2000) Neurofilament-L is a protein phosphatase-1-binding protein associated with neuronal plasma membrane and post-synaptic density. *J. Biol. Chem.* **275**, 2439–46.

Tojima T., Ito E. (2004) Signal transduction cascades underlying de novo protein synthesis required for neuronal morphogenesis in differentiating neurons. *Prog. Neurobiol.* **72**, 183–93.

Tomidokoro Y., Lashley T., Rostagno A., Neubert T. A., Bojsen-Møller M., Braendgaard H., Plant G., et al. (2005) Familial Danish dementia: co-existence of Danish and Alzheimer amyloid subunits (ADan AND A{beta}) in the absence of compact plaques. *J. Biol. Chem.* **280**, 36883–94.

Trinkle-Mulcahy L., Andrews P. D., Wickramasinghe S., Sleeman J., Prescott A., Lam Y. W., Lyon C., Swedlow J. R., Lamond A. I. (2003) Time-lapse imaging reveals dynamic relocalization of PP1gamma throughout the mammalian cell cycle. *Mol. Biol. Cell* **14**, 107–17.

Tsachaki M., Fotinopoulou A., Slavi N., Zarkou V., Ghiso J., Efthimiopoulos S. (2013) BRI2 interacts with BACE1 and regulates its cellular levels by promoting its degradation and reducing its mRNA levels. *Curr. Alzheimer Res.* **10**, 532–41.

Tsachaki M., Ghiso J., Efthimiopoulos S. (2008) BRI2 as a central protein involved in neurodegeneration. *Biotechnol. J.* **3**, 1548–54.

Tsachaki M., Ghiso J., Rostagno A., Efthimiopoulos S. (2010) BRI2 homodimerizes with the involvement of intermolecular disulfide bonds. *Neurobiol. Aging* **31**, 88–98.

Tsachaki M., Serlidaki D., Fetani A., Zarkou V., Rozani I., Ghiso J., Efthimiopoulos S. (2011) Glycosylation of BRI2 on asparagine 170 is involved in its trafficking to the cell surface but not in its processing by furin or ADAM10. *Glycobiology* **21**, 1382–8.

Udeshi N. D., Mani D. R., Eisenhaure T., Mertins P., Jaffe J. D., Clauser K. R., Hacohen N., Carr S. A. (2012) Methods for quantification of in vivo changes in protein ubiquitination following proteasome and deubiquitinase inhibition. *Mol. Cell. Proteomics* **11**, 148–59.

Ullrich S., Münch A., Neumann S., Kremmer E., Tatzelt J., Lichtenthaler S. F. (2010) The novel membrane protein TMEM59 modulates complex glycosylation, cell surface expression, and secretion of the amyloid precursor protein. *J. Biol. Chem.* **285**, 20664–74.

Vidal R., Calero M., Révész T., Plant G., Ghiso J., Frangione B. (2001) Sequence, genomic structure and tissue expression of Human BRI3, a member of the BRI gene family. *Gene* **266**, 95–102.

Vidal R., Delisle M. B., Ghetti B. (2004) Neurodegeneration caused by proteins with an aberrant carboxyl-terminus. *J. Neuropathol. Exp. Neurol.* **63**, 787–800.

Vidal R., Frangione B., Rostagno A., Mead S., Révész T., Plant G., Ghiso J. (1999) A stop-codon mutation in the BRI gene associated with familial British dementia. *Nature* **399**, 776–81.

Vidal R., Revesz T., Rostagno A., Kim E., Holton J. L., Bek T., Bojsen-Møller M., et al. (2000) A decamer duplication in the 3' region of the BRI gene originates an amyloid peptide that is associated with dementia in a Danish kindred. *Proc. Natl. Acad. Sci. U. S. A.* **97**, 4920–5.

Wagner S. A., Beli P., Weinert B. T., Nielsen M. L., Cox J., Mann M., Choudhary C. (2011) A proteome-wide, quantitative survey of in vivo ubiquitylation sites reveals widespread regulatory roles. *Mol. Cell. Proteomics* **10**, M111.013284.

Wakula P., Beullens M., Ceulemans H., Stalmans W., Bollen M. (2003) Degeneracy and function of the ubiquitous RVXF motif that mediates binding to protein phosphatase-1. *J. Biol. Chem.* **278**, 18817–23.

Wang H., Tannukit S., Zhu D., Snead M. L., Paine M. L. (2005) Enamel matrix protein interactions. *J. Bone Miner. Res.* **20**, 1032–40.

Watabe-Uchida M., John K. A., Janas J. A., Newey S. E., Aelst L. Van (2006) The Rac Activator DOCK7 Regulates Neuronal Polarity through Local Phosphorylation of Stathmin/Op18. *Neuron* **51**, 727–739.

Weber C., Schreiber T. B., Daub H. (2012) Dual phosphoproteomics and chemical proteomics analysis of erlotinib and gefitinib interference in acute myeloid leukemia cells. *J. Proteomics* **75**, 1343–56.

Westphal R. S., Tavalin S. J., Lin J. W., Alto N. M., Fraser I. D., Langeberg L. K., Sheng M., Scott J. D. (1999) Regulation of NMDA receptors by an associated phosphatase-kinase signaling complex. *Science* **285**, 93–6.

Whitford K. L., Dijkhuizen P., Polleux F., Ghosh A. (2002) Molecular control of cortical dendrite development. *Annu. Rev. Neurosci.* **25**, 127–49.

Wickham L., Benjannet S., Marcinkiewicz E., Chretien M., Seidah N. G. (2005) Beta-amyloid protein converting enzyme 1 and brain-specific type II membrane protein BRI3: binding partners processed by furin. *J. Neurochem.* **92**, 93–102.

Wilhelm M., Schlegl J., Hahne H., Gholami A. M., Lieberenz M., Savitski M. M., Ziegler E., et al. (2014)

Mass-spectrometry-based draft of the human proteome. *Nature* **509**, 582–7.

Willander H., Presto J., Askarieh G., Biverstål H., Frohm B., Knight S. D., Johansson J., Linse S. (2012) BRICHOS domains efficiently delay fibrillation of amyloid β-peptide. *J. Biol. Chem.* **287**, 31608–17.

Witte H., Bradke F. (2008) The role of the cytoskeleton during neuronal polarization. *Curr. Opin. Neurobiol.* **18**, 479–487.

Wittmann T., Bokoch G. M., Waterman-Storer C. M. (2004) Regulation of Microtubule Destabilizing Activity of Op18/Stathmin Downstream of Rac1. *J. Biol. Chem.* **279**, 6196–6203.

Woodgett J. R. (1990) Molecular cloning and expression of glycogen synthase kinase-3/factor A. *EMBO J.* **9**, 2431–8.

Worster-Drought C., Hill T. R., McMenemey W. H. (1933) Familial Presenile Dementia with Spastic Paralysis. *J. Neurol. Psychopathol.* **14**, 27–34.

Xia D., Stull J. T., Kamm K. E. (2005) Myosin phosphatase targeting subunit 1 affects cell migration by regulating myosin phosphorylation and actin assembly. *Exp. Cell Res.* **304**, 506–517.

Yan D., Guo L., Wang Y. (2006) Requirement of dendritic Akt degradation by the ubiquitin–proteasome system for neuronal polarity. *J. Cell Biol.* **174**, 415–424.

Yan Z., Hsieh-Wilson L., Feng J., Tomizawa K., Allen P. B., Fienberg A. A., Nairn A. C., Greengard P. (1999) Protein phosphatase 1 modulation of neostriatal AMPA channels: regulation by DARPP-32 and spinophilin. *Nat. Neurosci.* **2**, 13–7.

Yang L., Xiong Y., Hu X.-F., Du Y.-H. (2015) MicroRNA-323 regulates ischemia/reperfusion injury-induced neuronal cell death by targeting BRI3. *Int. J. Clin. Exp. Pathol.* **8**, 10725–33.

Yoshida T., Kato K., Yokoi K., Oguri M., Watanabe S., Metoki N., Yoshida H., et al. (2010) Association of genetic variants with hemorrhagic stroke in Japanese individuals. *Int. J. Mol. Med.* **25**, 649–56.

Yoshimura T., Kawano Y., Arimura N., Kawabata S., Kikuchi A., Kaibuchi K. (2005) GSK-3β Regulates Phosphorylation of CRMP-2 and Neuronal Polarity. *Cell* **120**, 137–149.

Yu H., Tardivo L., Tam S., Weiner E., Gebreab F., Fan C., Svrzikapa N., et al. (2011) Next-generation sequencing to generate interactome datasets. *Nat. Methods* **8**, 478–80.

Yuen E. C., Howe C. L., Li Y., Holtzman D. M., Mobley W. C. Nerve growth factor and the neurotrophic factor hypothesis. *Brain Dev.* **18**, 362–8.

Zagrebelsky M., Holz A., Dechant G., Barde Y.-A., Bonhoeffer T., Korte M. (2005) The p75 Neurotrophin Receptor Negatively Modulates Dendrite Complexity and Spine Density in Hippocampal Neurons. *J. Neurosci.* **25**.

Zhang Y., Li Y.-M., Liu L.-D., Jiang L., Ji M., Jiang R.-J., Guo L., Liao Y., Li Q.-H. (2011) Host cell protein C9orf9 promotes viral proliferation via interaction with HSV-1 UL25 protein. *Virol. Sin.* **26**, 171–80.

Zhou F.-Q., Snider W. D. (2006) Intracellular control of developmental and regenerative axon growth. *Philos. Trans. R. Soc. B Biol. Sci.* **361**, 1575–1592.

Zolessi F. R., Poggi L., Wilkinson C. J., Chien C.-B., Harris W. A. (2006) Polarization and orientation of retinal ganglion cells in vivo. *Neural Dev.* **1**, 2.

Aims

BRI2 and BRI3 are type II transmembrane proteins family members whose physiological functions are poorly understood. Two different autosomal dominant mutations in the *BRI2* gene are responsible for the development of two rare early-onset forms of dementia, Familial British and Danish dementias (FBD and FDD, respectively), that share clinical and neuropathological characteristics with Alzheimer´s disease (AD), involving brain deposition of abnormal proteins. The molecular and cellular mechanisms underlying these abnormal protein depositions are not fully elucidated. However, it is possible that this abnormal protein deposition might result from abnormal intracellular targeting, signaling, and processing of its precursors, which results in cellular/neuronal dysfunction that ultimately leads to degeneration and impaired brain function. Therefore, the elucidation of the mechanisms physiopathological associated with BRI2 abnormal targeting, signaling, and processing that results in neuronal/cellular dysfunction, which ultimately leads to degeneration and impaired brain function, is of paramount importance. For BRI3 no disease association has been determined so far, however, its enriched expression in the central nervous system strongly suggests a role for BRI3 in neuronal function. Previous work from our laboratory, using two-hybrid (YTH) screens with a brain cDNA library, resulted in the identification of several PP1 binding proteins, namely BRI3. The identification of PP1 containing complexes is of paramount importance since opened new avenues for the study of BRI3 and BRI2 intracellular signaling where PP1/protein phosphorylation represents a key regulatory mechanism.

Therefore, the aim of this thesis was to validate and characterize the BRI3/PP1 and BRI2/PP1 complexes and decipher its physiological relevance (**Aim 1**). In addition, we also identified novel protein partners of both BRI2 and BRI3, particularly in the brain, which provided new insights to unravel the physiological functions as well as the underlying signaling mechanisms in which they are involved (**Aim 2**).

Hence, the following specific aims for this thesis were proposed:

Aim 1. Validation and Functional Characterization of the BRI2:PP1 and BRI3:PP1 complexes (**Chapter II**):

1. Identification and validation of the interactions of BRI2 and BRI3 with PP1 (**Chapter II.A**).
2. Determine the physiological relevance of the BRI2:PP1 complex (**Chapter II.B**).

Aim 2. Identification of novel BRI2 and BRI3 protein interactors (**Chapter III**):

1. Identification of novel BRI2 interactors in the brain: construction and analysis of an interaction network (**Chapter III.A**).
2. Identification of novel BRI3 interactors: construction of a BRI3 interaction network in the brain (**Chapter III.B**).

CHAPTER II - VALIDATION AND FUNCTIONAL CHARACTERIZATION OF THE BRI2:PP1 AND BRI3:PP1 COMPLEXES

CHAPTER II.A – IDENTIFICATION AND VALIDATION OF THE INTERACTIONS OF BRI2 AND BRI3 WITH PP1

"BRI2 and BRI3 are functionally distinct phosphoproteins"

Filipa Martins, Sandra Rebelo, Mariana Santos, Cândida Zita Cotrim, Edgar F. da Cruz e Silva, Odete A.B. da Cruz e Silva

Neuroscience and Signaling Laboratory, Department of Medical Sciences, Institute of Biomedicine-iBiMED, University of Aveiro, Portugal

Corresponding author: Sandra Rebelo, Neuroscience and Signaling Laboratory, Department of Medical Sciences, Institute of Biomedicine-iBiMED, University of Aveiro, 3810-193 Aveiro, Portugal, Tel: +351-924406306, E-mail: srebelo@ua.pt

Martins F, Rebelo S, Santos M, Zita Cotrim C, da Cruz e Silva EF and da Cruz e Silva OCS (2016). BRI2 and BRI3 are functionally distinct phosphoproteins. *Cellular Signalling*, 28(1):130-44. doi: 10.1016/j.cellsig.2015.10.012

Abstract

Three BRI protein family members have been identified. Among these are BRI3 and BRI2, the latter is associated with Familial Danish and Familial British dementias. 'In silico' sequence analysis identified consensus PP1 binding sites in BRI2 and BRI3. This is singularly important, given that protein phosphorylation is a major mechanism regulating intracellular processes. Protein phosphatase 1 (PP1) interacting proteins are fundamental in determining substrate specificity and subcellular localization of this phosphatase. More than 200 PP1 interacting proteins (PIPs) have thus far been reported. It is plausible to hypothesize that BRI2 and BRI3 may be functionally regulated by protein phosphorylation.

Both BRI2 and BRI3 are type II transmembrane glycoproteins relevant in neuronal systems. Using Myc-BRI2 and Myc-BRI3, wild type and PP1 binding mutant constructs, it was possible to show, for the first time, that in fact BRI2 and BRI3 bind PP1. The complexes BRI2:PP1 and BRI3:PP1 were validated *in vitro* and *in vivo*. The subcellular distribution of BRI2 and BRI3 is similar; both localize to the perinuclear area and Golgi apparatus in non-neuronal cells. However, in SH-SY5Y cells BRI2 and BRI3 could also be detected in elongated cellular projections ('processes') and in rat cortical neurons both are broadly distributed throughout the cell body, neurites, and the nucleus. Consistently, co-localization of BRI2 and BRI3 with PP1 was evident. The functional significance of these complexes is apparent given that both BRI proteins are substrates of PP1, thus simultaneously this is the first report of BRI2 and BRI3 as phosphoproteins. Moreover, we show that when BRI2 is phosphorylated a significant increase in neuronal outgrowth and differentiation is evident.

This is the first report describing both BRI2 and BRI3 as PP1 binding proteins. Thus both are PP1 substrates, regulated by protein phosphorylation and in the case of BRI2, regulation by protein phosphorylation is crucial for neuronal differentiation. Interestingly, the Alzheimer's amyloid precursor protein (APP), forms a trimeric complex composed of PP1 and Fe65, with PP1 having the capacity to dephosphorylate APP at Thr668 residue. The emerging consensus appears to be that PP1 containing complexes are crucial in regulating signaling events underlying neuropathological conditions.

II.A.1. Introduction

Reversible protein phosphorylation is a major mechanism controlling key intracellular events in eukaryotic cells. In fact, recent phosphoproteomic studies have indicated that more than 70% of all eukaryotic cellular proteins are regulated by protein phosphorylation occurring mainly at serine (ser), threonine (Thr) and tyrosine (Tyr) residues (Olsen *et al*. 2010). Protein phosphatase 1 (PP1) is a ubiquitous serine/threonine phosphatase, estimated to dephosphorylate about a third of all proteins in eukaryotic cells (Cohen 2002; Ceulemans and Bollen 2004). In mammals there are four PP1 isoforms: PP1α, PP1β/δ and the splice variants PP1γ1 and PP1γ2 encoded for by three different genes *PPP1CA*, *PPP1CB* and *PPP1CC*, respectively (Cohen 2002). PP1 isoforms are extremely similar in their sequences and the differences are located mainly at the N- and C-terminals. However, they possess specific distinct tissue and subcellular distributions. PP1α, PP1β/δ and PP1γ1 are widely expressed across mammalian tissues, particularly in brain and PP1γ2 is testis-enriched (da Cruz e Silva *et al*. 1995; Bordelon *et al*. 2005; Peti *et al*. 2013; Sasaki *et al*. 1990). PP1 is a key protein, functionally diverse, involved in processes including a regulatory role in gene transcription, cell cycle regulation, protein targeting and intracellular processing (Cohen 2002; Bollen 2001; Ceulemans *et al*. 2002). The functional versatility and specificity of PP1 relies on the interaction of its catalytic subunit with many different specific regulatory subunits also known as PP1 interacting proteins (PIPs) (Bollen *et al*. 2010; Fardilha *et al*. 2011; Rebelo *et al*. 2015). These control PP1 subcellular localization and determine substrate specificity and activity (Cohen 2002; da Cruz e Silva *et al*. 1995; Bollen 2001; Ceulemans *et al*. 2002; Bollen *et al*. 2010; Fardilha *et al*. 2010; Heroes *et al*. 2013; Hsieh-Wilson *et al*. 1999; Küntziger *et al*. 2006). PIPs interact with the PP1 catalytic subunit (PP1c) through several PP1 binding motifs such as the RVxF, SILK and MyPhone domains (Hendrickx *et al*. 2009; Jones *et al*. 2005). Most PIPs interact with PP1c through the well-conserved domain, the RVxF motif. This motif has the consensus sequence [R/K]-$X_{A(0-1)}$-[V/I]-X_B-[F/W], where X_A is any amino acid and X_B is any amino acid except proline (Wakula *et al*. 2003). Recently, other consensus sequences have been proposed for the RVxF motif: [HKR]-[ACHKMNQRSTV]-V-[CHKNQRST]-[FW] and [KRL][KRSTAMVHNQ] [VI]{FIMYDP}[FW] (Hendrickx *et al*. 2009; Meiselbach *et al*. 2006). Given that the regulatory subunits control the specificity and the diversity of PP1 activity, the key to fully understanding PP1 function lies in studying these regulatory subunits as well as their cellular functions. Yeast two-hybrid (Y2H) screens, of a human brain cDNA library, using the three PP1 isoforms (PP1α, PP1γ1 and PP1γ2) as baits were used, and several PIPs were described including novel PP1 binding partners (Esteves *et al*.; Esteves *et al*. 2013). One of the novel putative PP1 interacting proteins identified, in these screens, was BRI3 which belongs to the BRI family of proteins (Esteves *et al*. 2013; Cotrim 2009). The *BRI* gene family comprises at least three members, *BRI1*/*ITM2A*, *BRI2*/*ITM2B* and *BRI3*/*ITM2C*, which encode three type II transmembrane

glycoproteins BRI1, BRI2 and BRI3, respectively. These three genes have homologues in chimpanzee, Rhesus monkey, cow, mouse, rat and humans, and their genomic organization consist of six exons and five introns (Rostagno *et al*. 2005; Tsachaki *et al*. 2008). The pattern of expression of these three members is quite different across different tissues (Tsachaki *et al*. 2008; Deleersnijder *et al*. 1996; Lashley *et al*. 2008). BRI1, is a 263-residue protein, expressed in several mesenchymal tissues and was found to be most abundantly expressed in chondro- and osteogenic tissues, in thymus and skeletal muscle (Deleersnijder *et al*. 1996; Kirchner and Bevan 1999; Pittois *et al*. 1999; Akiyama *et al*. 2004). Data suggests a possible involvement of BRI1 in chondro- and osteogenic differentiation (Deleersnijder *et al*. 1996; Pittois *et al*. 1999). The second BRI family member, BRI2, is a 266-residue protein ubiquitously expressed protein, with high levels of expression in the brain, placenta, pancreas, heart, kidney and liver. In the brain, the hippocampus and cerebellum are the regions with the highest mRNA expression levels for BRI2 (Tsachaki *et al*. 2008; Lashley *et al*. 2008; Akiyama *et al*. 2004). The precise biological function of BRI2 remains unknown. However, some reports indicate that it might be involved in the plasticity of neuronal processes and in the promotion of neuritic outgrowth (Choi *et al*. 2004). It has also been suggested that BRI2 may be involved in apoptosis and in signal transduction, acting as a cell surface receptor since it forms disulfide-linked homodimers that occur at the cell surface. Moreover, several studies demonstrated that BRI2 is post-translationally modified by N-glycosylation at asparagine 170, affecting its trafficking through the secretory pathway to the cell surface (Lashley *et al*. 2008; Akiyama *et al*. 2004; Del Campo and Teunissen 2014; Tsachaki *et al*. 2010). Additionally, bioinformatic analysis of the BRI2 sequence, suggests several putative phosphorylation sites, being only confirmed 4 phosphoresidues (Ser8, Tyr76, Tyr112, and Tyr165) (Tsachaki *et al*. 2011; Sharma *et al*. 2014; Demirkan *et al*. 2011). The third family member, BRI3, is a protein composed of 267 amino acids, it is mainly expressed in the brain with the highest levels of expression in cerebral cortex, medulla oblongata, amygdala, hippocampus, thalamus, striatum, caudate nucleus and spinal cord (Tsachaki *et al*. 2008; Vidal *et al*. 2001). This protein is also expressed in plasmocytoid dendritic cells, appendix, peripheral blood leukocytes, bone marrow and fetal liver (Rissoan *et al*. 2002). BRI3´s biological function remains to be fully elucidated, although it has been suggested that it may play a role in TNF-induced cell death and in neuronal differentiation (Wu *et al*. 2003; Gong *et al*. 2008). The sequence of BRI3 predicts a single site of N-glycosylation at Asn169 and some phosphorylation sites being 4 already identified (Ser5, Ser30, Thr32 and Thr37) (Wickham *et al*. 2005; Gauci *et al*. 2009; Sharma *et al*. 2014; Mertins *et al*. 2013; Shiromizu *et al*. 2013; Tweedie-Cullen *et al*. 2009; Munton *et al*. 2007).

BRI2 undergoes regulated intramembrane proteolysis (RIP). First, it is cleaved by a furin and related proteases in the ectodomain, generating a C-terminal 23-residue peptide (3KDa). Additionally, the

remaining membrane-bound, N-terminus undergoes processing by ADAM-10 and a peptide containing the BRICHOS domain (25KDa) is released. The resulting membrane associated N-terminal fragment (NTF; 22KDa) undergoes intramembrane cleavage by SPPL2a/2b to produce a small, secreted, BRI2 C-terminal domain and an intracellular domain (BRI2ICD; 10KDa), that can translocate to the nucleus (Tsachaki *et al*. 2008; Peng *et al*. 2010; Vidal *et al*. 1999; Mentrup *et al*. 2015). BRI3 is also processed by a furin in the ectodomain resulting in the secretion of a C-terminal 23-residue long peptide (Wickham *et al*. 2005). However, although BRI3 is highly homologous to BRI2, it seems that it fails to undergo shedding by ADAM-10 as well as intramembrane proteolysis by SPPL2a/b (Wickham *et al*. 2005; Martin *et al*. 2009). With respect to BRI1 processing, very little is known, although by aligning the BRI family members one would predict that BRI1 can be cleaved by furin or another related proprotein convertase (Wickham *et al*. 2005). To date, the precise biological functions and the proteolytic processing pathways of BRI family protein members have not been fully elucidated.

In the present study by *in silico* analysis the RVxF motif was identified in all the BRI family protein members, signifying that BRI1, BRI2 and BRI3 might be regulated by protein phosphorylation. Given that BRI1 is chondro- and osteogenic tissue-specific while the other two proteins, BRI2 and BRI3, are ubiquitous and brain specific, respectively, the work here presented focused on BRI2 and BRI3. Consequently, the putative complexes BRI2:PP1 and BRI3:PP1 were validated, using several *in vitro* and *in vivo* techniques, namely blot overlay assay and co-immunoprecipitations. Furthermore, we established that the KVTF and KISF motifs are the PP1 binding motifs responsible for the interaction between the phosphatase and BRI2 and BRI3 respectively. The functional relevance of the novel complexes was pursued and it was possible to establish that both BRI2 and BRI3 are novel PP1 substrates and both can be dephosphorylated by PP1 in vitro. Additionally, BRI2 is important for neuronal differentiation, particularly for neuronal outgrowth that is regulated by protein phosphorylation.

II.A.2. Materials and Methods

II.A.2.1. Antibodies

The following primary antibodies were used: mouse monoclonal BRI2 C-8 (Santa Cruz Biotechnology, Inc.), that recognizes the N-terminal of BRI2; rabbit polyclonal BRI3 (Abcam), raised against amino acids 110-258 of human BRI3; rabbit polyclonal CBC2C and CBC3C, that recognizes the C-terminal of PP1α and PP1γ, respectively (da Cruz e Silva *et al*. 1995); rabbit polyclonal APP (Cell Signaling), that recognizes the C-terminal of amyloid precursor protein; and Myc-tag antibody (Cell Signaling), that recognizes myc-fusion proteins. The secondary antibodies used were horseradish peroxidase-conjugated anti-mouse and anti-rabbit (GE Healthcare) for

enhanced chemiluminescence (ECL) detection, and Alexa 594-conjugated anti-mouse IgG and Alexa 488-conjugated anti-rabbit IgG (Molecular Probes) for co-localization analysis.

II.A.2.2. Expression vectors and DNA constructs

pCMV-BRI2 and pCMV-BRI3 were obtained from the I.M.A.G.E. consortium (MRC Geneservice, UK) and they correspond to BRI2 (GenBank Accession: BC016148) and BRI3 (GenBank Accession: BC098563) cDNAs, respectively, inserted into the mammalian expression vector pCMV-SPORT6. Full-length BRI2 and BRI3 were further subcloned into two different vectors: pET-28c vector (Novagen) and the mammalian expression vector pCMV-Myc (Clontech) to obtain myc-fusion proteins. BRI2 and BRI3 PP1 binding (PP1BM) mutants (Hendrickx *et al*. 2009) were generated with the QuikChange Site-Directed Mutagenesis Kit (Stratagene). The BRI2 F6A (KVTA; BRI2 single mutant), BRI2 V4AF6A (KATA; BRI2 double mutant), BRI3 F6A (KISA; BRI3 single mutant) and BRI3 K3AF6A (AISA; BRI3 double mutant) mutants cDNAs were generated using pCMV-Myc vectors containing wild-type BRI2 and BRI3 with appropriate primers (Table II.A.S1). All constructs and mutations were confirmed by DNA sequencing (ABI PRISM 310 Genetic Analyzer, Applied Biosystems).

II.A.2.3. Brain dissection

Wistar Hannover rats (9-12 weeks) were obtained from Harlan Interfaune Ibérica, SL. All experimental procedures observed the European legislation for animal experimentation (2010/63/EU). No specific ethics approval under EU guidelines was required for this project, since the rats were only euthanized, by cervical stretching followed by decapitation, for brain removal. This is within the European law (Council Directive 86/609/EEC) and during this procedure, we took all steps to ameliorate animal suffering and used the minimum number of animals possible. The procedures were approved and supervised by our Institutional Animal Care and Use Committee (IACUC): Comissão Responsável pela Experimentação e Bem-Estar Animal (CREBEA). Briefly, animals were sacrificed by cervical stretching followed by decapitation and both cortex and hippocampus were dissected out on ice. Tissues were further weighed and homogenized on ice with a Potter-Elvehjem tissue homogenizer with 10-15 pulses at 650-750 rpm, in non-denaturating lysis buffer (50 mM Tris-HCl pH 8.0, 120 mM NaCl and 4% CHAPS) containing protease inhibitors (1 mM PMSF, 10 mM Benzamidine, 2 μM Leupeptin, 1.5 μM Aprotinin and 5 μM Pepstatin A) (Santos *et al*. 2014b). The tissue extracts were used for immunoprecipitation analysis as described below.

II.A.2.4. Cell culture and transient transfection

HeLa cells (ATTC CRM-CCL-2) were grown in Minimal Essential Medium (MEM) with Earle´s salts and GlutaMAX supplemented with 10% FBS, 1% MEM non-essential amino acids, 100U/ml penicillin and 100 mg/ml streptomycin. SH-SY5Y (ATCC CRL-2266) cells were grown in Minimal Essential Medium (MEM) supplemented with F-12 nutrient mixture, 10% FBS, 1.5 mM L-glutamine, 100U/ml penicillin and 100 mg/ml streptomycin. Rat cortical primary cultures were established from Wistar Hannover 18 days embryos, as previously described (Henriques *et al*. 2007). Briefly, after dissociation with trypsin (0.45 mg/ml) in Hank´s balanced salt solution cells were plated onto poly-D-lysine-coated dishes at a density of $1.0x10^5$ cells/cm^2 in B27-supplemented Neurobasal medium (GIBCO Invitrogen), a serum-free medium combination. The medium was supplemented with glutamine (0.5 mM) and gentamicin (60 µg/ml). All cultures were maintained in an atmosphere of 5% CO_2 at 37ºC.

Transient transfections were performed using the cationic lipid LipofectAMINE 2000 (Invitrogen Life technologies), according to the manufacturer´s instructions and previous studies (Rebelo *et al*. 2007a). Upon 24 hours of transfection, cells were harvested for immunoprecipitation assays or fixed using 4% paraformaldehyde and processed for immunocytochemistry analysis as previously described (Rebelo *et al*. 2008).

II.A.2.5. Immunocytochemistry analysis

Once fixed as described above, cells were permeabilized with methanol for 2 minutes and washed with 1x PBS. For immunolocalization studies of BRI2 and BRI3, both wild-type and mutant proteins, cells were incubated with the primary antibody (anti-myc) for 2 hours at room temperature. After washing with 1x PBS, cells were subsequently incubated with anti-mouse Alexa 594-conjugated secondary antibody. For co-localization studies of both BRI2 and BRI3 with APP or PP1γ, HeLa cells were first incubated with one of the primary antibodies (APP C-terminal or CBC3C) followed by anti-rabbit Alexa 488-conjugated secondary antibody. After washing with 1x PBS, cells were subsequently incubated with a second primary antibody (anti-myc), followed by anti-mouse Alexa 594-conjugated secondary antibody. All preparations were washed with PBS, mounted using Vectashield mounting media with DAPI (Vector) and visualized using an LSM510-Meta confocal microscope (Zeiss) and 63x/1.4 oil immersion objectives. The argon laser lines of 405 nm (DAPI), 488 nm (Alexa 488), and a 561nm DPSS laser (Alexa 594) were used. Microphotographs were acquired in a sole section in the Z-axis (xy mode) and represent a mean of 16 scans.

II.A.2.6. Blot overlay assays

BRI2 and BRI3 proteins were generated by *in vitro* transcription and translation (IVT) from pET-BRI2 and pET-BRI3 expression vectors, respectively using the TnT-coupled transcription/translation kit (Promega), according to the manufacturer´s instructions. For the overlay assays, four samples of 200 ng of purified recombinant PP1γ1 (Watanabe *et al*. 2003) were on a 10% SDS-PAGE and subsequently transferred onto nitrocellulose membranes. One was overlaid for 1 hour with the BRI2-IVT while the other was overlaid with the BRI3-IVT. Afterward, membranes were washed to remove excess protein and bound proteins were detected by incubating with BRI2 or BRI3 antibody, respectively, and subsequently developed by ECL (GE Healthcare).

II.A.2.7. Co-immunoprecipitation assays

For analysis of endogenous proteins rat cortex and hippocampus were collected in lysis buffer (50 mM Tris-HCl pH 8, 120 mM NaCl and 4% CHAPS) containing protease inhibitors (1 mM PMSF, 10 mM Benzamidine, 2 μM Leupeptin, 1.5 μM Aprotinin and 5 μM Pepstatin A). Dynabeads Protein G (Dynal, Invitrogen) were washed in 3% BSA/1x PBS and primary antibodies were cross-linked to Dynabeads according to the manufacturer´s instructions. Afterward, lysates were pre-cleared with 0.6 mg Dynabeads for 1 hour at 4°C with agitation and incubated with antibody-Dynabeads overnight at 4°C with agitation. The immunoprecipitates were washed in 1x PBS and proteins denatured by boiling in loading buffer followed by SDS-PAGE and immunoblotting.

SH-SY5Y cells were transiently transfected with pCMV-Myc-BRI2, pCMV-Myc-BRI2 KVTA, pCMV-Myc-BRI2 KATA, pCMV-Myc-BRI3, pCMV-Myc-BRI3 KISA or with the pCMV-Myc-BRI3 AISA and immunoprecipitated as described above.

II.A.2.8. SDS-PAGE and Immunoblotting

Samples were separated on SDS-PAGE and electrophoretically transferred onto nitrocellulose, followed by immunological detection with specific antibodies as indicated. Membranes were saturated in 5% non-fat dry milk in TBS-T for 4 hours and further incubated with primary antibodies. The incubations with the CBC2C and CBC3C antibodies were performed overnight while the incubation with anti-myc was carried out for 4 hours. Detection was achieved using horseradish peroxidase-conjugated anti-mouse or anti-rabbit IgGs as secondary antibody and proteins were visualized by ECL (GE Healthcare).

II.A.2.9. Protein phosphorylation analysis by Phos-tag SDS-PAGE

SH-SY5Y cells were transfected with pCMV-Myc-BRI2 or with pCMV-Myc-BRI3 and treated with 0.25 nM or 500 nM okadaic acid (OA) for 3 hours. Cells were then harvested in PP1 buffer (50 mM Tris-HCl pH 7.5, 0.1 mM EGTA, 1 mM $MnCl_2$, 5 mM DTT) containing protease inhibitors (1 mM PMSF, 10 mM Benzamidine, 2 μM Leupeptin, 1.5 μM Aprotinin and 5 μM Pepstatin A). The lysates were incubated for 1 hour at 30°C with (100 ng or 200 ng) or without purified recombinant PP1γ1 (Watanabe *et al*. 2003). Samples were further analyzed by phos-tag SDS-PAGE performed with 8.5% polyacrylamide gels containing 50 μM phos-tag™ acrylamide (AAL-107, Wako Pure Chemicals Industries, Ltd) and 100 μM $MnCl_2$ as previously described (Santos *et al*. 2014a). After electrophoresis, phos-tag acrylamide gels were washed with transfer buffer (25 mM Tris, 192 mM glycine and 20% methanol) containing 10 mM EDTA, for 10 minutes with agitation and then with transfer buffer without EDTA for 10 minutes according to the manufacturer´s protocol. Proteins were transferred electrophoretically onto nitrocellulose membranes followed by immunoblotting detection as indicated above.

The same analysis was performed using lysates from SH-SY5Y cells transfected with pCMV-Myc-BRI2, pCMV-Myc-BRI2 KATA, pCMV-Myc-BRI3 KISA and pCMV-Myc-BRI3 AISA.

II.A.2.10. Data analysis and statistics

For the morphological analysis of BRI2 and BRI3 (wild-type and mutant proteins) transfected SH-SY5Y cells, after image acquisition, the analysis was carried out using ImageJ Fiji software. The number of processes per cell was determined by counting the projections arising from the cell body and process length was determined using the 'Measure' tool of the ImageJ Fiji software. Data were expressed as mean ± SEM from at least 3 different sets of experiments. Statistical analysis was additionally performed using GraphPad Prism software. The 1-way ANOVA was conducted followed by the Tukey-Kramer multi-comparison test. Three levels of significance were used, depending if the p-value was under 0.05, 0.01 or 0.001.

Regarding the co-localization studies, quantifications were performed using the Zeiss LSM 510 4.0 software as previously described (Santos *et al*. 2013).

II.A.3. Results and Discussion

II.A.3.1. BRI2 and BRI3 are novel putative PP1 binding proteins

More than 200 PIPs have been identified and it is expected that more will be discovered in the next few years (Fardilha *et al*. 2011; Fardilha *et al*. 2010; Heroes *et al*. 2013; Hendrickx *et al*. 2009; Esteves *et al*. 2013; Esteves *et al*.). Typically PIPs comprise at least one conserved PP1 binding

domain, namely the RVxF motif. From our previous work on yeast two-hybrid screens novel PIPs were identified using PP1α, PP1γ1 and PP1γ2 as baits (Esteves *et al*. 2013; Esteves *et al*.). Of the clones obtained 4 encoded a putative novel PP1 interacting protein; BRI3 (ITM2C) in the PP1 2 screen (Cotrim 2009). BRI3 belongs to the BRI family of proteins, which has three members (BRI1, BRI2 and BRI3), exhibiting tissue-specific expression. Further *in silico* analysis of all three BRI family members revealed that they have the conserved PP1 binding motif (RVxF): KIAF, KVTF and KISF, for BRI1, BRI2 and BRI3, respectively. Interestingly, the PP1 binding motif is localized to exactly the same intracellular domain position (amino acids 3-6) in each of the different human BRI proteins (Figure II.A.1A and II.A.1B). Given that the BRI1 expression is mainly in chondro- and osteogenic tissues, while BRI2 is ubiquitous and BRI3 is brain specific, the focus was placed on BRI2 and BRI3 proteins. *In silico* characterization of the two potential PP1 binding motifs, KVTF (BRI2) and KISF (BRI3) was achieved using the ClustalOmega algorithm, which allowed for the evaluation of the homology between species.

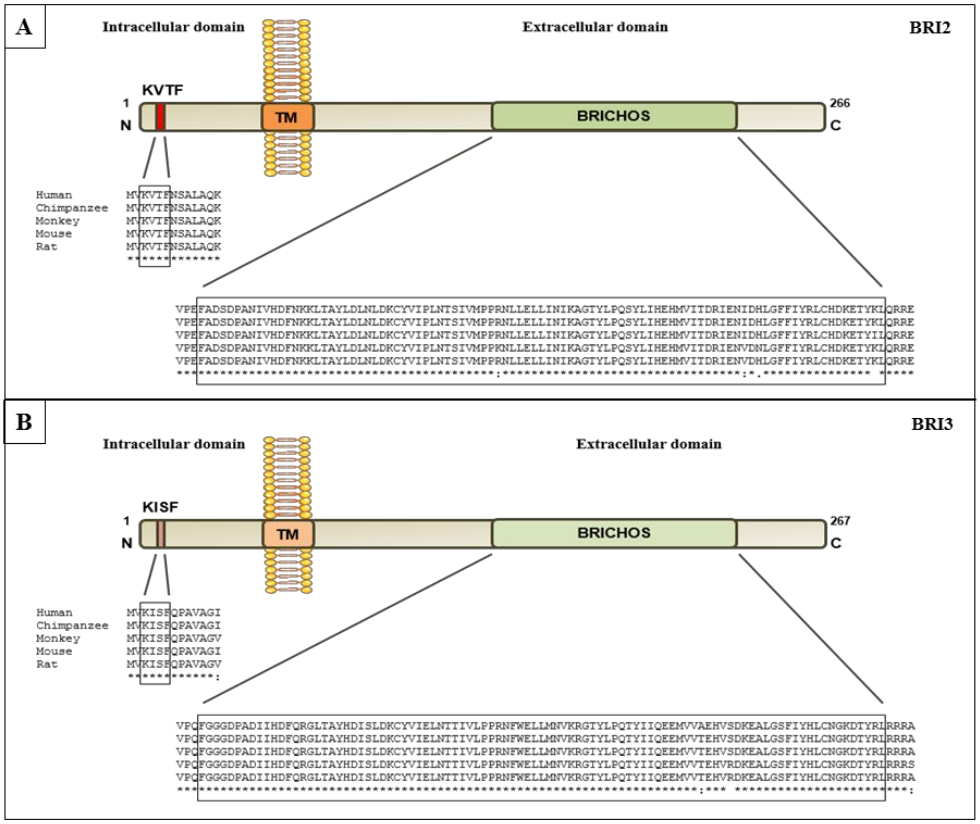

Figure II.A. 1 - Schematic representation of human BRI2 and BRI3. A- Schematic representation of BRI2 functional related domains and motifs. The conserved PP1 binding motif (KVTF) is highlighted in red (position 3-6 in aa sequence), the transmembrane domain is highlighted in orange (position 58-80 in aa sequence) and the BRICHOS domain highlighted in green (position 136-230 in aa sequence). Sequence of human BRI2 was aligned against others species using the ClustalOmega algorithm. Sequence conservation is indicated by asterisks (identical sequences), colons (conserved substitutions) and periods (semi-conserved substitutions). **B-** Schematic representation of BRI3 functional associated domains and motifs. The conserved PP1 binding motif (KISF) is highlighted in red (position 3-6 in aa sequence), the

transmembrane domain is highlighted in orange (position 58-80 in aa sequence) and the BRICHOS domain highlighted in green (position 136-230 in aa sequence). Sequence of human BRI2 was aligned against others species using ClustalOmega algorithm. Sequence conservation is indicated by asterisks (identical sequences), colons (conserved substitutions) and periods (semi-conserved substitutions). KVTF and KISF, RVxF-like PP1 binding motif; TM, transmembrane domain.

Remarkably, both motifs are totally conserved in the species analyzed (Human, Chimpanzee, Monkey, Mouse, and Rat). Moreover, both BRI2 and BRI3 proteins share a conserved domain, the BRICHOS domain, which seems to be involved in protein processing and/or targeting to the secretory pathway (Sánchez-Pulido *et al*. 2002). Our results regarding the homology between species of the BRICHOS domain also indicated that it is also highly conserved among the species analyzed, in the case of both BRI2 and BRI3 (Figure II.A.1A and II.A.1B). Given the YTH data and the BRI2 and BRI3 *in silico* characterization, the putatively novel BRI2:PP1 and BRI3:PP1 complexes were validated *in vitro* and *in vivo*.

II.A.3.2. BRI2 and BRI3 interact with PP1 *in vitro*

The *in vitro* validation of the BRI2:PP1 and BRI3:PP1 complexes was accomplished using a blot overlay assay. Briefly, BRI2 and BRI3 proteins were generated by *in vitro* transcription/translation (IVT). For the overlay assays, four samples of 200 ng of purified recombinant PP1γ1 were loaded and separated on an SDS-PAGE and subsequently transferred onto nitrocellulose membranes. Two of these membranes were overlaid for 1 hour with the BRI2-IVT or with the BRI3-IVT and the other two were subjected to the same procedure but were overlaid with the BRI2 and BRI3- IVT negative controls. Afterward, for all the four membranes, were subjected to specific antibodies directed against BRI2 or BRI3, respectively. The results are presented in Figure II.A.2. It was possible to detect a band around 37 kDa corresponding in size to PP1γ1 only in the membranes that were incubated with the BRI2-IVT and BRI3-IVT. No immunoreactive bands were detected in the negative controls. These results indicate that both BRI2 and BRI3 bind directly to PP1 *in vitro*, thus confirming the hypothesis that BRI2 and BRI3 are novel PP1 binding proteins.

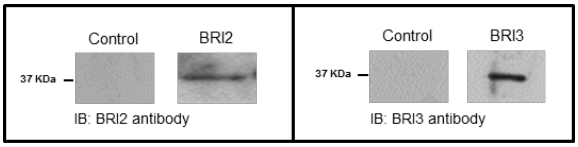

Figure II.A. 2 - Blot overlay assay of full-length BRI2 and BRI3. Samples of purified recombinant PP1γ protein were separated by SDS-PAGE and the resulting blot was overlaid with BRI2-IVT, BRI3-IVT or without (controls) and further detected using specific antibodies against BRI2 and BRI3 IB, immunoblotting.

II.A.3.3. BRI2:PP1 and BRI3:PP1 complexes are formed *in vivo*

Having shown that both BRI2 and BRI3 interact directly with PP1 *in vitro*, the existence of these complexes *in vivo* was addressed, using distinct models, namely a neuronal-like cell line (SH-SY5Y) and rat brain (cortex and hippocampus). Co-immunoprecipitations, using the specific antibodies directed against PP1α, PP1γ (recognizes both PP1γ1 and PP1γ2), BRI2 and BRI3 were carried out. Briefly, rat cortical and hippocampal extracts were immunoprecipitated with BRI2, BRI3, PP1γ and PP1α antibodies and the results are presented in Fig. II.A.3A. Using rat cortical (Figure II.A.3A1) and hippocampal (Figure II.A.3A2) brain extracts it was possible to confirm that both BRI2:PP1 and BRI3:PP1 complexes are formed in the brain, since a 37 kDa band was detected, corresponding to PP1α and PP1γ, after IP with BRI2 or BRI3 specific antibodies (Figure II.A.3, A1 and A2). Furthermore, since two specific antibodies directed against two different PP1 isoforms (PP1γ and PP1α) were used, in the immunoblotting, one we can confirm that both BRI2 and BRI3 interact *in vivo* with these two PP1 isoforms. However, the most intense bands were obtained for BRI3 hippocampal immunoprecipitated when blotted with PP1γ antibody, and for BRI3 cortical immunoprecipitated when blotted with PP1α. Additionally, when the immunoprecipitation was carried out with PP1γ and PP1α antibodies, BRI3 for both brain regions (cortex and hippocampus) could be detected (Figure II.A.3, A1 and A2).

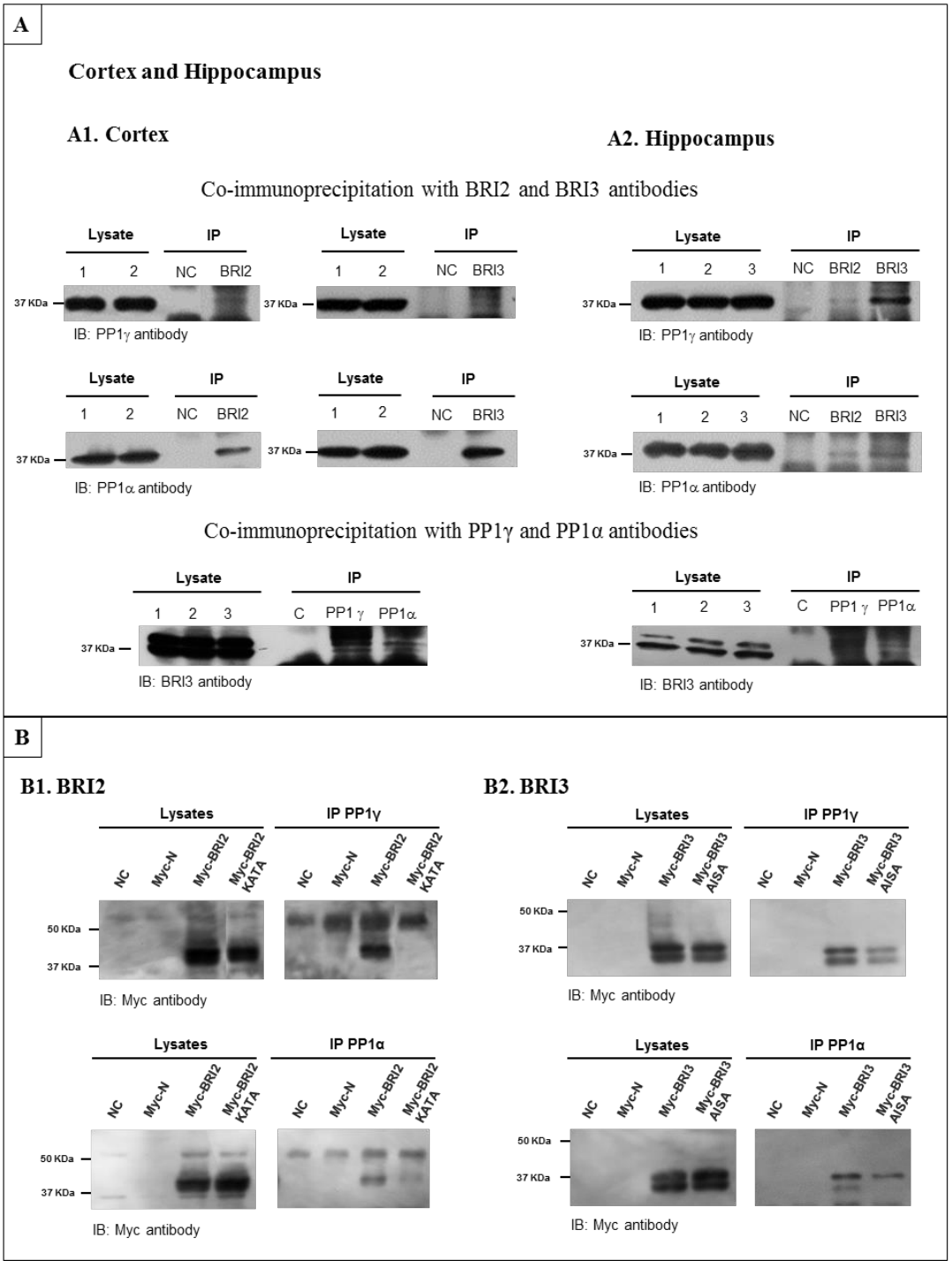

Figure II.A. 3 - In Vivo validation of BRI2:PP1 and BRI3:PP1 complexes. A- Co-immunoprecipitation of the BRI2:PP1 and BRI3:PP1 complexes in rat cortex and hippocampus lysates. Rat cortex (**A1**) and hippocampus (**B2**) extracts were immunoprecipitated with BRI2, BRI3, PP1γ and PP1α antibodies bound to protein G Dynabeads. The negative controls were performed by incubating cell extracts with G Dynabeads. Lysates 1 were subsequently used for negative controls and lysates 2 and 3 for immunoprecipitation with the respective antibodies. **B- Co-immunoprecipitation of the Myc-BRI2, Myc-BRI3 and the respective BRI2 and BRI3 PP1BM mutants.** SH-SY5Y transfected lysates with the following Myc-BRI2 and Myc-BRI2 KATA were immunoprecipitated with both the PP1γ and PP1α antibodies bound to protein G Dynabeads (**B1**). SH-SY5Y transfected lysates with the following Myc-BRI3 and Myc-BRI3 AISA were immunoprecipitated with both PP1γ and PP1α antibodies bound to protein G Dynabeads (**B2**). NC, Negative control; Myc-N, Empty Myc vector; IP, immunoprecipitation; IB, immunoblotting.

In a different experimental model, SH-SY5Y cells were transfected with both Myc-BRI2 and Myc-BRI3 and two PP1BM mutants (Myc-BRI2 KATA and Myc-BRI3 AISA). Consequently, immunoprecipitations (IP) were carried out with the PP1γ (CBC3C) and PP1α (CBC2C) antibodies (Figure II.A.3B). The use of the double mutants at the PP1BM for BRI2 and BRI3, allowed one to determine if PP1 bound the BRI proteins at the domains identified by the *in silico* analysis, as previously described (Korrodi-Gregório *et al*. 2013). The results presented in Figure II.A.3B indicated that it was possible to detect BRI2 and BRI3 when both the PP1 antibodies (PP1α and PP1γ) were used for the IP, indicating once again that BRI2 and BRI3 interact *in vivo* with these two PP1 isoforms. Consistently, when the PP1BM mutant for BRI2 was used, namely Myc-BRI2 KATA, the interaction with PP1α and PP1γ was abolished. These results show that the interaction between BRI2 and PP1 is mediated by the KVTF motif (Figure II.A.3A1). Considering the Myc-BRI3 AISA the results were not so evident, even though a dramatic reduction in the interaction between PP1 and BRI3 (Figure II.A.3A2) was clear. Thus it is reasonable to deduce that the KISF is important for the BRI3:PP1 interaction, but that PP1 mediated activity is being exerted at another level which is not abolished by the double BRI3 mutation.

Additionally, for both BRI2 and BRI3 PP1BM single mutants (Myc-BRI2 KVTA and Myc-BRI3 KISA) were evaluated, a decrease in the binding was evident although not as marked as that detected in the double mutants (data not shown).

II.A.3.4. Immunolocalization of BRI2 and BRI3 in non-neuronal and neuronal models

Given that both complexes are formed *in vivo*, it is evident that these two proteins are functionally related and therefore it became important to evaluate their localization. The localization of BRI2 and BRI3 was achieved using several models; a non-neuronal (HeLa cells), a neuronal-like (SH-SY5Y) and primary culture neuronal model (rat cortical neurons). For HeLa and SY-SY5Y cells, BRI2 was similarly localized, mainly in the ER, Golgi apparatus, membrane and vesicles (Figure II.A.4A and II.A.4B) as described in previous reports (Vidal *et al*. 2001; Choi *et al*. 2004). The enrichment of BRI2 in the Golgi apparatus was confirmed by co-localization with a Golgi marker (CFP-Golgi). However, in SH-SY5Y cells, it was also evident that BRI2 is present in a few elongated cellular projections (´processes') and in the cell membrane (Figure II.A.4B). The localization of BRI2 in rat cortical neurons is however quite different; it is distributed through the cell soma and neuritis. It can also be detected in the nucleus (Figure II.A.4C).

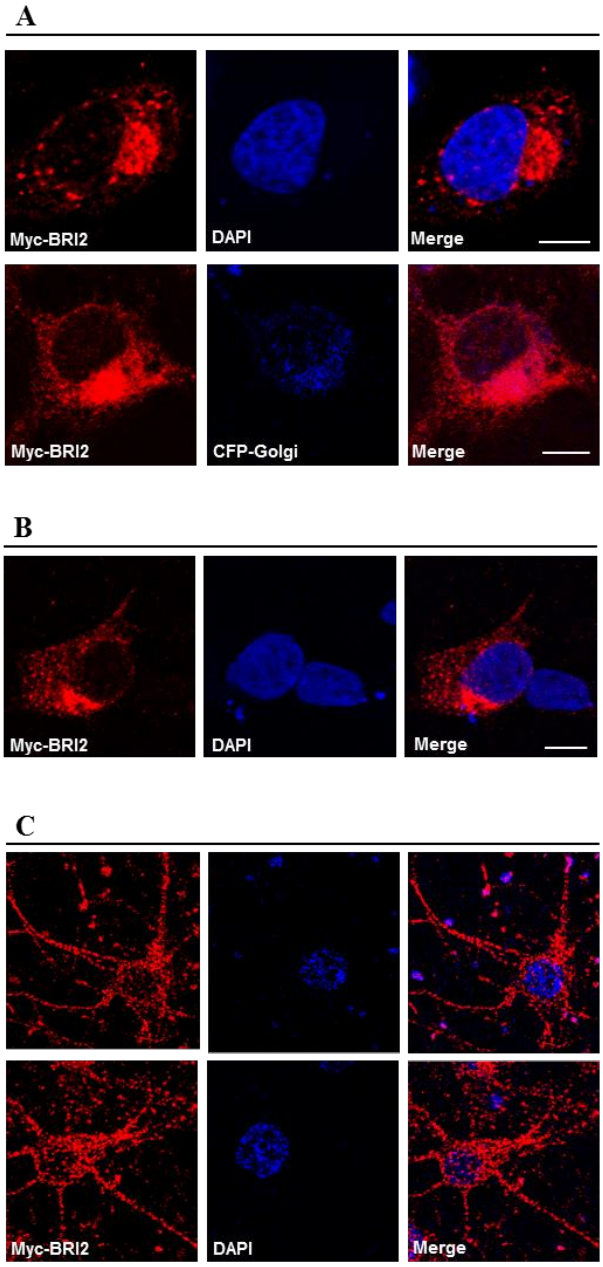

Figure II.A. 4 - Subcellular distribution of BRI2 protein in, HeLa cells, SH-SY5Y cells and rat cortical neurons. HeLa cells, SH-SY5Y cells and rat cortical neurons were transfected with Myc-BRI2 and then processed for immunofluorescence using specific antibodies against Myc-tag. **A-** Localization of Myc-BRI2 in HeLa cells and its co-localization with a Golgi marker (CFP-Golgi). **B-** Localization of Myc-BRI2 in SH-SY5Y cells. C- Localization of Myc-BRI2 in rat cortical neurons. Bars, 10 µm.

Regarding BRI3 localization (Figure II.A.5), it is apparently similar to that observed for BRI2 and as previously described (Gong *et al*. 2008; Martin *et al*. 2008). Hence, BRI3 is localized to the perinuclear space and Golgi apparatus. It also co-localized with CFP-Golgi indicating that it is strongly enriched in this subcellular compartment (Figure II.A.5A and II.A.5B). As observed for BRI2, BRI3 is presented in some elongated projections that in the case of BRI3 seem to be more

elongated (Figure II.A.5B). In rat cortical neurons BRI3 is broadly distributed through the cell body, neuritis and nucleus (Figure II.A.5C). Taken together these results show that BRI is positioned at key cellular compartments consistent with this being a RIP protein; expressed at the cell surface, undergoing cleavage and reaching the nucleus where it can influence gene expression. Furthermore, its localization in neuritis opens possibilities with respect to neuronal associated functions.

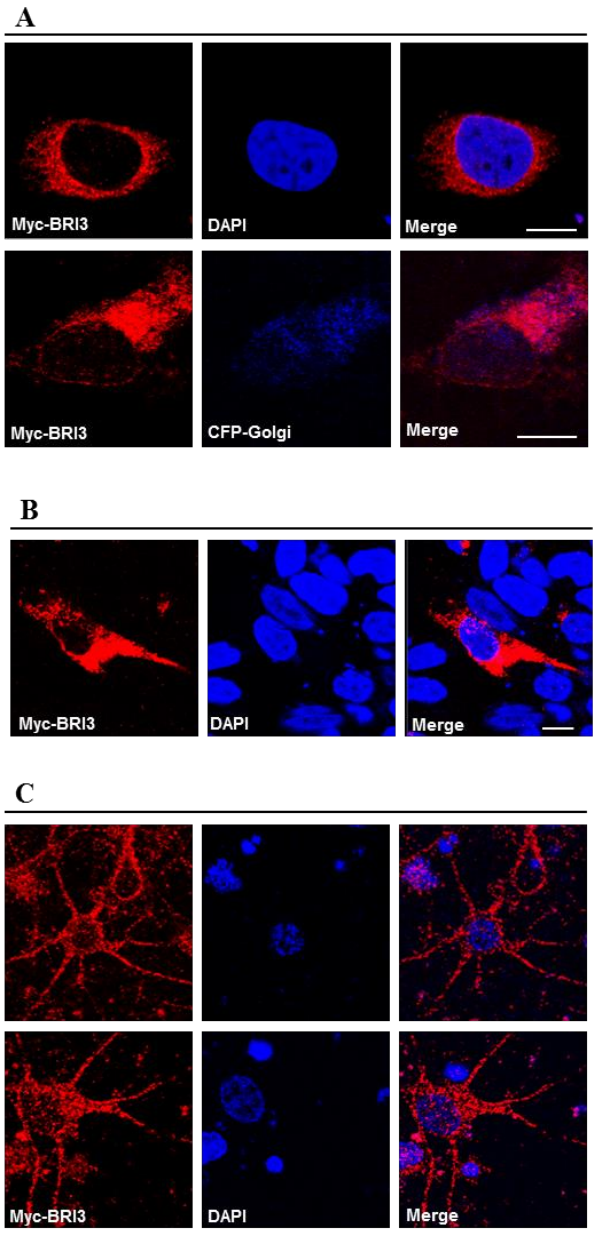

Figure II.A. 5 - Subcellular distribution of BRI3 protein in, HeLa cells, SH-SY5Y cells and rat cortical neurons. HeLa cells, SH-SY5Y cells and rat cortical neurons were transfected with Myc-BRI3 and then processed for immunofluorescence using specific antibodies against Myc-tag. **A-** Localization of Myc-BRI3 in HeLa cells and its co-localization with a Golgi marker (CFP-Golgi). **B-** Localization of Myc-BRI3 in SH-SY5Y cells. **C-** Localization of Myc-BRI3 in rat cortical neurons. Bars, 10 µm.

II.A.3.5. Co-localization of the novel complexes

Once the localization of BRI2 and BRI3 was determined, the co-localization of each with a previously described binding partner, the Alzheimer's amyloid precursor protein, APP (Matsuda *et al*. 2005; Matsuda *et al*. 2009) (Figure II.A.6A), was addressed, as well as their co-localization with the novel binding partner, PP1 (Figure II.A.6B). HeLa cells were transiently transfected with both Myc-BRI2 and Myc-BRI3 and subjected to immunocytochemistry using a Myc-tag antibody. Endogenous APP was detected, using a C-Terminal antibody against APP (Figure II.A.6A). All proteins have the expected subcellular distribution. APP is localized in ER, the Golgi apparatus, vesicles and plasma membrane (Rebelo *et al*. 2007b; da Cruz E Silva *et al*. 2004). Given the similar subcellular distribution between BRI proteins and APP it is evident that they co-localize as observed by the yellowish color (Figure II.A.6A). Quantitative analysis of the co-localization was performed; using a specific co-localization software (Zeiss LSM 510 4.0 software) as previously described (Santos *et al*. 2013; Rebelo *et al*. 2013). Essentially, BRI2 and BRI3 co-localize similarly with APP (49% ± 1.4 and 51% ± 1.5, respectively), whereas the co-localization of APP with both BRI2 and BRI3 is slightly lower (35% ± 1.4 and 44% ± 2, respectively).

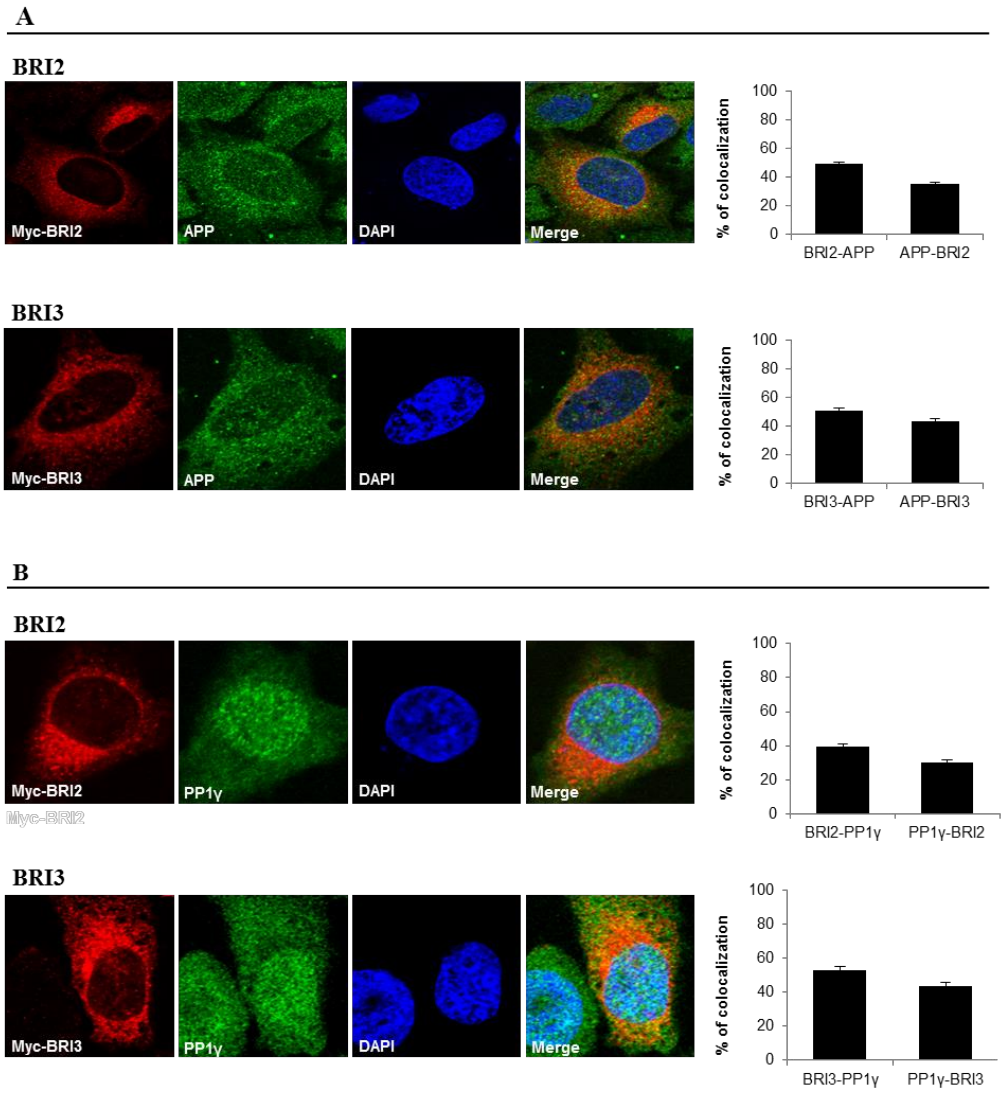

Figure II.A. 6 - Subcellular distribution of the BRI2:APP, BRI3:APP, BRI2:PP1 and BRI3:PP1 complexes in HeLa cells. HeLa cells were transfected with Myc-BRI2 and Myc-BRI3 and then processed for immunofluorescence using specific antibodies against Myc-tag and to endogenous APP and PP1γ. **A-** Co-localization of Myc-BRI2 and Myc-BRI3 with endogenous APP and respective quantification of the % of co-localization between BRI2 and BRI3 with APP. Values are mean ± SEM, n=32 cells for BRI2 and 30 cells for BRI3. **B-** Co-localization of Myc-BRI2 and Myc-BRI3 with endogenous PP1γ. The quantification of the % of co-localization between BRI2 and BRI3 with PP1γ. Values are mean ± SEM, n=35 cells for BRI2 and 39 cells for BRI3.

The co-localization of BRI2 and BRI3 with the new binding partner, PP1, is presented in Fig. II.A.6B. Once again BRI2 and BRI3 present the expected localization as well as PP1γ. PP1γ presented a normal subcellular distribution, and was found predominantly throughout the nucleus, and in the cytoplasm (Figure II.A.6B). Despite the different subcellular distribution of BRI2, BRI3 and PP1γ it is evident that they co-localize in the cytoplasm, mainly around the perinuclear area, as observed by the yellow color (Figure II.A.6B). The quantitative analysis of the percentage of co-localization was

calculated. Essentially, some differences in the co-localization of BRI2 and BRI3 with PP1γ were observed (40% ± 1.6 and 53% ± 1.8, respectively). BRI3 co-localizes more with PP1γ. However the co-localization of PP1γ with BRI2 and BRI3 is lower (30% ± 1.5 and 44% ± 1.9, respectively), but once again PP1γ co-localizes to a higher degree with BRI3. Interestingly, both BRI2 and BRI3 presented a similar percentage of co-localization with the well-known BRI2 or BRI3 binding partner (APP) or the novel binding protein, PP1. It is perhaps not surprising that the percentage of PP1 binding to BRI is comparatively lower, given that for PP1 many PIPs have been described.

II.A.3.6. PP1 regulation of both BRI2 and BRI3

Having determined that both complexes, BRI2:PP1 and BRI3:PP1, are formed *in vitro* and *in vivo* and that BRI proteins and PP1 co-localize at several subcellular compartments, it is reasonable to postulate that protein phosphorylation may play a regulatory role in BRI function. Therefore BRI2 and BRI3 were tested for their potential as PP1 substrates. To date, there are some data suggesting BRI2 and BRI3 as putative phosphoproteins but this was not directly shown before. In order to analyze the phosphorylation state of BRI2 and BRI3 proteins, both Myc-BRI2 and Myc-BRI3 constructs were used to transiently transfect SH-SY5Y cells, followed by incubation with two different concentrations of Okadaic Acid (OA, a protein phosphatase inhibitor) and further incubated with two different amounts of recombinant purified PP1γ1 protein. The resulting cellular extracts were analyzed by immunoblotting (Figure II.A.7A1 and II.A.7B1) and were also loaded onto Phos-tag polyacrylamide gels (Figure II.A.7A2 and II.A.7B2). The SDS-PAGE with the polyacrylamide-bound Mn_2-Phos-tag system, traps phosphorylated proteins by the Phos-tag sites, thus delaying their migration (Hosokawa *et al*. 2010; Kinoshita *et al*. 2006). The analysis of the Figure II.A.7A1 reveals two strong bands corresponding to BRI2 in the cellular extracts from SH-SY5Y cells transfected with Myc-BRI2 in all conditions. Of particular interest, the intensity of the immunoreactive bands increases in a linear fashion in response to OA addition. Given that OA inhibits protein dephosphorylation it is likely that the increased BRI phosphorylation is affecting the protein in some way, such as processing or turnover time, and this deserves further attention. This effect, of protein phosphorylation increasing the half-life of proteins, namely APP, has previously been reported (Vieira *et al*. 2010; Vieira *et al*. 2009). Of note, BRI phosphorylation can be partially reversed by the addition of purified PP1γ1 protein (Figure II.A.7A1). Consequently, BRI2 phosphorylation was addressed by resorting to the phos-tag SDS-PAGE (Figure II.A.7A2). Inhibition of protein phosphatases with OA, resulted in BRI2 separating as multiple bands which is consistent with an increase in BRI2 phosphorylation levels. The higher phosphorylation level was achieved when PP1 was inhibited (OA 500nM). When cells were treated with OA and further incubated with purified PP1γ1 protein (100ng and 200ng) the effects were partially reversed and the slower migrating bands

were barely detected. This indicates an *in vitro* dephosphorylation of BRI2 by PP1γ1 (Figure II.A.7A2).

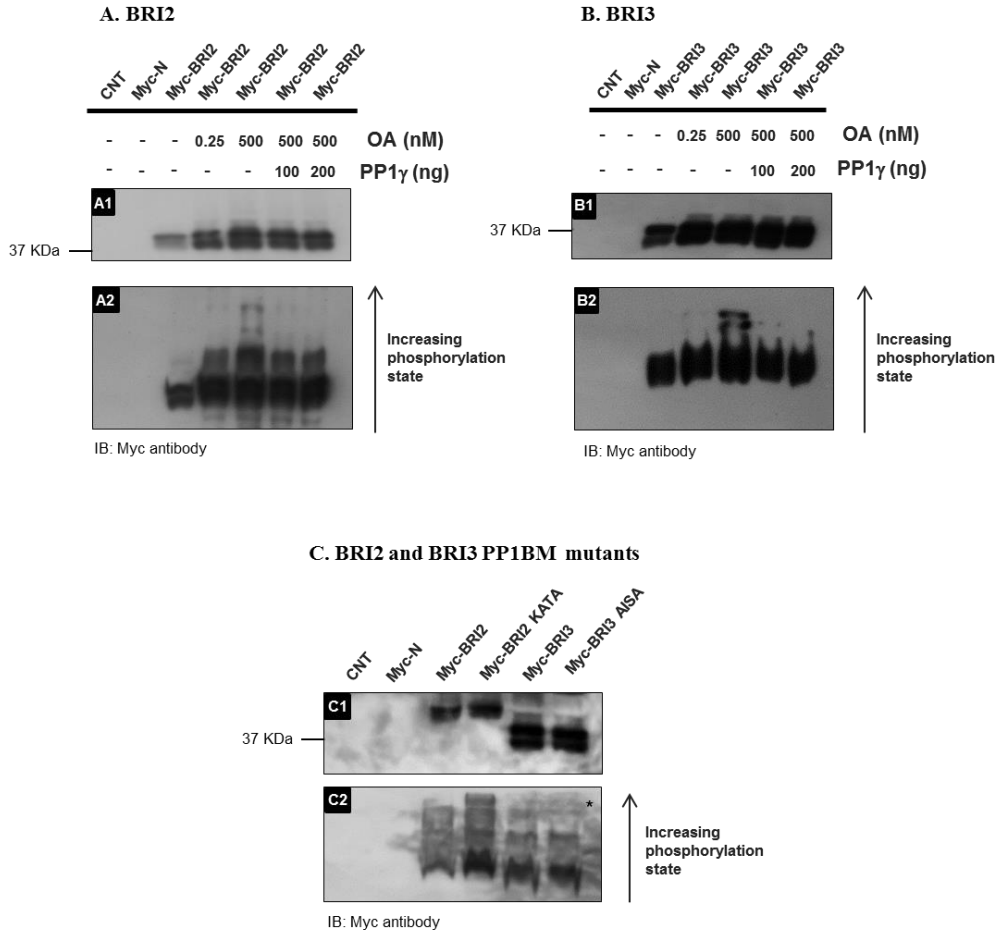

Figure II.A. 7 - Phosphorylation analysis of BRI2, BRI3 and PP1BM mutant proteins by phos-tag SDS-PAGE. Transfected SH-SY5Y cells with Myc-BRI2 or Myc-BRI3 were incubated with 0, 0.25 or 500 nM okadaic acid (OA) for 3 hours and collected in PP1 buffer. Lysates were further incubated at 30ºC for 1 hour with or without 100 ng of PP1γ1 protein. **A- SH-SY5Y cells transfected with Myc-BRI2**: **A1** – Samples were loaded onto a normal SDS-PAGE; **A2**- Samples were loaded onto a phos-tag SDS-PAGE. **B- SH-SY5Y cells transfected with Myc-BRI3**: **B1** – Samples were loaded onto a normal SDS-PAGE; **B2**- Samples were loaded onto a phos-tag SDS-PAGE. **C. SH-SY5Y cells transfected with Myc-BRI2, Myc-BRI3 and PP1BM mutants (Myc-BRI2 KATA and Myc-BRI3AISA)**: **C1**- Samples were loaded onto a normal SDS-PAGE; **C2**- Samples were loaded onto a phos-tag SDS-PAGE.

For BRI3 the results are quite similar. In the SDS-PAGE one can only detect two strong bands corresponding to BRI3 in the cellular extracts from SH-SY5Y cells transfected with Myc-BRI3 for all conditions tested (Figure II.A.7B1). In the phos-tag SDS-PAGE (Figure II.A.7B2) an increase is observed in BRI3 phosphorylation levels with OA treatment, particularly at the concentration that inhibits PP1 (OA 500 nM), as indicated by the presence of two slower migrating bands. Similarly to

BRI2 when cells are treated with OA and the lysates incubated with purified PP1γ1 protein (100ng and 200ng) a decrease in the intensity of the two slower bands is observed, it appears that BRI3, is likewise, dephosphorylated *in vitro* by PP1γ1. From the already suggested phosphorylated residues for BRI2 only Ser8 located at the intracellular domain. Regarding BRI3 the four suggested phosphorylated residues are located at the BRI3 intracellular domain. Given the localization of these residues, they are the putative PP1 target residues, and this issue deserves further investigation.

Moreover, when using the same phos-tag SDS-PAGE approach to evaluate the phosphorylation levels of both BRI2 and BRI3 PP1BM double mutants (Figure II.A.7C), the relevance of the PP1BM is reinforced. As shown before, in Figure II.A.3B, Myc-BRI2 KATA mutant abolishes the interaction between PP1 and BRI2, while Myc-BRI3 AISA mutant significantly decreases the interaction between PP1 and BRI3. Therefore, the phosphorylation levels of the BRI2 and BRI3 double mutants were evaluated. For the Myc-BRI2 KATA multiple bands were observed, which is consistent with an increase in BRI2 phosphorylation levels (Figure II.A.7C2), which cannot be dephosphorylated given that the PP1 BM has been mutated and therefore PP1 cannot bind. The result was not so evident for the Myc-BRI3 AISA mutant. Although an extra slower migrating band could be detected with this mutant (Figure II.A.7C2*). Thus there is a contribution of this PP1BM to BRI3 dephosphorylation, but consistent with the results shown in Figure II.A3, PP1 regulation of BRI3 dephosphorylation is likely to involve levels other than the KISF domain identified.

Given that both BRI2 and BRI3 PP1BM mutants produced dramatic alterations regarding PP1 binding and consequently BRI2 and BRI3 phosphorylation levels, the consequence of partially or totally disrupting the BRI2:PP1 and BRI3:PP1 complexes was evaluated. Briefly, the subcellular localization of transiently transfected SH-SY5Y cells with the following constructs: Myc-BRI2, Myc-BRI2 KVTA, Myc-BRI2 KATA, Myc-BRI3, Myc-BRI3 KISA and Myc-BRI2 AISA, was compared. The results for BRI2 and BRI3 are presented in Figure II.A.8 and Figure II.A.9, respectively. For the subcellular distribution of Myc-BRI2, results were as described before in Fig. 4B. Essentially, BRI2 is localized in ER, Golgi, vesicles and also to a few and short elongated cellular projections (‘processes’) (Figure II.A.8A and II.A.8B). For both the single (Myc-BRI2 KVTA) and double (Myc-BRI2 KATA) mutant there is a significant increase in the number of cellular projections and in the mean length of the higher elongated projection in the cell (Figure II.A.8A and II.A.8B). A remarkable phenotype was observed with the BRI2 double mutant, where a higher number of cellular processes per cell, and longer processes were clearly evident (Figure II.A.8A). A quantitative analysis using the ImageJ software was carried out, to determine the number of cellular projections and length of the longest process as previously described (da Rocha *et al*. 2015), results are presented in Figure II.A.8B. It was possible to establish that with Myc-BRI2 KATA, the mean value of cellular projections was around 14.81 ±1.94, and the mean length of the higher process around 22.98 μm ±

0.48 (Figure II.A.8B). As mentioned, these results were significantly different from those determined for the wild-type Myc-BRI2, with the following results for the number of processes and length of the higher process: 2.54 ± 0.20 and 10.14 μm ± 0.11, respectively (Figure II.A.8B). Consistently, the Myc-BRI2 KVTA (single mutant) produced an intermediate phenotype (Figure II.A.8A and II.A.8B). One can, therefore, conclude that BRI2 phosphorylation is a key event capable of modulating the number of neuritis, as well as the length of these processes in cells. This would place BRI2 at the forefront of neuritogenesis related events that will be further investigated.

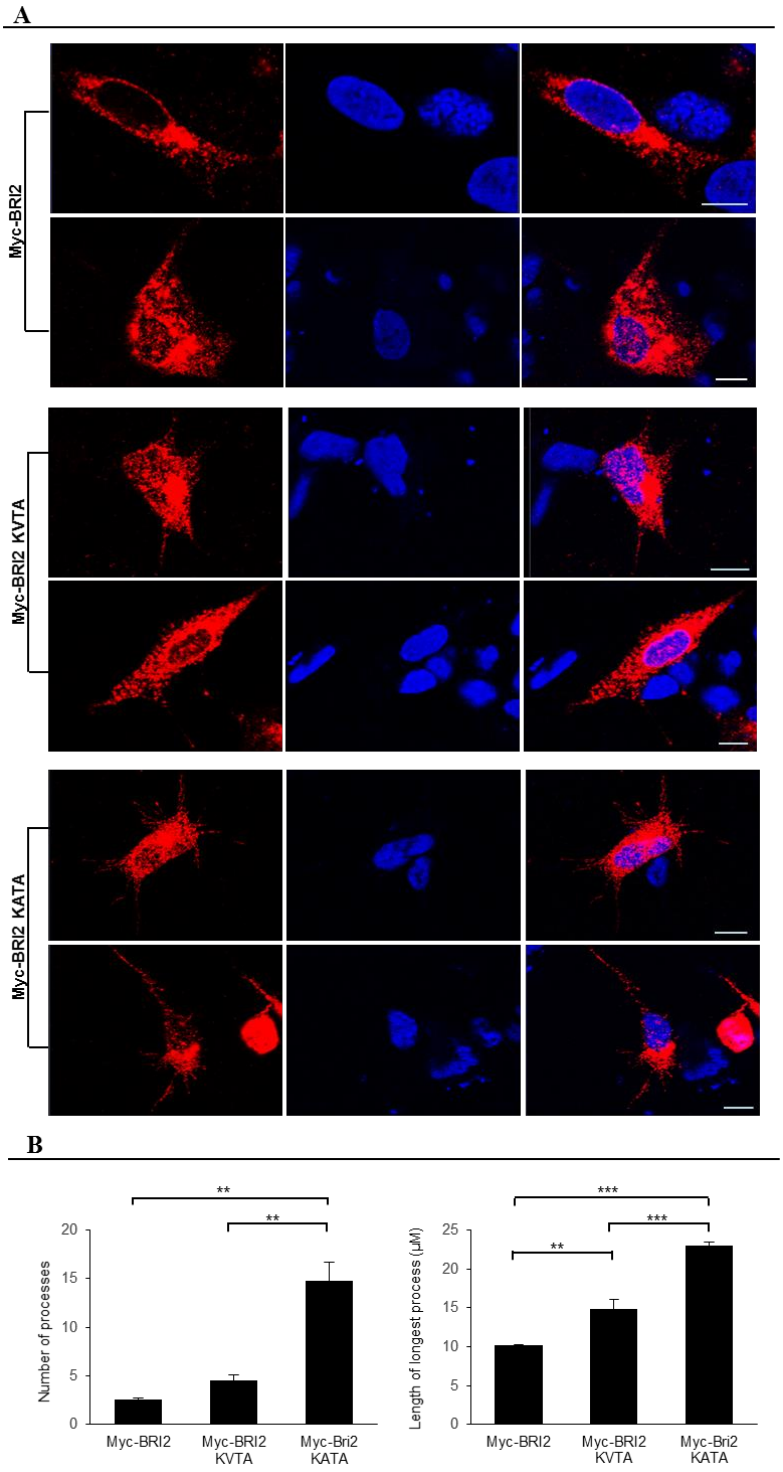

Figure II.A. 8 - Immunolocalization of both Myc-BRI2 and PP1BM mutants (Myc-BRI2 KVTA and Myc-BRI2 KATA). SH-SY5Y cells were transfected with Myc-BRI2 and both PP1BM mutants and then processed for immunofluorescence using specific antibodies against Myc-tag. **A-** Localization of Myc-BRI2, Myc-BRI2 KVTA and Myc-BRI2 KATA. **B-** Values are mean ± SEM (n=3, with each group containing 35 cells). Symbols represent the statistical significance: *, p-value<0.05; **, p-value<0.01; ***, p-value<0.001. Bars, 10 µm.

Myc-BRI3 subcellular distribution was similar to that previously presented in Fig. 5B, where it exhibits a higher number of elongated cellular projections (´processes'). Quantification was carried out using the ImageJ software and presented in Figure II.A.9A and II.A.9B. As for BRI2, the number of cellular projections emerging per cell was counted and the length of the longest projection for both Myc-BRI3 and its mutants were determined. Myc-BRI3 presented around 6.96 ± 0.09 projections per cell, the highest projection is around 19.77 μm ± 1,87 (Figure II.A.9B). These results were not so different for both mutants where values of 8.66 ± 1.42 and 6.77 ± 0.43 were obtained for the number of processes for the single and double mutant, respectively. Regarding the length of the higher process, a decrease was observed, around 15.24 ± 0.45 and 17.01 ± 0.64 for Myc-BRI3 KISA and Myc-BRI3 AISA, respectively. Thus in BRI3 protein phosphorylation does not appear to promote the number or the length of processes associated with each cell. This is in marked contrast to the results observed for BRI2, where protein phosphorylation is the regulatory event modulating neuritic number and process length. However, it is also evident that the basal levels for BRI3 are much higher than those for BRI2. That is, the neuronal BRI3 isoform can sustain a neuronal phenotype independent of the PP1 BM. Whereas BRI2 depends on PP1 binding to the KVTF domain to repress neuritogenesis, it appears that if the protein is not dephosphorylated then neurite outgrowth is promoted.

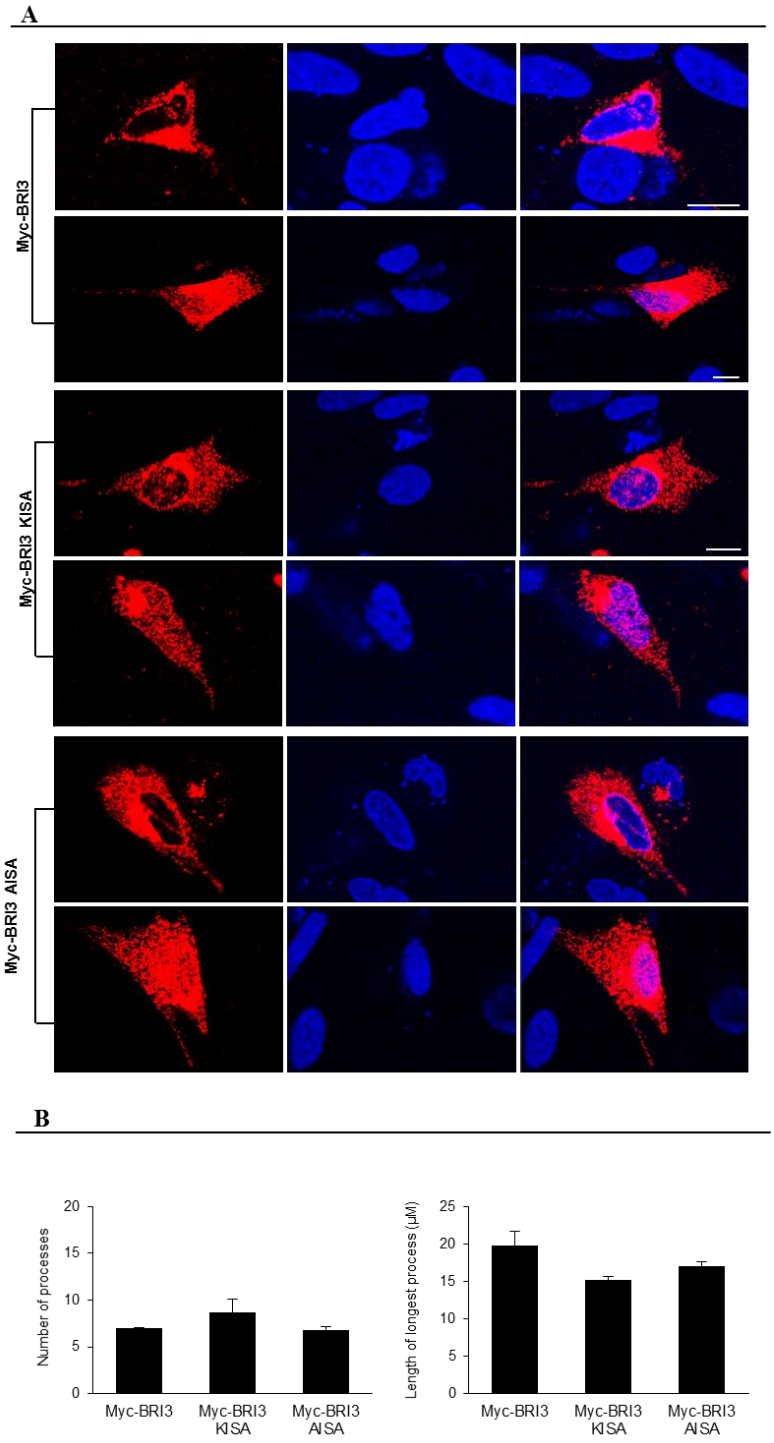

Figure II.A. 9 - Immunolocalization of both Myc-BRI3 and PP1BM mutants (Myc-BRI3 KVTA and Myc-BRI3 KATA). SH-SY5Y cells were transfected with Myc-BRI3 and both PP1BM mutants and then processed for immunofluorescence using specific antibodies against Myc-tag. **A-** Localization of Myc-BRI3, Myc-BRI3 KVTA and Myc-BRI3 KATA. **B-** Values are mean ± SEM (n=3, with each group containing 35 cells). Bars, 10 µm.

II.A.4. Conclusions

BRI2 and BRI3 are two novel PP1 interacting proteins and it was demonstrated that the BRI2:PP1 and BRI3:PP1 complexes exist *in vitro* and *in vivo*. The complexes appear to be physiologically relevant where BRI2 and BRI3 are phosphoproteins and simultaneously PP1 substrates.

The use of BRI2 and BRI3 PP1BM mutants was crucial for determining the importance of RVxF motif for the PP1-BRI interaction. For BRI2, the interaction with PP1was abolished in the BRI2 KATA mutant, presumably because that protein entered into an irreversible phosphorylation state; that is PP1 could no longer bind to dephosphorylate BRI2. For BRI3 it was not so clear since the interaction between BRI3 and PP1 was not completely abolished, it was nonetheless partially decreased, resulting in an increase in the phosphorylation levels of BRI3.

BRI2 and BRI3 are proteins whose main cellular functions remain to be elucidated. Thus, the identification of the novel complexes, BRI2:PP1 and BRI3:PP1 is of paramount importance since it opens new avenues for the study of intracellular targeting and signaling events where protein phosphorylation represents a key regulatory mechanism. In fact, the BRI2 function is highly regulated by protein phosphorylation and upon abolishing PP1 binding, a dramatic increase in neurite outgrowth and cellular differentiation is observed. It seems that BRI2 is important for neuronal differentiation, namely for neuronal outgrowth. Interestingly, APP is also relevant for neuronal function, it is up-regulated in the developing nervous system and it is found enriched in growing neurites and neuritic growth cones (Schubert *et al*. 1991; Masliah *et al*. 1992; Ferreira *et al*. 1993). Moreover, it was shown that APP mediates *in vitro* neuritic outgrowth promoted by NGF (Milward *et al*. 1992) and RA plus brain-derived neurotrophic factor (Ruiz-León and Pascual 2003; Holback *et al*. 2005). It is noteworthy that BRI binds APP, both are phosphoproteins and both are PP1 regulatory proteins.

Two mutations have been described in the gene encoding the BRI2 protein associated with the development of Familial British Dementia (FBD) and Familial Danish Dementia (FDD); two autosomal dominant neurodegenerative diseases that share clinical and neuropathological characteristics with AD (Peng *et al*. 2010; Vidal *et al*. 2000). As already described both BRI2 and BRI3 interact with APP and play a strong regulatory role in the processing of APP, consequently regulating Aβ production (Matsuda *et al*. 2009; Matsuda *et al*. 2008; Fotinopoulou *et al*. 2005; Matsuda *et al*. 2011). The Aβ peptide is the major constituent of AD amyloid plaques, a key player in AD pathology. Increased Aβ production and aggregation is associated with neurotoxicity, activation of the inflammatory response, and apoptotic cascades (Jakob-Roetne and Jacobsen 2009). Furthermore, abnormal protein phosphorylation levels have been associated with several neuropathological disorders including AD due to abnormal protein kinase and protein phosphatase activities (Chung 2009; Gong *et al*. 2006; da Cruz e Silva and da Cruz e Silva 2003; Oliveira *et al*.

2015). For instance, APP was found to be hyperphosphorylated at Thr668 residue in AD brains, which is thought to increase Aβ production (Chung 2009). Recently we also reported that APP forms a trimeric complex with PP1 and Fe65 and that PP1 is responsible for dephosphorylation of APP at the Thr668 residue (Rebelo *et al*. 2013). Thus it seems critical to explore the hypothesis of a common physiopathological mechanism between the above mentioned neurodegenerative diseases. In closing, PP1 containing complexes, such as APP:Fe65:PP1 (Rebelo *et al*. 2013), LAP1:PP1 (Santos *et al*. 2013), BRI2:PP1 and BRI3:PP1 are critical in regulating the phosphorylation-dependent molecular mechanisms associated with neuropathologies.

References

Akiyama H., Kondo H., Arai T., Ikeda K., Kato M., Iseki E., Schwab C., McGeer P. L. (2004) Expression of BRI, the normal precursor of the amyloid protein of familial British dementia, in human brain. *Acta Neuropathol*. **107**, 53–8.

Bollen M. (2001) Combinatorial control of protein phosphatase-1. *Trends Biochem. Sci*. **26**, 426–31.

Bollen M., Peti W., Ragusa M. J., Beullens M. (2010) The extended PP1 toolkit: designed to create specificity. *Trends Biochem. Sci*. **35**, 450–8.

Bordelon J. R., Smith Y., Nairn A. C., Colbran R. J., Greengard P., Muly E. C. (2005) Differential localization of protein phosphatase-1alpha, beta and gamma1 isoforms in primate prefrontal cortex. *Cereb. Cortex* **15**, 1928–37.

Campo M. Del, Teunissen C. E. (2014) Role of BRI2 in Dementia. *J. Alzheimers. Dis*.

Ceulemans H., Bollen M. (2004) Functional diversity of protein phosphatase-1, a cellular economizer and reset button. *Physiol. Rev*. **84**, 1–39.

Ceulemans H., Stalmans W., Bollen M. (2002) Regulator-driven functional diversification of protein phosphatase-1 in eukaryotic evolution. *Bioessays* **24**, 371–81.

Choi S.-I., Vidal R., Frangione B., Levy E. (2004) Axonal transport of British and Danish amyloid peptides via secretory vesicles. *FASEB J*. **18**, 373–5.

Chung S.-H. (2009) Aberrant phosphorylation in the pathogenesis of Alzheimer's disease. *BMB Rep*. **42**, 467–74.

Cohen P. T. W. (2002) Protein phosphatase 1--targeted in many directions. *J. Cell Sci*. **115**, 241–56.

Cotrim C. Z. (2009) *Identification of neuronal proteins that interact with PP1γ2*. University of Aveiro.

Cruz e Silva E. F. da, Cruz e Silva O. A. B. da (2003) Protein phosphorylation and APP metabolism. *Neurochem. Res*. **28**, 1553–61.

Cruz e Silva E. F. da, Fox C. A., Ouimet C. C., Gustafson E., Watson S. J., Greengard P. (1995) Differential expression of protein phosphatase 1 isoforms in mammalian brain. *J. Neurosci*. **15**, 3375–89.

Cruz E Silva O. A. B. da, Vieira S. I., Rebelo S., Cruz e Silva E. F. da (2004) A model system to study intracellular trafficking and processing of the Alzheimer's amyloid precursor protein. *Neurodegener. Dis*. **1**, 196–204.

Deleersnijder W., Hong G., Cortvrindt R., Poirier C., Tylzanowski P., Pittois K., Marck E. Van, Merregaert J. (1996) Isolation of markers for chondro-osteogenic differentiation using cDNA library subtraction. Molecular cloning and characterization of a gene belonging to a novel multigene family of integral membrane proteins. *J. Biol. Chem*. **271**, 19475–82.

Demirkan G., Yu K., Boylan J. M., Salomon A. R., Gruppuso P. A. (2011) Phosphoproteomic profiling of in vivo signaling in liver by the mammalian target of rapamycin complex 1 (mTORC1). *PLoS One* **6**, e21729.

Esteves S. L. C., Domingues S. C., Cruz e Silva O. A. B. da, Fardilha M., Cruz e Silva E. F. da Protein phosphatase 1α interacting proteins in the human brain. *OMICS* **16**, 3–17.

Esteves S. L. C., Korrodi-Gregório L., Cotrim C. Z., Kleeff P. J. M. van, Domingues S. C., Cruz e Silva O. A. B. da, Fardilha M., Cruz e Silva E. F. da (2013) Protein phosphatase 1γ isoforms linked interactions in the brain. *J. Mol. Neurosci*. **50**, 179–97.

Fardilha M., Esteves S. L. C., Korrodi-Gregório L., Cruz e Silva O. A. B. da, Cruz e Silva F. F. da (2010) The physiological relevance of protein phosphatase 1 and its interacting proteins to health and disease. *Curr. Med. Chem*. **17**, 3996–4017.

Fardilha M., Esteves S. L. C., Korrodi-Gregório L., Vintém A. P., Domingues S. C., Rebelo S., Morrice N.,

Cohen P. T. W., Cruz e Silva O. A. B. da, Cruz e Silva E. F. da (2011) Identification of the human testis protein phosphatase 1 interactome. *Biochem. Pharmacol.* **82**, 1403–15.

Ferreira A., Caceres A., Kosik K. S. (1993) Intraneuronal compartments of the amyloid precursor protein. *J. Neurosci.* **13**, 3112–23.

Fotinopoulou A., Tsachaki M., Vlavaki M., Poulopoulos A., Rostagno A., Frangione B., Ghiso J., Efthimiopoulos S. (2005) BRI2 interacts with amyloid precursor protein (APP) and regulates amyloid beta (Abeta) production. *J. Biol. Chem.* **280**, 30768–72.

Gauci S., Helbig A. O., Slijper M., Krijgsveld J., Heck A. J. R., Mohammed S. (2009) Lys-N and trypsin cover complementary parts of the phosphoproteome in a refined SCX-based approach. *Anal. Chem.* **81**, 4493–501.

Gong C.-X., Liu F., Grundke-Iqbal I., Iqbal K. (2006) Dysregulation of protein phosphorylation/dephosphorylation in Alzheimer's disease: a therapeutic target. *J. Biomed. Biotechnol.* **2006**, 31825.

Gong Y., Wu J., Qiang H., Liu B., Chi Z., Chen T., Yin B., Peng X., Yuan J. (2008) BRI3 associates with SCG10 and attenuates NGF-induced neurite outgrowth in PC12 cells. *BMB Rep.* **41**, 287–93.

Hendrickx A., Beullens M., Ceulemans H., Abt T. Den, Eynde A. Van, Nicolaescu E., Lesage B., Bollen M. (2009) Docking Motif-Guided Mapping of the Interactome of Protein Phosphatase-1. *Chem. Biol.* **16**, 365–371.

Henriques A. G., Vieira S. I., Rebelo S., Domingues S. C. T. S., Cruz e Silva E. F. da, Cruz e Silva O. A. B. da (2007) Isoform specific amyloid-beta protein precursor metabolism. *J. Alzheimers. Dis.* **11**, 85–95.

Heroes E., Lesage B., Görnemann J., Beullens M., Meervelt L. Van, Bollen M. (2013) The PP1 binding code: a molecular-lego strategy that governs specificity. *FEBS J.* **280**, 584–95.

Holback S., Adlerz L., Iverfeldt K. (2005) Increased processing of APLP2 and APP with concomitant formation of APP intracellular domains in BDNF and retinoic acid-differentiated human neuroblastoma cells. *J. Neurochem.* **95**, 1059–68.

Hosokawa T., Saito T., Asada A., Fukunaga K., Hisanaga S.-I. (2010) Quantitative measurement of in vivo phosphorylation states of Cdk5 activator p35 by Phos-tag SDS-PAGE. *Mol. Cell. Proteomics* **9**, 1133–43.

Hsieh-Wilson L. C., Allen P. B., Watanabe T., Nairn A. C., Greengard P. (1999) Characterization of the neuronal targeting protein spinophilin and its interactions with protein phosphatase-1. *Biochemistry* **38**, 4365–73.

Jakob-Roetne R., Jacobsen H. (2009) Alzheimer's disease: from pathology to therapeutic approaches. *Angew. Chem. Int. Ed. Engl.* **48**, 3030–59.

Jones J. A., Rawles R., Hannun Y. A. (2005) Identification of a novel phosphatidic acid binding domain in protein phosphatase-1. *Biochemistry* **44**, 13235–45.

Kinoshita E., Kinoshita-Kikuta E., Takiyama K., Koike T. (2006) Phosphate-binding tag, a new tool to visualize phosphorylated proteins. *Mol. Cell. Proteomics* **5**, 749–57.

Kirchner J., Bevan M. J. (1999) ITM2A is induced during thymocyte selection and T cell activation and causes downregulation of CD8 when overexpressed in CD4(+)CD8(+) double positive thymocytes. *J. Exp. Med.* **190**, 217–28.

Korrodi-Gregório L., Vieira S. I., Esteves S. L. C., Silva J. V, Freitas M. J., Brauns A.-K., Luers G., et al. (2013) TCTEX1D4, a novel protein phosphatase 1 interactor: connecting the phosphatase to the microtubule network. *Biol. Open* **2**, 453–65.

Küntziger T., Rogne M., Folstad R. L. S., Collas P. (2006) Association of PP1 with its regulatory subunit AKAP149 is regulated by serine phosphorylation flanking the RVXF motif of AKAP149. *Biochemistry*

45, 5868–77.

Lashley T., Revesz T., Plant G., Bandopadhyay R., Lees A. J., Frangione B., Wood N. W., et al. (2008) Expression of BRI2 mRNA and protein in normal human brain and familial British dementia: its relevance to the pathogenesis of disease. *Neuropathol. Appl. Neurobiol.* **34**, 492–505.

Martin L., Fluhrer R., Haass C. (2009) Substrate requirements for SPPL2b-dependent regulated intramembrane proteolysis. *J. Biol. Chem.* **284**, 5662–70.

Martin L., Fluhrer R., Reiss K., Kremmer E., Saftig P., Haass C. (2008) Regulated intramembrane proteolysis of Bri2 (Itm2b) by ADAM10 and SPPL2a/SPPL2b. *J. Biol. Chem.* **283**, 1644–52.

Masliah E., Mallory M., Ge N., Saitoh T. (1992) Amyloid precursor protein is localized in growing neurites of neonatal rat brain. *Brain Res.* **593**, 323–8.

Matsuda S., Giliberto L., Matsuda Y., Davies P., McGowan E., Pickford F., Ghiso J., Frangione B., D'Adamio L. (2005) The familial dementia BRI2 gene binds the Alzheimer gene amyloid-beta precursor protein and inhibits amyloid-beta production. *J. Biol. Chem.* **280**, 28912–6.

Matsuda S., Giliberto L., Matsuda Y., McGowan E. M., D'Adamio L. (2008) BRI2 inhibits amyloid beta-peptide precursor protein processing by interfering with the docking of secretases to the substrate. *J. Neurosci.* **28**, 8668–76.

Matsuda S., Matsuda Y., D'Adamio L. (2009) BRI3 inhibits amyloid precursor protein processing in a mechanistically distinct manner from its homologue dementia gene BRI2. *J. Biol. Chem.* **284**, 15815–25.

Matsuda S., Matsuda Y., Snapp E. L., D'Adamio L. (2011) Maturation of BRI2 generates a specific inhibitor that reduces APP processing at the plasma membrane and in endocytic vesicles. *Neurobiol. Aging* **32**, 1400–8.

Meiselbach H., Sticht H., Enz R. (2006) Structural analysis of the protein phosphatase 1 docking motif: molecular description of binding specificities identifies interacting proteins. *Chem. Biol.* **13**, 49–59.

Mentrup T., Häsler R., Fluhrer R., Saftig P., Schröder B. (2015) A Cell-Based Assay Reveals Nuclear Translocation of Intracellular Domains Released by SPPL Proteases. *Traffic* **16**, 871–92.

Mertins P., Qiao J. W., Patel J., Udeshi N. D., Clauser K. R., Mani D. R., Burgess M. W., Gillette M. A., Jaffe J. D., Carr S. A. (2013) Integrated proteomic analysis of post-translational modifications by serial enrichment. *Nat. Methods* **10**, 634–7.

Milward E. A., Papadopoulos R., Fuller S. J., Moir R. D., Small D., Beyreuther K., Masters C. L. (1992) The amyloid protein precursor of Alzheimer's disease is a mediator of the effects of nerve growth factor on neurite outgrowth. *Neuron* **9**, 129–37.

Munton R. P., Tweedie-Cullen R., Livingstone-Zatchej M., Weinandy F., Waidelich M., Longo D., Gehrig P., et al. (2007) Qualitative and quantitative analyses of protein phosphorylation in naive and stimulated mouse synaptosomal preparations. *Mol. Cell. Proteomics* **6**, 283–93.

Oliveira J. M., Henriques A. G., Martins F., Rebelo S., Cruz E Silva O. A. B. da (2015) Amyloid-β Modulates Both AβPP and Tau Phosphorylation. *J. Alzheimers. Dis.*

Olsen J. V, Vermeulen M., Santamaria A., Kumar C., Miller M. L., Jensen L. J., Gnad F., et al. (2010) Quantitative phosphoproteomics reveals widespread full phosphorylation site occupancy during mitosis. *Sci. Signal.* **3**, ra3.

Peng S., Fitzen M., Jörnvall H., Johansson J. (2010) The extracellular domain of Bri2 (ITM2B) binds the ABri peptide (1-23) and amyloid beta-peptide (Abeta1-40): Implications for Bri2 effects on processing of amyloid precursor protein and Abeta aggregation. *Biochem. Biophys. Res. Commun.* **393**, 356–61.

Peti W., Nairn A. C., Page R. (2013) Structural basis for protein phosphatase 1 regulation and specificity. *FEBS J.* **280**, 596–611.

Pittois K., Wauters J., Bossuyt P., Deleersnijder W., Merregaert J. (1999) Genomic organization and chromosomal localization of the Itm2a gene. *Mamm. Genome* **10**, 54–6.

Rebelo S., Domingues S. C., Santos M., Fardilha M., Esteves S. L. C., Vieira S. I., Vintém A. P. B., Wu W., Cruz E Silva E. F. da, Cruz E Silva O. A. B. da (2013) Identification of a novel complex AβPP:Fe65:PP1 that regulates AβPP Thr668 phosphorylation levels. *J. Alzheimers. Dis.* **35**, 761–75.

Rebelo S., Santos M., Martins F., Cruz E Silva E. F. da, Cruz E Silva O. A. B. da (2015) Protein Phosphatase 1 is a key player in nuclear events. *Cell. Signal.*

Rebelo S., Vieira S. I., Cruz E Silva E. F. da, Cruz E Silva O. A. B. da (2008) Monitoring "De Novo"APP synthesis by taking advantage of the reversible effect of cycloheximide. *Am. J. Alzheimers. Dis. Other Demen.* **23**, 602–8.

Rebelo S., Vieira S. I., Esselmann H., Wiltfang J., Cruz e Silva E. F. da, Cruz e Silva O. A. B. da (2007a) Tyrosine 687 phosphorylated Alzheimer's amyloid precursor protein is retained intracellularly and exhibits a decreased turnover rate. *Neurodegener. Dis.* **4**, 78–87.

Rebelo S., Vieira S. I., Esselmann H., Wiltfang J., Cruz e Silva E. F. da, Cruz e Silva O. A. B. da (2007b) Tyrosine 687 phosphorylated Alzheimer's amyloid precursor protein is retained intracellularly and exhibits a decreased turnover rate. *Neurodegener. Dis.* **4**, 78–87.

Rissoan M.-C., Duhen T., Bridon J.-M., Bendriss-Vermare N., Péronne C., Saint Vis B. de, Brière F., Bates E. E. M. (2002) Subtractive hybridization reveals the expression of immunoglobulin-like transcript 7, Eph-B1, granzyme B, and 3 novel transcripts in human plasmacytoid dendritic cells. *Blood* **100**, 3295–303.

Rocha J. F. da, Cruz E Silva O. A. B. da, Vieira S. I. (2015) Analysis of the amyloid precursor protein role in neuritogenesis reveals a biphasic SH-SY5Y neuronal cell differentiation model. *J. Neurochem.* **134**, 288–301.

Rostagno A., Tomidokoro Y., Lashley T., Ng D., Plant G., Holton J., Frangione B., Revesz T., Ghiso J. (2005) Chromosome 13 dementias. *Cell. Mol. Life Sci.* **62**, 1814–25.

Ruiz-León Y., Pascual A. (2003) Induction of tyrosine kinase receptor b by retinoic acid allows brain-derived neurotrophic factor-induced amyloid precursor protein gene expression in human SH-SY5Y neuroblastoma cells. *Neuroscience* **120**, 1019–26.

Sánchez-Pulido L., Devos D., Valencia A. (2002) BRICHOS: a conserved domain in proteins associated with dementia, respiratory distress and cancer. *Trends Biochem. Sci.* **27**, 329–32.

Santos M., Costa P., Martins F., Cruz E Silva E. F. da, Cruz E Silva O. A. B. da, Rebelo S. (2014a) LAP1 is a crucial protein for the maintenance of the nuclear envelope structure and cell cycle progression. *Mol. Cell. Biochem.* **399**, 143–53.

Santos M., Domingues S. C., Costa P., Muller T., Galozzi S., Marcus K., Cruz E Silva E. F. da, Cruz E Silva O. A. da, Rebelo S. (2014b) Identification of a Novel Human LAP1 Isoform That Is Regulated by Protein Phosphorylation. *PLoS One* **9**, e113732.

Santos M., Rebelo S., Kleeff P. J. M. Van, Kim C. E., Dauer W. T., Fardilha M., Cruz E Silva O. A. da, Cruz E Silva E. F. da (2013) The nuclear envelope protein, LAP1B, is a novel protein phosphatase 1 substrate. *PLoS One* **8**, e76788.

Sasaki K., Shima H., Kitagawa Y., Irino S., Sugimura T., Nagao M. (1990) Identification of members of the protein phosphatase 1 gene family in the rat and enhanced expression of protein phosphatase 1 alpha gene in rat hepatocellular carcinomas. *Jpn. J. Cancer Res.* **81**, 1272–80.

Schubert W., Prior R., Weidemann A., Dircksen H., Multhaup G., Masters C. L., Beyreuther K. (1991) Localization of Alzheimer beta A4 amyloid precursor protein at central and peripheral synaptic sites. *Brain Res.* **563**, 184–94.

Sharma K., D'Souza R. C. J., Tyanova S., Schaab C., Wiśniewski J. R., Cox J., Mann M. (2014) Ultradeep Human Phosphoproteome Reveals a Distinct Regulatory Nature of Tyr and Ser/Thr-Based Signaling.

Cell Rep. **8**, 1583–94.

Shiromizu T., Adachi J., Watanabe S., Murakami T., Kuga T., Muraoka S., Tomonaga T. (2013) Identification of missing proteins in the neXtProt database and unregistered phosphopeptides in the PhosphoSitePlus database as part of the Chromosome-centric Human Proteome Project. *J. Proteome Res*. **12**, 2414–21.

Tsachaki M., Ghiso J., Efthimiopoulos S. (2008) BRI2 as a central protein involved in neurodegeneration. *Biotechnol. J*. **3**, 1548–54.

Tsachaki M., Ghiso J., Rostagno A., Efthimiopoulos S. (2010) BRI2 homodimerizes with the involvement of intermolecular disulfide bonds. *Neurobiol. Aging* **31**, 88–98.

Tsachaki M., Serlidaki D., Fetani A., Zarkou V., Rozani I., Ghiso J., Efthimiopoulos S. (2011) Glycosylation of BRI2 on asparagine 170 is involved in its trafficking to the cell surface but not in its processing by furin or ADAM10. *Glycobiology* **21**, 1382–8.

Tweedie-Cullen R. Y., Reck J. M., Mansuy I. M. (2009) Comprehensive mapping of post-translational modifications on synaptic, nuclear, and histone proteins in the adult mouse brain. *J. Proteome Res*. **8**, 4966–82.

Vidal R., Calero M., Révész T., Plant G., Ghiso J., Frangione B. (2001) Sequence, genomic structure and tissue expression of Human BRI3, a member of the BRI gene family. *Gene* **266**, 95–102.

Vidal R., Frangione B., Rostagno A., Mead S., Révész T., Plant G., Ghiso J. (1999) A stop-codon mutation in the BRI gene associated with familial British dementia. *Nature* **399**, 776–81.

Vidal R., Revesz T., Rostagno A., Kim E., Holton J. L., Bek T., Bojsen-Møller M., et al. (2000) A decamer duplication in the 3' region of the BRI gene originates an amyloid peptide that is associated with dementia in a Danish kindred. *Proc. Natl. Acad. Sci. U. S. A*. **97**, 4920–5.

Vieira S. I., Rebelo S., Domingues S. C., Cruz e Silva E. F. da, Cruz e Silva O. A. B. da (2009) S655 phosphorylation enhances APP secretory traffic. *Mol. Cell. Biochem*. **328**, 145–54.

Vieira S. I., Rebelo S., Esselmann H., Wiltfang J., Lah J., Lane R., Small S. A., Gandy S., Cruz E Silva E. F. da, Cruz E Silva O. A. da (2010) Retrieval of the Alzheimer's amyloid precursor protein from the endosome to the TGN is S655 phosphorylation state-dependent and retromer-mediated. *Mol. Neurodegener*. **5**, 40.

Wakula P., Beullens M., Ceulemans H., Stalmans W., Bollen M. (2003) Degeneracy and function of the ubiquitous RVXF motif that mediates binding to protein phosphatase-1. *J. Biol. Chem*. **278**, 18817–23.

Watanabe T., Cruz e Silva E. F. da, Huang H.-B., Starkova N., Kwon Y.-G., Horiuchi A., Greengard P., Nairn A. C. (2003) Preparation and characterization of recombinant protein phosphatase 1. *Methods Enzymol*. **366**, 321–38.

Wickham L., Benjannet S., Marcinkiewicz E., Chretien M., Seidah N. G. (2005) Beta-amyloid protein converting enzyme 1 and brain-specific type II membrane protein BRI3: binding partners processed by furin. *J. Neurochem*. **92**, 93–102.

Wu H., Liu G., Li C., Zhao S. (2003) bri3, a novel gene, participates in tumor necrosis factor-alpha-induced cell death. *Biochem. Biophys. Res. Commun*. **311**, 518–24.

Supplementary Data

Table II.A.S 1 - Oligonucleotides used to generate BRI2 and BRI3 PP1BM mutants generated by Site-Directed Mutagenesis.

Plasmid Name	Template DNA	Oligonucleotide sequence (5´-3´)	
		FW	**RV**
pCMV-Myc-BRI2 KVTA	pCMV-Myc-BRI2	ATGGTGAAGGTGACGGCCAACTCCGCTCTG	CAGAGCGGAGTTGGCCGTCACCTTCACCAT
pCMV-Myc-BRI2 KATA	pCMV-Myc-BRI2 KVTA	ATGGTGAAGGCGACGGCCAACTCCGCTCTG	CAGAGCGGAGTTGGCCGTCGCCTTCACCAT
pCMV-Myc-BRI3 KISA	pCMV-Myc-BRI3	GTGAAGATTAGCGCCCAGCCCGCCGTGGCTG	CAGCCACGGCGGGCTGGGCGCTAATCTTCAC
pCMV-Myc-BRI3 AISA	pCMV-Myc-BRI3 KISA	ATGGTGGCGATTAGCGCCCAGCCCGCCGT	ACGGCGGGCTGGGCGCTAATCGCCAC CAT

CHAPTER II.B – FUNCTIONAL CHARACTERIZATION OF THE BRI2:PP1 COMPLEX

"BRI2 processing and its neuritogenic role are modulated by protein phosphatase 1 complexing"

Filipa Martins[1], Joana B. Serrano[1], Thorsten Müller[2], Odete A. B. da Cruz e Silva[1] and Sandra Rebelo[1]

[1] Neuroscience and Signalling Laboratory, Department of Medical Sciences, Institute of Biomedicine-iBiMED, University of Aveiro, 3810-193 Aveiro, Portugal
[2] Leibniz-Institut für Analytische Wissenschaften -ISAS- e. V., Dortmund, Germany

Corresponding author: Sandra Rebelo, Neuroscience and Signalling Laboratory, Department of Medical Sciences, Institute of Biomedicine-iBiMED, University of Aveiro, 3810-193 Aveiro, Portugal, Tel: +351-924406306, E-mail: srebelo@ua.pt

Martins F, Serrano JB, Müller T, da Cruz e Silva OCS and Rebelo S (2017). BRI2 processing and its neuritogenic role are modulated by protein phosphatase 1 complexing. *Journal of Cellular Biochemistry*, in press. doi: 10.1002/jcb.25925

Abstract

BRI2 is a ubiquitously expressed type-II transmembrane phosphoprotein. BRI2 undergoes proteolytic processing into secreted fragments and during the maturation process it suffers post-translational modifications. Of particular relevance, BRI2 is a protein phosphatase 1 (PP1) interacting protein, where PP1 is able to dephosphorylate the former. Further, disruption of the BRI2:PP1 complex, using BRI2 PP1 binding motif mutants, leads to increased BRI2 phosphorylation levels. However, the physiological function of BRI2 remains elusive; although findings suggest a role in neurite outgrowth and neuronal differentiation.

In the work here presented, BRI2 expression during neuronal development was investigated. This increases during neuronal differentiation and an increase in its proteolytic processing is also evident. To elucidate the importance of BRI2 phosphorylation for both proteolytic processing and neuritogenesis, SH-SY5Y cells were transfected with the BRI2 PP1 binding motif mutant constructs. For the first time, it was possible to show that BRI2 phosphorylation is an important regulatory mechanism for its proteolytic processing and its neuritogenic role. Furthermore, by modulating BRI2 processing using an ADAM10 inhibitor, a dual role for BRI2 in neurite outgrowth is suggested: phosphorylated full-length BRI2 appears to be important for the formation of neuritic processes, and BRI2 NTF promotes neurite elongation. This work significantly contributed to the understanding of the physiological function of BRI2 and its regulation by protein phosphorylation.

II.B.1. Introduction

Reversible protein phosphorylation is a major regulatory mechanism for controlling several intracellular events in eukaryotic cells. PP1 catalyzes the majority of protein dephosphorylation events and it is involved in various cellular functions (Bollen *et al*. 2010; Heroes *et al*. 2013). PP1 functional diversity is largely determined by the binding of its catalytic subunit to different specific regulatory subunits. For instance, when associated with its regulatory proteins, PP1 is involved in neuronal responses at several levels; neurotransmission, neurite outgrowth and synapse formation (Shi 2009; Wakula *et al*. 2003; Rebelo *et al*. 2015; da Cruz e Silva *et al*. 2004).

BRI2 is a ubiquitously expressed type-II transmembrane protein. In the brain, it is particularly abundant in the hippocampus and cerebellum, when compared to the cerebral cortex (Vidal *et al*. 1999). Interestingly, BRI2 undergoes proteolytic processing resulting in the formation of several secreted peptides. Cleavage in its ectodomain by a furin-like protease results in the release of a C-terminal peptide of 23 amino acids and the remaining membrane-bound N-terminal portion was identified as the mature form of BRI2. Mature BRI2 is further cleaved by disintegrin and metalloproteinase domain-containing protein 10 (ADAM10) resulting in the secretion of a 25 kDa peptide which contains the conserved BRICHOS domain. The remaining membrane-associated N-terminal fragment (NTF) can be further processed by SPPL2a/b; releasing an intracellular domain (BRI2 ICD) to the cytosol and a secreted C-terminal domain (Choi *et al*. 2004; Tsachaki *et al*. 2008; Lashley *et al*. 2008; Vidal *et al*. 1999). Moreover, during the maturation process in the cis-medial Golgi, the protein suffers post-translational modifications, such as glycosylation and phosphorylation, leading to various forms of BRI2 that may have different cellular locations and physiological functions (Martins *et al*. 2016; Lashley *et al*. 2008; Akiyama *et al*. 2004; Del Campo and Teunissen 2014; Tsachaki *et al*. 2011). In fact, four phosphorylatable residues have already been confirmed for BRI2: Ser8, Tyr76, Tyr112 and Tyr165 (Sharma *et al*. 2014; Demirkan *et al*. 2011). The precise physiological role of BRI2 remains elusive, however, some functions have been ascribed. Recently, using several techniques including BRI2 PP1-binding motif (PP1-BM) mutant constructs (Myc-BRI2 KVTA and Myc-BRI2 KATA constructs), we established that BRI2 is a novel PP1 interacting protein, thus determining the importance of the RVxF motif (^{3}KVTF^{6}) for BRI2:PP1 complex formation. Additionally, by using the Myc-BRI2 KATA mutant it was possible to completely abolish the interaction between BRI2 and PP1 and as a consequence, the BRI2 mutants mimic an irreversibly phosphorylated state in which PP1 is no longer able to dephosphorylate it. Interestingly, an increase in neurite outgrowth was observed when these mutants were expressed in SH-SY5Y cells (Martins *et al*. 2016). Moreover, BRI2 morphological distribution within proximal dendrites and axons, as well as cell bodies, and its presence in some pathological structures such as dystrophic neurites in senile plaques, suggests that BRI2 is transported along the axons' processes

(Akiyama *et al*. 2004; Martins *et al*. 2016). Thus, it is plausible to assume that BRI2 is involved in the plasticity of neuronal processes and that it may also have a role at the nerve terminals (Akiyama *et al*. 2004; Choi *et al*. 2004). In fact, it was demonstrated that BRI2 promotes neurite outgrowth in BRI2 overexpressing human neuronal cells (Choi *et al*. 2004).

Neuritogenesis is a complex and dynamic phenomenon in which neurites first emerge from the cell body and then begin extending away. These neurites are critical to generate the axons and dendrites of mature neurons that will further compose the adult brain. Therefore, neurite outgrowth is considered a prerequisite and early event for neuronal differentiation that involves several highly dynamic morphogenetic processes including neurite initiation, elongation, branching, growth cone motility, and collapse (da Silva and Dotti 2002). Interestingly, each of these phases involves morphological changes that are determined mostly by the regulation of specific signaling cascades, which in turn controls neuronal cytoskeletal dynamics, trafficking and also cellular adhesion.

Thus, the aim of this study was to explore the functional relevance of the BRI2 phosphorylation on both BRI2 proteolytic processing and its neuritogenic role. BRI2 processing was monitored and modulated using an ADAM10 inhibitor in SH-SY5Y cells transfected with BRI2 PP1 binding motif mutants. Concomitantly a detailed characterization of the alterations related with neuritogenic phenotype was performed. BRI2 phosphorylation was further modulated using okadaic acid, a well-established phosphatase inhibitor. Our results suggest a strong relationship between BRI2 phosphorylation, namely PP1 dephosphorylation, and its processing. Based on the findings here presented, a role for the BRI2:PP1 complex in neurite outgrowth and neuronal differentiation is proposed, whereby phosphorylated full-length BRI2 seems to be crucial for the formation of neurites while increased BRI2 NTF assists neurite elongation.

II.B.2. Materials and Methods

II.B.2.1. Cell line culture and transfection

The SH-SY5Y human neuroblastoma cell line was maintained in Minimal Essential Medium /F-12 Nutrient Mixture (Gibco) using procedures previously described (Santos *et al*. 2013). Transient transfections of SH-SY5Y cells with the following constructs: Myc-BRI2; Myc-BRI2 ^{3}KVTA^{6} and Myc-BRI2 ^{3}KATA^{6} (mutated in the consensus PP1 binding motif ^{3}KVTF^{6}; PP1-BM mutants) were performed using TurboFect reagent (ThermoFisher Scientific) according to the manufacturer's protocols. These constructs were previously produced and described (Martins *et al*. 2016).

II.B.2.2. Neuronal primary cultures time-course

Pregnant Wistar rats (12-16 weeks) were obtained from Harlan Interfaune Ibérica, SL. All experimental procedures followed the European legislation for animal experimentation

(2010/63/EU) and our Institutional Animal Care and Use Committee (IACUC): Comissão Responsável pela Experimentação e Bem-Estar Animal (CREBEA), approved the procedures performed. Essentially, the E18 pregnant rats were euthanized, by cervical stretching following decapitation and the 18 days rat embryos were decapitated and used for the isolation of cortex. This is within the European law (Council Directive 86/609/EEC), and during this procedure, all steps were taken to ameliorate animal suffering. Rat cortical primary cultures were established as previously described (Santos *et al*. 2014). Briefly, after dissociation with 0.45 mg/ml trypsin, cells were plated onto poly-D-lysine-coated dishes at a density of $1.06x10^5$ cells/ cm^2 in B27-supplemented Neurobasal medium (Gibco), a serum-free medium combination. The medium was supplemented with glutamine (0.5 mM) and gentamicin (60 mg/ml). Cultures were maintained in an atmosphere of 5% CO^2 at 37˚C. The cortical neurons were collected every two days, until 14 days in vitro (DIV), and further analyzed by SDS-PAGE and immunoblotting.

II.B.2.3. Modulation of BRI2 phosphorylation levels

SH-SY5Y cells were transfected with Myc-BRI2 and treated with 0.25 nM or 500 nM okadaic acid (OA) for 3 hours, and controls were exposed to vehicle (DMSO) for the same period. The cells were further harvested and processed for SDS-PAGE.

II.B.2.4. Modulation of BRI2 processing

SH-SY5Y transiently transfected cells were incubated for 48 hours with 10 μM of the GI254023X inhibitor, and controls were exposed to vehicle (DMSO) for the same period. GI254023X is a potent and selective ADAM10 metalloproteinase inhibitor that hinders BRI2 cleavage into BRI2 NTF. The cells were further processed for SDS-PAGE, and immunocytochemistry followed by morphometric analysis.

II.B.2.5. SDS-PAGE and immunoblotting

Cells were harvested using 1% boiling SDS and subsequently collected. Cell lysates were sonicated for 30 s and the total protein content was determined using Pierce´s BCA kit (ThermoFisher Scientific). Mass-normalized samples were resolved on 5-20% gradient SDS-PAGE and electrophoretically transferred onto nitrocellulose membranes. These were initially stained with Ponceau S in order to assess gel loading, as previously described (Santos *et al*. 2015a; Klein *et al*. 1995; Romero-Calvo *et al*. 2010). Primary antibodies used were: mouse monoclonal anti-Myc (Cell Signaling Technology), mouse monoclonal anti-BRI2 (raised against amino acids 1-54 at the N-terminus of ITM2B of human origin; Santa Cruz Biotechnology), rabbit polyclonal anti-PP1γ (da Cruz e Silva *et al*. 1995), rabbit polyclonal anti-PP1α (da Cruz e Silva *et al*. 1995), mouse monoclonal

anti-acetylated α-tubulin (Sigma-Aldrich), mouse monoclonal anti-synaptophysin (Synaptic Systems GmbH), mouse monoclonal anti-β-III tubulin (Promega) and mouse monoclonal anti-β-actin (Novus Biologicals). These primary antibodies were incubated for 2 hours (anti-β-actin, anti-acetylated α-tubulin, and anti-synaptophysin) to overnight (anti-Myc, anti-BRI2, anti-PP1γ and anti-PP1α). Detection was achieved using anti-mouse or anti-rabbit horseradish peroxidase-linked secondary antibodies (GE Healthcare) and proteins visualized by an enhanced chemiluminescence-based system.

II.B.2.6. Morphological analysis by confocal microscopy

For immunocytochemistry analysis, cells grown on coverslips were fixed using 4% paraformaldehyde and permeabilized with 0.2% TRITON X-100 (Rebelo *et al*. 2008). The following primary antibodies and secondary antibodies were used and incubated for 1hr to 2hrs: mouse monoclonal anti-Myc (Cell Signaling Technology), rabbit polyclonal anti-Myc (Cell Signaling Technology); mouse monoclonal acetylated α-tubulin (Sigma-Aldrich); Alexa Fluor® 488, 594 and 405- conjugated IgGs (Molecular Probes). To stain filamentous actin (F-actin) Alexa Fluor® 568 Phalloidin (Molecular Probes) in 1% bovine serum albumin phosphate-buffered saline was added for 30 min. Preparations were mounted with Vectashield® media with or without DAPI (Vector Laboratories) and visualized using an LSM510-Meta confocal microscope (Carl Zeiss Microimaging GmbH) and a 63x/1.4 oil immersion objective. Microphotographs were acquired in a sole section in the Z-axis (xy mode) and represent a mean of 16 scans. Morphometric analyses of SH-SY5Y cells were performed using ImageJ software (U. S. National Institutes of Health). The total numbers of cellular processes emerging from the cell were counted and the length of the longest process was measured. Processes were categorized as indicated: '< 20 μM' – processes shorter than '20 μM; 20-35 μM' – processes longer than 20 μM but shorter than 35 μM (also named pre-neurites); '> 35 μM' – processes longer than 35 μM (also named neurites, since they are longer than two cell body lengths) (da Rocha *et al*. 2015; Dehmelt and Halpain 2004). Data were expressed as the number of processes per cell and the percentages of cells that possess each of the categories of the processes. The fluorescence intensity of F-actin staining was also quantified using the ImageJ software and data were expressed as the ratio of the fluorescence intensity of the transfected cells per the fluorescence intensity of the non-transfected cells (Santos *et al*. 2015b).

II.B.2.7. Data analysis and statistics

Ponceau-S stained membranes and autoradiograms were scanned (GS-800 calibrated imaging densitometer; Bio-Rad) and protein bands quantified using the Image Lab software. All data were corrected relative to loading control (Ponceau-S) and were expressed as mean ± SEM (standard error)

of at least three independent experiments. Statistical significance analysis was conducted (GraphPad Prism6 software) and, when appropriate, data were analyzed using unpaired two-tailed student's t-test and one-way ANOVA followed by the Dunnett's multi-comparisons test, for comparison of data with control values.

II.B.3. Results

II.B.3.1. BRI2 protein levels during neuronal development

Given our previous results and the work of Choi and colleagues (Choi *et al*. 2004), BRI2 seems to have a relevant but undisclosed role in neuritogenesis, which incited the work here presented. Hence, BRI2 intracellular levels were assessed during neuronal development (establishment of rat cortical primary cultures up to 14 DIV). The data showed that full-length BRI2 levels significantly increased during neuronal development (Figure II.B.1) reaching a maximum level between 10 DIV and 12 DIV and decreased slightly at 14 DIV. Of note, the mature BRI2 was more evident upon 10 DIV, which is consistent with a robust increase in the BRI2 NTF (Figure II.B.1). These results indicated that BRI2 is highly expressed in functional mature neurons since its intracellular levels correlated well with synaptophysin levels, a pre-synaptic marker. Interestingly, the full-length BRI2 and BRI2 NTF levels also seemed to correlate with the levels of a neuron-specific and well-characterized marker of neuronal differentiation, β-III tubulin. Both PP1γ and PP1α were used as additional differentiation markers confirming that BRI2 expression appeared to correlate with neuronal differentiation. Ponceau S staining was used as a loading control, as previously described (Romero-Calvo *et al*. 2010; Klein *et al*. 1995; Santos *et al*. 2014) (Figure II.B.1).

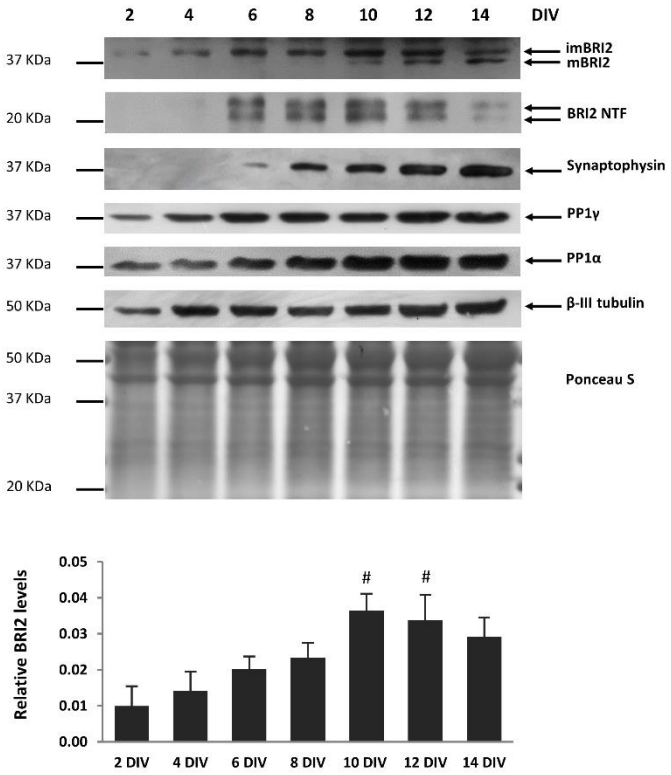

Figure II.B. 1 - BRI2 expression during neuronal differentiation. Endogenous BRI2 levels were detected for 14 days in vitro (DIV), during the establishment of rat cortical primary neurons from 2 DIV to 14 DIV. Synaptophysin, PP1α, PP1γ, and β-III tubulin levels of expression are also presented. Ponceau S staining was used to assess gel loading. The quantitative data for relative BRI2 levels are presented graphically on the bottom as mean ± SEM of 3 independent experiments. # $p < 0.05$ for comparisons to 2DIV condition by using one-way ANOVA followed by the Dunnett's test. imBRI2, immature BRI2; mBRI2, mature BRI2; BRI2 NTF, BRI2 N-terminal fragment.

II.B.3.2. BRI2 processing is modulated by protein phosphatase 1 binding

Given that both BRI2 and BRI2 NTFs levels in cortical neurons seem to correlate with neuronal differentiation we hypothesized that the same was occurring with our previously described BRI2 PP1-BM mutants. Therefore, BRI2 processing was monitored in SH-SY5Y cells transiently transfected with the Myc-BRI2, Myc-BRI2 KVTA and Myc-BRI2 KATA constructs (BRI2 PP1-BM mutants) for 24 hrs and 48 hrs (Figure II.B.2). Essentially, at the 24hrs time point, an intracellular accumulation of BRI2 NTFs with the Myc-BRI2 KATA construct was observed, resulting from an increase in its processing (Figure II.B.2A). The result was quite robust at the 48hrs time point, where a significant increase of the BRI2 NTFs was observed with both mutants, Myc-BRI2 KVTA ($p<0.05$ by the one-way ANOVA) and Myc-BRI2 KATA ($p<0.001$ by the one-way ANOVA). Additionally, given that during neuronal development there appears to be an increase in BRI2 NTF, which correlates with an increase in β-III tubulin (Figure II.B.1), the levels of the latter protein were also assessed. The neuron-specific β-III tubulin, which is a well-established SH-SY5Y differentiation

marker (Dwane *et al*. 2013; Forster *et al*. 2016), was present in non-transfected cells, but the levels increased in cells transfected with either the Myc-BRI2 or the BRI2 PP1-BM constructs. After 24hrs of transfection, the levels of β-III tubulin showed a tendency to increase, particularly with the BRI2 PP1-BM (Figure II.B.2B). At the 48 hrs time point, this tendency rendered a significant increase in β-III tubulin levels with the BRI2 PP1-BM mutant constructs ($p<0.001$ by the one-way ANOVA for Myc-BRI2 KVTA and $p<0.0001$ by the one-way ANOVA for Myc-BRI2 KATA; Figure II.B.2B), which suggests the appearance of neuronal features.

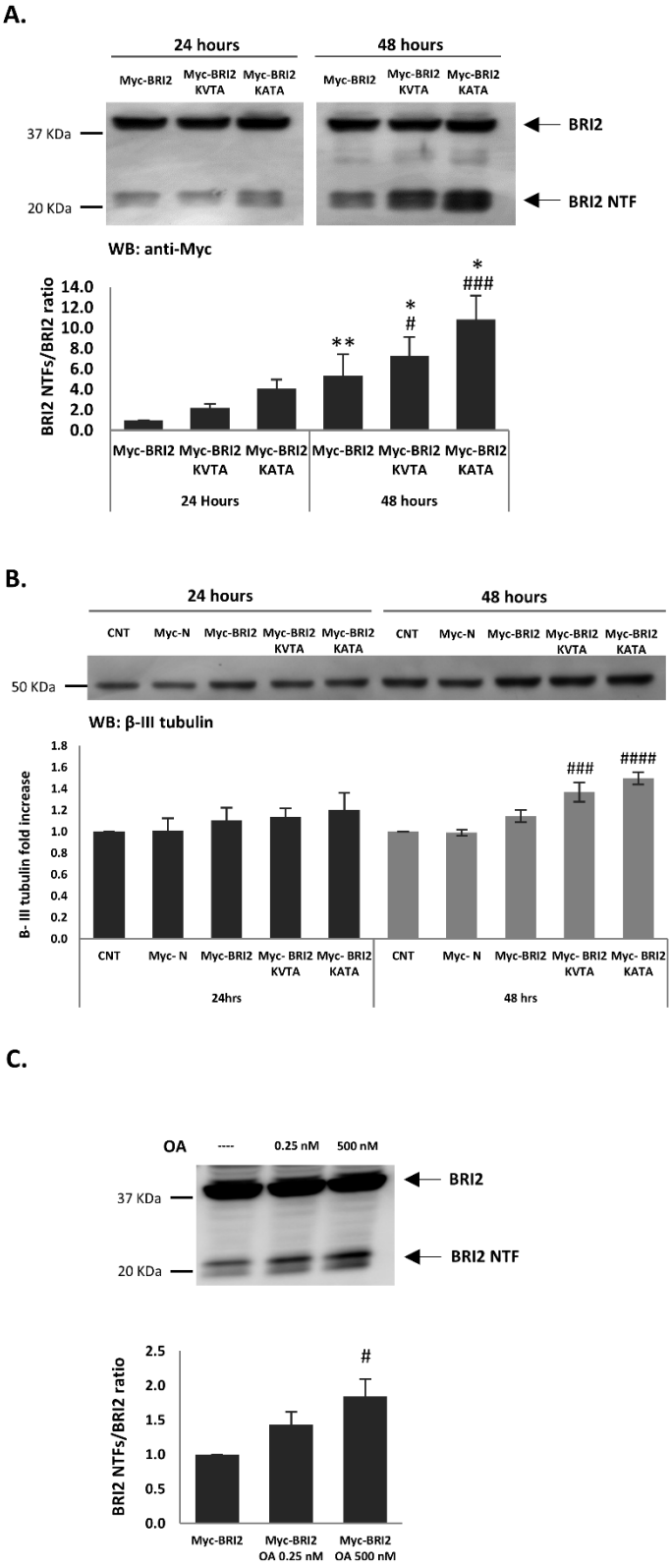

Figure II.B. 2 - BRI2 processing analysis in SH-SY5Y cells transfected with Myc-BRI2 constructs. Analysis of Myc-tagged BRI2 proteins by immunoblotting were performed using a Myc monoclonal antibody. In order to assess BRI2 processing, the ratio of BRI2 N-terminal fragments (BRI2 NTFs) with BRI2 full-length protein was calculated. Of note, the same results were obtained when an N-terminal BRI2 antibody was used (data not shown). **A -**SH-SY5Y cells were

transfected with Myc-BRI2, Myc-BRI2 KVTA and Myc-BRI2 KATA constructs for 24 hrs and 48 hrs. The quantitative data are presented as mean ± SEM of at least 4 independent experiments. #/* $p < 0.05$, ** $p < 0.01$, ### $p < 0.001$. Statistical symbols: (#) for comparisons with the Myc-BRI2 24 hrs by using one-way ANOVA followed by the Dunnett's test; (*) for comparisons between each construct at 24 hrs and 48 hrs by using t-student´s test. **B** – SH-SY5Y cells were transfected with Myc-BRI2, Myc-BRI2 KVTA and Myc-BRI2 KATA constructs for 24 hrs and 48 hrs and analyzed the β-III tubulin levels by immunoblotting. The protein levels were plotted as fold increases of CNT for both 24 hrs and 48 hrs. The quantitative data are presented as mean ± SEM of at least 4 independent experiments. ### $p < 0.001$, #### $p < 0.001$ for comparisons to 48 hrs CNT by using one-way ANOVA followed by the Dunnett's test**.** BRI2 NTF, BRI2 N-terminal fragment; CNT, non-transfected control. **C** - SH-SY5Y cells were transfected with Myc-BRI2 were incubated with 0, 0.25 or 500 nM of okadaic acid (OA) for 3 hours. The quantitative data are presented as mean ± SEM of 3 independent experiments. # $p < 0.05$, for comparisons with the Myc-BRI2 without okadaic acid by using one-way ANOVA followed by the Dunnett's test.

Our previous studies using a phos-tag SDS-PAGE approach revealed an increase in the BRI2 phosphorylation levels upon treatment with okadaic acid (OA), a protein phosphatase inhibitor. Remarkably, higher BRI2 phosphorylation levels were achieved when PP1 was inhibited (higher OA concentration - OA 500 nM) this is partially reversed when purified PP1 protein is added (Martins *et al*. 2016). Therefore, in order to clearly determine if protein phosphorylation is an important regulatory mechanism of BRI2 processing, particularly by involving PP1 mediated dephosphorylation, SH-SY5Y cells transfected with the Myc-BRI2 construct, were incubated with two concentrations of OA, for 3 hours. In fact, upon OA treatment an increase in the BRI2 processing (BRI2 NTF/BRI2 ratio) was achieved, being only significant when PP1 was inhibited (OA 500 nM) (Figure II.B.2C).

II.B.3.3. Characterization of the BRI2 neuritogenic-related alterations

A detailed cellular morphometric analysis was performed upon transient transfection of SH-SY5Y cells, for 24hrs and 48hrs, with wild-type BRI2 and BRI2 PP1-BM constructs. Overall, there was an increase in the total number of cellular processes upon 48hrs of transfection with Myc-BRI2 (Figure II.B.3A1), Myc-BRI2 KVTA (Figure II.B.3A2) and Myc-BRI2 KATA (Figure II.B.3A3), when compared with the 24 hrs time point. The mean value of cellular processes significantly increased from 2.5 to 7.3 ($p<0.01$ by the two-tailed Student's t-test) for Myc-BRI2, from 4.6 to 15.8 ($p<0.001$ by the two-tailed Student's t-test) for Myc-BRI2 KVTA and from 14.8 to 36.9 ($p<0.01$ by the two-tailed Student's t-test) for Myc-BRI2 KATA (Figure II.B.3A1, 3A.2 and 3A.3). Neuritogenesis was further evaluated by scoring the length of the longest cellular process presented by the transfected cells as described in the materials and methods sections. Upon 24hrs of transfection with Myc-BRI2, more than 86 % of the cells analyzed had processes shorter than 20 μm, while only 9% and 4.5 % of cells presented processes that were between 20-35 μm and > 35 μm, respectively (Figure II.B.3B). The phenotype observed with Myc-BRI2 KVTA was slightly different, presenting a higher percentage of cells with pre-neurites and neurites (Figure II.B.3B). However, the phenotype changed dramatically with the Myc-BRI2 KATA displaying a significant decrease in the number of processes

shorter than 20 μm ($p<0.001$ by the one-way ANOVA) and a concomitant increase in the number of processes with 20-35 μm and longer > 35 μm ($p<0.01$ and $p<0.01$, respectively, by the one-way ANOVA) when compared with Myc-BRI2 (Figure II.B.3B). Interestingly, upon 48hrs of transfection, the results were quite different from those observed at the 24hrs time point. With Myc-BRI2 a significant decrease in the % of cells with smaller length processes (<20 μm) was observed ($p<0.001$ by the two-tailed Student's t-test), while for the other two categories of processes the percentage significantly increased (pre-neurites and neurites; $p<0.001$ by the two-tailed Student's t-test) (Figure II.B.3B). A dramatic alteration was evident with the Myc-BRI2 KVTA and Myc-BRI2 KATA mutants; where a significant decrease in the number of processes shorter than 20 μm was scored ($p<0.0001$ by the two-tailed Student's t-test), as well as a corresponding increase in the processes with a longer length, particularly those more than 35 μm ($p<0.05$ for Myc-BRI2 KVTA and $p<0.001$ for Myc-BRI2 KATA, by the two-tailed Student's t-test) (Figure II.B.3B).

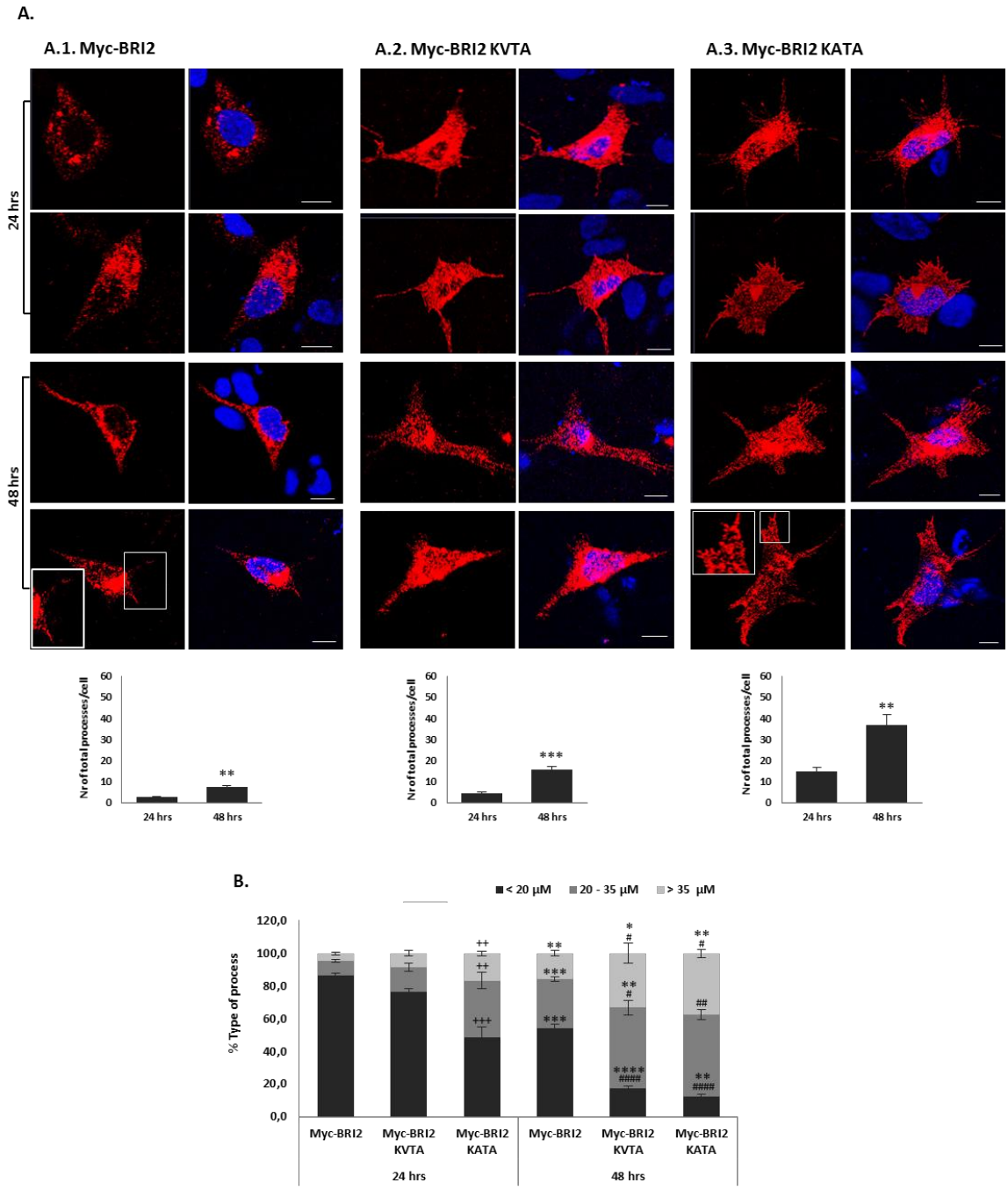

Figure II.B. 3 - Morphometric analysis of the cellular processes in SH-SY5Y cells transfected with Myc-BRI2, Myc-BRI2 KVTA and Myc-BRI2 KATA constructs. A- Subcellular distribution of Myc-BRI2 (A.1), Myc-BRI2 KVTA (A.2) and Myc-BRI2 KATA (A.3) and the respective quantitative analysis of the total number of processes in SH-SY5Y cells transfected for 24 hrs and 48 hrs. Quantitative data are presented as mean ± SEM and obtained by analyzing at least 30 cells per condition from three independent experiments. ** $p < 0.01$, *** $p < 0.001$ for comparisons between 24 hrs and 48 hrs, by using t-student´s test. Bars, 10 µm. **B** – Percentage of cells with each type of processes in SH-SY5Y cells transfected with Myc-BRI2, Myc-BRI2 KVTA and Myc-BRI2 KATA constructs for 24 hrs and 48 hrs. Processes were categorized according to their lengths, and the percentages of processes with length inferior to 20 µm (< 20 µm), pre-neurites (20–35 µm) and neurites (≥ 35 µm) calculated out of the total number of processes. The quantitative data are presented as mean ± SEM and was obtained by analyzing at least 30 cells per condition from three independent experiments. #/* $p < 0.05$, ++/##/** $p < 0.01$, +++/*** $p < 0.001$, #### $p < 0.0001$. Statistical symbols: (+) for comparisons to Myc-BRI2 at 24 hrs by using one-way ANOVA followed by the Dunnett's test; (#) for comparisons to Myc-BRI2 at 48 hrs by using one-way ANOVA followed by the Dunnett's test; (*) for comparisons between each construct at 24 hrs and 48 hrs by using t-student´s test.

Given that the morphological alterations observed when BRI2 became phosphorylated (BRI2 PP1-BM mutants) are consistent with neurite outgrowth and neuronal differentiation, cytoskeleton alterations were subsequently investigated. Essentially, the levels of acetylated α-tubulin (microtubules (MT) stabilization), β-actin and F-actin (actin remodeling) were evaluated upon transfection with Myc-BRI2 and both BRI2 PP1-BM mutants for 24 hrs and 48 hrs (Figure II.B.4 and Figure II.B.5). Acetylated α-tubulin levels (an indirect measure of MTs stabilization) were significantly lower with both mutants, Myc-BRI2 KVTA ($p<0.05$ by the one-way ANOVA) and Myc-BRI2 KATA ($p<0.05$ by the one-way ANOVA) after 24 hrs of transfection (Figure II.B.4A). This decrease correlates with the requirement of MTs instability, during the initial steps of neuritogenesis, and is associated with the emergence of processes and the elongation of smaller processes (da Rocha *et al*. 2015). Interestingly, after 48 hrs of transfection, the acetylated α-tubulin levels increased significantly for Myc-BRI2 KVTA ($p<0.05$ by the one-way ANOVA) and Myc-BRI2 KATA ($p<0.01$ by the one-way ANOVA) constructs, which are associated with the longer neuritic elongation observed in these conditions (Figure II.B.4A). Upon evaluating the levels of β-actin a slight increase, at 24 hrs and 48 hrs of transfection with both BRI2 PP1-BM constructs, was observed (Figure II.B.4B).

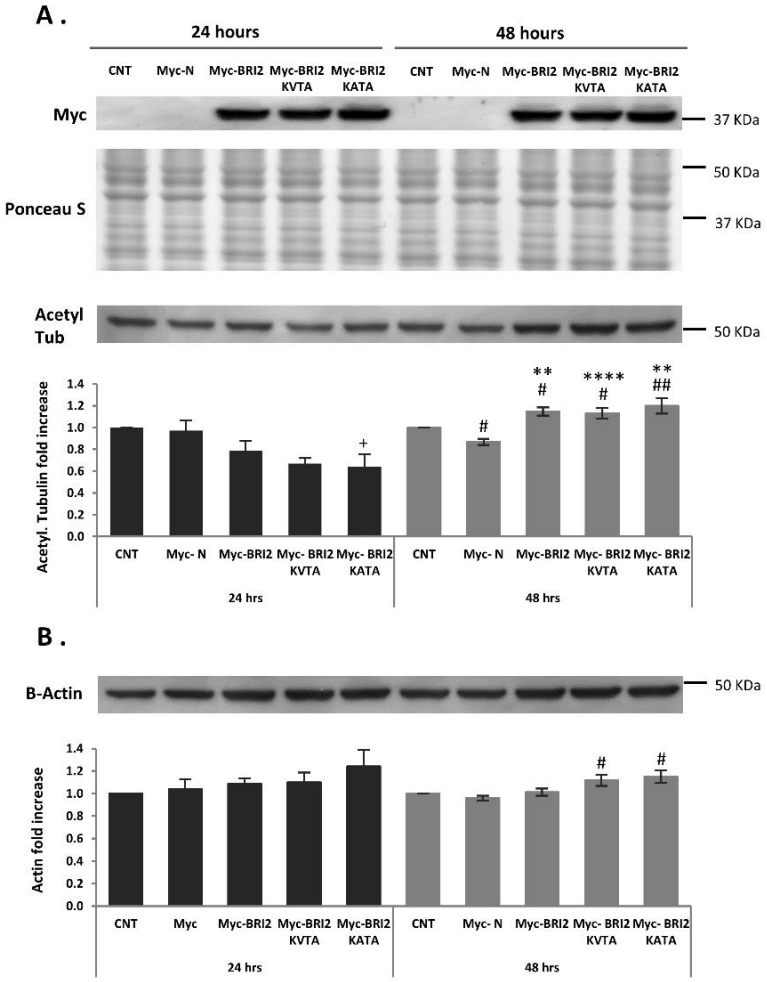

Figure II.B.4 - Profiles of acetylated α-tubulin and β-actin in SH-SY5Y cells transfected with Myc-BRI2, Myc-BRI2 KVTA and Myc-BRI2 KATA constructs. Analysis of acetylated α-tubulin (**A**) and β-actin (**B**) levels by immunoblotting in SH-SY5Y transfected cells with Myc-BRI2, Myc-BRI2 KVTA and Myc-BRI2 KATA constructs for 24 hrs and 48 hrs. The protein levels were plotted as fold increases of CNT for both 24 hrs and 48 hrs. The quantitative data are presented as mean ± SEM of at least 4 independent experiments. +/# $p < 0.05$, ##/** $p < 0.01$, **** $p < 0.0001$. Statistical symbols: (+) for comparisons to CNT at 24 hrs by using one-way ANOVA followed by the Dunnett's test; (#) for comparisons to CNT at 48 hrs by using one-way ANOVA followed by the Dunnett's test; (*) for comparisons between each construct at 24 hrs and 48 hrs by using t-student´s test. CNT, non-transfected control; Acetyl Tub, acetylated α-tubulin.

Furthermore, we investigated actin remodeling by immunocytochemistry using F-actin as a specific marker of actin polymerization, thereby monitoring actin dynamics (Figure II.B.5). Overall, it was clear that the F-actin levels in transfected cells were higher than in the non-transfected cells for both time points analyzed (24 hrs and 48 hrs of transfection; Figure II.B.5A and B, respectively). Quantification clearly indicated that F-actin levels significantly increased with both Myc-BRI2 mutants ($p<0.0001$ by the one-way ANOVA for Myc-BRI2 KVTA, and $p<0.0001$ by the one-way ANOVA for Myc-BRI2 KATA) at the 24 hrs time point compared with Myc-BRI2 (Figure II.B.5A and C). This increase was also observed with both mutants at the 48 hrs time point (Figure II.B.5B

and C), being significant for the Myc-BRI2 KATA mutant ($p<0.05$ by the one-way ANOVA). Consistent with the previous results, we observed decreased α-tubulin acetylation upon 24 hrs of transfection and an increase after 48 hrs (Figure II.B.5A and B).

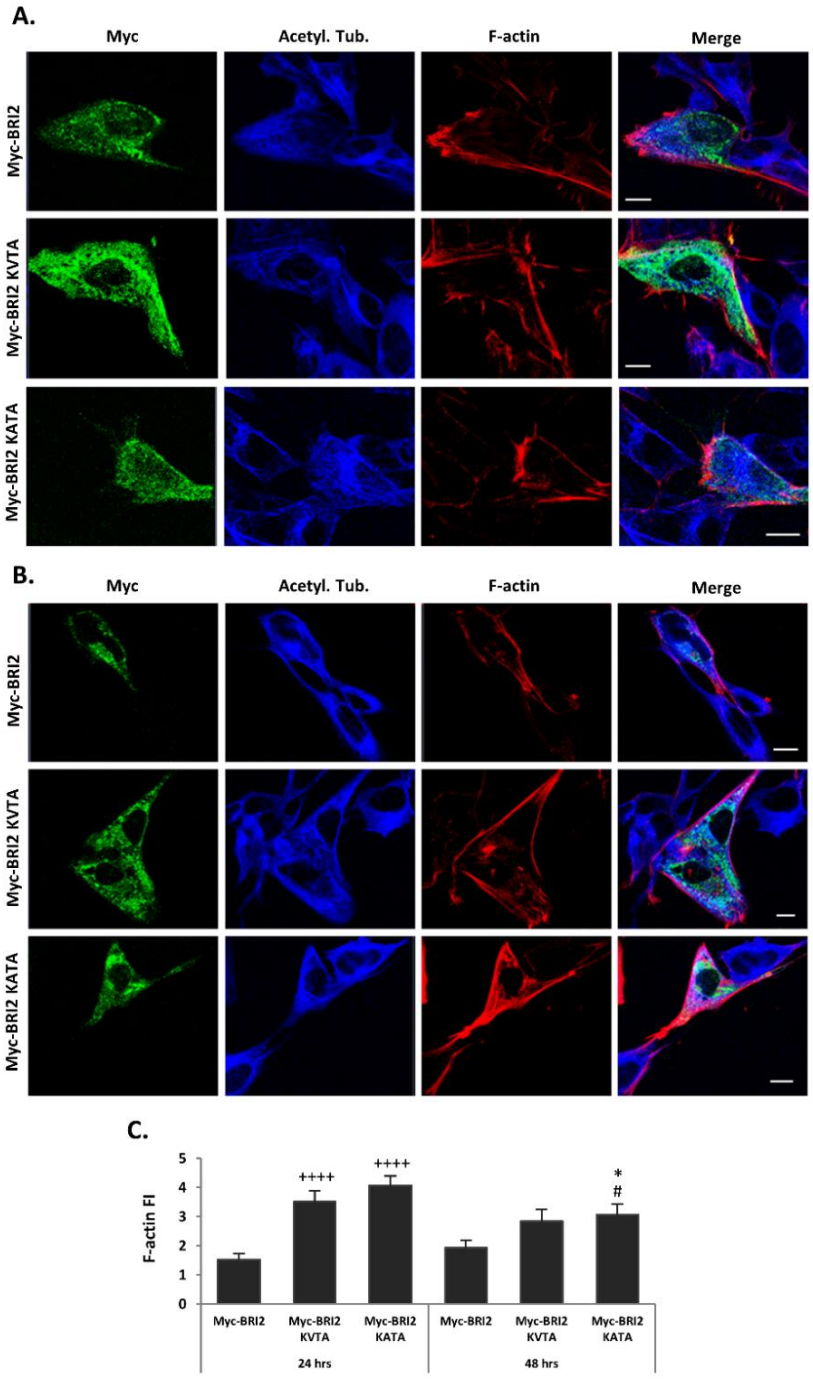

Figure II.B. 5 - Cellular localization of Myc-tagged BRI2 proteins, acetylated α-tubulin, and F-actin in SH-SY5Y cells transfected with Myc-BRI2, Myc-BRI2 KVTA and Myc-BRI2 KATA constructs. Subcellular localization of Myc-tagged BRI2 (green) and acetylated α-tubulin (blue) were analyzed by immunocytochemistry analysis using the polyclonal Myc-tag and monoclonal acetylated α-tubulin antibodies upon 24 hrs (**A**) or 48 hrs (**B**) of SH-SY5Y cells transfection. F-actin was probed with red fluorescent-labelled phalloidin. **C**- The quantitative data for F-actin stain are

presented as mean ± SEM of the ratio of the fluorescence intensity of the transfected cells per the fluorescence intensity of the non-transfected cells (n = 30). #/* $p < 0.05$, ++++ $p < 0.0001$. Statistical symbols: (+) for comparisons to Myc-BRI2 at 24 hrs by using one-way ANOVA followed by the Dunnett's test; (#) for comparisons to Myc-BRI2 at 48 hrs by using one-way ANOVA followed by the Dunnett's test; (*) for comparisons between each construct at 24 hrs and 48 hrs by using t-student´s test. Bars, 10 µm. Acetyl. Tub., acetylated α-tubulin; F-actin FI, F-actin fluorescence intensity.

II.B.3.4. Modulating BRI2 NTF levels using an ADAM10 inhibitor

As presented above, it was possible to establish that BRI2 phosphorylation induced robust morphological alterations consistent with neuritogenesis. Interestingly, this neuritogenic phenotype not only correlated well with BRI2 phosphorylation levels but also with the BRI2 processing profile. Thus, further evidence for the involvement of BRI2 NTF on the neuritogenic phenotype induced by BRI2 phosphorylation was sought. Hence, BRI2 NTFs levels were modulated in SH-SY5Y cells expressing either the Myc-BRI2 or the Myc-BRI2 PP1-BM mutants by inhibiting BRI2 cleavage by ADAM10 using 10 µM of GI254023X inhibitor for 48 hrs. Upon modulation of BRI2 processing (Fig. II.B.6), morphological evaluation of the cells was performed and the quantitative data is presented in figure II.B.7. In fact, using the specific ADAM10 inhibitor (GI254023X) for 48 hrs a significant decrease was observed in the levels of BRI2 NTF ($p<0.0001$ by the two-tailed Student's t-test for Myc-BRI2, and $p<0.05$ by the two-tailed Student's t-test for Myc-BRI2 KVTA) when compared with control (Fig. II.B.6).

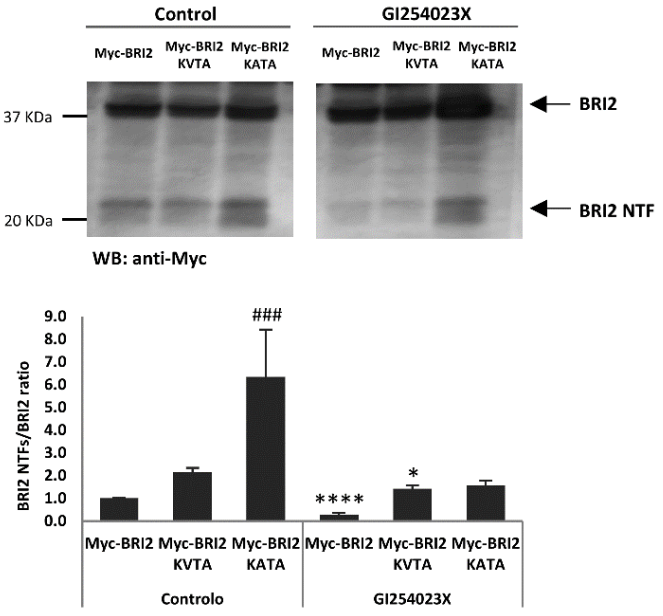

Figure II.B. 6 - Modulation of BRI2 processing in SH-SY5Y cells transfected with Myc-BRI2, Myc-BRI2 KVTA and Myc-BRI2 KATA constructs. SH-SY5Y cells were transfected with Myc-BRI2, Myc-BRI2 KVTA and Myc-BRI2 KATA constructs for 24 hrs and 48 hrs, incubated with GI254023X inhibitor. Controls were exposed to vehicle (DMSO). Analysis of Myc-tagged BRI2 proteins by immunoblotting after 24 hrs and 48 hrs of transfection. The quantitative data are

presented as mean ± SEM of the ratio of BRI2 N-terminal fragments (BRI2 NTFs) with BRI2 full-length protein. * $p < 0.05$, ### $p < 0.001$, **** $p < 0.0001$. Statistical symbols: (#) for comparisons with the Myc-BRI2 24 hrs by using one-way ANOVA followed by the Dunnett's test; (*) for comparisons between each construct at 24 hrs and 48 hrs by using t-student´s test. BRI2 NTF, BRI2 N-terminal fragment.

Moreover, morphometric analysis clearly indicated that when the BRI2 NTF's levels are diminished a significant increase in the number of cellular processes was evident ($p<0.001$ for Myc-BRI2 (Fig. II.B.7A.1), $p<0.05$ for Myc-BRI2 KVTA (Fig. II.B.7A.2) and $p<0.05$ for Myc-BRI2 KATA (Fig. II.B.7A.3), all determined by the two-tailed Student's t-test; Fig. II.B.7A). Neuritogenesis was further evaluated as previously described, by scoring the length of the longest cellular process presented by the transfected cells in control and inhibitor conditions (Fig. II.B.7B). Interestingly, upon 48 hrs of transfection with GI254023X exposure, the results were quite different from those observed in the control condition. With Myc-BRI2 the % of cells with smaller length processes (<20 μm) were quite similar, while for the higher length processes (neurites) the percentage decreased (Fig. II.B.7B). Similar results were observed for PP1-BM mutants, however, a significant decrease in the number of processes higher than 35 μm was clear ($p<0.05$ by the two-tailed Student's t-test), mirrored by a corresponding increase of processes between 20-35 μm length ($p<0.05$ by the two-tailed Student's t-test) with Myc-BRI2 KATA (Fig. II.B.7B).

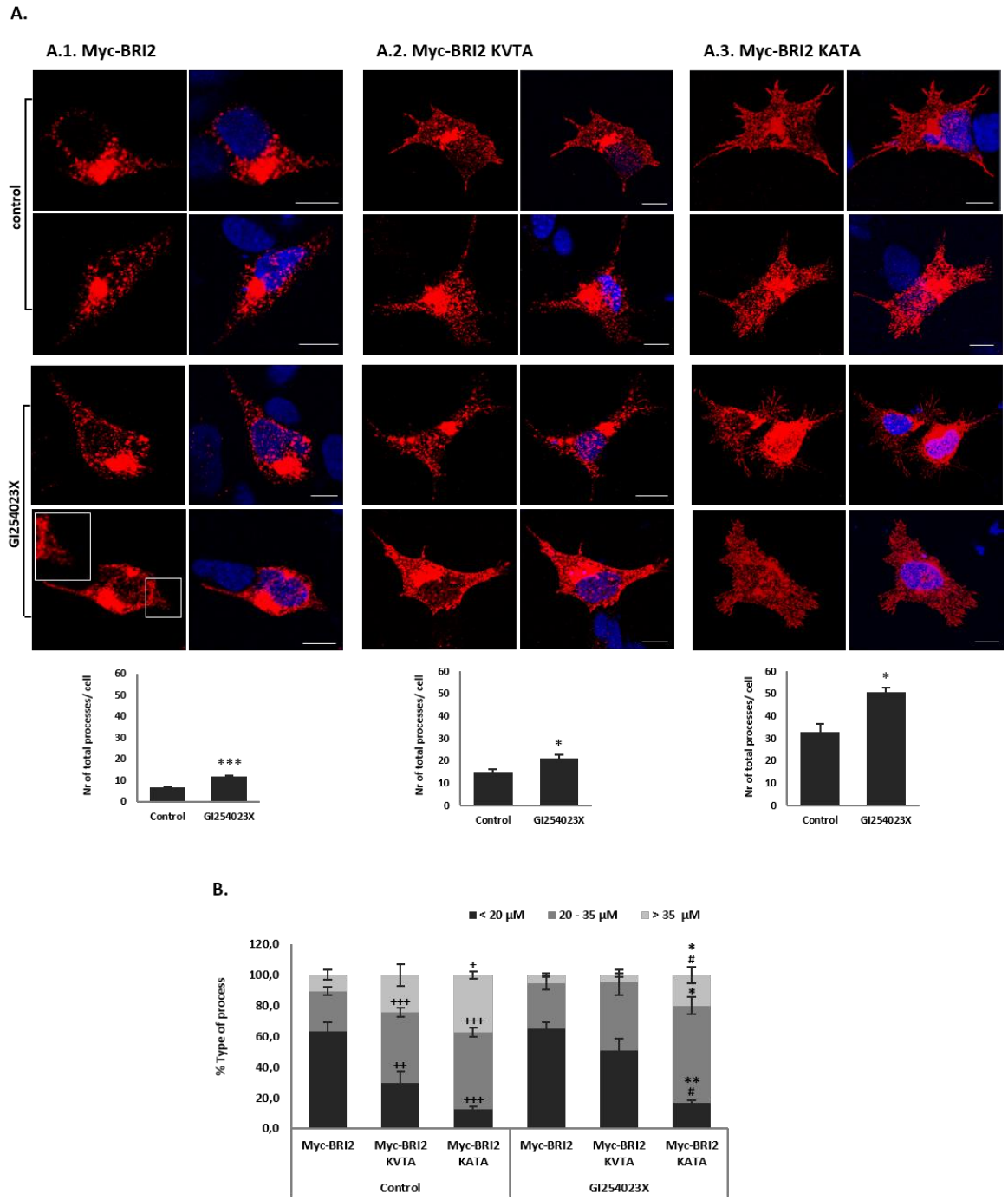

Figure II.B. 7 - Morphometric analysis of the cellular processes in SH-SY5Y cells transfected with Myc-BRI2, Myc-BRI2 KVTA and Myc-BRI2 KATA constructs followed by treatment with GI254023X inhibitor. **A-** Subcellular distribution of Myc-BRI2, Myc-BRI2 KVTA and Myc-BRI2 KATA after 48 hrs of transfection and the respective quantitative analysis of the total number of processes. Quantitative data are presented as mean ± SEM and obtained by analyzing at least 30 cells per condition from 3 independent experiments. * $p < 0.05$, *** $p < 0.001$ for comparisons between control and GI254023X conditions, by using t-student´s test. Bars, 10 µm. **B –** Percentage of cells with each type of processes. Processes were categorized according to their lengths, and the percentages of processes with length inferior to 20 µm (< 20 µm), pre-neurites (20–35 µm) and neurites (≥ 35 µm) calculated out of the total number of processes. The quantitative data are presented as mean ± SEM and was obtained by analyzing at least 30 cells per condition from three independent experiments. +/#/* $p < 0.05$, ++/** $p < 0.01$, +++ $p < 0.001$. Statistical symbols: (+) for comparisons to Myc-

BRI2 at control condition by using one-way ANOVA followed by the Dunnett's test; (#) for comparisons to Myc-BRI2 at GI254023X condition by using one-way ANOVA followed by the Dunnett's test; (*) for comparisons between each construct at control and GI254023X conditions by using t-student´s test.

II.B.4. Discussion

BRI2 is a type II transmembrane protein whose main physiological role remains to be elucidated. Nevertheless, some functions have already been proposed, namely its association with neurite outgrowth and neuronal differentiation (Akiyama *et al*. 2004; Martins *et al*. 2016; Choi *et al*. 2004). In fact, here we showed that both BRI2 levels and processing significantly increased during neuronal development (Figure II.B.1). The impact of BRI2 phosphorylation in the suggested BRI2 neuritogenic role was unequivocally demonstrated upon, a detailed morphometric analysis of SH-SY5Y cells transfected with BRI2 and BRI2 PP1-BM constructs. It was extremely clear that when BRI2:PP1 interaction is abolished a phenotype consistent with neurite outgrowth and neuronal differentiation is observed. Of note, morphological changes and remodeling occurring during neuronal differentiation depend on cytoskeleton alterations. In line with this, we found that upon 24 hrs of transfection, particularly with the BRI2 PP1-BM constructs, a significant decrease in acetylated α-tubulin and a significant increase in actin polymerization were evident (Figure II.B.4A and Fig. 5, respectively). This is consistent with the emergence and elongation of cellular processes, which requires MT instability and remodeling of actin filaments (da Rocha *et al*. 2015; Sliogeryte *et al*. 2014; Xu *et al*. 2009). At the 48 hrs time point, the significant increase in actin polymerization was maintained with the transfection of BRI2 PP1-BM constructs (Figure II.B.5). Interestingly, at this time point with the PP1-BM mutants acetylated tubulin increases significantly (Fig. 4A) which is related to the neuritic elongation and stabilization (da Rocha *et al*. 2015). Taken together, these findings suggest protein phosphorylation, namely dephosphorylation by PP1, is a regulatory mechanism for BRI2's neuritogenic role. This hypothesis is in line with numerous evidence implicating post-translational modifications in the regulation of dynamic events such as neurite outgrowth, hence the downstream signaling pathways deserve to be investigated. Interestingly, it is well known that phosphorylation of APP which has been previously shown to be functionally related to BRI2, plays a significant role in neurite outgrowth (Ando *et al*. 1999). These neurotrophic activities were attributed to both full- length APP and the sAPPα (secreted APP fragment derived from α-secretase APP processing) (Perez *et al*. 1997; Young-Pearse *et al*. 2008).

Moreover, in this manuscript we provide for the first time evidence suggesting that BRI2 phosphorylation, namely PP1 dephosphorylation, regulates BRI2 processing (Figure II.B.2A and 2C) since when BRI2:PP1 interaction is abolished (using BRI2 PP1-BM mutants) or PP1 inhibition (using OA) an increase in BRI2 phosphorylation is observed; that is well correlated with a significant increase in BRI2 processing. Therefore, having established that BRI2 phosphorylation is well correlated with its processing and neuritogenic role, we further investigated the involvement of BRI2 NTF on neurite outgrowth. By decreasing BRI2 cleavage by ADAM10 with a specific inhibitor, GI254023X, in SH-SY5Y cells transfected with BRI2 and the BRI2 PP1-BM constructs (Figure

II.B.6) there was an increase in the number of total processes per cell compared to control and a decrease in the % of cells with longer processes (>35 μM), with both of the PP1-BM mutants that correlated well with the decrease in BRI2 NTF. It can, therefore, be contemplated that for BRI2 mediated neurite outgrowth, phosphorylation of full-length protein promotes the emergence of neurites, whereas the increased BRI2 NTFs play a relevant role in neurites' elongation and stabilization. BRI2 is able to form homodimers linked by disulfide bonds that together with monomers appear at the cell surface (Tsachaki *et al*. 2010). As described for other proteins, BRI2 may act as a cell surface receptor that participates in signal transduction pathways, namely neurite outgrowth signaling pathways, triggered by ligand interaction. It is also possible that the importance of full-length BRI2 in mediating neurite outgrowth was modulated by protein interactions that require BRI2 phosphorylation since it induces conformational changes in the protein, potentially affecting binding specificity and affinity. Regarding the role of BRI2 processing in neuritogenesis, it is reasonable to assume that if BRI2´s NTF increase, the secreted fragment which contains the conserved BRICHOS domain also increases, where ADAM10 is responsible for the increased processing. In addition, it is possible that subsequent intramembrane cleavage of this fragment by SPPL2a/2b is also augmented. As a result of this proteolysis, a small secreted BRI2 C-terminal domain, and an intracellular domain, the BRI2ICD are generated. Recently it was described that BRI2ICD can translocate to the nucleus suggesting a particular function for this fragment in signal transduction and transcriptional regulation as already demonstrated for the APP intracellular domain (AICD) (Mentrup *et al*. 2015; Rebelo *et al*. 2013). Actually, AICD translocation to the nucleus is regulated by APP phosphorylation and facilitates neurite outgrowth (Zhou *et al*. 2012; Chang *et al*. 2006). Thus, further studies are required to unravel the precise mechanisms underlying the BRI2 neuritogenic role.

In summary, the data here presented supports a functional role for the BRI2:PP1 complex by modulating BRI2 phosphorylation, and simultaneously regulating BRI2 processing and consequently its neuritogenic role. Thereby, we further suggest that the BRI2:PP1 complex is essential to dynamically regulate neurite outgrowth (Figure II.B.8).

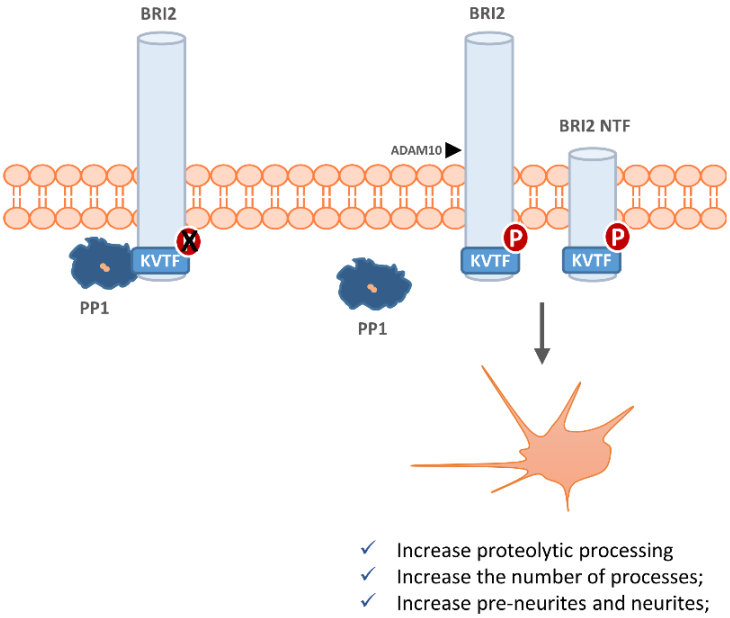

Figure II.B. 8 - Schematic depiction of BRI2 phosphorylation induced neurite outgrowth. BRI2 and PP1 interact through the RVTF motif (RVxF conserved motif) present in BRI2 protein regulating its phosphorylation levels, namely dephosphorylation by PP1. When BRI2:PP1 complex formation is impaired BRI2 becomes phosphorylated. The increase in BRI2 phosphorylation levels favors its processing and greatly induces neurite outgrowth: promotes the formation of cellular processes and its elongation and stabilization.

BRI2 was found mutated in two autosomal dominant neurodegenerative diseases, Familial British Dementia (FBD) and Familial Danish Dementia (FDD) that share clinical and neuropathological features with Alzheimer´s disease. Both disorders are characterized by the deposition of the amyloidogenic peptides ABri and ADan in the patients' brains. These peptides derive from the proteolytic processing of mutated forms of BRI2 (ABriPP and ADanPP) by furin in FBD and FDD, respectively (Rostagno *et al*. 2005). Interestingly, Choi and colleagues demonstrated that expression of ABriPP and ADanPP in N2a cells induces elongation of neurites (Choi *et al*. 2004). By unraveling the importance of BRI2 phosphorylation and proteolytic processing for the function of BRI2 we are contributing to the understanding of the pathological events leading to FBD and FDD. Functionally, the BRI2:PP1 complex may have important direct implications for the development of all these neurodegenerative disorders and this issue should be further investigated in the future.

References

Akiyama H., Kondo H., Arai T., Ikeda K., Kato M., Iseki E., Schwab C., McGeer P. L. (2004) Expression of BRI, the normal precursor of the amyloid protein of familial British dementia, in human brain. *Acta Neuropathol*. **107**, 53–8.

Ando K., Oishi M., Takeda S., Iijima K., Isohara T., Nairn A. C., Kirino Y., Greengard P., Suzuki T. (1999) Role of phosphorylation of Alzheimer's amyloid precursor protein during neuronal differentiation. *J. Neurosci*. **19**, 4421–7.

Bollen M., Peti W., Ragusa M. J., Beullens M. (2010) The extended PP1 toolkit: designed to create specificity. *Trends Biochem. Sci*. **35**, 450–8.

Campo M. Del, Teunissen C. E. (2014) Role of BRI2 in Dementia. *J. Alzheimers. Dis*. **40**, 481–94.

Chang K.-A., Kim H.-S., Ha T.-Y., Ha J.-W., Shin K. Y., Jeong Y. H., Lee J.-P., et al. (2006) Phosphorylation of amyloid precursor protein (APP) at Thr668 regulates the nuclear translocation of the APP intracellular domain and induces neurodegeneration. *Mol. Cell. Biol*. **26**, 4327–38.

Choi S.-I., Vidal R., Frangione B., Levy E. (2004) Axonal transport of British and Danish amyloid peptides via secretory vesicles. *FASEB J*. **18**, 373–5.

Cruz e Silva E. F. da, Fox C. A., Ouimet C. C., Gustafson E., Watson S. J., Greengard P. (1995) Differential expression of protein phosphatase 1 isoforms in mammalian brain. *J. Neurosci*. **15**, 3375–89.

Cruz e Silva O. A. B. da, Fardilha M., Henriques A. G., Rebelo S., Vieira S., Cruz e Silva E. F. da (2004) Signal transduction therapeutics: relevance for Alzheimer's disease. *J. Mol. Neurosci*. **23**, 123–42.

Dehmelt L., Halpain S. (2004) Actin and microtubules in neurite initiation: Are MAPs the missing link? *J. Neurobiol*. **58**, 18–33.

Demirkan G., Yu K., Boylan J. M., Salomon A. R., Gruppuso P. A. (2011) Phosphoproteomic profiling of in vivo signaling in liver by the mammalian target of rapamycin complex 1 (mTORC1). *PLoS One* **6**, e21729.

Dwane S., Durack E., Kiely P. A. (2013) Optimising parameters for the differentiation of SH-SY5Y cells to study cell adhesion and cell migration. *BMC Res. Notes* **6**, 366.

Forster J. I., Köglsberger S., Trefois C., Boyd O., Baumuratov A. S., Buck L., Balling R., Antony P. M. A. (2016) Characterization of Differentiated SH-SY5Y as Neuronal Screening Model Reveals Increased Oxidative Vulnerability. *J. Biomol. Screen*. **21**, 496–509.

Heroes E., Lesage B., Görnemann J., Beullens M., Meervelt L. Van, Bollen M. (2013) The PP1 binding code: a molecular-lego strategy that governs specificity. *FEBS J*. **280**, 584–95.

Klein D., Kern R. M., Sokol R. Z. (1995) A method for quantification and correction of proteins after transfer to immobilization membranes. *Biochem. Mol. Biol. Int*. **36**, 59–66.

Lashley T., Revesz T., Plant G., Bandopadhyay R., Lees A. J., Frangione B., Wood N. W., et al. (2008) Expression of BRI2 mRNA and protein in normal human brain and familial British dementia: its relevance to the pathogenesis of disease. *Neuropathol. Appl. Neurobiol*. **34**, 492–505.

Martins F., Rebelo S., Santos M., Cotrim C. Z., Cruz E Silva E. F. da, Cruz E Silva O. A. B. da (2016) BRI2 and BRI3 are functionally distinct phosphoproteins. *Cell. Signal*. **28**, 130–44.

Mentrup T., Häsler R., Fluhrer R., Saftig P., Schröder B. (2015) A Cell-Based Assay Reveals Nuclear Translocation of Intracellular Domains Released by SPPL Proteases. *Traffic* **16**, 871–92.

Perez R. G., Zheng H., Ploeg L. H. Van der, Koo E. H. (1997) The beta-amyloid precursor protein of Alzheimer's disease enhances neuron viability and modulates neuronal polarity. *J. Neurosci*. **17**, 9407–14.

Rebelo S., Domingues S. C., Santos M., Fardilha M., Esteves S. L. C., Vieira S. I., Vintém A. P. B., Wu W., Cruz E Silva E. F. da, Cruz E Silva O. A. B. da (2013) Identification of a novel complex AβPP:Fe65:PP1

that regulates AβPP Thr668 phosphorylation levels. *J. Alzheimers. Dis.* **35**, 761–75.

Rebelo S., Santos M., Martins F., Cruz E Silva E. F. da, Cruz E Silva O. A. B. da (2015) Protein Phosphatase 1 is a key player in nuclear events. *Cell. Signal.* **27**, 2589–98.

Rebelo S., Vieira S. I., Cruz E Silva E. F. da, Cruz E Silva O. A. B. da (2008) Monitoring "De Novo"APP synthesis by taking advantage of the reversible effect of cycloheximide. *Am. J. Alzheimers. Dis. Other Demen.* **23**, 602–8.

Rocha J. F. da, Cruz E Silva O. A. B. da, Vieira S. I. (2015) Analysis of the amyloid precursor protein role in neuritogenesis reveals a biphasic SH-SY5Y neuronal cell differentiation model. *J. Neurochem.* **134**, 288–301.

Romero-Calvo I., Ocón B., Martínez-Moya P., Suárez M. D., Zarzuelo A., Martínez-Augustin O., Medina F. S. de (2010) Reversible Ponceau staining as a loading control alternative to actin in Western blots. *Anal. Biochem.* **401**, 318–320.

Rostagno A., Tomidokoro Y., Lashley T., Ng D., Plant G., Holton J., Frangione B., Revesz T., Ghiso J. (2005) Chromosome 13 dementias. *Cell. Mol. Life Sci.* **62**, 1814–25.

Santos M., Costa P., Martins F., Cruz E Silva E. F. da, Cruz E Silva O. A. B. da, Rebelo S. (2015a) LAP1 is a crucial protein for the maintenance of the nuclear envelope structure and cell cycle progression. *Mol. Cell. Biochem.* **399**, 143–53.

Santos M., Domingues S. C., Costa P., Muller T., Galozzi S., Marcus K., Cruz E Silva E. F. da, Cruz E Silva O. A. da, Rebelo S. (2014) Identification of a Novel Human LAP1 Isoform That Is Regulated by Protein Phosphorylation. *PLoS One* **9**, e113732.

Santos M., Rebelo S., Cruz e Silva E. F. da, Cruz e Silva O. A. B. da (2015b) DYT1 dystonia-associated mutant affects cytoskeletal dynamics. *Microsc. Microanal.* **21**, 26–27.

Santos M., Rebelo S., Kleeff P. J. M. Van, Kim C. E., Dauer W. T., Fardilha M., Cruz E Silva O. A. da, Cruz E Silva E. F. da (2013) The nuclear envelope protein, LAP1B, is a novel protein phosphatase 1 substrate. *PLoS One* **8**, e76788.

Sharma K., D'Souza R. C. J., Tyanova S., Schaab C., Wiśniewski J. R., Cox J., Mann M. (2014) Ultradeep Human Phosphoproteome Reveals a Distinct Regulatory Nature of Tyr and Ser/Thr-Based Signaling. *Cell Rep.* **8**, 1583–94.

Shi Y. (2009) Serine/threonine phosphatases: mechanism through structure. *Cell* **139**, 468–84.

Silva J. S. da, Dotti C. G. (2002) Breaking the neuronal sphere: regulation of the actin cytoskeleton in neuritogenesis. *Nat. Rev. Neurosci.* **3**, 694–704.

Sliogeryte K., Thorpe S. D., Lee D. A., Botto L., Knight M. M. (2014) Stem cell differentiation increases membrane-actin adhesion regulating cell blebability, migration and mechanics. *Sci. Rep.* **4**, 7307.

Tsachaki M., Ghiso J., Efthimiopoulos S. (2008) BRI2 as a central protein involved in neurodegeneration. *Biotechnol. J.* **3**, 1548–54.

Tsachaki M., Ghiso J., Rostagno A., Efthimiopoulos S. (2010) BRI2 homodimerizes with the involvement of intermolecular disulfide bonds. *Neurobiol. Aging* **31**, 88–98.

Tsachaki M., Serlidaki D., Fetani A., Zarkou V., Rozani I., Ghiso J., Efthimiopoulos S. (2011) Glycosylation of BRI2 on asparagine 170 is involved in its trafficking to the cell surface but not in its processing by furin or ADAM10. *Glycobiology* **21**, 1382–8.

Vidal R., Frangione B., Rostagno A., Mead S., Révész T., Plant G., Ghiso J. (1999) A stop-codon mutation in the BRI gene associated with familial British dementia. *Nature* **399**, 776–81.

Wakula P., Beullens M., Ceulemans H., Stalmans W., Bollen M. (2003) Degeneracy and function of the ubiquitous RVXF motif that mediates binding to protein phosphatase-1. *J. Biol. Chem.* **278**, 18817–23.

Xu X., Harder J., Flynn D. C., Lanier L. M. (2009) AFAP120 regulates actin organization during neuronal

differentiation. *Differentiation*. **77**, 38–47.

Young-Pearse T. L., Chen A. C., Chang R., Marquez C., Selkoe D. J. (2008) Secreted APP regulates the function of full-length APP in neurite outgrowth through interaction with integrin beta1. *Neural Dev*. **3**, 15.

Zhou F., Gong K., Song B., Ma T., Laar T. van, Gong Y., Zhang L. (2012) The APP intracellular domain (AICD) inhibits Wnt signalling and promotes neurite outgrowth. *Biochim. Biophys. Acta* **1823**, 1233–41.

CHAPTER III - IDENTIFICATION OF NOVEL BRI2 AND BRI3 PROTEIN INTERACTORS

CHAPTER III.A - IDENTIFICATION OF NOVEL BRI2 INTERACTORS IN THE BRAIN: CONSTRUCTION AND ANALYSIS OF AN INTERACTION NETWORK

"Identification and characterization of the BRI2 interactome in the brain"

Filipa Martins[1], Ana M. Marafona[1], Cátia D. Pereira[1], Thorsten Müller[2], Christina Loosse[2], Katharina Kolbe[2], Odete A.B. da Cruz e Silva[1] and Sandra Rebelo[1]

[1] Neuroscience and Signalling Laboratory, Department of Medical Sciences, Institute of Biomedicine-iBiMED, University of Aveiro, 3810-193 Aveiro, Portugal

[2] Leibniz-Institut für Analytische Wissenschaften -ISAS- e. V., Dortmund, Germany

Corresponding author: Sandra Rebelo, Neuroscience and Signalling Laboratory, Department of Medical Sciences, Institute of Biomedicine-iBiMED, University of Aveiro, 3810-193 Aveiro, Portugal, Tel: +351-924406306, E-mail: srebelo@ua.pt

Martins F, Marafona AM, Pereira CD, Müller T, Loosse C, Kolbe K, da Cruz e Silva OCS and Rebelo S (2017). Identification and characterization of the BRI2 interactome in the brain. Submitted to *Scientific Reports*.

Abstract

BRI family proteins are ubiquitous type II transmembrane proteins but BRI2 is highly expressed in some neuronal tissues. Possible BRI2 functions include neuronal maturation and differentiation. BRI2 protein complexes appear to be important in mediating some of the functions attributed to this protein. Previously described BRI2 interactors include Alzheimer's amyloid precursor protein and protein phosphatase 1, however the identification of novel interactors provides an important tool to understand the role and function of BRI2. To this end three rat brain regions (cerebellum, hippocampus, and cerebral cortex) were processed for BRI2 immunoprecipitation; co-precipitating proteins were identified by Nano-HPLC-MS/MS. The pool of the brain regions resulted in 511 BRI2 interacting proteins (BRI2 brain interactome) of which 120 were brain specific and 49 involved in neuronal differentiation. Brain region specific analyses were also carried out for the cerebellum, hippocampus, and cerebral cortex. Several novel BRI2 interactors were identified among them DLG4/PSD-95, which is singularly important as it places BRI2 in the postsynaptic compartment. In essence, the results elucidating the BRI2 brain interactome, associated this protein with neurite outgrowth and neuronal differentiation, and synaptic signaling and plasticity. It follows that further studies should address BRI2 particularly given its relevance to neuropathological conditions.

III.A.1 Introduction

BRI2 (also known as ITM2B, integral membrane protein 2B) is a ubiquitously expressed type II transmembrane protein that belongs to a family comprising two additional members, BRI1 and BRI3. BRI2 mRNA was found highly expressed in the brain, placenta, pancreas, and kidney, whereas lower expression levels were observed in heart, lung, liver and skeletal muscle. Remarkably, in the brain, BRI2 is predominantly detected in the cerebellum, spinal cord, subthalamic nucleus, substantia nigra, and hippocampus. However, lower expression levels were detected in the cerebral cortex, amygdala, and thalamus (Vidal *et al*. 1999). Moreover, using *in situ* hybridization it was demonstrated that within the brain, BRI2 mRNA is distributed in different cellular populations, namely in neurons, astrocytes and microglial cells as well as in smooth muscle and cerebral endothelial cells (Rostagno *et al*. 2005). Subcellularly, BRI2 is mainly localized in the endoplasmic reticulum (ER), Golgi apparatus, plasma membrane and cytoplasmic vesicles (Choi *et al*. 2004). BRI2 undergoes regulated intramembrane proteolysis (RIP) in the cis- or medial-Golgi resulting in the formation of several secreted peptides, including the C-terminal 23-residue peptide, the BRICHOS domain, the NTF and BRI2 C-terminal domain, and an intracellular domain (BRI2 ICD), as consequence of the activity of several proteases (Choi *et al*. 2004).

The distribution of BRI2 within proximal dendrites and axons, as well as cell bodies, and its presence in some neuropathological structures like dystrophic neurites, suggests that BRI2 could be anterogradely transported to the nerve terminals, where it may have a role (Akiyama *et al*. 2004). In fact, BRI2 overexpression in human neuronal cells induces neurites' elongation, indicating that BRI2 could be involved in neurite outgrowth (Choi *et al*. 2004; Martins *et al*. 2016). Moreover, BRI2 expression increases during neuronal maturation and differentiation suggesting an important role for BRI2 both during neuronal development but also in the adult brain (Martins *et al*. 2017). In addition, some BRI2 binding proteins have been identified; as is the case with the Alzheimer's amyloid precursor protein (APP). BRI2:APP interaction occurs at the cell surface and in endocytic compartments, and this complex could potentially regulate APP processing and inhibit Abeta production (Matsuda *et al*. 2005; Matsuda *et al*. 2011). Interestingly, BRI2 accumulates in the hippocampus in the early stages of Alzheimer's disease (AD) preventing the BRI2:APP complex formation and therefore resulting in increased APP processing and consequently more $Abeta_{1-40}$ and $Abeta_{1-42}$ is produced (Del Campo *et al*. 2014). Additionally, we recently reported that BRI2 interacts with protein phosphatase 1 (PP1) via a BRI2 well conserved RVxF motif (^{3}KVTF^{6}). Further, we established that BRI2 is dephosphorylated by this protein phosphatase; given that when the BRI2:PP1 interaction is abolished, BRI2 phosphorylation levels increase dramatically. The morphological consequence of inhibiting PP1 binding was a phenotype consistent with neurite outgrowth and neuronal differentiation (Martins *et al*. 2016; Martins *et al*. 2017).

In addition to AD, the clinical relevance of this protein lies in two different autosomal dominant mutations in the *ITM2B* gene, which are associated with two rare early-onset forms of dementia, the Familial British and Danish dementias (FBD and FDD, respectively). These diseases share several clinical symptoms, such as progressive cognitive impairment cerebellar ataxia and spasticity (Tsachaki *et al*. 2008). Neuropathological hallmarks of FBD consist in the presence of pre-amyloid and amyloid parenchymal lesions in the brain (primarily localized to the hippocampus and cerebellum), extensive cerebral amyloid angiopathy (CAA) and intraneuronal formation of neurofibrillary tangles (NFT) within the limbic regions (Plant *et al*. 1990; Revesz *et al*. 1999). Neuropathological lesions in FDD patients are closely similar to those found in FBD, however in FDD co-deposition of Abeta and Danish amyloid is found, but parenchymal compact plaques are absent (Holton *et al*. 2002; Vidal *et al*. 2000).

To date, the precise physiological BRI2 function is not fully elucidated. Even so several lines of evidence strengthen the association of BRI2 with neuronal functions, in particular, the identification and functional characterization of BRI2 interactors, namely APP and PP1. Therefore, the identification of novel BRI2 interactors that may play important roles in regulating its trafficking, processing and signaling effect is an essential point. Additionally, specific cellular signaling pathways and processes which are crucial to the understanding of the physiological and pathological role of BRI2, in particular in the brain, may be forthcoming. The work here described proposes novel BRI2 interactors in rat brain, which represent a valuable tool to study the brain function in mammals. BRI2 interactors in three different brain regions were investigated; the cerebellum, hippocampus, and cerebral cortex, followed by *in silico* analysis, such as Gene Ontology (GO), biological pathways, and protein-protein interaction (PPI) network analysis. This permitted identifying potentially novel BRI2 functional relationships via analyzing its interacting proteins in the brain.

III.A.2 Materials and Methods

III.A.2.1 Preparation of rat brain lysates

Wistar Hannover rats (9-12 weeks) were obtained from Harlan Interfaune Ibérica, SL, and all experimental procedures were conducted in accordance with the European legislation for animal experimentation (2010/63/EU). No specific ethics approval under EU guidelines was required for this project, since the rats were euthanized, by cervical stretching followed by decapitation, for brain removal. This is within the European law (Council Directive 86/609/EEC) and the number and suffering of the animals were minimized as much as possible. The procedures were approved and supervised by our Institutional Animal Care and Use Committee (IACUC): Comissão Responsável pela Experimentação e Bem-Estar Animal (CREBEA). Briefly, animals were sacrificed by cervical stretching followed by decapitation and the cerebral cortex, hippocampus and cerebellum were

dissected on ice. Tissues were further weighed and homogenized on ice with a Potter-Elvehjem tissue homogenizer with 10-15 pulses at 650-750 rpm, in non-denaturating lysis buffer (50 mM Tris-HCl pH 8.0, 120 mM NaCl and 4% CHAPS) containing protease inhibitors (1 mM PMSF, 10 mM Benzamidine, 2 μM Leupeptin, 1.5 μM Aprotinin and 5 μM Pepstatin A) (Santos *et al*. 2014). The tissue extracts were used for immunoprecipitation analysis as described below.

III.A.2.2 Co-immunoprecipitation

The lysates from rat cerebral cortex, hippocampus and cerebellum extracts were divided into three equal parts (2 controls and 1 BRI2 co-immunoprecipitation) and pre-cleared separately using Dynabeads Protein G (Life Technologies). A direct immunoprecipitation approach was performed using mouse anti-BRI2 antibody (1μg/500μg protein; sc-374362, Santa Cruz Biotechnology), pre-incubated with Dynabeads Protein G for 1 hour at 4°C with rotation. After, the pre-cleared extracts were applied to antibody-Dynabeads and incubated overnight at 4°C with rotation. The immunoprecipitates were washed three times with PBS in 3% BSA for 10 min at 4°C with rotation and beads were re-suspended in 1% SDS. As a control extracts only incubated with dynabeads protein G or with dynabeads protein G coupled with mouse IgGs were used. The whole procedure was triplicated for each of the distinct brain regions.

III.A.2.3 In-gel protein digestion, nano-HPLC and mass spectrometry

The eluted fractions from the brain BRI2 co-IP assays were separated by SDS-PAGE on a 12% Bis-Tris gel and gels bands excised, cut into small pieces, and alternately washed with buffer A (50 mM ammonium hydrogen carbonate (NH_4HCO_3)) and B (50 mM NH_4HCO_3/50% ACN (acetonitrile)). Following dehydration of gel pieces *in vacuo*, trypsin (Serva, Germany) was solved in 10 mM HCl and 50 mM NH_4HCO_3 and used for overnight in gel digestion at 37 °C (trypsin:protein ratio 1:20). Peptides were then extracted once with 200 μl of 50% ACN/0.05% TFA (trifluoroacetic acid) and once with 100 μl of 50% ACN/0.05% TFA. Extracts were combined and centrifuged for 5 min at 16,000 ×g. The supernatant was transferred to a new vial in order to get rid of potential gel residuals. Then, ACN was removed *in vacuo*. For LC–MS analysis, a final volume of 16 μl was prepared by addition of 0.1% TFA.

Peptide extracts were used for mass spectrometry analysis. Therefore, samples were injected via the autosampler of an RSLC nano system (Thermo Scientific), concentrated on a C_{18} trapping column (2 cm length, 100 μm i.d., 5 μm particle size, Thermo Scientific), and separated on a C_{18} analytical column (50 cm length, 75 μm i.d., 2 μm particle size, Thermo Scientific) heated at 60 °C before being emitted via a coated silica tip (FS360-20-10-D-20, New Objective, USA) of the nanospray-

electrospray source of an Q Exactive (Thermo Scientific). The HPLC separation was performed with a gradient method of in total 120 min consisting of: 7 min of loading the sample and washing the column with 0.1% TFA at a flow rate of 30 µl min^{-1} on the trapping column, followed by separation applying a linear gradient at a flow rate of 400 nl min^{-1} with the solvents A (0.1% FA (formic acid) in HPLC grade water) and B (84% ACN/0.1% FA in HPLC grade water) starting from 5% B to 40% B in 98 min on the heated analytical column, a linear gradient of 40% B to 95% B in 2 min, and washing for 7 min with 95% B. Finally, a gradient was applied from 95% B to 5% B in 1 min followed by equilibration for 5 min with 5% B. For ionization a spray voltage of 1.6 kV and capillary temperature of 250 °C was used. The acquisition method consisted of two scan events, Full MS and MS/MS. The Full MS was monitored from m/z 350 to 1400, with an Orbitrap resolution of 70,000, a maximum injection time of 80 ms and an automatic gain control (AGC) value of 3e6. The m/z values initiating MS/MS were set on a dynamic exclusion list for 35 s. Lock mass polydimethylcyclosiloxane (m/z 445.120) was used for internal recalibration. The 10 most intensive ions (charge N1) were selected for MS/MS-fragmentation and fragments were scanned at a resolution of 35,000, with a maximum injection time of 120 ms and an AGC value of 2e5. Fragments were generated by higher-energy collisional-induced dissociation (HCD) on isolated ions.

For peptide identification .raw files were processed in Proteome Discoverer 1.4 and analyzed using the Mascot search algorithm with a mass tolerance of 10 ppm and a fragment mass tolerance of 0.02 Da. Searches were performed allowing one missed cleavage site after tryptic digestion. Oxidation (M) and phosphorylation (STY) were considered as variable modifications. Targeted Decoy PSM Validator was implemented with an FDR of 1%. All data were searched against a database containing the whole Uniprot/Swissprot entries of the taxonomy *Rattus norvegicus*.

For each sample condition (i.e. for each specific brain region), two mock IPs were used as negative controls. Therefore, the proteins identified in the mock IPs were excluded from the list of the proteins identified in the BRI2 co-IPs, with one exception: the ratio between the number of peptide-spectrum matches (PSM) for a given protein in a BRI2 co-IP sample and the PSM in the mock IPs, of the same brain region, were equal or higher than 2.0. In addition, well-described common contaminants as presented in (Hodge *et al*. 2013) and proteins characteristic of hair, skin/epidermis, tongue and gums (KRT33A, KRT78, KRT85, KRT14, KRT5, KRT3, KRT31, KRT32, KRT33B, KRT35, KRT36, KRT4, KRT77, KRT8, KRT17) which are also highly probable contaminants, were excluded.

III.A.2.4 Bioinformatic data analysis

Experimentally detected BRI2 protein-protein interactions already described in the literature were retrieved using PSIQUIC View web service (del-Toro *et al*. 2013) (version 1.4.5, downloaded October 2016), which enabled access to multiple PSI-MI compliant resources. In addition, two BRI2

interacting proteins identified and validated recently in our laboratory, protein phosphatase 1 alpha (PPP1CA) and protein phosphatase 1 gamma (PPP1CC), were added manually.

Tissue expression analysis was performed using the following databases: The Human Protein Atlas (HPA; available from www.proteinatlas.org) (Uhlén *et al*. 2015); TiGER (available from http://bioinfo.wilmer.jhu.edu/tiger) (Liu *et al*. 2008); and UniGene (Wheeler *et al*. 2003). The HPA was searched for proteins strongly expressed in the brain and a list of proteins within the brain 'Tissue enriched', 'Tissue enhanced' and 'Group enriched' categories was obtained. Annotated protein expression is a manually curated score based on IHC staining patterns in normal tissues from two or more paired antibodies binding to different epitopes of the same protein, which describes the distribution and strength of expression of each protein in cells. The TiGER database was searched for proteins, preferentially expressed in the brain, based on ESTs by searching 'Brain' in 'Tissue View'. The UniGene database was searched for brain-restricted genes by using the following search criteria: [brain][restricted].

Functional enrichment analysis of Gene Ontology (GO) categories (biological process and cellular component) was performed using PANTHER (Protein Annotation Through Evolutionary Relationship; version 11.1, accessed January 2016), online resource (Mi *et al*. 2017). For the PANTHER enrichment analysis, the overall set of rat/human protein-coding genes were used as reference set, and only enriched annotation with a p-value <0.05 were considered. In addition, functional enrichment analysis of KEGG pathways was performed using the ClueGo plugin version 2.3.2, (accessed January 2016) (Bindea *et al*. 2009) of the Cytoscape software version 3.4.0, freely available online (Shannon *et al*. 2003). Construction of protein-protein interaction (PPI) networks was achieved also using the Cytoscape software and further analyzed using the NetworkAnalyzer plugin version 3.3.1 (accessed January 2016). In order to perform network augmentation, protein-protein data was retrieved from the International Molecular Exchange (IMEx) consortium partners. Given the lack of information for *Rattus norvergicus* in these databases, the lists of proteins were extrapolated by homology to *Homo sapiens*. Rat UniProt accession numbers were converted to a human using the Uniprot tool available online - Uniprot Retrieve/ID mapping (http://www.uniprot.org/uploadlists/).

III.A.2.5 Interaction validation by immunoblotting

Brain lysates and eluted proteins from the co-immunoprecipitation assays were resolved on 5-20% gradient SDS-PAGE and electrophoretically transferred onto nitrocellulose membranes. Nonspecific protein-binding sites were blocked using 5% nonfat dry milk in TBST. Afterward, the membranes were incubated with the following primary antibodies: anti-BRI2 antibody (catalog no.: sc-374362, Santa Cruz Biotechnology) and anti-PSD95 (catalog no.: AB9708, Merck Millipore) overnight at

4°C with shaking. The membranes were then washed three times for 10 minutes with TBST and incubated for 2 h at room temperature with horseradish peroxidase-linked secondary antibodies (GE Healthcare). Finally, the membranes were washed three times for 10 minutes with TBST and enhanced chemiluminescence-based system were used for protein detection.

III.A.3 Results

III.A.3.1 Identification of BRI2 brain interactome

Given that BRI2 has been recently associated with neuronal functions, the identification of BRI2 brain interactors is of paramount importance. Therefore, our main goal was the identification of novel putative BRI2 interacting proteins in rat brain. Given the expression pattern of BRI2 in the brain, three different regions were chosen, namely cerebral cortex, hippocampus and cerebellum, and the workflow carried out was summarized and presented in Figure III.A.1. Briefly, the mentioned brain regions were dissected out and further subjected to co-immunoprecipitation (co-IP) using a BRI2 specific antibody against the N-terminal region of the protein. For the co-IP experiments, two negative controls were used for each specific brain region. The first one consists, in addition, Dynabeads Protein G in the absence of the BRI2 antibody to the tissue lysates, while in the second control Dynabeads Protein G was conjugated with anti-mouse IgGs. The co-IP proteins were further analyzed by HPLC-MS. The co-IPs experiments followed by MS analysis were repeated at least three times for each specific brain region. The obtained set of proteins was subjected to data processing and filtering since some proteins were only identified in the BRI2 co-IP samples and never in the controls, while others appear both controls and co-IPs samples but were found significantly enriched in BRI2 co-IP samples. These were considered as a BRI2 interactor candidate if peptide spectrum matches (PSM) ratio between co-IP samples and controls ≥ 2.0.

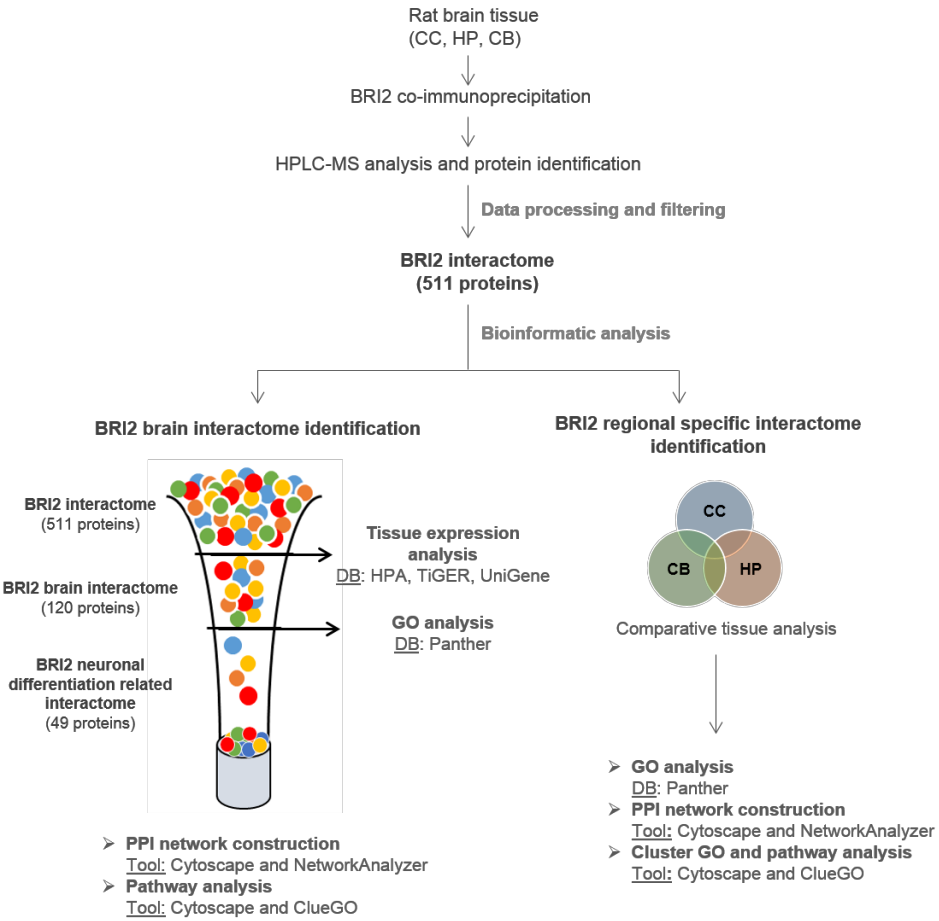

Figure III.A. 1 - Workflow for the identification of novel brain BRI2 interacting proteins using rat brain tissue lysates. Two different approaches were used, the first one is represented on left and the second one on the right. DB, database; CC, cerebral cortex; HP, hippocampus; CB, cerebellum; MS, mass-spectrometry.

Overall, upon data processing 511 putative BRI2 interacting proteins were identified in the rat brain (Supplementary Table III.A.S1). Of note, 342 proteins were identified in the cerebral cortex, 257 in the hippocampus and 262 in the cerebellum (Supplementary Table III.A.S1). In Supplementary Table III.A.S1, the Uniprot accession numbers are listed as well as the gene and protein name, and the rat brain region in which the peptides were detected. The first analysis of the BRI2 brain interactome (pool of the three brain regions studied) using bioinformatic approaches indicates that the majority of proteins identified in this study belong to the protein classes of cytoskeletal proteins (16%; half of which belong to the actin family), hydrolases (12%), enzyme modulators (11%; mainly G-proteins) and transporters (11%; half of which belong to cation transporters family). Other represented protein classes included membrane traffic proteins (7%), oxidoreductases (7%), calcium-binding proteins (5%), ion channels (5%; being 2 % anion channels), dehydrogenases (5%), chaperones (3%),

structural proteins (3%), ATP synthases (2%), transmembrane receptor regulatory/adaptor proteins (2%) and transcription factors (1%) (Figure III.A.2 and Supplementary Table III.A.S2).

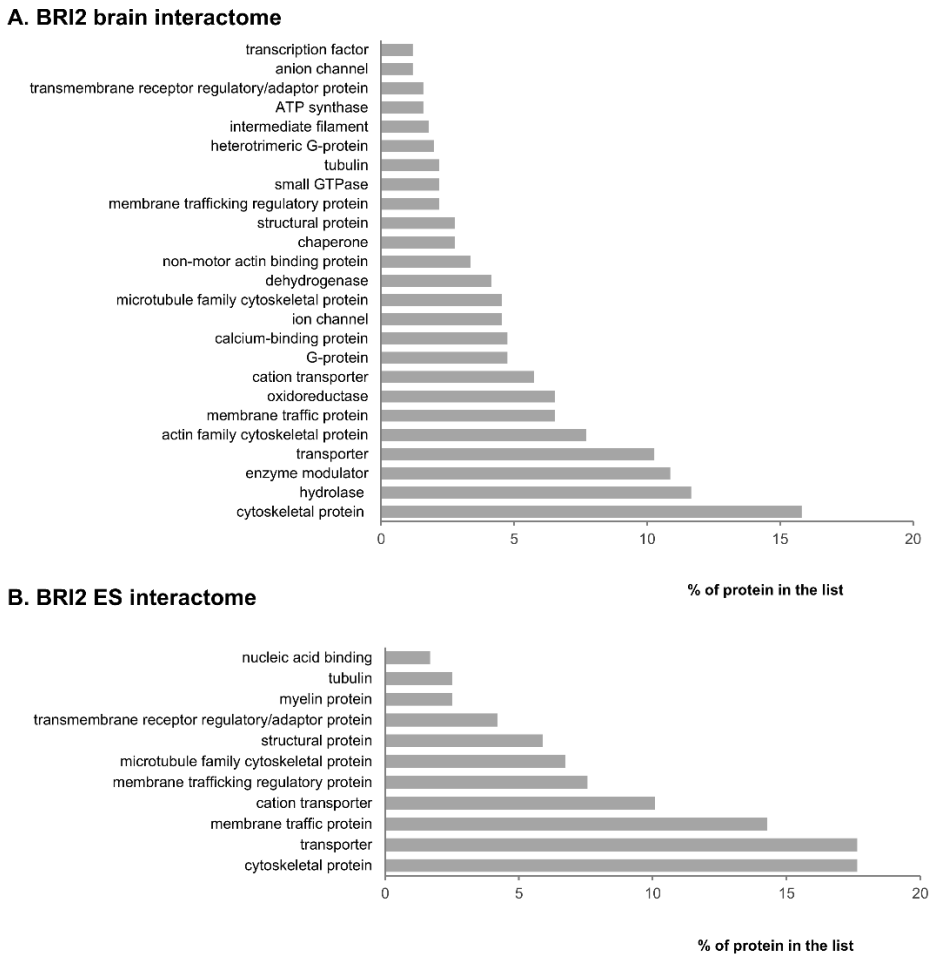

Figure III.A. 2 - Panther Protein class of the novel BRI2 interactome using the PANTHER online resource. The percentage of the BRI2 interacting proteins in each category was calculated and plotted. **A** – Panther Protein class of all the identified BRI2 interacting proteins (BRI2 brain interactome). **B -** Panther Protein class of the identified brain-enriched or specific BRI2 interacting proteins (BRI2 brain ES interactome).

In parallel, a curated list of 45 proteins that were previously identified as putative BRI2 interacting proteins was retrieved, as described above (Supplementary Table III.A.S3). Overall, most of these proteins were identified by yeast-two-hybrid and high-throughput screens and were not further validated by additional assays. Of note, in the study here described, 2 of the 45 previously reported BRI2 interacting proteins were also identified: the dihydropyridine-sensitive L-type, calcium channel alpha-2/delta subunit (Cacna2d1) and the serine/threonine-protein phosphatase PP1-alpha catalytic subunit (Ppp1ca).

III.A.3.2 Highly enriched and specific brain BRI2 interacting proteins

Given that the main goal of this work is to unravel putative associations of BRI2 to specific cellular functions as well as pathways where BRI2 participates in the brain related processes, a tissue-specific/enriched network approach was employed. For this purpose, the enriched and specific brain proteins from the candidate BRI2 pooled interactome (cerebral cortex + hippocampus + cerebellum) using three different databases were retrieved, as explained in the materials and methods section. From the 511 putative BRI2 interacting proteins identified by Nano-HPLC-MS/MS, a total of 120 proteins are highly enriched/specifically (ES) expressed in the brain (BRI2 ES interactome) (Table III.A.1).

Table III.A. 1 – Novel candidate BRI2 interacting proteins highly enriched or specific for the brain tissue. Uniprot accession numbers, gene and protein names, are listed, as well as the rat brain tissues where the proteins were found. CC, cerebral cortex; HP, hippocampus; CB, cerebellum.

Uniprot accession	Gene name	Protein name	Brain regions
P13233	Cnp	2',3'-cyclic-nucleotide 3'-phosphodiesterase	CC, HP, CB
P23565	Ina	Alpha-internexin	CC, HP, CB
O08838	Amph	Amphiphysin	CC, HP, CB
P0C6S7	Anks1b	Ankyrin repeat and sterile alpha motif domain-containing protein 1B	CC
Q8CGU4	Agap2	Arf-GAP with GTPase, ANK repeat and PH domain-containing protein 2	CC
Q6PST4	Atl1	Atlastin-1	CC
Q05764	Add2	Beta-adducin	HP
P85969	Napb	Beta-soluble NSF attachment protein	HP
Q05175	Basp1	Brain acid soluble protein 1	HP
P55068	Bcan	Brevican core protein	HP, CB
P11275	Camk2a	Calcium/calmodulin-dependent protein kinase type II subunit alpha	CC, HP
P08413	Camk2b	Calcium/calmodulin-dependent protein kinase type II subunit beta	CC, HP, CB
Q62717	Cadps	Calcium-dependent secretion activator 1	HP
Q63092	Camkv	CaM kinase-like vesicle-associated protein	HP
Q1WIM1	Cadm4	Cell adhesion molecule 4	CB
Q5FVI4	Cend1	Cell cycle exit and neuronal differentiation protein 1	CC, HP
Q05140	Snap91	Clathrin coat assembly protein AP180	CC, HP
P63041	Cplx1	Complexin-1	HP
Q9Z1T4	Cnksr2	Connector enhancer of kinase suppressor of ras 2	CC
Q63198	Cntn1	Contactin-1	CC, HP
P97846	Cntnap1	Contactin-associated protein 1	CC, CB
Q5BJS7	Cpne9	Copine-9	HP
Q62950	Crmp1	Dihydropyrimidinase-related protein 1	HP
Q62951	Dpysl4	Dihydropyrimidinase-related protein 4	CB
Q63622	Dlg2	Disks large homolog 2	CC

Uniprot accession	Gene name	Protein name	Brain regions
P31016	Dlg4	Disks large homolog 4	CC, HP, CB
P97836	Dlgap1	Disks large-associated protein 1	CC
P97837	Dlgap2	Disks large-associated protein 2	CC
P97838	Dlgap3	Disks large-associated protein 3	CC
P21575	Dnm1	Dynamin-1	CC, HP
Q8R491	Ehd3	EH domain-containing protein 3	HP
Q8CH84	Elavl2	ELAV-like protein 2	CC
O35179	Sh3gl2	Endophilin-A1	CC, CB
P24942	Slc1a3	Excitatory amino acid transporter 1	CC, HP, CB
P31596	Slc1a2	Excitatory amino acid transporter 2	CC, HP, CB
O35921	Slc1a6	Excitatory amino acid transporter 4	CB
O88871	Gabbr2	Gamma-aminobutyric acid type B receptor subunit 2	CC
P47819	Gfap	Glial fibrillary acidic protein	CC, HP, CB
P19490	Gria1	Glutamate receptor 1	CC
P19491	Gria2	Glutamate receptor 2	CC, HP, CB
P35439	Grin1	Glutamate receptor ionotropic, NMDA 1	CC
Q00960	Grin2b	Glutamate receptor ionotropic, NMDA 2B	CC
Q9WTT6	Gda	Guanine deaminase	CC
P19627	Gnaz	Guanine nucleotide-binding protein G	CC, HP
P59215	Gnao1	Guanine nucleotide-binding protein G	CC, HP, CB
Q9Z214	Homer1	Homer protein homolog 1	CC
Q9ESM2	Hapln2	Hyaluronan and proteoglycan link protein 2	CC, CB
Q9QYU4	Crym	Ketimine reductase mu-crystallin	HP
Q6QLM7	Kif5a	Kinesin heavy chain isoform 5A	CC, HP, CB
P56536	Kif5c	Kinesin heavy chain isoform 5C	CC, CB
P37285	Klc1	Kinesin light chain 1	CC, HP, CB
Q62813	Lsamp	Limbic system-associated membrane protein	CC, CB
P34926	Map1a	Microtubule-associated protein 1A	CC, HP
P15205	Map1b	Microtubule-associated protein 1B	CC, HP, CB
P15146	Map2	Microtubule-associated protein 2	CC
Q63560	Map6	Microtubule-associated protein 6	CC, HP, CB
Q505J6	Slc25a18	Mitochondrial glutamate carrier 2	CC
P02688	Mbp	Myelin basic protein	CC
P60203	Plp1	Myelin proteolipid protein	CC, CB
P07722	Mag	Myelin-associated glycoprotein	CC, CB
Q63345	Mog	Myelin-oligodendrocyte glycoprotein	CC, CB
P13596	Ncam1	Neural cell adhesion molecule 1	CB
P55067	Ncan	Neurocan core protein	CC, HP, CB
O35095	Ncdn	Neurochondrin	CC
P19527	Nefl	Neurofilament light polypeptide	CC, HP, CB
P12839	Nefm	Neurofilament medium polypeptide	CC, CB
P07936	Gap43	Neuromodulin	CC
Q9ESI7	Dcx	Neuronal migration protein doublecortin	CC

Uniprot accession	Gene name	Protein name	Brain regions
Q9WU34	Sept3	Neuronal-specific septin-3	HP
Q62718	Ntm	Neurotrimin	CC, CB
P11506	Atp2b2	Plasma membrane calcium-transporting ATPase 2	CC
Q64568	Atp2b3	Plasma membrane calcium-transporting ATPase 3	HP
P10499	Kcna1	Potassium voltage-gated channel subfamily A member 1	CC
Q6MG82	Prrt1	Proline-rich transmembrane protein 1	HP
O88778	Bsn	Protein bassoon	CC, CB
P63319	Prkcg	Protein kinase C gamma type	CC, HP, CB
Q9JKS6	Pclo	Protein piccolo	CC
P47709	Rph3a	Rabphilin-3A	CC, HP
P63012	Rab3a	Ras-related protein Rab-3A	CC, HP, CB
P62824	Rab3c	Ras-related protein Rab-3C	CC, HP
Q9JIR4	Rims1	Regulating synaptic membrane exocytosis protein 1	CC
Q64548	Rtn1	Reticulon-1	CC, HP, CB
Q9JKE3	Scamp5	Secretory carrier-associated membrane protein 5	CC, HP
Q9JJM9	Sept5	Septin-5	CC, HP
O08875	Dclk1	Serine/threonine-protein kinase DCLK1	CC, HP
Q9WV48	Shank1	SH3 and multiple ankyrin repeat domains protein 1	CC, CB
P0DJJ3	Sgip1	SH3-containing GRB2-like protein 3-interacting protein 1	CC, HP
P31647	Slc6a11	Sodium- and chloride-dependent GABA transporter 3	CC, CB
P48768	Slc8a2	Sodium/calcium exchanger 2	CC
P06686	Atp1a2	Sodium/potassium-transporting ATPase subunit alpha-2	CC
P06687	Atp1a3	Sodium/potassium-transporting ATPase subunit alpha-3	CC, HP
P13638	Atp1b2	Sodium/potassium-transporting ATPase subunit beta-2	CC, HP, CB
Q63633	Slc12a5	Solute carrier family 12 member 5	HP
Q9QWN8	Sptbn2	Spectrin beta chain, non-erythrocytic 2	CC, CB
Q9QXY2	Srcin1	SRC kinase signaling inhibitor 1	CC, CB
P09951	Syn1	Synapsin-1	CC, HP
Q63537	Syn2	Synapsin-2	CC
Q02563	Sv2a	Synaptic vesicle glycoprotein 2A	CC, HP, CB
Q63564	Sv2b	Synaptic vesicle glycoprotein 2B	CC, HP
P07825	Syp	Synaptophysin	CC, HP
P60881	Snap25	Synaptosomal-associated protein 25	HP, CB
P21707	Syt1	Synaptotagmin-1	CC, HP, CB
P97610	Syt12	Synaptotagmin-12	CC, CB
P29101	Syt2	Synaptotagmin-2	CB
Q62747	Syt7	Synaptotagmin-7	CB
P32851	Stx1a	Syntaxin-1A	CC
P61265	Stx1b	Syntaxin-1B	CC, HP, CB
P61765	Stxbp1	Syntaxin-binding protein 1	CC, HP
Q05546	Tnr	Tenascin-R	CC, HP, CB
P70566	Tmod2	Tropomodulin-2	CC, CB
P85108	Tubb2a	Tubulin beta-2A chain	CC, HP, CB

Uniprot accession	Gene name	Protein name	Brain regions
Q3KRE8	Tubb2b	Tubulin beta-2B chain	CC, HP
Q4QRB4	Tubb3	Tubulin beta-3 chain	CC, HP, CB
Q9QUL6	Nsf	Vesicle-fusing ATPase	CC, HP, CB
Q62634	Slc17a7	Vesicular glutamate transporter 1	CC, HP
Q9JI12	Slc17a6	Vesicular glutamate transporter 2	CC
O35458	Slc32a1	Vesicular inhibitory amino acid transporter	CC, HP
P62762	Vsnl1	Visinin-like protein 1	CB
Q71RJ2	Cacng2	Voltage-dependent calcium channel gamma-2 subunit	CB
Q6QIX3	Slc30a3	Zinc transporter 3	CC

Almost half of these interactors are cytoskeletal proteins (around 18%; mainly actin and microtubules) or transporters (around 18%; half of which belong to cation transporters family), followed by membrane traffic proteins (14%; half of which are regulatory), structural proteins (6%: half of which are myelin proteins), transmembrane receptor regulatory/adaptor proteins (3%) and nucleic acid binding proteins (2%) (Figure III.A.2B and Supplementary Table III.A.S4).

In order to elucidate if the proteins identified in BRI2 ES interactome could be assigned to specific functions, and ultimately to provide more information regarding the physiological role of BRI2, particularly in the brain, a further classification was performed into functional categories according to Gene Ontology (GO) annotation using the PANTHER online resource. Regarding the analysis of the over-represented biological process GO terms (Figure III.A.3A and Supplementary Table III.A.S5), the results revealed that the BRI2 ES interactome included proteins involved in several functional roles, from which the synaptic vesicle cycle (60.3%), neuron development (32.2%), brain development (26.4%), regulation of synaptic plasticity (24.0%), ion transport (22.3%), and cytoskeleton organization (16.5%) stand out (Figure III.A.3A). Cellular component annotation analysis revealed several statistically enriched categories (Supplementary Table S6). Of note, a high percentage of proteins in the BRI2 ES interactome that localized to the synapse (57.0%), dendrite (30.6%), postsynaptic density (25.6%), synaptic vesicle (24.0%), axon terminus (17.4%) and presynaptic membrane (10.7%) were found (Figure III.A.3B).

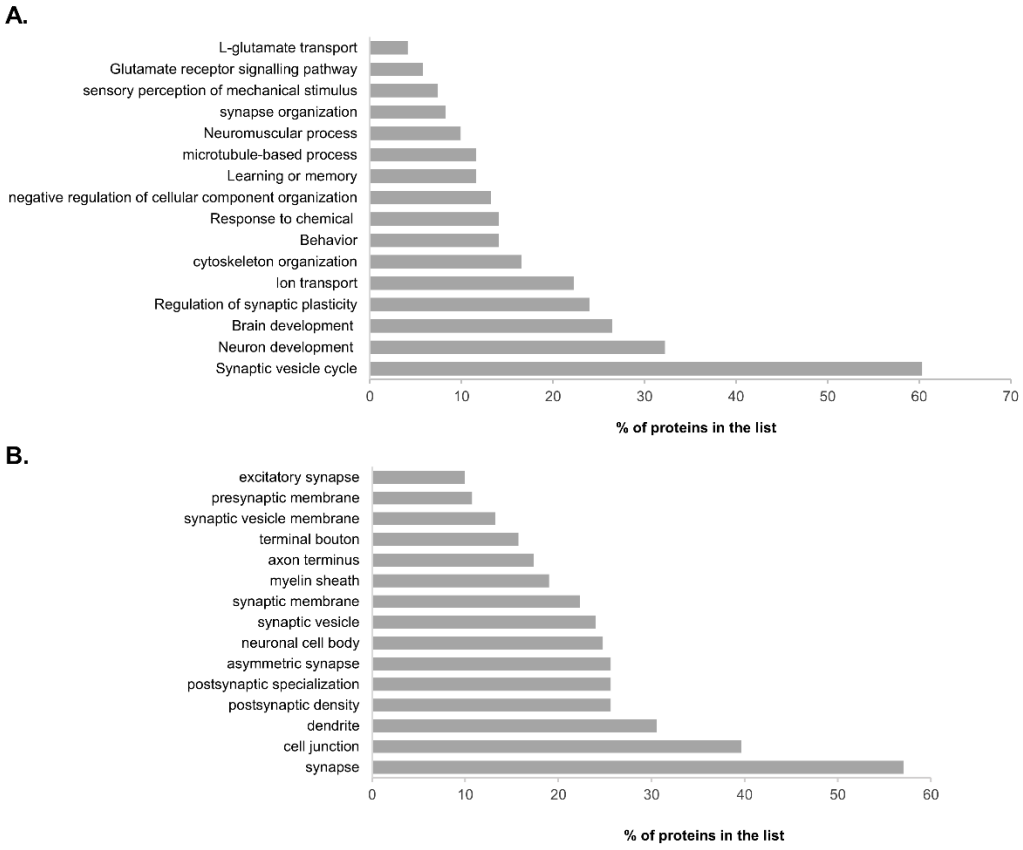

Figure III.A. 3 - Functional enrichment analysis of the BRI2 brain ES interactome using the PANTHER online resource. The percentage of the BRI2 interacting proteins in each category was calculated and plotted. **A** – Biological process analysis of the identified BRI2 interacting proteins particularly brain-enriched or specific. **B** – Cellular component analysis of the identified BRI2 interacting proteins particularly brain-enriched or specific.

III.A.3.3 BRI2 role in neuronal differentiation

Previous results strongly suggested a role for BRI2 in neuronal differentiation (Akiyama *et al*. 2004; Martins *et al*. 2016; Martins *et al*. 2017), however to date the exact mechanisms or pathways involving BRI2 have not been revealed. Hence from the BRI2 brain ES interactors, the proteins annotated with GO terms related to neuronal differentiation were retrieved. This resulted in a list of 49 proteins corresponding to the BRI2 ES neuronal differentiation interactome (Supplementary Table III.A.S7). To evaluate the interconnection of these BRI2 candidate interactors, a PPI network augmentation was performed, using the Cytoscape software (Shannon *et al*. 2003), which enhanced the experimental data with additional known and experimentally validated PPI from public databases (see materials and methods section). In addition, the proteins annotated with GO terms related to neuronal differentiation from the previously identified list of BRI2 interactors (Supplementary Table S3), were manually added to this PPI network. The PPI network augmentation provides interesting

and valuable information, permitting a systems approach to analyze the complexes formed from the co-immunoprecipitating proteins rather than a single interaction.

The network construction and analysis were achieved using the NetworkAnalyzer plugin of the Cytoscape (Shannon *et al*. 2003). In the resulting BRI2 (gene *ITM2B*) PPI network (Figure III.A.4), the grey nodes correspond to PPI added by the Cytoscape analysis, the colored nodes to the proteins identified in this study (blue for proteins identified in cerebral cortex, orange for proteins identified in hippocampus, and green for proteins identified in cerebellum) annotated with GO terms related to neuronal differentiation, and the node size corresponds to its degree (k; the number of edges linked to it). The total number of proteins mapped in the neuronal differentiation-specific PPI network was 144 (nodes), and the total number of connections between them was 286 (edges) (Figure III.A.4). The average number of neighbors for a node in the network, which indicates the average connectivity of a node in the network, is 3.972. The mean clustering coefficient of the network, which characterizes how nearest neighboring nodes of a node are connected to each other, is 0.09, being 4.5 times larger than the clustering coefficient expected for a sparse random uncorrelated network (0.02) (Doncheva *et al*. 2012; Newman 2006).

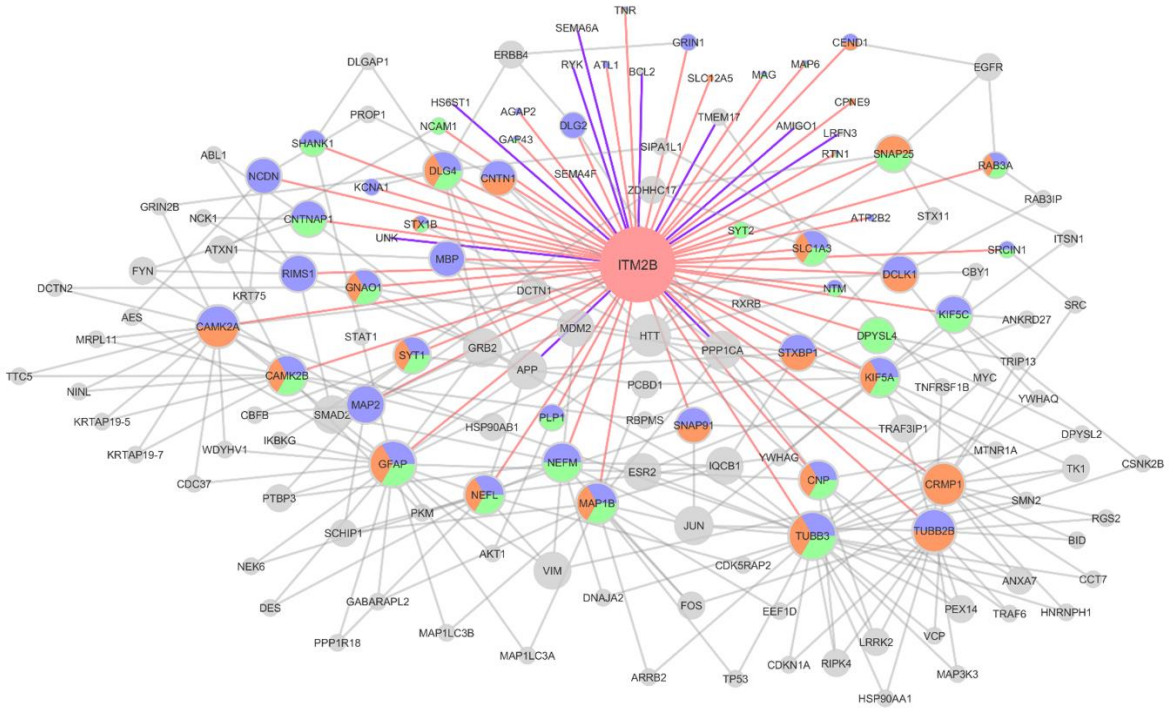

Figure III.A.4 - BRI2 brain ES sub-network for neuronal differentiation annotated proteins. Node colors represent the source of the protein: blue nodes correspond to proteins identified in this study in the cerebral cortex, orange nodes correspond to proteins identified in this study in the hippocampus, green nodes correspond to proteins identified in this study in the cerebellum, and grey nodes are proteins added by network augmentation. Node size according to the degree in the network. Edge color represents the source of interaction: light red edges correspond to the novel BRI2 interactions identified in our study, whereas the grey edges correspond to interactions added by network augmentation.

From all the nodes, the TUBB3 (k=23) was noteworthy since it presents the highest node degree and in this study, it was identified in the three different brain regions analyzed (Figure III.A.4). TUBB3 (Tubulin beta-3 chain), is a neuron-specific beta-tubulin which has been suggested to have a critical role in proper axon guidance and maintenance (Tischfield *et al*. 2010). Additionally, the following proteins were highlighted in the network: the TUBB2B (k=16), CAMK2A (k=15), CRMP1 (k=15), MAP1B (k=13), CAMK2B (k=11), NEFL (k=11), KIF5A (k=11), NEFM (K=10) and DLG4 (k=9) (Figure III.A.4).

In order to establish the signaling pathways that are most associated with BRI2, an integrated KEGG pathway enrichment analysis of the 144 proteins in BRI2 brain ES neuronal differentiation PPI network was performed using the ClueGo plugin of the Cytoscape software (Bindea *et al*. 2009). This analysis placed BRI2 into signalling networks well related to neuronal differentiation, namely ErbB signalling pathway (pValue = 1.812E-08), neurotrophin signalling pathway (pValue =6.443E-05), estrogen signalling pathway (pValue =1.163E-05), FoxO signalling pathway (pValue = 5.248E-03), axon guidance (pValue =1.571E-03), adherens junction (pValue =2.896E-02) and HIF-1 signalling pathway (pValue =2.675E-02) (Table III.A.2).

Table III.A. 2 - KEGG category enrichment analysis of the neuronal differentiation annotated network obtained using ClueGo plugin of the Cytoscape software. Enriched categories identified are those with p-value <0.05.

KEGG Term ID	KEGG Term	Nr. Genes	% Associated Genes	pValue	Associated Genes Found
KEGG:04721	Synaptic vesicle cycle	6	9.523809	3.4E-03	RAB3A, RIMS1, SNAP25, STX1B, STXBP1, SYT1
KEGG:05014	Amyotrophic lateral sclerosis (ALS)	8	15.686275	6.070E-06	BCL2, BID, GRIN1, GRIN2B, NEFL, NEFM, TNFRSF1B, TP53
KEGG:05130	Pathogenic Escherichia coli infection	6	10.909091	1.699E-03	ABL1, FYN, NCK1, TUBB2B, TUBB3, YWHAQ
KEGG:04360	Axon guidance	10	5.681818	1.571E-03	ABL1, CAMK2A, CAMK2B, DPYSL2, FYN, NCK1, RYK, SEMA4F, SEMA6A, SRC
KEGG:04520	Adherens junction	5	6.756757	2.896E-02	CSNK2B, EGFR, FYN, SMAD2, SRC
KEGG:04066	HIF-1 signaling pathway	6	5.8252425	2.675E-02	AKT1, BCL2, CAMK2A, CAMK2B, CDKN1A, EGFR
KEGG:04725	Cholinergic synapse	7	6.3063064	8.587E-03	AKT1, BCL2, CAMK2A, CAMK2B, FOS, FYN, GNAO1
KEGG:04728	Dopaminergic synapse	10	7.6923075	1.195E-04	AKT1, ARRB2, CAMK2A, CAMK2B, FOS, GNAO1, GRIN2B, KIF5A, KIF5C, PPP1CA
KEGG:04921	Oxytocin signaling pathway	10	6.289308	6.652E-04	CAMK2A, CAMK2B, CDKN1A, EGFR, FOS, GNAO1, JUN, PPP1CA, RGS2, SRC
KEGG:05031	Amphetamine addiction	7	10.294118	5.916E-04	CAMK2A, CAMK2B, FOS, GRIN1, GRIN2B, JUN, PPP1CA
KEGG:04713	Circadian entrainment	7	7.2916665	4.341E-03	CAMK2A, CAMK2B, FOS, GNAO1, GRIN1, GRIN2B, MTNR1A
KEGG:04720	Long-term potentiation	5	7.4626865	2.505E-02	CAMK2A, CAMK2B, GRIN1, GRIN2B, PPP1CA
KEGG:04724	Glutamatergic synapse	7	6.140351	9.391E-03	DLG4, DLGAP1, GNAO1, GRIN1, GRIN2B, SHANK1, SLC1A3
KEGG:05030	Cocaine addiction	4	8.163265	4.038E-02	DLG4, GRIN1, GRIN2B, JUN
KEGG:04012	ErbB signaling pathway	12	13.636364	1.812E-08	ABL1, AKT1, CAMK2A, CAMK2B, CDKN1A, EGFR, ERBB4, GRB2, JUN, MYC, NCK1, SRC
KEGG:04068	FoxO signaling pathway	8	5.970149	5.248E-03	AGAP2, AKT1, CDKN1A, EGFR, GABARAPL2, GRB2, MDM2, SMAD2
KEGG:04110	Cell cycle	8	6.451613	3.526E-03	ABL1, CDKN1A, MDM2, MYC, SMAD2, TP53, YWHAG, YWHAQ
KEGG:04210	Apoptosis	7	5.0	2.714E-02	AKT1, BCL2, BID, FOS, IKBKG, JUN, TP53
KEGG:04380	Osteoclast differentiation	8	6.060606	5.022E-03	AKT1, FOS, FYN, GRB2, IKBKG, JUN, STAT1, TRAF6
KEGG:04620	Toll-like receptor signaling pathway	6	5.6603775	2.808E-02	AKT1, FOS, IKBKG, JUN, STAT1, TRAF6
KEGG:04660	T cell receptor signaling pathway	7	6.6666665	6.308E-03	AKT1, FOS, FYN, GRB2, IKBKG, JUN, NCK1
KEGG:04662	B cell receptor signaling pathway	5	6.849315	2.886E-02	AKT1, FOS, GRB2, IKBKG, JUN
KEGG:04722	Neurotrophin signaling pathway	10	8.264462	6.443E-05	ABL1, AKT1, BCL2, CAMK2A, CAMK2B, GRB2, JUN, MAP3K3, TP53, TRAF6
KEGG:04912	GnRH signaling pathway	7	7.6086955	3.597E-03	CAMK2A, CAMK2B, EGFR, GRB2, JUN, MAP3K3, SRC
KEGG:04915	Estrogen signaling pathway	10	10.0	1.163E-05	AKT1, EGFR, ESR2, FOS, GNAO1, GRB2, HSP90AA1, HSP90AB1, JUN, SRC

KEGG Term ID	KEGG Term	Nr. Genes	% Associated Genes	pValue	Associated Genes Found
KEGG:04917	Prolactin signaling pathway	6	8.333333	5.765E-03	AKT1, ESR2, FOS, GRB2, SRC, STAT1
KEGG:04919	Thyroid hormone signaling pathway	7	5.9322033	1.114E-02	AKT1, MDM2, MYC, RXRB, SRC, STAT1, TP53
KEGG:05142	Chagas disease (American trypanosomiasis)	7	6.730769	6.148E-03	AKT1, FOS, GNAO1, IKBKG, JUN, SMAD2, TRAF6
KEGG:05145	Toxoplasmosis	6	5.084746	3.829E-02	AKT1, BCL2, GNAO1, IKBKG, STAT1, TRAF6
KEGG:05160	Hepatitis C	8	6.0150375	5.137E-03	AKT1, CDKN1A, EGFR, GRB2, IKBKG, STAT1, TP53, TRAF6
KEGG:05161	Hepatitis B	12	8.219178	6.068E-06	AKT1, BCL2, CDKN1A, FOS, GRB2, IKBKG, JUN, MYC, SRC, STAT1, TP53, YWHAQ
KEGG:05169	Epstein-Barr virus infection	13	6.372549	3.203E-05	AKT1, BCL2, CDKN1A, CSNK2B, IKBKG, JUN, MDM2, MYC, TP53, TRAF6, VIM, YWHAG, YWHAQ
KEGG:05205	Proteoglycans in cancer	13	6.3414636	3.324E-05	AKT1, CAMK2A, CAMK2B, CDKN1A, EGFR, ERBB4, GRB2, MDM2, MYC, PPP1CA, SMAD2, SRC, TP53
KEGG:05210	Colorectal cancer	7	11.290322	3.318E-04	AKT1, BCL2, FOS, JUN, MYC, SMAD2, TP53
KEGG:05212	Pancreatic cancer	6	9.090909	4.118E-03	AKT1, EGFR, IKBKG, SMAD2, STAT1, TP53
KEGG:05213	Endometrial cancer	5	9.615385	9.083E-03	AKT1, EGFR, GRB2, MYC, TP53
KEGG:05214	Glioma	8	12.121212	4.402E-05	AKT1, CAMK2A, CAMK2B, CDKN1A, EGFR, GRB2, MDM2, TP53
KEGG:05215	Prostate cancer	10	11.235955	4.003E-06	AKT1, BCL2, CDKN1A, EGFR, GRB2, HSP90AA1, HSP90AB1, IKBKG, MDM2, TP53
KEGG:05218	Melanoma	5	7.0422535	2.831E-02	AKT1, CDKN1A, EGFR, MDM2, TP53
KEGG:05219	Bladder cancer	6	14.634147	3.292E-04	CDKN1A, EGFR, MDM2, MYC, SRC, TP53
KEGG:05220	Chronic myeloid leukemia	8	10.958904	9.260E-05	ABL1, AKT1, CDKN1A, GRB2, IKBKG, MDM2, MYC, TP53
KEGG:05222	Small cell lung cancer	7	8.139535	2.458E-03	AKT1, BCL2, IKBKG, MYC, RXRB, TP53, TRAF6
KEGG:05223	Non-small cell lung cancer	5	8.928572	1.144E-02	AKT1, EGFR, GRB2, RXRB, TP53
KEGG:05224	Breast cancer	9	6.1643834	1.997E-03	AKT1, CDKN1A, EGFR, ESR2, FOS, GRB2, JUN, MYC, TP53

III.A.3.4 BRI2 brain region specific interactome

A second analytical approach used in this study of the BRI2 interactome, took into account the different brain regions, since this could be important and may reveal differences providing novel insights into specific BRI2 associated brain region-dependent processes. Therefore, the identification and characterization of the specific candidate BRI2 interactors from the three different brain regions: cerebral cortex, hippocampus, and cerebellum, was carried out (Figure III.A.5). A comparative analysis of the 511 candidate BRI2 interacting proteins identified in this study revealed that 108 proteins were specifically identified in the cerebral cortex, 62 in the hippocampus and 85 in the cerebellum (Figure III.A.5A). Further, 92 proteins were common to all regions, while 61 were shared by the cerebral cortex and cerebellum, 23 between cerebellum and hippocampus and 80 between cerebral cortex and hippocampus (Figure III.A.5A). Furthermore, given the particular interest in studying BRI2 function(s) in the CNS (central nervous system), a comparative analysis of the BRI2 ES interactome was also carried out (Figure III.A.5C). The results evidenced that while the majority of proteins were shared between brain regions (27 shared in all three regions, 17 shared in the cerebral cortex and cerebellum, 21 shared in cerebral cortex and hippocampus, and 2 shared in cerebellum and hippocampus), a subset of proteins were found to co-IP with BRI2 in specific brain regions (31 in cerebral cortex, 14 in hippocampus, and 8 in cerebellum) (Figure III.A.5C).

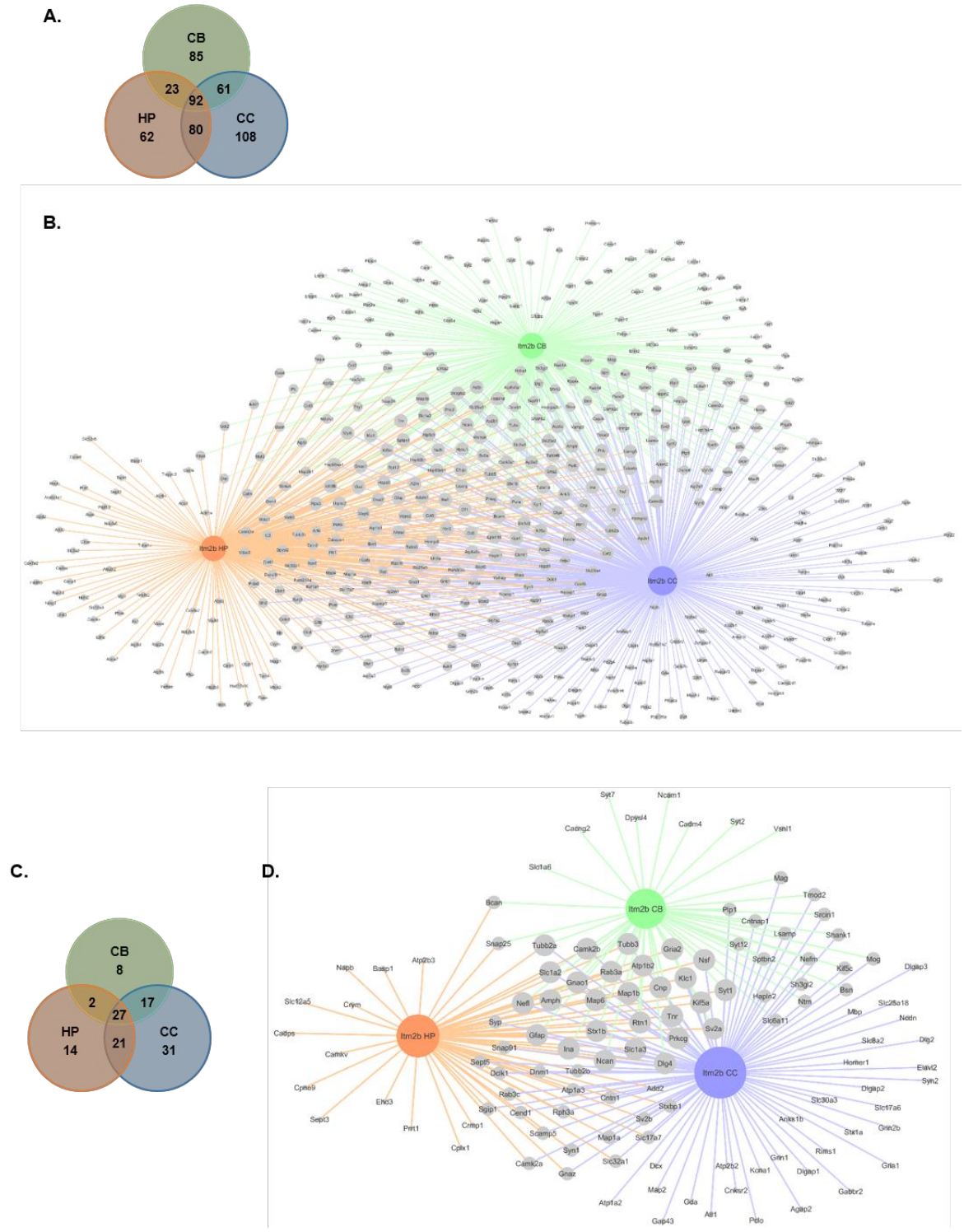

Figure III.A. 5 - Brain region specific protein interactions in the BRI2 interactome. (A, B) - Brain region specific protein interactions revealed in the identified BRI2 interactome. A- Venn diagram comparison of the brain region (cerebral cortex, hippocampus, and cerebellum) specific BRI2 protein interactions identified in this study. B- BRI2 interactome identified in this study. Node size according to the degree in the network. Edge color represents the source of interaction: blue edges correspond to the BRI2 interactions identified in the cerebral cortex, orange edges correspond to the BRI2 interactions identified in the hippocampus, and green edges correspond to the BRI2 interactions identified in the cerebellum. **(C, D)** - Brain region specific protein interactions revealed in the identified BRI2 ES interactome. C- Venn diagram comparison of the brain region (cerebral cortex, hippocampus, and cerebellum) specific BRI2 protein interactions

identified in this study, highly enriched or specific for the brain. D- BRI2 ES interactome identified in this study. Node size according to the degree in the network. Edge color represents the source of interaction: blue edges correspond to the BRI2 interactions identified in the cerebral cortex, orange edges correspond to the BRI2 interactions identified in the hippocampus, and green edges correspond to the BRI2 interactions identified in the cerebellum.

Once the BRI2 ES region specific interactomes were established (Fig. 4D), network augmentation was performed to enhance the experimental data with additional known and experimentally validated protein partners and obtain PPI networks (BRI2 ES region specific networks). For the cerebral cortex specific PPI network (Supplementary Figure III.A.S1A), a total of 292 proteins (nodes) with 330 connections (edges) between them was mapped. This network presents an average number of 2.243 neighbors. Regarding the hippocampus specific PPI network (Supplementary Figure III.A.S1B), 160 proteins, with 165 connections between them was mapped. The topological analysis revealed an average number of neighbors of 2.0625. The cerebellum-specific PPI network (Supplementary Figure III.A.S1C) was the smallest, with only 47 nodes connected by 47 edges, and with an average of 2.0 neighbors. To further address if the BRI2 interactome could be assigned to selective brain region-dependent processes, functional enrichment analysis of the BRI2 ES region specific networks, using the PANTHER online resource, was performed (Table III.A.3). Remarkably, biological process annotation evidenced that for the three BRI2 ES region specific networks, the highly enriched terms were similar to those previously associated with the BRI2 ES interactome, namely neuron differentiation and synaptic vesicle cycling (Table III.A.3 and Figure III.A.3A)

Table III.A. 3 -- Biological process enrichment analysis of the BRI2 ES regional specific networks (cerebral cortex, hippocampus and cerebellum) using Panther online resource. Enriched categories are identified as those with p-value <0.05, and GO terms presented correspond to the two most specific for each category retrieved in the analysis. Nr. Number.

GO term	Nr. proteins	Fold enrichment (%)	p-value	Associated proteins
BRI2 ES cerebral cortex specific network analysis				
synaptic vesicle fusion to presynaptic active zone membrane (GO:0031629)	9	55.78	1.28E-09	SNAP25, SNAP23, SNAP47, STX3, STX2, SNAP29, STX11, STX1A, STX4
vesicle fusion with Golgi apparatus (GO:0048280)	6	44.62	5.70E-05	VTI1B, SEC22B, BET1, GOSR2, STX5, SEC22A
dendrite morphogenesis (GO:0048813)	9	13.66	2.62E-04	DLG4, ITGB1, FYN, DCX, ABI1, SHANK3, SHANK1, CAMK2A, MAP2
protein localization to membrane (GO:0072657)	22	4.07	3.48E-04	RTP2, TNF, VAMP4, VAMP3, VAMP2, DLG4, SNAP25, ITGB7, SNAP47, NUP54, DLG2, TMED2, STX3, SHANK3, DLG1, DLG3, STX1A, NSF, VAMP5, EGFR, RPS8, TNIK
learning (GO:0007612)	13	7.11	5.05E-04	DLG4, SNAP25, SLC8A2, ITGB1, SHANK2, FYN, HTT, SHANK3, ATP1A2, SHANK1, APP, PARK2, GRIN1
regulation of protein localization to plasma membrane (GO:1903076)	10	10.47	5.25E-04	VTI1B, ITGB1, PIK3R1, STX8, STX3, GOPC, DLG1, STX7, EGFR, STX4
ERBB2 signaling pathway (GO:0038128)	8	15.26	6.70E-04	GRB2, CDC37, PTPN12, SRC, PIK3R1, ERBB4, ERBB2, EGFR
long-term synaptic potentiation (GO:0060291)	8	14.87	8.11E-04	VAMP2, SNAP25, SLC8A2, SHANK2, SNAP47, STX3, SHANK3, STX4
retrograde vesicle-mediated transport, Golgi to ER (GO:0006890)	10	9.18	1.74E-03	TMED9, RINT1, SEC22B, KDELR1, TMED2, KIF18A, HTT, USE1, BNIP1, NSF
retrograde transport, endosome to Golgi (GO:0042147)	10	9.07	1.95E-03	TRIM27, VAMP3, TMED9, DCTN1, VTI1B, STX10, STX16, GOSR2, STX5, STX6
post-Golgi vesicle-mediated transport (GO:0006892)	10	8.55	3.32E-03	VAMP4, VAMP3, VAMP2, VTI1B, SNAP23, GOSR2, GOPC, NSF, VAMP5, STX4
receptor localization to synapse (GO:0097120)	5	33.80	4.14E-03	DLG4, DLG2, ANKS1B, DLG1, DLG3
regulation of ion transport (GO:0043269)	25	3.17	4.50E-03	TRIM27, CREB3, VAMP3, KCNA3, PRKACA, VAMP2, PLN, DLG4, GPM6B, YWHAE, KCNA1, PLCG1, HTT, SHANK3, ATP1A2, PRKCD, ATP2B2, ABL1, HOMER1, SHANK1, DLG1, CALCA, KCNA10, CAMK2A, PARK2
vesicle-mediated transport to the plasma membrane (GO:0098876)	9	9.70	4.52E-03	VAMP4, VAMP3, VAMP2, SNAP25, SNAP47, STX3, GOPC, NSF, VAMP5
positive regulation of excitatory postsynaptic potential (GO:2000463)	6	20.28	5.65E-03	RIMS1, DLG4, SHANK3, SHANK1, STX1A, GRIN1
GDP metabolic process (GO:0046710)	5	28.60	9.33E-03	MAGI3, DLG4, DLG2, DLG1, DLG3
neuromuscular process (GO:0050905)	10	7.36	1.25E-02	DLG4, KCNA1, PTPRQ, SHANK3, ATP2B2, ABL1, SHANK1, APP, PARK2, GRIN1
SNARE complex assembly (GO:0035493)	4	49.58	1.33E-02	VAMP4, VAMP3, VAMP1, STX4
protein localization to synapse (GO:0035418)	6	17.16	1.47E-02	DLG4, SNAP25, SNAP47, STX3, SHANK1, PCLO
regulation of intracellular transport (GO:0032386)	22	3.24	1.54E-02	CREB3, TNF, VAMP3, RIMS1, VAMP2, PLN, NAPB, SRC, EMD, YWHAE, RINT1, NUP54, PIK3R1, RNASE2, ERBB4, ERBB2, PRKCD, HMOX1, MDM2, STX1A, PARK2, EGFR
peptidyl-tyrosine phosphorylation (GO:0018108)	13	5.14	1.83E-02	TRIM27, INSR, CDC37, SRC, ABI3, FYN, PIBF1, ERBB4, ERBB2, ABI1, PRKCD, ABL1, EGFR
COPII vesicle coating (GO:0048208)	8	9.75	1.86E-02	GOLGA2, GRIA1, SEC22B, BET1, TMED2, GOSR2, STX5, NSF

GO term	Nr. proteins	Fold enrichment (%)	p-value	Associated proteins
activation of protein kinase activity (GO:0032147)	16	4.09	2.38E-02	TNF, AGAP2, INSR, ITGB3, PRKACA, SRC, PIBF1, CRK, PLCG1, PRKCD, ABL1, CD81, DLG1, CALCA, EGFR, TNIK
synaptic vesicle docking (GO:0016081)	4	37.18	4.12E-02	SNAP25, STX3, BLOC1S6, STX1A
BRI2 ES hippocampus specific network analysis				
synaptic vesicle fusion to presynaptic active zone membrane (GO:0031629)	7	77.92	6.23E-08	STX19, STX1B, STX3, STX2, SNAP29, STX1A, STX4
cytoskeleton organization (GO:0007010)	28	3.97	3.85E-06	CRMP1, PFN1, DPYSL3, UBE2B, MYO18A, KLHL20, DPYSL2, ACTR2, SRC, FLNA, ADD2, DBN1, SDCBP, LIMA1, ZAK, ANK2, KIF18A, HTT, PIP5K1A, ANLN, SPRY2, SEPT1, SYNE4, CCDC155, AXIN1, MYH9, VIM, CDK5RAP2
vesicle docking (GO:0048278)	9	20.73	6.79E-06	STX19, STX1B, STX3, STX2, STX16, STX5, STX1A, STX4, STX6
intracellular protein transport (GO:0006886)	23	4.15	7.66E-05	AP3M1, CDC37, NAPB, STX19, EHD3, YWHAE, SDCBP, STX1B, VCP, STX3, MICALL1, ANK2, STX2, PIP5K1A, MYO1C, MCM3AP, STX16, BID, STX5, ARL6IP1, STX1A, STX4, STX6
cell projection organization (GO:0030030)	25	3.23	1.95E-03	CRMP1, MAPK8IP2, UBE2B, IQCB1, RTN4, DPYSL2, HMGB1, ACTR2, SRC, FLNA, EHD3, TMEM17, YWHAE, SDCBP, RPS6KA5, LIMA1, INTU, STX3, MICALL1, IQGAP1, PIP5K1A, SNAP29, SLC12A5, MYH9, CDK5RAP2
Golgi vesicle transport (GO:0048193)	14	5.62	2.22E-03	MYO18A, KLHL20, EHD3, RBSN, BET1, TFG, VCP, ANK2, KIF18A, HTT, STX5, STX4, ANKFY1, STX6
spindle localization (GO:0051653)	6	20.04	5.83E-03	ACTR2, HTT, SPRYZ, CCDC155, MYH9, CDK5RAP2
cell differentiation (GO:0030154)	50	1.95	1.00E-02	CRMP1, DPYSL3, MAPK8IP2, UBE2B, MAPK6, RTN4, ATF2, DPYSL2, HMGB1, ACTR2, SRC, FLNA, AGR2, DBN1, IL33, YWHAE, PSMD11, RPS6KA5, BASP1, STX1B, INTU, STX3, CDK5RAP3, ZAK, MICALL1, ANK2, IQGAP1, STX2, RNF8, FXR1, PIP5K1A, ANLN, SMPD3, SPRY2, HNRNPH3, RIPK3, SYNE4, SLC12A5, HSPE1, CCDC155, AXIN1, GNB2L1, MYH9, ANXA7, VIM, TRIP13, CDK5RAP2, CPNE9, FAS, RGS2
protein complex assembly (GO:0006461)	23	3.04	1.75E-02	DPYSL3, MAPK8IP2, TK1, RTN4, SRC, ADD2, EHD3, PSMD11, BET1, TFG, VCP, CADPS, NDUFV2, STX2, AMFR, ANLN, SNAP29, RIPK3, BID, STX5, AXIN1, STX4, FAZ
regulation of cysteine-type endopeptidase activity involved in apoptotic process (GO:0043281)	10	6.61	2.92E-02	HMGB1, SRC, YWHAE, VCP, SERPINB9, BID, ARL6IP1, HSPE1, GNB2L1, FAZ
actin filament-based process (GO:0030029)	15	4.14	3.50E-02	PFN1, DPYSL3, MYO18A, ACTR2, SRC, FLNA, ADD2, DBN1, SDCBP, LIMA1, ANK2, PIP5K1A, CCDC155, MYH9, VIM
supramolecular fiber organization (GO:0097435)	13	4.72	3.97E-02	DPYSL3, ACTR2, SRC, FLNA, ADD2, DBN1, LIMA1, KIF18A, RIPK3, CCDC155, AXIN1, VIM, HSP90AB1
positive regulation of intracellular signal transduction (GO:1902533)	21	3.08	4.21E-02	MAPK8IP2, RGL2, PELI2, HMGB1, SRC, FLNA, SDCBP, TFG, CDK5RAP3, ZAK, IQGAP1, HTT, PLA2G2A, SPRY2, RIPK3, BID, CCL18, AXIN1, GNB2L1, EEF1D, FAS
cytosolic transport (GO:0016482)	8	8.62	4.29E-02	KLHL20, ACTR2, EHD3, RBSN, STX16, STX5, ANKFY1, STX6
BRI2 ES cerebellum specific network analysis				
synaptic vesicle recycling (GO:0036465)	4	60.13	5.56E-03	SH3GL2, SYT2, SYT7, SH3GL1
endocytosis (GO:0006897)	9	7.44	2.22E-02	SH3GL3, SH3GL2, WIPF1, DPYSL2, SYT2, SYT7, CSNK1E, SH3GL1, CACNG2
developmental process (GO:0032502)	28	2.42	2.29E-03	SH3GL3, COL10A1, SH3GL2, GFI1B, DPYSL4, DPYSL2, PRKD2, RHEB, SYT2, SIAH1, ITM2B, KIF18A, PTPRO, HTT, SRPK2, CSNK1E, SH3GL1,

GO term	Nr. proteins	Fold enrichment (%)	p-value	Associated proteins
				SPRED1, TFF1, LITAF, SYNE4, UCHL1, CCDC155, TRIP13, ARIH2, SPRY3, SPRED2, NCAM1

III.A.3.5 Validation of HPLC-MS/MS-identified BRI2 interactors by immunoblotting analysis

The identification of DLG4, also known as PSD-95, in the BRI2 ES interactome is of paramount importance since it suggests, for the first time, the presence of BRI2 in the postsynaptic compartment, particularly at the postsynaptic density (PSD). For this reason, PSD-95 was selected for experimental validation. Briefly, we co-immunoprecipitated BRI2 from the three brain regions as well as the mock negative controls using a specific antibody. These Co-IPs were analyzed using SDS-PAGE and immunoblotted with the BRI2 antibody (Figure III.A.6). First, it was possible to confirm that the BRI2 co-immunoprecipitation approach in the 3 brain regions was effective since when a BRI2 antibody was used in immunoblotting, a signal in the range of 37-40 kDa was detected, corresponding to the full-length BRI2 protein (Figure III.A.6). Nonetheless, lower signals in the negative controls (mock IP controls – dynabeads protein G coupled with mouse IgG; Figure III.A.6) were also detected. Moreover, using a PSD-95 specific antibody, a prominent signal in the range of 95-100 kDa was evident in all the BRI2 co-immunoprecipitations, which is consistent with the molecular weight of the PSD-95 protein. These results were consistent with the mass spectrometry data, validating the formation of a complex containing BRI2 and PSD-95 (Figure III.A.4 and Figure III.A.6).

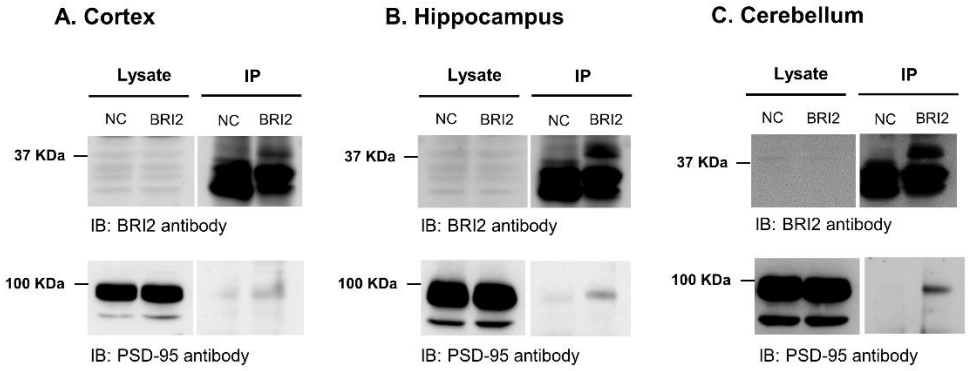

Figure III.A. 6 - Co-immunoprecipitation of the BRI2 in rat brain tissue lysate and western blot for BRI2 and PSD-95. Rat cerebral cortex (A), hippocampus (B) and cerebellum (C) were immunoprecipitated with a mouse monoclonal BRI2 antibody bound to protein G Dynabeads. The mock IP negative controls were performed by incubating cell extracts with G Dynabeads coupled with mouse IgG. NC, mock IP negative controls.

III.A.4 Discussion

BRI2 is a relevant protein in the pathogenesis of the neurodegenerative diseases FBD and FDD, as well as in AD, given its association with APP and its effects on Abeta production, aggregation and degradation (Fotinopoulou *et al*. 2005; Matsuda *et al*. 2005; Matsuda *et al*. 2011; Willander *et al*. 2012). Several lines of evidence suggest a role for BRI2 at the nerve terminals (Akiyama *et al*. 2004) and in neurite outgrowth (Choi *et al*. 2004; Martins *et al*. 2016; Martins *et al*. 2017), however, its precise physiological function and associated signaling pathways remain elusive. The study of PPI networks is a valuable methodology to uncover the role of previously uncharacterized proteins in pathways or protein complexes, both in healthy and diseased states. Therefore, the identification of the BRI2 interactome is crucial for understanding the biological functions of BRI2 in the CNS. This study focused on elucidating and characterizing the BRI2 brain interactome, which was isolated from rat cerebral cortex, hippocampus and cerebellum by co-immunoprecipitation assays, using a specific BRI2 antibody. This approach identified 511 protein candidates as potential BRI2 brain interactors, of which two were previously reported in public protein interaction databases: Ppp1ca and Cacna2d1. PP1 is a major serine/threonine phosphatase that was recently found to interact directly with BRI2. The BRI2:PP1 complex seems to be of paramount importance in the nervous system since BRI2 dephosphorylation by PP1 appears to be responsible for the regulation of its role in neurite outgrowth (Martins *et al*. 2016; Martins *et al*. 2017). In total, approximately 5% of the currently suggested BRI2 interacting proteins were identified in the work here presented. Of note, only a small number of these previously reported BRI2 interacting proteins have actually been validated. Moreover, the failure to identify other known BRI2 interactors might be due to several factors. For instance, limitations of this study include the possibility of poor recovery of the membrane and nuclear proteins, not detecting weak or transient interactions, and the cellular/tissue expression of the proteins previously detected. It is also crucial to take into account that the HPLC-MS/MS technique identifies co-complex interactions which include direct physical interactions but also indirect co-complex associations (Kim *et al*. 2010). Remarkably, although the BRI2 interactors here identified do not present a high overlap with the others previously reported in the literature, many were functionally similar or related. It is also important to note that a specific BRI2 antibody that recognizes the N-terminal of the protein was used. Since BRI2 suffers proteolytic cleavages that originate different BRI2 N-terminal fragments, when we perform the co-IP experiments we isolated not only full-length BRI2 but also the different BRI2 N-terminal fragments.

In this study, the BRI2 brain interactome was identified, and thus a tissue-specific network-based approach was used. Of the 511 candidate BRI2 brain interactors identified in this study, 120 were highly specific or strongly expressed in the brain. Functional enrichment analysis for cellular component of the brain BRI2 interactome suggests a subcellular localization for the BRI2 protein in

neuron projections, synapses, both presynapse and postsynapse, and associated with synaptic vesicles (Figure III.A.3B). These results together with the fact that the majority of these BRI2 interactors are cytoskeletal proteins, transporters and membrane traffic proteins (Figure III.A.2) are consistent with the concept that BRI2 in the CNS has a role in nerve terminals and neuronal differentiation (Choi *et al*. 2004; Akiyama *et al*. 2004; Martins *et al*. 2016; Martins *et al*. 2017). Analysis of the BRI2 ES interactome resulted in the identification of proteins associated with several processes of the synaptic vesicle cycle, such as neurotransmitter uptake and vesicle docking, priming, fusion and exocytosis (Figure III.A.3A and Supplementary Table III.A.S5). For instance, syntaxin 1 (Stx1a; Stx1b) and synaptosome-associated protein 25 (Snap25) are core components of a SNARE (soluble N-ethylmaleimide-sensitive factor [NSF]-attachment protein receptor) complex, formed by V and T-SNARE proteins. This complex assembly between vesicle and plasma membrane constitutes a key step in exocytosis and neurotransmitter release that is rendered Ca^{2+}-dependent by interaction with synaptotagmin-1 (Syt1), a Ca^{2+} sensor synaptic vesicle-associated protein (Sørensen *et al*. 2006; Südhof and Rothman 2009; Jahn and Fasshauer 2012; Geppert *et al*. 1994; Voets *et al*. 2001). Moreover, several proteins in the BRI2 ES interactome associated with the microtubule transport machinery were found, in particular β-tubulin isotype III (Tubb3b), β-tubulin isotype IIb (Tubb2b), kinesin heavy chain isoforms 5a and 5c (Kif5a and kif5c, respectively), and kinesin light chain isoform 1 (Klc1). Neuronal trafficking is a crucial process to the formation and dynamics of both presynaptic and postsynaptic structures and depends on molecular motor proteins that move along the cytoskeleton. Kif5a and Kif5c are two kinesin heavy chain (KHC) neuron-specific isoforms, and klc1 is a neuronally enriched kinesin light chain (KLC) isoform that are components of the kinesin I, a motor protein important for trafficking in axons and dendrites (Rahman *et al*. 1998; Xia *et al*. 1998). Therefore, these results suggest that in neurons, BRI2 is transported within axons by anterograde axonal transport to the distal nerve terminals where the full-length protein or even its N-terminal fragments may interact with the neurotransmitter machinery release and contribute to synaptic signaling.

The present results regarding the BRI2 ES interactome also suggest an association for BRI2 with synaptic transmission, plasticity, and learning. Several BRI2 brain interactome members including disk large homolog 4 (Dlg4/PSD-95), calcium/calmodulin-dependent protein kinase II alpha (Camk2a/CamkIIα), calcium/calmodulin-dependent protein kinase II beta (Camk2b/CamkIIβ), protein phosphatase 1 (PP1/Ppp1ca), (glutamate receptor ionotropic NMDA1 (Grin1/NR1/GluN1), glutamate receptor ionotropic NMDA2B (Grin2b/GluN2B/NR2B), glutamate receptor ionotropic AMPA1 (Gria1/GluA1/GluR-1) and glutamate receptor ionotropic AMPA2 (Gria2/GluA2/GluR-2) all participate in these processes. The PSD-95 protein was identified in our interactome firstly by MS analysis and further validated by immunoblotting analysis as novel BRI2 interactor in all three brain

regions, suggesting the presence of BRI2 in the postsynaptic compartments. PSD-95 is a major scaffold protein in the brain and concentrated in the postsynaptic density (PSD) of excitatory synapses, implicated in synapse maturation and in regulating synaptic strength and plasticity (Nelson *et al*. 2013; Yoshii and Constantine-Paton 2014; Kim *et al*. 2007). PSD-95 interacts with both AMPA receptors (AMPARs) and NMDA-type glutamate receptors (NMDARs) through its PDZ (PSD-95/Dlg/ZO-1) domain, and its overexpression increases the number of synapses expressing AMPARs (Béïque and Andrade 2003; El-Husseini *et al*. 2000). The NMDAR subunit GluN2B was also found to bind directly and to colocalize with PSD-95 in rat hippocampal neurons, and the interaction serves to anchor the NMDARs to the submembrane cytoskeleton (Niethammer *et al*. 1996; Kornau *et al*. 1995). Therefore, it is plausible to hypothesize that BRI2 may also be involved in synaptic transmission and plasticity by altering the AMPAR and NMDAR trafficking which affects excitatory synaptic transmission. Consistent with a role for BRI2 in synaptic plasticity, learning and memory, *Itm2b* (+/-) mice exhibit synaptic and memory deficits. Knock-in mouse models of FDD and FBD, FDD_{KI} and FBD_{KI} respectively, exhibit similar deficits which are attributed to the loss of BRI2 function in those neurodegenerative diseases (Tamayev *et al*. 2010a; Tamayev *et al*. 2010b). Moreover, in a synaptosomal proteome characterization of the mouse model FDD_{KI}, PSD-95 expression was found decreased and pointed as a potential player in the altered synaptic transmission and activity observed in this mice (Vitale *et al*. 2012). PSD-95 knockout mice display several phenotypic similarities, such as abnormal synaptic plasticity as well as abnormal memory and learning (Feyder *et al*. 2010). The synaptic accumulation of PSD-95 is a key feature in its ability to potentiate synaptic transmission. PSD-95 phosphorylation of Ser295 by JNK1 enhances its synaptic accumulation, whereas dephosphorylation of this PSD-95 residue by PP1/PP2A is required for AMPA receptor internalization and LTD (Kim *et al*. 2007). However, there are no clear evidence whether Ser295 phosphorylation enhances synaptic transport or postsynaptic stability of PSD-95.

An exciting feature of this BRI2 interactome, is the high number of cytoskeleton proteins which translated into an overrepresentation of functions like cytoskeleton organization and microtubule-based processes, evidently important for neuronal differentiation (Figure III.A.3A). Rearrangements of actin and microtubules cytoskeletons are crucial to establish and maintain polarity in neurons, in neural migration and vesicle trafficking (Barnes and Polleux 2009; Stiess and Bradke 2011). In fact, almost 50% (49 out of the 120) of the brain BRI2 ES interactome proteins are annotated with neuronal differentiation related biological processes (Supplementary Table III.A.S7), and the construction of a BRI2-neuronal differentiation-specific PPI subnetwork (Figure III.A.4) allowed us to explore the biological functionalities and the potential underlying molecular mechanisms of BRI2 in these processes. In line with this observation, functional enrichment pathway analysis of the expanded BRI2-neuronal differentiation-specific interactome associated BRI2 interactors to

signalling pathways involved in several neuronal differentiation related events, namely adherens junction, axon guidance, ErbB signalling pathway (Iwakura and Nawa 2013; Mei and Nave 2014), FoxO signalling pathway (Wen *et al*. 2012), neurotrophin signalling pathway (Reichardt 2006) and estrogen signalling pathway (Wang *et al*. 2003) (Table III.A.2). These results strengthen the proposed role for BRI2 in neuronal differentiation and neurite outgrowth and an association of BRI2 with these signaling pathways deserve further investigations.

The identification of adhesion proteins, such as neural cell adhesion molecule (Ncam1), a member of the Ig superfamily of cell-adhesion molecules (Kleene *et al*. 2010) in the study here presented lead us to propose that one of the mechanisms by which BRI2 promotes neurite outgrowth might be by regulating cell-cell adhesion. Ncam associates with numerous cytoskeletal components but also with some signaling pathways associated with a neurite outgrowth response (Hansen *et al*. 2008). For instance, Ncam interacts with spectrin, a protein involved in linking cellular membranes to the actin filament cytoskeletal system, which in turns interacts with the growth-associated protein 43 (GAP-43), a protein that is highly expressed in growth cones and believed to be important for growth cone extension. Likewise, Ncam-mediated neurite outgrowth was inhibited in neurons from GAP-43 knockout mice, supporting a functional relationship between Ncam and GAP-43 (Hansen *et al*. 2008). Remarkably, both spectrin (Sptbn2) and GAP-43 (Gap43) were identified in our BRI2 interactome and therefore these mechanisms deserve further investigation. Moreover, it has already been described that BRI2 is able to form homodimers linked by disulfide bonds that appear at the cell surface resembling the structure of a cell-surface receptor (Tsachaki *et al*. 2010). Although a receptor function for BRI2 has not been established it is possible to hypothesize that BRI2, triggered by ligand interaction, may act as a cell surface receptor participating in the above-mentioned signaling pathways. It was recently demonstrated by our group that BRI2 phosphorylation modulates its proteolytic processing and neuritogenic role. Moreover, for BRI2 mediated neurite outgrowth, it appears that phosphorylation of full-length protein promotes the emergence of neurites whereas the increased BRI2 NTFs play a relevant role in neurites' elongation and stabilization (Martins *et al*. 2017). Thus, it is also plausible to assume that mechanisms underlying BRI2 role in neurite outgrowth may also involve: (1) BRI2 full-length phosphorylation induces conformational changes in the protein which affect protein-protein binding, and for instance could affect binding to neurotrophic effectors of the above signalling pathways; (2) increased BRI2 proteolytic processing to its secreted fragment (containing the BRICHOS domain) which can activate the above signalling pathways via a growth factor receptor.

Finally, a comparative analysis approach of the BRI2 ES interactome in the three different brain regions was employed, resulting in the identification of 31 proteins specifically in the cerebral cortex, 14 in the hippocampus, and 8 in the cerebellum (Figure III.A.5C). The results evidenced that in the

different brain regions BRI2 seems to be associated to cellular processes also highlighted in the analysis of the total BRI2 ES interactome, namely neuron development and synaptic vesicle cycle (Table III.A.3), supporting that the majority of the biological functions of BRI2 in the CNS are in fact relatively stable across the three brain regions.

In summary, these results provide important insights on BRI2 brain interactome, comprising several new putative interacting partners. We observed a complex interaction of BRI2 with proteins related to neuronal differentiation, neurite outgrowth, synaptic signaling and plasticity. Further, we validated both PSD-95 as novel BRI2 interactor in the brain using co-IP and immunoblotting analysis. Therefore, the work here presented provides a valuable list of BRI2 interacting proteins for further studies to investigate their potential roles in BRI2 biology and the underlying molecular mechanisms, as well as novel insights in its associated pathologies (FBD, FDD, and AD).

References

Akiyama H., Kondo H., Arai T., Ikeda K., Kato M., Iseki E., Schwab C., McGeer P. L. (2004) Expression of BRI, the normal precursor of the amyloid protein of familial British dementia, in human brain. *Acta Neuropathol*. **107**, 53–8.

Barnes A. P., Polleux F. (2009) Establishment of axon-dendrite polarity in developing neurons. *Annu. Rev. Neurosci*. **32**, 347–81.

Béïque J.-C., Andrade R. (2003) PSD-95 regulates synaptic transmission and plasticity in rat cerebral cortex. *J. Physiol*. **546**, 859–67.

Bell R., Hubbard A., Chettier R., Chen D., Miller J. P., Kapahi P., Tarnopolsky M., Sahasrabuhde S., Melov S., Hughes R. E. (2009) A human protein interaction network shows conservation of aging processes between human and invertebrate species. *PLoS Genet*. **5**, e1000414.

Berndt J. D., Aoyagi A., Yang P., Anastas J. N., Tang L., Moon R. T. (2011) Mindbomb 1, an E3 ubiquitin ligase, forms a complex with RYK to activate Wnt/β-catenin signaling. *J. Cell Biol*. **194**, 737–50.

Bindea G., Mlecnik B., Hackl H., Charoentong P., Tosolini M., Kirilovsky A., Fridman W.-H., Pagès F., Trajanoski Z., Galon J. (2009) ClueGO: a Cytoscape plug-in to decipher functionally grouped gene ontology and pathway annotation networks. *Bioinformatics* **25**, 1091–3.

Campo M. Del, Hoozemans J. J. M., Dekkers L.-L., Rozemuller A. J., Korth C., Müller-Schiffmann A., Scheltens P., et al. (2014) BRI2-BRICHOS is increased in human amyloid plaques in early stages of Alzheimer's disease. *Neurobiol. Aging* **35**, 1596–604.

Choi S.-I., Vidal R., Frangione B., Levy E. (2004) Axonal transport of British and Danish amyloid peptides via secretory vesicles. *FASEB J*. **18**, 373–5.

Cross M., Nguyen T., Bogdanoska V., Reynolds E., Hamilton J. A. (2005) A proteomics strategy for the enrichment of receptor-associated complexes. *Proteomics* **5**, 4754–63.

Danielsen J. M. R., Sylvestersen K. B., Bekker-Jensen S., Szklarczyk D., Poulsen J. W., Horn H., Jensen L. J., Mailand N., Nielsen M. L. (2011) Mass spectrometric analysis of lysine ubiquitylation reveals promiscuity at site level. *Mol. Cell. Proteomics* **10**, M110.003590.

del-Toro N., Dumousseau M., Orchard S., Jimenez R. C., Galeota E., Launay G., Goll J., et al. (2013) A new reference implementation of the PSICQUIC web service. *Nucleic Acids Res*. **41**, W601-6.

El-Husseini A. E., Craven S. E., Chetkovich D. M., Firestein B. L., Schnell E., Aoki C., Bredt D. S. (2000) Dual Palmitoylation of Psd-95 Mediates Its Vesiculotubular Sorting, Postsynaptic Targeting, and Ion Channel Clustering. *J. Cell Biol*. **148**.

Feyder M., Karlsson R.-M., Mathur P., Lyman M., Bock R., Momenan R., Munasinghe J., et al. (2010) Association of Mouse *Dlg4* (PSD-95) Gene Deletion and Human *DLG4* Gene Variation With Phenotypes Relevant to Autism Spectrum Disorders and Williams' Syndrome. *Am. J. Psychiatry* **167**, 1508–1517.

Fleischer A., Ayllón V., Dumoutier L., Renauld J.-C., Rebollo A. (2002) Proapoptotic activity of ITM2B(s), a BH3-only protein induced upon IL-2-deprivation which interacts with Bcl-2. *Oncogene* **21**, 3181–9.

Fotinopoulou A., Tsachaki M., Vlavaki M., Poulopoulos A., Rostagno A., Frangione B., Ghiso J., Efthimiopoulos S. (2005) BRI2 interacts with amyloid precursor protein (APP) and regulates amyloid beta (Abeta) production. *J. Biol. Chem*. **280**, 30768–72.

Geppert M., Goda Y., Hammer R. E., Li C., Rosahl T. W., Stevens C. F., Südhof T. C. (1994) Synaptotagmin I: a major Ca2+ sensor for transmitter release at a central synapse. *Cell* **79**, 717–27.

Gupta G. D., Coyaud É., Gonçalves J., Mojarad B. A., Liu Y., Wu Q., Gheiratmand L., et al. (2015) A Dynamic Protein Interaction Landscape of the Human Centrosome-Cilium Interface. *Cell* **163**, 1483–1499.

Han C., Park I., Lee B., Jin S., Choi H., Kwon J. T., Kwon Y., Kim D. H., Park Z. Y., Cho C. (2011) Identification of heat shock protein 5, calnexin and integral membrane protein 2B as Adam7-interacting membrane proteins in mouse sperm. *J. Cell. Physiol*. **226**, 1186–95.

Hansen S. M., Berezin V., Bock E. (2008) Signaling mechanisms of neurite outgrowth induced by the cell adhesion molecules NCAM and N-Cadherin. *Cell. Mol. Life Sci*. **65**, 3809–3821.

Hein M. Y., Hubner N. C., Poser I., Cox J., Nagaraj N., Toyoda Y., Gak I. A., et al. (2015) A human interactome in three quantitative dimensions organized by stoichiometries and abundances. *Cell* **163**, 712–23.

Hodge K., Have S., Hutton L., Lamond A. (2013) Cleaning up the masses: Exclusion lists to reduce contamination with HPLC-MS/MS. *J. Proteomics* **88**, 92–103.

Holton J. L., Lashley T., Ghiso J., Braendgaard H., Vidal R., Guerin C. J., Gibb G., et al. (2002) Familial Danish dementia: a novel form of cerebral amyloidosis associated with deposition of both amyloid-Dan and amyloid-beta. *J. Neuropathol. Exp. Neurol.* **61**, 254–67.

Huttlin E. L., Ting L., Bruckner R. J., Gebreab F., Gygi M. P., Szpyt J., Tam S., et al. (2015) The BioPlex Network: A Systematic Exploration of the Human Interactome. *Cell* **162**, 425–40.

Iwakura Y., Nawa H. (2013) ErbB1-4-dependent EGF/neuregulin signals and their cross talk in the central nervous system: pathological implications in schizophrenia and Parkinson's disease. *Front. Cell. Neurosci.* **7**, 4.

Jahn R., Fasshauer D. (2012) Molecular machines governing exocytosis of synaptic vesicles. *Nature* **490**, 201–207.

Kim E. D., Sabharwal A., Vetta A. R., Blanchette M. (2010) Predicting direct protein interactions from affinity purification mass spectrometry data. *Algorithms Mol. Biol.* **5**, 34.

Kim M. J., Futai K., Jo J., Hayashi Y., Cho K., Sheng M. (2007) Synaptic Accumulation of PSD-95 and Synaptic Function Regulated by Phosphorylation of Serine-295 of PSD-95. *Neuron* **56**, 488–502.

Kim W., Bennett E. J., Huttlin E. L., Guo A., Li J., Possemato A., Sowa M. E., et al. (2011) Systematic and quantitative assessment of the ubiquitin-modified proteome. *Mol. Cell* **44**, 325–40.

Kleene R., Mzoughi M., Joshi G., Kalus I., Bormann U., Schulze C., Xiao M.-F., Dityatev A., Schachner M. (2010) NCAM-Induced Neurite Outgrowth Depends on Binding of Calmodulin to NCAM and on Nuclear Import of NCAM and fak Fragments. *J. Neurosci.* **30**, 10784–10798.

Kornau H. C., Schenker L. T., Kennedy M. B., Seeburg P. H. (1995) Domain interaction between NMDA receptor subunits and the postsynaptic density protein PSD-95. *Science* **269**, 1737–40.

Liu X., Yu X., Zack D. J., Zhu H., Qian J. (2008) TiGER: a database for tissue-specific gene expression and regulation. *BMC Bioinformatics* **9**, 271.

Martin L., Fluhrer R., Reiss K., Kremmer E., Saftig P., Haass C. (2008) Regulated intramembrane proteolysis of Bri2 (Itm2b) by ADAM10 and SPPL2a/SPPL2b. *J. Biol. Chem.* **283**, 1644–52.

Martins F., Rebelo S., Santos M., Cotrim C. Z., Cruz E Silva E. F. da, Cruz E Silva O. A. B. da (2016) BRI2 and BRI3 are functionally distinct phosphoproteins. *Cell. Signal.* **28**, 130–44.

Martins F., Serrano J., Muller T., Cruz e Silva O. da, Rebelo S. (2017) BRI2 processing and its neuritogenic role are modulated by protein phosphatase 1 complexing. *J. Cell. Biochem.* **in press**.

Matsuda S., Giliberto L., Matsuda Y., Davies P., McGowan E., Pickford F., Ghiso J., Frangione B., D'Adamio L. (2005) The familial dementia BRI2 gene binds the Alzheimer gene amyloid-beta precursor protein and inhibits amyloid-beta production. *J. Biol. Chem.* **280**, 28912–6.

Matsuda S., Matsuda Y., Snapp E. L., D'Adamio L. (2011) Maturation of BRI2 generates a specific inhibitor that reduces APP processing at the plasma membrane and in endocytic vesicles. *Neurobiol. Aging* **32**, 1400–8.

Mei L., Nave K.-A. (2014) Neuregulin-ERBB signaling in the nervous system and neuropsychiatric diseases. *Neuron* **83**, 27–49.

Mi H., Huang X., Muruganujan A., Tang H., Mills C., Kang D., Thomas P. D. (2017) PANTHER version 11: expanded annotation data from Gene Ontology and Reactome pathways, and data analysis tool enhancements. *Nucleic Acids Res.* **45**, D183–D189.

Murn J., Zarnack K., Yang Y. J., Durak O., Murphy E. A., Cheloufi S., Gonzalez D. M., et al. (2015) Control of a neuronal morphology program by an RNA-binding zinc finger protein, Unkempt. *Genes Dev.* **29**, 501–12.

Nelson C. D., Kim M. J., Hsin H., Chen Y., Sheng M. (2013) Phosphorylation of threonine-19 of PSD-95 by GSK-3β is required for PSD-95 mobilization and long-term depression. *J. Neurosci.* **33**, 12122–35.

Niethammer M., Kim E., Sheng M. (1996) Interaction between the C terminus of NMDA receptor subunits and multiple members of the PSD-95 family of membrane-associated guanylate kinases. *J. Neurosci.* **16**, 2157–63.

Odom D. T., Zizlsperger N., Gordon D. B., Bell G. W., Rinaldi N. J., Murray H. L., Volkert T. L., et al. (2004) Control of pancreas and liver gene expression by HNF transcription factors. *Science* **303**, 1378–81.

Plant G. T., Révész T., Barnard R. O., Harding A. E., Gautier-Smith P. C. (1990) Familial cerebral amyloid angiopathy with nonneuritic amyloid plaque formation. *Brain*, 721–47.

Rahman A., Friedman D. S., Goldstein L. S. (1998) Two kinesin light chain genes in mice. Identification and characterization of the encoded proteins. *J. Biol. Chem.* **273**, 15395–403.

Reichardt L. F. (2006) Neurotrophin-regulated signalling pathways. *Philos. Trans. R. Soc. Lond. B. Biol. Sci.* **361**, 1545–64.

Revesz T., Holton J. L., Doshi B., Anderton B. H., Scaravilli F., Plant G. T. (1999) Cytoskeletal pathology in familial cerebral amyloid angiopathy (British type) with non-neuritic amyloid plaque formation. *Acta Neuropathol.* **97**, 170–6.

Rolland T., Taşan M., Charloteaux B., Pevzner S. J., Zhong Q., Sahni N., Yi S., et al. (2014) A proteome-scale map of the human interactome network. *Cell* **159**, 1212–26.

Rostagno A., Tomidokoro Y., Lashley T., Ng D., Plant G., Holton J., Frangione B., Revesz T., Ghiso J. (2005) Chromosome 13 dementias. *Cell. Mol. Life Sci.* **62**, 1814–25.

Santos M., Domingues S. C., Costa P., Muller T., Galozzi S., Marcus K., Cruz E Silva E. F. da, Cruz E Silva O. A. da, Rebelo S. (2014) Identification of a Novel Human LAP1 Isoform That Is Regulated by Protein Phosphorylation. *PLoS One* **9**, e113732.

Shannon P., Markiel A., Ozier O., Baliga N. S., Wang J. T., Ramage D., Amin N., Schwikowski B., Ideker T. (2003) Cytoscape: A Software Environment for Integrated Models of Biomolecular Interaction Networks. *Genome Res.* **13**, 2498–2504.

Sincennes M.-C., Humbert M., Grondin B., Lisi V., Veiga D. F. T., Haman A., Cazaux C., et al. (2016) The LMO2 oncogene regulates DNA replication in hematopoietic cells. *Proc. Natl. Acad. Sci. U. S. A.* **113**, 1393–8.

Sørensen J. B., Wiederhold K., Müller E. M., Milosevic I., Nagy G., Groot B. L. de, Grubmüller H., Fasshauer D. (2006) Sequential N- to C-terminal SNARE complex assembly drives priming and fusion of secretory vesicles. *EMBO J.* **25**, 955–66.

Stiess M., Bradke F. (2011) Neuronal polarization: the cytoskeleton leads the way. *Dev. Neurobiol.* **71**, 430–44.

Südhof T. C., Rothman J. E. (2009) Membrane Fusion: Grappling with SNARE and SM Proteins. *Science (80-.).* **323**.

Tamayev R., Giliberto L., Li W., d'Abramo C., Arancio O., Vidal R., D'Adamio L. (2010a) Memory deficits due to familial British dementia BRI2 mutation are caused by loss of BRI2 function rather than amyloidosis. *J. Neurosci.* **30**, 14915–24.

Tamayev R., Matsuda S., Fà M., Arancio O., D'Adamio L. (2010b) Danish dementia mice suggest that loss of function and not the amyloid cascade causes synaptic plasticity and memory deficits. *Proc. Natl. Acad. Sci. U. S. A.* **107**, 20822–7.

Tischfield M. A., Baris H. N., Wu C., Rudolph G., Maldergem L. Van, He W., Chan W.-M., et al. (2010) Human TUBB3 mutations perturb microtubule dynamics, kinesin interactions, and axon guidance. *Cell* **140**, 74–87.

Tsachaki M., Fotinopoulou A., Slavi N., Zarkou V., Ghiso J., Efthimiopoulos S. (2013) BRI2 interacts with BACE1 and regulates its cellular levels by promoting its degradation and reducing its mRNA levels. *Curr. Alzheimer Res.* **10**, 532–41.

Tsachaki M., Ghiso J., Efthimiopoulos S. (2008) BRI2 as a central protein involved in neurodegeneration. *Biotechnol. J.* **3**, 1548–54.

Tsachaki M., Ghiso J., Rostagno A., Efthimiopoulos S. (2010) BRI2 homodimerizes with the involvement of intermolecular disulfide bonds. *Neurobiol. Aging* **31**, 88–98.

Uhlén M., Fagerberg L., Hallström B. M., Lindskog C., Oksvold P., Mardinoglu A., Sivertsson Å., et al. (2015) Tissue-based map of the human proteome. *Science (80-.).* **347**.

Vidal R., Frangione B., Rostagno A., Mead S., Révész T., Plant G., Ghiso J. (1999) A stop-codon mutation in

the BRI gene associated with familial British dementia. *Nature* **399**, 776–81.

Vidal R., Revesz T., Rostagno A., Kim E., Holton J. L., Bek T., Bojsen-Møller M., et al. (2000) A decamer duplication in the 3' region of the BRI gene originates an amyloid peptide that is associated with dementia in a Danish kindred. *Proc. Natl. Acad. Sci. U. S. A.* **97**, 4920–5.

Vitale M., Renzone G., Matsuda S., Scaloni A., D'Adamio L., Zambrano N. (2012) Proteomic characterization of a mouse model of familial Danish dementia. *J. Biomed. Biotechnol.* **2012**, 728178.

Voets T., Moser T., Lund P. E., Chow R. H., Geppert M., Südhof T. C., Neher E. (2001) Intracellular calcium dependence of large dense-core vesicle exocytosis in the absence of synaptotagmin I. *Proc. Natl. Acad. Sci. U. S. A.* **98**, 11680–5.

Wagner S. A., Beli P., Weinert B. T., Nielsen M. L., Cox J., Mann M., Choudhary C. (2011) A proteome-wide, quantitative survey of in vivo ubiquitylation sites reveals widespread regulatory roles. *Mol. Cell. Proteomics* **10**, M111.013284.

Wang L., Andersson S., Warner M., Gustafsson J.-A. (2003) Estrogen receptor (ER) knockout mice reveal a role for ER in migration of cortical neurons in the developing brain. *Proc. Natl. Acad. Sci.* **100**, 703–708.

Wen Q., Wang H., Little P. J., Quirion R., Zheng W. (2012) Forkhead family transcription factor FoxO and neural differentiation. *Neurogenetics* **13**, 105–113.

Wheeler D. L., Church D. M., Federhen S., Lash A. E., Madden T. L., Pontius J. U., Schuler G. D., et al. (2003) Database resources of the National Center for Biotechnology. *Nucleic Acids Res.* **31**, 28–33.

Willander H., Presto J., Askarieh G., Biverstål H., Frohm B., Knight S. D., Johansson J., Linse S. (2012) BRICHOS domains efficiently delay fibrillation of amyloid β-peptide. *J. Biol. Chem.* **287**, 31608–17.

Xia C., Rahman A., Yang Z., Goldstein L. S. B. (1998) Chromosomal Localization Reveals Three Kinesin Heavy Chain Genes in Mouse. *Genomics* **52**, 209–213.

Yoshii A., Constantine-Paton M. (2014) Postsynaptic localization of PSD-95 is regulated by all three pathways downstream of TrkB signaling. *Front. Synaptic Neurosci.* **6**, 6.

Yu H., Tardivo L., Tam S., Weiner E., Gebreab F., Fan C., Svrzikapa N., et al. (2011) Next-generation sequencing to generate interactome datasets. *Nat. Methods* **8**, 478–80.

Supplementary Data

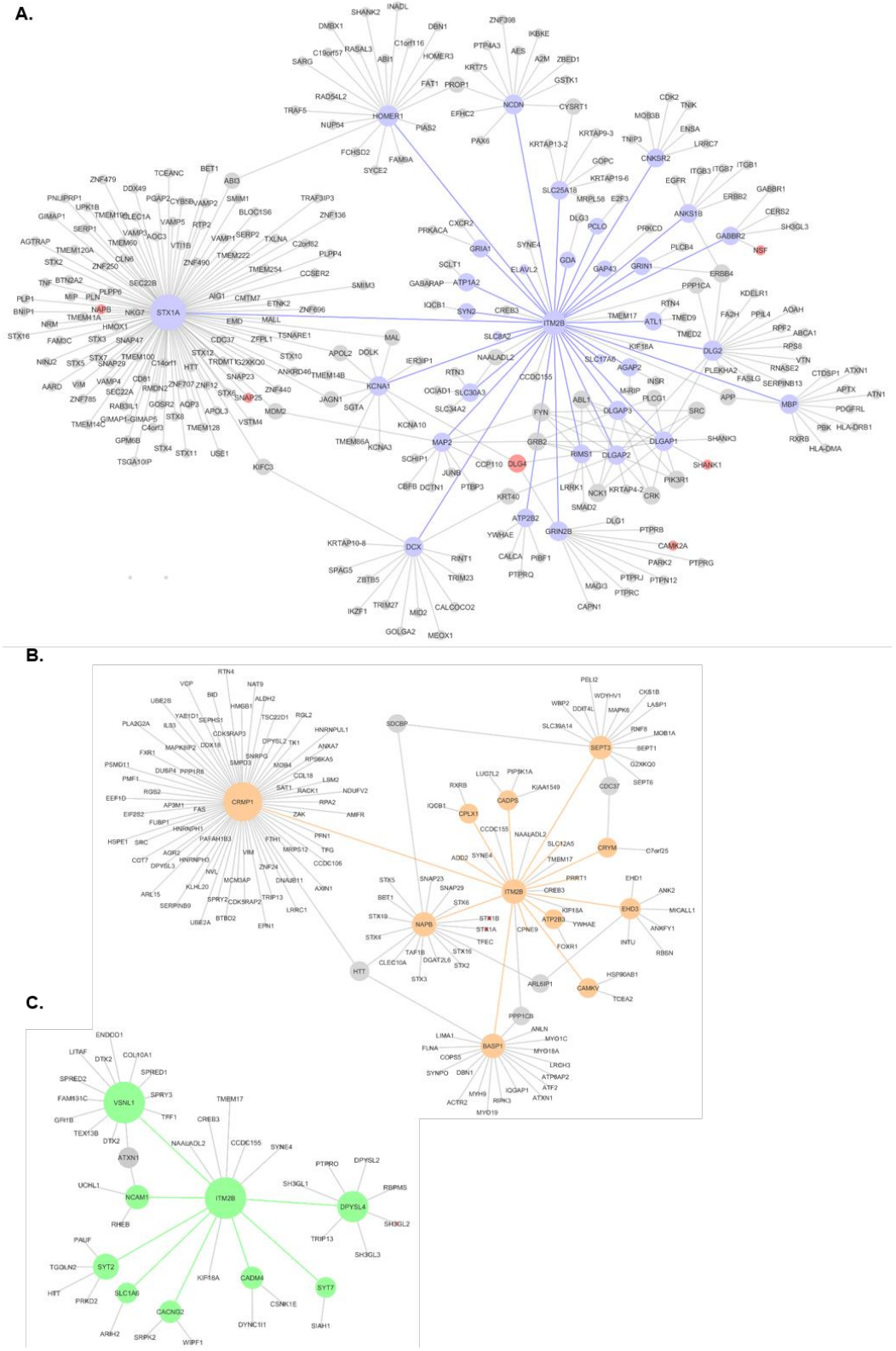

Figure III.A.S 1 - BRI2 ES-based region specific sub-networks. A- BRI2 ES-based sub-network for the cerebral cortex. Node colors represent the source of the protein: blue nodes correspond to proteins identified in this study in the

cerebral cortex, grey nodes to proteins added by network augmentation, and red nodes correspond to protein added by network augmentation that are also identified in this study as BRI2 ES interactors. Node size according to the degree in the network. Edge color represent the source of interaction: blue edges correspond to the cortex specific BRI2 interactions enriched or specific for brain identified in our study, whereas the grey edges correspond to interactions added by network augmentation. **B- BRI2 ES-based sub-network for the hippocampus.** Node colors represent the source of the protein: orange nodes correspond to proteins identified in this study in the cerebral cortex, grey nodes to proteins added by network augmentation, and red nodes correspond to protein added by network augmentation that are also identified in this study as BRI2 ES interactors. Node size according to the degree in the network. Edge color represent the source of interaction: orange edges correspond to the cortex specific BRI2 interactions enriched or specific for brain identified in our study, whereas the grey edges correspond to interactions added by network augmentation. **C- BRI2 ES-based sub-network for the cerebellum.** Node colors represent the source of the protein: green nodes correspond to proteins identified in this study in the cerebral cortex, grey nodes to proteins added by network augmentation, and red nodes correspond to protein added by network augmentation that are also identified in this study as BRI2 ES interactors. Node size according to the degree in the network. Edge color represent the source of interaction: green edges correspond to the cortex specific BRI2 interactions enriched or specific for brain identified in our study, whereas the grey edges correspond to interactions added by network augmentation.

Table III.A.S 1- Candidate BRI2 interacting proteins identified by Nano-HPLC-MS/MS. Uniprot accession numbers, gene and protein names, are listed, as well as the rat brain tissues where the proteins were identified. CC, cerebral cortex; HP, hippocampus; CB, cerebellum.

Uniprot accession	Gene name	Protein name	Brain regions
P62260	Ywhae	14-3-3 protein epsilon	HP
P61983	Ywhag	14-3-3 protein gamma	CC, HP
P68255	Ywhaq	14-3-3 protein theta	CC
P63102	Ywhaz	14-3-3 protein zeta/delta	CB
P13233	Cnp	2',3'-cyclic-nucleotide 3'-phosphodiesterase	CC, HP, CB
Q4FZT9	Psmd2	26S proteasome non-ATPase regulatory subunit 2	CC, CB
P11960	Bckdha	2-oxoisovalerate dehydrogenase subunit alpha, mitochondrial	CC
O70351	Hsd17b10	3-hydroxyacyl-CoA dehydrogenase type-2	HP
P63326	Rps10	40S ribosomal protein S10	CB
P62282	Rps11	40S ribosomal protein S11	CC
P62278	Rps13	40S ribosomal protein S13	CC, CB
P62250	Rps16	40S ribosomal protein S16	CC, CB
P17074	Rps19	40S ribosomal protein S19	CC, CB
P60868	Rps20	40S ribosomal protein S20	CB
P62853	Rps25	40S ribosomal protein S25	CB
P62856	Rps26	40S ribosomal protein S26	CB
P62909	Rps3	40S ribosomal protein S3	CC, HP, CB
P49242	Rps3a	40S ribosomal protein S3a	CB
P62703	Rps4x	40S ribosomal protein S4, X isoform	CC, CB
P62083	Rps7	40S ribosomal protein S7	CB
P38983	Rpsa	40S ribosomal protein SA	CC, CB
Q794F9	Slc3a2	4F2 cell-surface antigen heavy chain	HP
P63039	Hspd1	60 kDa heat shock protein, mitochondrial	CC, HP
P19945	Rplp0	60S acidic ribosomal protein P0	CB
P62914	Rpl11	60S ribosomal protein L11	CB
P23358	Rpl12	60S ribosomal protein L12	CC, HP, CB

P41123	Rpl13	60S ribosomal protein L13	CB
P47198	Rpl22	60S ribosomal protein L22	CC
P61354	Rpl27	60S ribosomal protein L27	CC, CB
P50878	Rpl4	60S ribosomal protein L4	CB
P21533	Rpl6	60S ribosomal protein L6	CB
P05426	Rpl7	60S ribosomal protein L7	CC, CB
P06761	Hspa5	78 kDa glucose-regulated protein	CC, HP, CB
P49911	Anp32a	Acidic leucine-rich nuclear phosphoprotein 32 family member A	CC, CB
Q9ER34	Aco2	Aconitate hydratase, mitochondrial	HP
P68035	Actc1	Actin, alpha cardiac muscle 1	CC
P60711	Actb	Actin, cytoplasmic 1	CC, HP, CB
P63269	Actg2	Actin, gamma-enteric smooth muscle	CC, HP, CB
Q6KC51	Ablim2	Actin-binding LIM protein 2	CC, CB
Q4V7C7	Actr3	Actin-related protein 3	CB
P69682	Necap1	Adaptin ear-binding coat-associated protein 1	CC, HP
B5DFN2	Ahcyl1	Adenosylhomocysteinase 2	CB
P39069	Ak1	Adenylate kinase isoenzyme 1	HP
P52481	Cap2	Adenylyl cyclase-associated protein 2	CC, HP
Q05962	Slc25a4	ADP/ATP translocase 1	CC, HP
Q09073	Slc25a5	ADP/ATP translocase 2	CC, HP
P61751	Arf4	ADP-ribosylation factor 4	CC, HP
Q62848	Arfgap1	ADP-ribosylation factor GTPase-activating protein 1	CB
P07897	Acan	Aggrecan core protein	HP
P06238	A2m	Alpha-2-macroglobulin	CC, HP, CB
Q9Z1P2	Actn1	Alpha-actinin-1	CC
Q63028	Add1	Alpha-adducin	HP, CB
P85515	Actr1a	Alpha-centractin	HP
P04764	Eno1	Alpha-enolase	CC, HP
P23565	Ina	Alpha-internexin	CC, HP, CB
P54921	Napa	Alpha-soluble NSF attachment protein	HP, CB
P21396	Maoa	Amine oxidase [flavin-containing] A	HP
O08838	Amph	Amphiphysin	CC, HP, CB
P0C6S7	Anks1b	Ankyrin repeat and sterile alpha motif domain-containing protein 1B	CC
O70511	Ank3	Ankyrin-3	CC, HP, CB
P52303	Ap1b1	AP-1 complex subunit beta-1	CC, HP
Q32Q06	Ap1m1	AP-1 complex subunit mu-1	CC
P18484	Ap2a2	AP-2 complex subunit alpha-2	CC, HP, CB
P62944	Ap2b1	AP-2 complex subunit beta	CC, HP, CB
P84092	Ap2m1	AP-2 complex subunit mu	CC, HP
P62744	Ap2s1	AP-2 complex subunit sigma	CC, HP, CB
P0C1X8	Aak1	AP2-associated protein kinase 1	CC, HP
Q8CGU4	Agap2	Arf-GAP with GTPase, ANK repeat and PH domain-containing protein 2	CC
P00507	Got2	Aspartate aminotransferase, mitochondrial	CB
P15178	Dars	Aspartate--tRNA ligase, cytoplasmic	CB

Q6PST4	Atl1	Atlastin-1	CC
P19511	Atp5f1	ATP synthase F	CC, HP
P15999	Atp5a1	ATP synthase subunit alpha, mitochondrial	CC, HP
P10719	Atp5b	ATP synthase subunit beta, mitochondrial	HP
P31399	Atp5h	ATP synthase subunit d, mitochondrial	HP
P35434	Atp5d	ATP synthase subunit delta, mitochondrial	HP
P29419	Atp5i	ATP synthase subunit e, mitochondrial	CC
D3ZAF6	Atp5j2	ATP synthase subunit f, mitochondrial	HP, CB
Q6PDU7	Atp5l	ATP synthase subunit g, mitochondrial	HP, CB
P35435	Atp5c1	ATP synthase subunit gamma, mitochondrial	CC, HP, CB
Q06647	Atp5o	ATP synthase subunit O, mitochondrial	CC, HP, CB
P21571	Atp5j	ATP synthase-coupling factor 6, mitochondrial	HP
Q7TNJ2	Abca7	ATP-binding cassette sub-family A member 7	HP
P47858	Pfkm	ATP-dependent 6-phosphofructokinase, muscle type	HP
P47860	Pfkp	ATP-dependent 6-phosphofructokinase, platelet type	HP
Q9WTP0	Epb41l1	Band 4.1-like protein 1	CC, HP, CB
Q9ESS6	Bcam	Basal cell adhesion molecule	CC, HP, CB
Q05764	Add2	Beta-adducin	HP
P29066	Arrb1	Beta-arrestin-1	CC
P85969	Napb	Beta-soluble NSF attachment protein	HP
O35567	Atic	Bifunctional purine biosynthesis protein PURH	CB
Q05175	Basp1	Phosphoribosylaminoimidazolecarboxamide formyltransferase Brain acid soluble protein 1	HP
Q6GMN2	Baiap2	Brain-specific angiogenesis inhibitor 1-associated protein 2	CC
P55068	Bcan	Brevican core protein	HP, CB
P11275	Camk2a	Calcium/calmodulin-dependent protein kinase type II subunit alpha	CC, HP
P08413	Camk2b	Calcium/calmodulin-dependent protein kinase type II subunit beta	CC, HP, CB
P15791	Camk2d	Calcium/calmodulin-dependent protein kinase type II subunit delta	CC, CB
P11730	Camk2g	Calcium/calmodulin-dependent protein kinase type II subunit gamma	CC, CB
Q66HR5	Calcoco1	Calcium-binding and coiled-coil domain-containing protein 1	CC, HP
Q62717	Cadps	Calcium-dependent secretion activator 1	HP
P62161	Calm1	Calmodulin	HP, CB
Q07009	Capn2	Calpain-2 catalytic subunit	CB
Q63092	Camkv	CaM kinase-like vesicle-associated protein	HP
P27791	Prkaca	cAMP-dependent protein kinase catalytic subunit alpha	CC
P48284	Ca4	Carbonic anhydrase 4	CB
P19139	Csnk2a1	Casein kinase II subunit alpha	CC, HP, CB
P67874	Csnk2b	Casein kinase II subunit beta	CC
Q9WU82	Ctnnb1	Catenin beta-1	CC, CB
B5D5N9	Slc7a2	Cationic amino acid transporter 2	CC, HP
Q5M7A7	Cnrip1	CB1 cannabinoid receptor-interacting protein 1	CB
P40241	Cd9	CD9 antigen	CC, HP, CB
B0K020	Cisd1	CDGSH iron-sulfur domain-containing protein 1	CC
Q1WIM1	Cadm4	Cell adhesion molecule 4	CB
Q5FVI4	Cend1	Cell cycle exit and neuronal differentiation protein 1	CC, HP

B2RYL1	Chtf8	Chromosome transmission fidelity protein 8 homolog isoform 2	CC
Q8VHF5	Cs	Citrate synthase, mitochondrial	CC
Q05140	Snap91	Clathrin coat assembly protein AP180	CC, HP
P11442	Cltc	Clathrin heavy chain 1	CC, HP
P08081	Clta	Clathrin light chain A	CC, HP
P08082	Cltb	Clathrin light chain B	CC, HP
Q99P82	Cldn11	Claudin-11	CC
Q99JD4	Clasp2	CLIP-associating protein 2	CB
P45592	Cfl1	Cofilin-1	CC, HP, CB
P13941	Col3a1	Collagen alpha-1	CB
P31720	C1qa	Complement C1q subcomponent subunit A	HP
P31721	C1qb	Complement C1q subcomponent subunit B	CC, HP, CB
P31722	C1qc	Complement C1q subcomponent subunit C	CC
P01026	C3	Complement C3 [Cleaved into: Complement C3 beta chain; C3-beta-c	CC, HP
O35796	C1qbp	Complement component 1 Q subcomponent-binding protein, mitochondrial	CB
P63041	Cplx1	Complexin-1	HP
Q9Z1T4	Cnksr2	Connector enhancer of kinase suppressor of ras 2	CC
Q63198	Cntn1	Contactin-1	CC, HP
P97846	Cntnap1	Contactin-associated protein 1	CC, CB
Q5BJS7	Cpne9	Copine-9	HP
Q02874	H2afy	Core histone macro-H2A.1	CB
P48199	Crp	C-reactive protein	CB
P00564	Ckm	Creatine kinase M-type	CB
P25809	Ckmt1	Creatine kinase U-type, mitochondrial	CC, HP, CB
P97536	Cand1	Cullin-associated NEDD8-dissociated protein 1	CB
O08565	Cxcr4	C-X-C chemokine receptor type 4	HP
Q03114	Cdk5	Cyclin-dependent-like kinase 5	CC
P97874	Gak	Cyclin-G-associated kinase	CC, HP
P32551	Uqcrc2	Cytochrome b-c1 complex subunit 2, mitochondrial	CC, HP, CB
Q7TQ16	Uqcrq	Cytochrome b-c1 complex subunit 8	CC, HP, CB
P20788	Uqcrfs1	Cytochrome b-c1 complex subunit Rieske, mitochondrial	HP, CB
P00406	Mtco2	Cytochrome c oxidase subunit 2	HP
P10888	Cox4i1	Cytochrome c oxidase subunit 4 isoform 1, mitochondrial	CC, HP
P11240	Cox5a	Cytochrome c oxidase subunit 5A, mitochondrial	CB
P12075	Cox5b	Cytochrome c oxidase subunit 5B, mitochondrial	CC, HP
P11951	Cox6c2	Cytochrome c oxidase subunit 6C-2	HP
P35171	Cox7a2	Cytochrome c oxidase subunit 7A2, mitochondrial	HP
P38650	Dync1h1	Cytoplasmic dynein 1 heavy chain 1	CC, HP
Q6Q0N1	Cndp2	Cytosolic non-specific dipeptidase	CB
O08651	Phgdh	D-3-phosphoglycerate dehydrogenase	CC, CB
P29147	Bdh1	D-beta-hydroxybutyrate dehydrogenase, mitochondrial	CC, HP
P08461	Dlat	Dihydrolipoyllysine-residue acetyltransferase component of pyruvate dehydrogenase complex, mitochondrial	CC
Q01205	Dlst	Dihydrolipoyllysine-residue succinyltransferase component of 2-oxoglutarate dehydrogenase complex, mitochondrial	HP, CB
Q62950	Crmp1	Dihydropyrimidinase-related protein 1	HP

P47942	Dpysl2	Dihydropyrimidinase-related protein 2	CC, HP
Q62951	Dpysl4	Dihydropyrimidinase-related protein 4	CB
Q63342	Dmgdh	Dimethylglycine dehydrogenase, mitochondrial	CC
Q62696	Dlg1	Disks large homolog 1	CC, CB
Q63622	Dlg2	Disks large homolog 2	CC
P31016	Dlg4	Disks large homolog 4	CC, HP, CB
P97836	Dlgap1	Disks large-associated protein 1	CC
P97837	Dlgap2	Disks large-associated protein 2	CC
P97838	Dlgap3	Disks large-associated protein 3	CC
Q07266	Dbn1	Drebrin	CC, HP
Q01986	Map2k1	Dual specificity mitogen-activated protein kinase kinase 1	HP, CB
Q6AYH5	Dctn2	Dynactin subunit 2	CC, HP
P21575	Dnm1	Dynamin-1	CC, HP
O35303	Dnm1l	Dynamin-1-like protein	CC, HP
Q2TA68	Opa1	Dynamin-like 120 kDa protein, mitochondrial	CC
B0BND0	Enpp6	Ectonucleotide pyrophosphatase/phosphodiesterase family member 6	CB
Q8R491	Ehd3	EH domain-containing protein 3	HP
Q8CH84	Elavl2	ELAV-like protein 2	CC
Q9JI66	Slc4a4	Electrogenic sodium bicarbonate cotransporter 1	HP, CB
P62630	Eef1a1	Elongation factor 1-alpha 1	CC, HP
Q68FR6	Eef1g	Elongation factor 1-gamma	CB
P05197	Eef2	Elongation factor 2	CC, HP, CB
P85834	Tufm	Elongation factor Tu, mitochondrial	CC, HP, CB
O35179	Sh3gl2	Endophilin-A1	CC, CB
Q5PPJ9	Sh3glb2	Endophilin-B2	CC, HP, CB
Q66HD0	Hsp90b1	Endoplasmin	CC, HP, CB
O88339	Epn1	Epsin-1	CC
B5DEH2	Erlin2	Erlin-2	CB
Q5RKI1	Eif4a2	Eukaryotic initiation factor 4A-II	HP, CB
P24942	Slc1a3	Excitatory amino acid transporter 1	CC, HP, CB
P31596	Slc1a2	Excitatory amino acid transporter 2	CC, HP, CB
O35921	Slc1a6	Excitatory amino acid transporter 4	CB
B2GUZ5	Capza1	F-actin-capping protein subunit alpha-1	CB
Q3T1K5	Capza2	F-actin-capping protein subunit alpha-2	CC
Q5XI32	Capzb	F-actin-capping protein subunit beta	CC, CB
P12785	Fasn	Fatty acid synthase	HP
Q5XI81	Fxr1	Fragile X mental retardation syndrome-related protein 1	CB
P05065	Aldoa	Fructose-bisphosphate aldolase A	CC, HP
O88871	Gabbr2	Gamma-aminobutyric acid type B receptor subunit 2	CC
P08050	Gja1	Gap junction alpha-1 protein	CC, HP, CB
Q68FP1	Gsn	Gelsolin	CC, CB
Q63228	Gmfb	Glia maturation factor beta	CC
P47819	Gfap	Glial fibrillary acidic protein	CC, HP, CB
P19490	Gria1	Glutamate receptor 1	CC

P19491	Gria2	Glutamate receptor 2	CC, HP, CB
Q63226	Grid2	Glutamate receptor ionotropic, delta-2	CB
P35439	Grin1	Glutamate receptor ionotropic, NMDA 1	CC
Q00960	Grin2b	Glutamate receptor ionotropic, NMDA 2B	CC
P28492	Gls2	Glutaminase liver isoform, mitochondrial	HP
P09606	Glul	Glutamine synthetase	CC, HP, CB
P04797	Gapdh	Glyceraldehyde-3-phosphate dehydrogenase	CC
P35571	Gpd2	Glycerol-3-phosphate dehydrogenase, mitochondrial	HP
P53534	Pygb	Glycogen phosphorylase, brain form	CC, HP
P08644	Kras	GTPase KRas	CC
Q63942	Rab3d	GTP-binding protein Rab-3D	HP
Q9WTT6	Gda	Guanine deaminase	CC
P43425	Gng7	Guanine nucleotide-binding protein G(I)/G(S)/G(O) subunit gamma-7	CC
P63095	Gnas	Guanine nucleotide-binding protein G(s) subunit alpha isoforms short	CC
P52287	Gnb3	Guanine nucleotide-binding protein G(I)/G(S)/G(T) subunit beta-3	CC
P82471	Gnaq	Guanine nucleotide-binding protein G(q) subunit alpha	CB
P54311	Gnb1	Guanine nucleotide-binding protein G(I)/G(S)/G(T) subunit beta-1	CC, HP
P10824	Gnai1	Guanine nucleotide-binding protein G(i) subunit alpha-1	CC, HP
P19627	Gnaz	Guanine nucleotide-binding protein G(z) subunit alpha	CC, HP
P59215	Gnao1	Guanine nucleotide-binding protein G(o) subunit alpha	CC, HP, CB
P04897	Gnai2	Guanine nucleotide-binding protein G(i) subunit alpha-2	CC, HP, CB
O35353	Gnb4	Guanine nucleotide-binding protein subunit beta-4	HP, CB
P55063	Hspa1l	Heat shock 70 kDa protein 1-like	CC
O88600	Hspa4	Heat shock 70 kDa protein 4	CB
P63018	Hspa8	Heat shock cognate 71 kDa protein	CC
P82995	Hsp90aa1	Heat shock protein HSP 90-alpha	CC, HP, CB
P34058	Hsp90ab1	Heat shock protein HSP 90-beta	CC, HP, CB
P11517	ND	Hemoglobin subunit beta-2	CB
Q6URK4	Hnrnpa3	Heterogeneous nuclear ribonucleoprotein A3	CC, CB
G3V9R8	Hnrnpc	Heterogeneous nuclear ribonucleoprotein C	CC, CB
Q9JJ54	Hnrnpd	Heterogeneous nuclear ribonucleoprotein D0	CC, CB
Q3SWU3	Hnrnpdl	Heterogeneous nuclear ribonucleoprotein D-like	CC, HP, CB
Q794E4	Hnrnpf	Heterogeneous nuclear ribonucleoprotein F	CC, CB
Q8VHV7	Hnrnph1	Heterogeneous nuclear ribonucleoprotein H	CC
Q6AY09	Hnrnph2	Heterogeneous nuclear ribonucleoprotein H2	CC, HP, CB
P61980	Hnrnpk	Heterogeneous nuclear ribonucleoprotein K	CC, HP, CB
Q62826	Hnrnpm	Heterogeneous nuclear ribonucleoprotein M	CB
Q7TP47	Syncrip	Heterogeneous nuclear ribonucleoprotein Q	CB
A7VJC2	Hnrnpa2bl	Heterogeneous nuclear ribonucleoproteins A2/B1	CC, CB
P05708	Hk1	Hexokinase-1	CC, HP
P02262	ND	Histone H2A type 1	CC, CB
P0C0S7	H2afz	Histone H2A.Z	CC, HP
Q00715	ND	Histone H2B type 1	CC, HP, CB
P62804	Hist1h4b	Histone H4	CC, HP, CB

Q9Z214	Homer1	Homer protein homolog 1	CC
Q9Z2X5	Homer3	Homer protein homolog 3	CB
P03994	Hapln1	Hyaluronan and proteoglycan link protein 1	CC, HP, CB
Q9ESM2	Hapln2	Hyaluronan and proteoglycan link protein 2	CC, CB
Q9WVK7	Hadh	Hydroxyacyl-coenzyme A dehydrogenase, mitochondrial	CC, HP
Q63617	Hyou1	Hypoxia up-regulated protein 1	CC, HP, CB
P20761	Igh-1a	Ig gamma-2B chain C region	CC, HP
P29994	Itpr1	Inositol 1,4,5-trisphosphate receptor type 1	CB
Q63269	Itpr3	Inositol 1,4,5-trisphosphate receptor type 3	CB
D3ZGS3	Ocrl	Inositol polyphosphate 5-phosphatase OCRL-1	CC, HP
Q63416	Itih3	Inter-alpha-trypsin inhibitor heavy chain H3	CC, HP
Q7TP98	Ilf2	Interleukin enhancer-binding factor 2	CB
Q9WVE9	Itsn1	Intersectin-1	CC, HP
Q99NA5	Idh3a	Isocitrate dehydrogenase [NAD] subunit alpha, mitochondrial	CC, HP
Q68FX0	Idh3B	Isocitrate dehydrogenase [NAD] subunit beta, mitochondrial	CC, HP, CB
P41565	Idh3g	Isocitrate dehydrogenase [NAD] subunit gamma 1, mitochondrial	CC
P56574	Idh2	Isocitrate dehydrogenase [NADP], mitochondrial	CB
Q9QYU4	Crym	Ketimine reductase mu-crystallin	HP
Q6QLM7	Kif5a	Kinesin heavy chain isoform 5A	CC, HP, CB
P56536	Kif5c	Kinesin heavy chain isoform 5C	CC, CB
P37285	Klc1	Kinesin light chain 1	CC, HP, CB
Q2PQA9	Kif5b	Kinesin-1 heavy chain	CC, HP, CB
Q9WV63	Kif2a	Kinesin-like protein KIF2A	CB
Q5XI51	Kif2b	Kinesin-like protein KIF2B	CC
P70615	Lmnb1	Lamin-B1	CB
Q5XIN6	Letm1	LETM1 and EF-hand domain-containing protein 1, mitochondrial	CB
P97829	Cd47	Leukocyte surface antigen CD47	CC, HP
Q62813	Lsamp	Limbic system-associated membrane protein	CC, CB
P04642	Ldha	L-lactate dehydrogenase A chain	HP
P04636	Mdh2	Malate dehydrogenase, mitochondrial	HP
O08873	Madd	MAP kinase-activating death domain protein	HP
P43244	Matr3	Matrin-3	CC, HP
Q4L1J4	Magi1	Membrane-associated guanylate kinase, WW and PDZ domain-containing protein 1	HP
Q00566	Mecp2	Methyl-CpG-binding protein 2	CB
D4A7N1	Chchd6	MICOS complex subunit Mic25	CC, CB
Q3KR86	Immt	MICOS complex subunit Mic60	CC, HP, CB
D3ZHV2	Macf1	Microtubule-actin cross-linking factor 1	CC, CB
P34926	Map1a	Microtubule-associated protein 1A	CC, HP
P15205	Map1b	Microtubule-associated protein 1B	CC, HP, CB
P15146	Map2	Microtubule-associated protein 2	CC
Q5M7W5	Map4	Microtubule-associated protein 4	CC, HP
Q63560	Map6	Microtubule-associated protein 6	CC, HP, CB
F1LP90	Mink1	Misshapen-like kinase 1	CC, HP
P97700	Slc25a11	Mitochondrial 2-oxoglutarate/malate carrier protein	CC, HP, CB

Q505J6	Slc25a18	Mitochondrial glutamate carrier 2	CC
O08839	Bin1	Myc box-dependent-interacting protein 1	CC, HP
P02688	Mbp	Myelin basic protein	CC
P60203	Plp1	Myelin proteolipid protein	CC, CB
P07722	Mag	Myelin-associated glycoprotein	CC, CB
Q63345	Mog	Myelin-oligodendrocyte glycoprotein	CC, CB
Q6VBQ5	Myadm	Myeloid-associated differentiation marker	CC
Q9QZ76	Mb	Myoglobin	HP
P02600	Myl1	Myosin light chain 1/3, skeletal muscle isoform	HP
P16409	Myl3	Myosin light chain 3	HP, CB
Q64119	Myl6	Myosin light polypeptide 6	CC, HP, CB
P13832	Rlc-a	Myosin regulatory light chain RLC-A	CC, CB
Q64122	Myl9	Myosin regulatory light polypeptide 9	CC
Q9JLT0	Myh10	Myosin-10	CC, CB
Q62812	Myh9	Myosin-9	CC, CB
Q5RJQ4	Sirt2	NAD-dependent protein deacetylase sirtuin-2	CC, CB
Q561S0	Ndufa10	NADH dehydrogenase [ubiquinone] 1 alpha subcomplex subunit 10, mitochondrial	HP, CB
Q5BK63	Ndufa9	NADH dehydrogenase [ubiquinone] 1 alpha subcomplex subunit 9, mitochondrial	HP
P19234	Ndufv2	NADH dehydrogenase [ubiquinone] flavoprotein 2, mitochondrial	HP, CB
Q641Y2	Ndufs2	NADH dehydrogenase [ubiquinone] iron-sulfur protein 2, mitochondrial	HP
P52504	Ndufs6	NADH dehydrogenase [ubiquinone] iron-sulfur protein 6, mitochondrial	HP
Q66HF1	Ndufs1	NADH-ubiquinone oxidoreductase 75 kDa subunit, mitochondrial	CC, HP, CB
O35867	Ppp1r9a	Neurabin-1	CC
P13596	Ncam1	Neural cell adhesion molecule 1	CB
P55067	Ncan	Neurocan core protein	CC, HP, CB
O35095	Ncdn	Neurochondrin	CC
P97685	Nfasc	Neurofascin	CC, HP, CB
P16884	Nefh	Neurofilament heavy polypeptide	CC, HP, CB
P19527	Nefl	Neurofilament light polypeptide	CC, HP, CB
P12839	Nefm	Neurofilament medium polypeptide	CC, CB
P07936	Gap43	Neuromodulin	CC
Q9ESI7	Dcx	Neuronal migration protein doublecortin	CC
Q9WU34	Sept3	Neuronal-specific septin-3	HP
P97546	Nptn	Neuroplastin	CC
Q62718	Ntm	Neurotrimin	CC, CB
P08460	Nid1	Nidogen-1	CB
Q9EPI6	Nsmf	NMDA receptor synaptonuclear signaling and neuronal migration factor	CC
A1L1I3	Numbl	Numb-like protein	CC
P04218	Cd200	OX-2 membrane glycoprotein	CC
P10111	Ppia	Peptidyl-prolyl cis-trans isomerase A	CB
Q9QVC8	Fkbp4	Peptidyl-prolyl cis-trans isomerase FKBP4	CB
Q63716	Prdx1	Peroxiredoxin-1	CC, HP
P35704	Prdx2	Peroxiredoxin-2	CC
O35244	Prdx6	Peroxiredoxin-6	CC, HP

Q642G4	Pex14	Peroxisomal membrane protein PEX14	CC
P16036	Slc25a3	Phosphate carrier protein, mitochondrial	CC, HP, CB
O08662	Pi4ka	Phosphatidylinositol 4-kinase alpha	CC
P16617	Pgk1	Phosphoglycerate kinase 1	HP
P16290	Pgam2	Phosphoglycerate mutase 2	CB
P11505	Atp2b1	Plasma membrane calcium-transporting ATPase 1	CC
P11506	Atp2b2	Plasma membrane calcium-transporting ATPase 2	CC
Q64568	Atp2b3	Plasma membrane calcium-transporting ATPase 3	HP
Q64542	Atp2b4	Plasma membrane calcium-transporting ATPase 4	CC
P30427	Plec	Plectin	CC, CB
Q9EPH8	Pabpc1	Polyadenylate-binding protein 1	CB
P0CG51	Ubb	Polyubiquitin-B [Cleaved into: Ubiquitin]	CC
P10499	Kcna1	Potassium voltage-gated channel subfamily A member 1	CC
P48679	Lmna	Prelamin-A/C [Cleaved into: Lamin-A/C]	CB
Q9JMJ4	Prpf19	Pre-mRNA-processing factor 19	HP
P62963	Pfn1	Profilin-1	CC
P67779	Phb	Prohibitin	CC, HP, CB
Q5XIH7	Phb2	Prohibitin-2	CC, HP, CB
P04961	Pcna	Proliferating cell nuclear antigen	CB
Q6AYD3	Pa2g4	Proliferation-associated protein 2G4	CC
Q6MG82	Prrt1	Proline-rich transmembrane protein 1	HP
O88778	Bsn	Protein bassoon	CC, CB
O88767	Park7	Protein deglycase DJ-1	CC
P04785	P4hb	Protein disulfide-isomerase	CB
P63319	Prkcg	Protein kinase C gamma type	CC, HP, CB
Q8VBU2	Ndrg2	Protein NDRG2	HP
Q9JKS6	Pclo	Protein piccolo	CC
Q6MG48	Prrc2a	Protein PRRC2A	CC
P23606	Tgm1	Protein-glutamine gamma-glutamyltransferase K	CB
P52873	Pc	Pyruvate carboxylase, mitochondrial	HP, CB
P26284	Pdha1	Pyruvate dehydrogenase E1 component subunit alpha, somatic form, mitochondrial	CC, CB
P49432	Pdhb	Pyruvate dehydrogenase E1 component subunit beta, mitochondrial	CC, HP, CB
P11980	Pkm	Pyruvate kinase PKM	CC, HP
P50399	Gdi2	Rab GDP dissociation inhibitor beta	HP, CB
P47709	Rph3a	Rabphilin-3A	CC, HP
F1M386	Rapgef2	Rap guanine nucleotide exchange factor 2	CC
Q9QUH6	Syngap1	Ras/Rap GTPase-activating protein SynGAP	CC
Q6RUV5	Rac1	Ras-related C3 botulinum toxin substrate 1	CC, CB
P35281	Rab10	Ras-related protein Rab-10	CC, HP
P61107	Rab14	Ras-related protein Rab-14	CC, CB
Q6NYB7	Rab1A	Ras-related protein Rab-1A	CC, CB
P10536	Rab1b	Ras-related protein Rab-1B	CB
P05712	Rab2a	Ras-related protein Rab-2A	CC
P63012	Rab3a	Ras-related protein Rab-3A	CC, HP, CB

Q63941	Rab3b	Ras-related protein Rab-3B	CC
P62824	Rab3c	Ras-related protein Rab-3C	CC, HP
M0RC99	Rab5a	Ras-related protein Rab-5A	CB
P09527	Rab7a	Ras-related protein Rab-7a	CB
P61227	Rap2b	Ras-related protein Rap-2b	HP
P63245	Rack1	Receptor of activated protein C kinase 1	CC, CB
Q6AXX6	Fam213a	Redox-regulatory protein FAM213A	CC, HP
Q9JIR4	Rims1	Regulating synaptic membrane exocytosis protein 1	CC
Q62703	Rcn2	Reticulocalbin-2	CB
Q64548	Rtn1	Reticulon-1	CC, HP, CB
Q6RJR6	Rtn3	Reticulon-3	CC, HP, CB
Q9JK11	Rtn4	Reticulon-4	CC
D4AE41	Rbmxl1	RNA binding motif protein, X-linked-like-1	CC, CB
Q3B7K9	Rundc3b	RUN domain-containing protein 3B	CC, HP
Q64578	Atp2a1	Sarcoplasmic/endoplasmic reticulum calcium ATPase 1	CC, CB
P11507	Atp2a2	Sarcoplasmic/endoplasmic reticulum calcium ATPase 2	HP
O88453	Safb	Scaffold attachment factor B1	CB
P56603	Scamp1	Secretory carrier-associated membrane protein 1	CC, HP
Q9JKE3	Scamp5	Secretory carrier-associated membrane protein 5	CC, HP
B3GNI6	Sept11	Septin-11	CC, CB
Q9JJM9	Sept5	Septin-5	CC, HP
Q9WVC0	Sept7	Septin-7	CB
G3V6S8	Srsf6	Serine/arginine-rich splicing factor 6	CB
O08875	Dclk1	Serine/threonine-protein kinase DCLK1	CC, HP
O08679	Mark2	Serine/threonine-protein kinase MARK2	CC
Q4QQT4	Ppp2r1b	Serine/threonine-protein phosphatase 2A 65 kDa regulatory subunit A beta isoform	CC
P63329	Ppp3ca	Serine/threonine-protein phosphatase 2B catalytic subunit alpha isoform	CC
Q64620	Ppp6c	Serine/threonine-protein phosphatase 6 catalytic subunit	CC
Q562B5	Pgam5	Serine/threonine-protein phosphatase PGAM5, mitochondrial	CC
P62138	Ppp1ca	Serine/threonine-protein phosphatase PP1-alpha catalytic subunit	CC
Q6P799	Sars	Serine--tRNA ligase, cytoplasmic	CB
P12346	Tf	Serotransferrin	CC, HP, CB
P23680	Apcs	Serum amyloid P-component	CB
Q9WV48	Shank1	SH3 and multiple ankyrin repeat domains protein 1	CC, CB
Q9QX74	Shank2	SH3 and multiple ankyrin repeat domains protein 2	CC, CB
Q9JLU4	Shank3	SH3 and multiple ankyrin repeat domains protein 3	CC
P0DJJ3	Sgip1	SH3-containing GRB2-like protein 3-interacting protein 1	CC, HP
Q63965	Sfxn1	Sideroflexin-1	CC, HP
Q9JHY2	Sfxn3	Sideroflexin-3	CC, CB
P31647	Slc6a11	Sodium- and chloride-dependent GABA transporter 3	CC, CB
P48768	Slc8a2	Sodium/calcium exchanger 2	CC
P06685	Atp1a1	Sodium/potassium-transporting ATPase subunit alpha-1	CC
P06686	Atp1a2	Sodium/potassium-transporting ATPase subunit alpha-2	CC
P06687	Atp1a3	Sodium/potassium-transporting ATPase subunit alpha-3	CC, HP

P07340	Atp1b1	Sodium/potassium-transporting ATPase subunit beta-1	CC, HP, CB
P13638	Atp1b2	Sodium/potassium-transporting ATPase subunit beta-2	CC, HP, CB
Q63633	Slc12a5	Solute carrier family 12 member 5	HP
Q66HR0	Slc12a9	Solute carrier family 12 member 9	HP
P11167	Slc2a1	Solute carrier family 2, facilitated glucose transporter member 1	CC, HP, CB
O35413	Sorbs2	Sorbin and SH3 domain-containing protein 2	CC
P16086	Sptan1	Spectrin alpha chain, non-erythrocytic 1	CC, HP, CB
Q9QWN8	Sptbn2	Spectrin beta chain, non-erythrocytic 2	CC, CB
Q9QXY2	Srcin1	SRC kinase signaling inhibitor 1	CC, CB
Q4FZT0	Stoml2	Stomatin-like protein 2, mitochondrial	CC
D4AB66	Ston2	Stonin-2	CC, HP
P21913	Sdhb	Succinate dehydrogenase [ubiquinone] iron-sulfur subunit, mitochondrial	CB
P13086	Suclg1	Succinate--CoA ligase [ADP/GDP-forming] subunit alpha, mitochondrial	CB
P09951	Syn1	Synapsin-1	CC, HP
Q63537	Syn2	Synapsin-2	CC
Q02563	Sv2a	Synaptic vesicle glycoprotein 2A	CC, HP, CB
Q63564	Sv2b	Synaptic vesicle glycoprotein 2B	CC, HP
Q62876	Syngr1	Synaptogyrin-1	CC, CB
Q62910	Synj1	Synaptojanin-1	CC, HP
P07825	Syp	Synaptophysin	CC, HP
Q9Z327	Synpo	Synaptopodin	CC
P60881	Snap25	Synaptosomal-associated protein 25	HP, CB
P21707	Syt1	Synaptotagmin-1	CC, HP, CB
P97610	Syt12	Synaptotagmin-12	CC, CB
P29101	Syt2	Synaptotagmin-2	CB
Q62747	Syt7	Synaptotagmin-7	CB
P32851	Stx1a	Syntaxin-1A	CC
P61265	Stx1b	Syntaxin-1B	CC, HP, CB
P61765	Stxbp1	Syntaxin-binding protein 1	CC, HP
Q5XIM9	Cct2	T-complex protein 1 subunit beta	HP, CB
Q7TPB1	Cct4	T-complex protein 1 subunit delta	HP, CB
Q68FQ0	Cct5	T-complex protein 1 subunit epsilon	CC, HP, CB
Q6P502	Cct3	T-complex protein 1 subunit gamma	HP, CB
Q05546	Tnr	Tenascin-R	CC, HP, CB
Q920J4	Txnl1	Thioredoxin-like protein 1	HP
P01830	Thy1	Thy-1 membrane glycoprotein	HP, CB
Q5U1Z2	Trappc3	Trafficking protein particle complex subunit 3	HP
P86252	Pura	Transcriptional activator protein Pur-alpha	CC, HP, CB
Q68A21	Purb	Transcriptional activator protein Pur-beta	CC, HP, CB
Q5M7W4	Tmc5	Transmembrane channel-like protein 5	HP
Q64428	Hadha	Trifunctional enzyme subunit alpha, mitochondrial	CC
Q60587	Hadhb	Trifunctional enzyme subunit beta, mitochondrial	HP
P48500	Tpi1	Triosephosphate isomerase	CC
Q6AYT3	Rtcb	tRNA-splicing ligase RtcB homolog	CB

P70566	Tmod2	Tropomodulin-2	CC, CB
Q63610	Tpm3	Tropomyosin alpha-3 chain	CC
P09495	Tpm4	Tropomyosin alpha-4 chain	HP
Q6P7B0	Wars	Tryptophan--tRNA ligase, cytoplasmic	CC, HP
P68370	Tuba1a	Tubulin alpha-1A chain	CC, HP, CB
Q6AYZ1	Tuba1c	Tubulin alpha-1C chain	HP
Q68FR8	Tuba3a	Tubulin alpha-3 chain	CC
Q5XIF6	Tuba4a	Tubulin alpha-4A chain	CC, HP, CB
Q6AY56	Tuba8	Tubulin alpha-8 chain	CB
P85108	Tubb2a	Tubulin beta-2A chain	CC, HP, CB
Q3KRE8	Tubb2b	Tubulin beta-2B chain	CC, HP
Q4QRB4	Tubb3	Tubulin beta-3 chain	CC, HP, CB
Q6P9T8	Tubb4b	Tubulin beta-4B chain	CC, HP, CB
P69897	Tubb5	Tubulin beta-5 chain	CC, HP, CB
B2RYG6	Otub1	Ubiquitin thioesterase OTUB1	HP
Q63357	Myo1d	Unconventional myosin-Id	CC
Q9QYF3	Myo5a	Unconventional myosin-Va	CC, CB
Q9JJW3	Usmg5	Up-regulated during skeletal muscle growth protein 5	CC, HP, CB
Q793F9	Vps4a	Vacuolar protein sorting-associated protein 4A	CB
Q04462	Vars	Valine--tRNA ligase	CB
Q9ERB4	Vcan	Versican core protein	CB
Q63666	Vamp1	Vesicle-associated membrane protein 1	CB
P63045	Vamp2	Vesicle-associated membrane protein 2	CB
P63025	Vamp3	Vesicle-associated membrane protein 3	CC, CB
Q9Z270	Vapa	Vesicle-associated membrane protein-associated protein A	HP, CB
Q9QUL6	Nsf	Vesicle-fusing ATPase	CC, HP, CB
Q62634	Slc17a7	Vesicular glutamate transporter 1	CC, HP
Q9JI12	Slc17a6	Vesicular glutamate transporter 2	CC
O35458	Slc32a1	Vesicular inhibitory amino acid transporter	CC, HP
P31000	Vim	Vimentin	CC, CB
P62762	Vsnl1	Visinin-like protein 1	CB
Q9Z2L0	Vdac1	Voltage-dependent anion-selective channel protein 1	CC, HP
P81155	Vdac2	Voltage-dependent anion-selective channel protein 2	CC, HP
Q9R1Z0	Vdac3	Voltage-dependent anion-selective channel protein 3	CC, HP, CB
Q71RJ2	Cacng2	Voltage-dependent calcium channel gamma-2 subunit	CB
P54290	Cacna2d1	Voltage-dependent calcium channel subunit alpha-2/delta-1	CC
P54287	Cacnb3	Voltage-dependent L-type calcium channel subunit beta-3	HP
Q5J3M4	Vom1r94	Vomeronasal type-1 receptor 94	CC
P25286	Atp6v0a1	V-type proton ATPase 116 kDa subunit a isoform 1	CC, HP, CB
P63081	Atp6v0c	V-type proton ATPase 16 kDa proteolipid subunit	CC, HP, CB
P62815	Atp6v1b2	V-type proton ATPase subunit B, brain isoform	CC
Q6PCU2	Atp6v1e1	V-type proton ATPase subunit E 1	HP
O54715	Atp6ap1	V-type proton ATPase subunit S1	CC
Q9ERH3	Wdr7	WD repeat-containing protein 7	CC

Q6QIX3	Slc30a3	Zinc transporter 3	CC

Table III.A.S 2 -Panther Protein class analysis of all candidate BRI2 interactors identified in this study. In the table are listed the Panther protein class terms and the respective IDs, as well as the Uniprot accessions of the proteins that belong to each class

Panther Protein Class (term ID)	Uniprot accessions of mapped proteins
ATP synthase (PC00227)	P15999, Q06647, P25286, O54715, D3ZAF6, P62815, P10719, P63081
G-protein (PC00095)	B3GNI6, P62630, P61227, P21575, O35303, P08644, P10824, P61751, P54311, P59215, P82471, P05197, Q9JJM9, P19627, Q9WVC0, Q6RUV5, Q6PST4, P85834, P43425, O35353, Q9WU34, Q2TA68, P04897, P52287
actin family cytoskeletal protein (PC00085)	P0DJJ3, O35413, P63269, Q05764, P09495, Q9QYF3, P45592, B2GUZ5, Q64122, P85515, P68035, Q64119, Q3T1K5, Q63610, Q5XI32, Q9Z1P2, P16409, P52481, O08839, D3ZHV2, P70566, P30427, P16086, Q9JLT0, O08838, Q07266, P13832, Q68FP1, Q4V7C7, Q9QWN8, Q6KC51, P60711, Q62812, Q9Z327, Q63028, P09951, P02600, Q63357, Q63537
anion channel (PC00002)	P15999, P81155, Q9R1Z0, P62815, P10719, Q9Z2L0
calcium-binding protein (PC00060)	Q9QVC8, P62161, P97700, Q8R491, Q05962, P62161, Q64122, Q505J6, Q07009, Q5XIN6, Q64119, Q64620, P16409, Q62717, P63319, P62161, P62138, P13832, Q62703, Q9WVE9, P63329, Q09073, P02600, P16036
cation transporter (PC00227)	P15999, P06687, Q06647, Q9JI12, Q9JHY2, P11507, P13638, P11505, Q63965, P25286, P06685, P48768, O54715, D3ZAF6, O35921, P07340, P11506, P62815, Q62634, Q64542, P06686, Q64568, P31596, Q9JI66, P10719, P63081, P24942, Q64578, P31647
chaperone (PC00072)	P68255, Q9QVC8, P82995, Q7TPB1, P97874, Q6P502, P34058, P63102, P61983, P62260, P63039, Q66HD0, Q5XIM9, Q68FQ0
cytoskeletal protein (PC00085)	P34926, P0DJJ3, O35413, Q9WV63, P47819, B3GNI6, P63269, Q05764, P09495, Q9QYF3, P45592, B2GUZ5, P85108, P21575, Q68FR6, O35303, Q64122, P85515, Q4QRB4, Q5XI51, Q6P9T8, Q63279, P68035, P12839, Q64119, Q3T1K5, O70511, Q63610, Q5XI32, Q9Z1P2, P31000, P56536, P16409, Q68FR8, P52481, O08839, P70615, P19527, Q6AY56, Q5XIF6, Q9JJM9, P38650, Q3KRE8, P15205, Q4FZT0, D3ZHV2, Q6IG00, P70566, Q6QLM7, P30427, P16086, Q9WVC0, Q9JLT0, O08838, Q9WU82, P68370, P69897, Q07266, P13832, P48679, Q68FP1, Q4V7C7, Q9QWN8, Q9WU34, Q6KC51, Q2TA68, P60711, Q6AYH5, Q2PQA9, Q62812, Q9Z327, Q793F9, P23565, Q63028, Q6AYZ1, P09951, Q68FR8, P02600, Q63357, Q63537
dehydrogenase (PC00176	P11960, P04636, P29147, O70351, P04642, P19234, Q64428, O08651, Q9WVK7, Q641Y2, P41565, Q68FX0, Q99NA5, P21913, Q63342, P26284, P49432, P04797, Q5BK63, P12785, Q66HF1
enzyme modulator (PC00095)	O35413, B3GNI6, F1M386, Q9QYF3, Q63228, Q8R491, P62630, P61227, P21575, O35303, P08644, P10824, Q5PPJ9, P29066, P49911, P61751, P54311, P59215, P67874, P82471, P05197, Q9QUH6, O08839, P50399, Q9JJM9, P06238, Q9JIR4, P97846, P19627, Q9WVC0, Q8CGU4, Q9JLT0, O08838, Q6RUV5, Q6PST4, P85834, P01026, P43425, O35179, O35353, Q7TP98, Q9WVE9, Q9WU34, Q2TA68, Q62848, Q9ERH3, P97829, P04897, Q4FZT9, Q62812, Q63416, P52287, P61980, Q9Z1T4, Q63357
heterotrimeric G-protein (PC00095)	P10824, P54311, P59215, P82471, P19627, Q6PST4, P43425, O35353, P04897, P52287
hydrolase (PC00121)	P15999, P06687, Q06647, Q62950, P62630, P21575, O35303, P32551, Q62951, O08565, Q794F9, P11507, Q07009, Q63198, Q5RJQ4, P13233, P54311, Q64620, D3ZGS3, P11505, B5DFN2, O35567, P25286, B0BND0, P05197, Q9WTT6, P06685, O54715, B2RYG6, Q6AYD3, P38650, P11506, P62815, P97846, P62138, P13596, P85834, Q4QQT4, Q6Q0N1, O35353, Q64542, P06686, Q7TP98, Q2TA68, P28492, Q64568, Q62910, Q9ERH3, P97685, P63329, P12346, P10719, P63081, Q9QUL6, P52287, Q64578, P12785, P47942, O88767
intermediate filament (PC00085)	P47819, Q63279, P12839, P31000, P70615, P19527, Q6IG00, P48679, P23565
ion channel (PC00068)	P15999, P06687, Q63226, P81155, P54287, P11507, P11505, P06685, Q9R1Z0, P11506, P62815, Q71RJ2, P19491, Q63269, Q64542, Q00960, P06686, P29994, Q64568, P10719, Q9Z2L0, Q64578, P19490
membrane traffic protein (PC00150)	P0DJJ3, Q3B7K9, Q8R491, P63025, P61765, P21707, P97610, Q9JK11, P54921, Q6RJR6, P07825, P08081, P11442, P61265, P29101, P08082, P32851, P52303, Q63666, Q9WVE9, Q64548, P62944, P85969, P09951, Q5BJS7, P63045, Q9Z270, Q05140, P62744, P47709, P60881, Q62876, Q63537
membrane trafficking regulatory protein (PC00150)	P0DJJ3, P61765, P21707, P97610, P07825, P29101, P09951, Q9Z270, P47709, Q62876, Q63537
microtubule family cytoskeletal protein (PC00085)	P34926, Q9WV63, P85108, P21575, O35303, Q4QRB4, Q5XI51, Q6P9T8, P56536, Q68FR8, Q6AY56, Q5XIF6, P38650, Q3KRE8, P15205, Q6QLM7, P68370, P69897, Q2TA68, Q6AYH5, Q2PQA9, Q793F9, Q6AYZ1, Q68FR8

Panther Protein Class (term ID)	Uniprot accessions of mapped proteins
non-motor actin binding protein (PC00085)	Q05764, P45592, B2GUZ5, Q3T1K5, Q5XI32, Q9Z1P2, D3ZHV2, P70566, P30427, P16086, Q07266, Q68FP1, Q9QWN8, Q9Z327, Q63028, P09951, Q63537
oxidoreductase (PC00176)	P11960, P04636, P29147, O70351, P21396, P04642, Q68FR6, P19234, Q64428, O08651, Q9WVK7, Q641Y2, P35171, P41565, P11240, O35244, Q68FX0, Q99NA5, P21913, P52504, Q920J4, P12075, Q63342, P00406, P97846, P26284, P49432, Q63716, P35704, P04797, Q5BK63, P12785, Q66HF1
small GTPase (PC00095)	B3GNI6, P61227, P21575, O35303, P08644, P61751, Q9JJM9, Q9WVC0, Q6RUV5, Q9WU34, Q2TA68
structural protein (PC00211)	Q99JD4, P47819, P60203, Q63279, P12839, P31000, P70615, P19527, Q6IG00, P02688, P48679, Q6KC51, P07722, P23565
transcription factor (PC00218)	P97536, Q6MG48, P86252, Q68A21, Q6AYD3, O88767
transmembrane receptor regulatory/adaptor protein (PC00226)	Q62696, P97838, P0C6S7, P31016, P18484, P97546, P97837, P97836
transporter (PC00227)	P15999, P06687, Q06647, P97700, Q63226, Q9JI12, P81155, Q05962, Q505J6, P54287, Q9JHY2, P61765, P11507, O35458, P13638, P11505, Q63965, Q6QIX3, P25286, P06685, P48768, O54715, D3ZAF6, O35921, P07340, Q9R1Z0, P11506, P62815, Q71RJ2, P97846, P19491, P69682, Q63269, Q62634, Q64542, Q00960, P06686, P29994, Q64568, B5D5N9, Q7TNJ2, P31596, Q9JI66, P10719, P63081, P24942, Q09073, Q9Z2L0, Q64578, P19490, P16036, P31647
tubulin (PC00085)	P85108, Q4QRB4, Q6P9T8, Q68FR8, Q6AY56, Q5XIF6, Q3KRE8, P68370, P69897, Q6AYZ1, Q68FR8

Table III.A.S 3 - BRI2 interactors retrieve from online databases. The BRI2 interactors, as well as, the uniprot accession number, the species and the experimental evidence supporting the interactions, as well as the cell line or tissue where they were detected is indicated.

Gene	Protein	Uniprot accession number	Species	Experimental evidence	Cell line/Tissue	References
Adam7	Desintegrin and metalloproteinase domain-containing protein 7	O35227	*Mus Musculus*	Affinity Capture-MS	Mouse sperm	(Han *et al.* 2011)
AMIGO1	Adhesion molecule with Ig-like domain 1	Q86WK6	*Homo sapiens*	Affinity Capture-MS	HEK293T cells	(Huttlin *et al.* 2015)
APP	Amyloid beta A4 protein	P05067	*Homo sapiens*	Two-hybrid Co-IP	HEK293 cells stably expressing APP751, transfected with myc-tagged BRI2	(Matsuda *et al.* 2005; Fotinopoulou *et al.* 2005)
ATF6B	cAMP response element-binding protein-related protein	Q99941	*Homo sapiens*	Affinity Capture-MS	HEK293T cells	(Huttlin *et al.* 2015)
B4GALNT1	UDP-N-acetyl-alpha-D-galactosamine:(N-acetylneuraminyl)-galactosylglucosylceramide N-acetylgalactosaminyltransferase (GalNAc-T)	Q00973	*Homo sapiens*	Affinity Capture-MS	HEK293T cells	(Huttlin *et al.* 2015)
BACE1	β-secretase β-amyloid protein converting enzyme 1	P56817	*Homo sapiens*	Co-IP	SH-SY5Y cells	(Tsachaki *et al.* 2013)
Bcl2	Apoptosis regulator Bcl-2 (protein phosphatase 1, regulatory subunit 50)	P10415	*Mus musculus*	Co-IP	TS1 alpha beta cells	(Fleischer *et al.* 2002)
BTN2A2	Butyrophilin, subfamily 2, member A2	Q8WVV5	*Homo sapiens*	Affinity Capture-MS	HEK293T cells	(Huttlin *et al.* 2015)
CACNA2D1	Dihydropyridine-sensitive L-type, calcium channel alpha-2/delta subunit	P54289	*Homo sapiens*	Affinity Capture-MS	HEK293T cells	(Huttlin *et al.* 2015)
CCDC155	Protein KASH5	Q8N6L0	*Homo sapiens*	Two-hybrid	----	(Rolland *et al.* 2014)
CHST12	Carbohydrate (chondroitin 4) sulfotransferase 12	Q9NRB3	*Homo sapiens*	Affinity Capture-MS	HEK293T cells	(Huttlin *et al.* 2015)
CREB3	Cyclic AMP-responsive element-binding protein 3	O43889	*Homo sapiens*	Two-hybrid; Affinity Capture-MS	HeLa cells expressing GFP-tagged proteins	(Yu *et al.* 2011; Hein *et al.* 2015)
Csf1	Macrophage colony-stimulating factor 1	P07141	*Mus musculus*	Pull-down	M1 myeloid cells	(Cross *et al.* 2005)
DCBLD2	Discoidin, CUB and LCCL domain-containing protein 2	Q96PD2	*Homo sapiens*	Affinity Capture-MS	HEK293T cells	(Huttlin *et al.* 2015)
FCGRT	IgG receptor FcRn large subunit p51	P55899	*Homo sapiens*	Affinity Capture-MS	HEK293T cells	(Huttlin *et al.* 2015)
GLG1	Cysteine-rich fibroblast growth factor receptor	Q92896	*Homo sapiens*	Affinity Capture-MS	HEK293T cells	(Huttlin *et al.* 2015)

Gene	Protein	Uniprot accession number	Species	Experimental evidence	Cell line/Tissue	References
HLA-A	HLA class I histocompatibility antigen, A-1 alpha chain	P30443	*Homo sapiens*	Affinity Capture-MS	HEK293T cells	(Huttlin *et al.* 2015)
HNF1A	Hepatocyte nuclear factor 1-alpha	P20823	*Homo sapiens*	Cross-linking study	Liver and pancreas	(Odom *et al.* 2004)
HS6ST1	Heparan sulfate 6-O-sulfotransferase 1	O60243	*Homo sapiens*	Affinity Capture-MS	HEK293T cells	(Huttlin *et al.* 2015)
KIAA1467	Uncharacterized protein KIAA1467	A2RU67	*Homo sapiens*	Affinity Capture-MS	HEK293T cells	(Huttlin *et al.* 2015)
KIF18A	Kinesin-like protein KIF18A	Q8NI77	*Homo sapiens*	Affinity Capture-MS	HeLa cells	(Hein *et al.* 2015)
Lmo2	Rhombotin-2	P25801	*Mus musculus*	Two-hybrid	----	(Sincennes *et al.* 2016)
LRFN3	Leucine-rich repeat and fibronectin type-III domain-containing protein 3	Q9BTN0	*Homo sapiens*	Affinity Capture-MS	HEK293T cells	(Huttlin *et al.* 2015)
MR1	Bajor histocompatibility complex class I-related gene protein	Q95460	*Homo sapiens*	Affinity Capture-MS	HEK293T cells	(Huttlin *et al.* 2015)
NAALADL2	Inactive N-acetylated-alpha-linked acidic dipeptidase-like protein 2	Q58DX5	*Homo sapiens*	Two-hybrid	----	(Rolland *et al.* 2014)
Nek2	Serine/threonine-protein kinase Nek2	O35942	BRI2 *Hs* - Nek2 *Ms*	Affinity Capture-MS	HeLa cells	(Hein *et al.* 2015)
PGAP1	Post-GPI attachment to proteins factor 1	Q75T13	*Homo sapiens*	Affinity Capture-MS	HEK293T cells	(Huttlin *et al.* 2015)
PPP1CA/Ppp1ca	Serine/threonine-protein phosphatase PP1-alpha catalytic subunit	P62136	*Homo sapiens*	Co-IP	SH-SY5Y cells transfected with myc-bri2	(Martins *et al.* 2016)
		P62138	*Rattus norvegicus*	Co-IP	Rat primary cortical and hippocampal cultures	
PPP1CC/Ppp1cc	Serine/threonine-protein phosphatase PP1-gamma catalytic subunit	P36873	*Homo sapiens*	Co-IP	SH-SY5Y cells transfected with myc-bri2	(Martins *et al.* 2016)
		P63088	*Rattus norvegicus*	Co-IP	Rat primary cortical and hippocampal cultures	
RPL31	60S ribosomal protein L31	P62899	*Homo sapiens*	Two-hybrid	----	(Bell *et al.* 2009)
RYK	RYK receptor-like tyrosine kinase	P34925	*Homo sapiens*	Affinity Capture-MS	HEK293T cells	(Berndt *et al.* 2011)
SEMA4F	Semaphorin-4F	O95754	*Homo sapiens*	Affinity Capture-MS	HEK293T cells	(Huttlin *et al.* 2015)
SEMA6A	Semaphorin-6A	Q9H2E6	*Homo sapiens*	Affinity Capture-MS	HEK293T cells	(Huttlin *et al.* 2015)

Gene	Protein	Uniprot accession number	Species	Experimental evidence	Cell line/Tissue	References
Shoc2	Leucine-rich repeat protein SHOC-2	O88520	BRI2 *Hs* - SHOC2 *Ms*	Affinity Capture-MS	HeLa cells expressing GFP-tagged proteins	(Hein *et al.* 2015)
SPPL2A	Signal peptide peptidase-like 2A	Q8TCT8	*Homo sapiens*	Co-IP	HEK293T cells	(Martin *et al.* 2008)
SPPL2B	Signal peptide peptidase-like 2B	Q8TCT7	*Homo sapiens*	Co-IP	HEK293T cells	(Martin *et al.* 2008)
SYNE4	Nesprin-4	Q8N205	*Homo sapiens*	Two-hybrid	----	(Rolland *et al.* 2014)
TGFBR3	Transforming growth factor beta receptor type 3	Q03167	*Homo sapiens*	Affinity Capture-MS	HEK293T cells	(Huttlin *et al.* 2015)
TMEM17	Transmembrane protein 17	Q86X19	*Homo sapiens*	Proximity Label-MS	----	(Gupta *et al.* 2015)
TMEM219	Insulin-like growth factor binding protein-3 receptor	Q86XT9	*Homo sapiens*	Affinity Capture-MS	HEK293T cells	(Huttlin *et al.* 2015)
TMEM59L	Brain-specific membrane-anchored protein (C19orf4)	Q9UK28	*Homo sapiens*	Affinity Capture-MS	HEK293T cells	(Huttlin *et al.* 2015)
UBC	Polyubiquitin-C	P0CG48	*Homo sapiens*	Affinity Capture-MS	HEK293T cells expressing HA-tagged ubiquitin; HEK293Tcells expressing strep-HA tagged ubiquitin; HEK293T and HCT116 cells	(Danielsen *et al.* 2011; Wagner *et al.* 2011; Kim *et al.* 2011)
UBR1	Ubiquitin protein ligase E3 component n-recognin 1	Q8IWV7	*Homo sapiens*	Affinity Capture-MS	HEK293T cells	(Huttlin *et al.* 2015)
UNK	RING finger protein unkempt homolog	Q9C0B0	*Homo sapiens*	Affinity Capture-RNA	SH-SY5Y and HeLa cells	(Murn *et al.* 2015)

Co-IP, co-immunoprecipitation; MS, mass spectrometry; Hs, *Homo sapiens*; Ms, *Mus musculus*

Table III.A.S4 - Panther Protein class analysis of candidate BRI2 interactors identified by Nano-HPLC-MS/MS, and highly enriched or specific in the brain tissue. Panther protein class terms and the respective IDs, as well as the Uniprot accessions of the proteins that belong to each class are listed.

Panther Protein Class (term ID)	Uniprot accessions of mapped proteins
cation transporter (PC00227)	P06687, Q9JI12, P13638, P48768, O35921, P11506, Q62634, P06686, Q64568, P31596, P24942, P31647
cytoskeletal protein (PC00085)	P34926, P0DJJ3, P47819, Q05764, P85108, P21575, Q4QRB4, P12839, P56536, P19527, Q9JJM9, Q3KRE8, P15205, P70566, Q6QLM7, O08838, Q9QWN8, Q9WU34, P23565, P09951, Q63537
membrane traffic protein (PC00150)	P0DJJ3, Q8R491, P61765, P21707, P97610, P07825, P61265, P29101, P32851, Q64548, P85969, P09951, Q5BJS7, Q05140, P47709, P60881, Q63537
membrane trafficking regulatory protein (PC00150)	P0DJJ3, P61765, P21707, P97610, P07825, P29101, P09951, P47709, Q63537
microtubule family cytoskeletal protein (PC00085)	P34926, P85108, P21575, Q4QRB4, P56536, Q3KRE8, P15205, Q6QLM7, Q63537
myelin protein (PC00211)	P60203, P02688, P07722
nucleic acid binding(PC00022)	Q505J6, Q8CGU4
structural protein (PC00129)	P47819, P60203, P12839, P19527, P02688, P07722, P23565
transmembrane receptor regulatory/adaptor protein(PC00226)	P97838, P0C6S7, P31016, P97837, P97836
transporter(PC00227)	P06687, Q9JI12, Q505J6, P61765, O35458, P13638, Q6QIX3, P48768, O35921, P11506, Q71RJ2, P97846, P19491, Q62634, Q00960, P06686, Q64568, P31596, P24942, P19490, P31647
tubulin(PC00085)	P85108, Q4QRB4, Q3KRE8

Table III.A.S5 - Biological process enrichment analysis of the brain specific BRI2 interactome using Panther online resource. Enriched categories are identified as those with p-value <0.05, and GO terms presented correspond to the two most specific for each category retrieved in the analysis. Nr. Number.

Biological Process	GO term	Nr. proteins	Fold enrichment (%)	p-value	Associated proteins
Brain development (GO:0007420)	brain development (GO:0007420)	31	7.39	1.31E-14	Slc17a6, Plp1, Ntm, Bcan, Syt1, Basp1, Cntn1, Nefm, Cnp, Gnao1, Slc32a1, Grin1, Dclk1, Slc8a2, Nefl, Atp2b2, Dcx, Mbp, Cend1, Ncaml, Kcna1, Slc17a7, Grin2b, Sptbn2, Mag, Atp2b3, Tnr, Slc1a2, Ina, Rph3a, Slc6a11
	forebrain development (GO:0030900)	16	7.07	1.02E-05	Slc17a6, Bcan, Nefm, Cnp, Gnao1, Slc32a1, Grin1, Dclk1, Slc8a2, Nefl, Dcx, Ncaml, Kcna1, Grin2b, Tnr, Slc1a2
	substantia nigra development (GO:0021762)	6	25.51	1.42E-03	Plp1, Basp1, Cnp, Mbp, Mag, Ina
	telencephalon development (GO:0021537)	12	7.99	3.69E-04	Slc17a6, Bcan, Nefm, Slc32a1, Grin1, Slc8a2, Nefl, Dcx, Kcna1, Grin2b, Tnr, Slc1a2
	hippocampus development (GO:0021766)	8	14.80	7.56E-04	Slc17a6, Bcan, Nefm, Slc32a1, Nefl, Dcx, Kcna1, Grin2b
Neuron development (GO:0048666)	positive regulation of dendrite extension (GO:1903861)	4	42.07	2.51E-02	Syt1, Syt2, Rims1, Cpne9
	regulation of dendrite extension (GO:1903859)	4	39.97	3.06E-02	Syt1, Syt2, Rims1, Cpne9
	neuron projection regeneration (GO:0031102)	5	24.98	1.75E-02	Gfap, Nefm, Nefl, Map1b, Ncaml
	neuron projection development (GO:0031175)	31	10.22	1.33E-18	Gfap, Crmp1, Plp1, Dpysl4, Tubb3, Stxbp1, Ncdn, Cntn1, Nefm, Dlg4, Cnp, Gnao1, Dclk1, Kif5c, Map6, Slc12a5, Nefl, Map1b, Dcx, Rab3a, Kif5a, Map2, Cntnap1, Agap2, Ncaml, Atl1, Gap43, Shank1, Snap91, Snap25, Camk2a
	dendrite morphogenesis (GO:0048813)	7	23.71	2.12E-04	Dlg4, Dclk1, Map6, Dcx, Map2, Shank1, Camk2a
	dendrite development (GO:0016358)	9	16.65	4.23E-05	Dlg4, Dclk1, Map6, Slc12a5, Map1b, Dcx, Map2, Shank1, Camk2a
	neuron projection morphogenesis (GO:0048812)	24	11.08	2.40E-14	Crmp1, Dpysl4, Tubb3, Stxbp1, Dlg4, Cnp, Dclk1, Kif5c, Map6, Nefl, Map1b, Dcx, Rab3a, Kif5a, Map2, Cntnap1, Agap2, Ncaml, Atl1, Gap43, Shank1, Snap91, Snap25, Camk2a
	cell morphogenesis involved in neuron differentiation (GO:0048667)	23	11.58	5.08E-14	Crmp1, Tubb3, Stxbp1, Dlg4, Cnp, Dclk1, Kif5c, Map6, Map1b, Atp2b2, Dcx, Rab3a, Kif5a, Map2, Agap2, Ncaml, Atl1, Gap43, Shank1, Slc1a3, Snap91, Snap25, Camk2a
	axonogenesis (GO:0007409)	17	10.26	9.76E-09	Crmp1, Tubb3, Stxbp1, Cnp, Dclk1, Kif5c, Map1b, Dcx, Rab3a, Kif5a, Map2, Agap2, Ncaml, Atl1, Gap43, Snap91, Snap25
	axon development (GO:0061564)	20	10.95	2.51E-11	Crmp1, Plp1, Tubb3, Stxbp1, Nefm, Cnp, Dclk1, Kif5c, Nefl, Map1b, Dcx, Rab3a, Kif5a, Map2, Agap2, Ncaml, Atl1, Gap43, Snap91, Snap25
Regulation of synaptic plasticity (GO:0048167)	positive regulation of excitatory postsynaptic potential (GO:2000463)	6	42.82	6.87E-05	Dlg4, Grin1, Stx1b, Rims1, Stx1a, Shank1
	modulation of excitatory postsynaptic potential (GO:0098815)	6	31.55	4.12E-04	Dlg4, Grin1, Stx1b, Rims1, Stx1a, Shank1
	positive regulation of synaptic transmission (GO:0050806)	17	24.98	5.86E-15	Gfap, Syt1, Syt12, Dlg4, Grin1, Stx1b, Slc8a2, Rims1, Gria2, Stx1a, Grin2b, Tnr, Shank1, Slc1a3, Camk2b, Snap25, Gria1
	neuron-neuron synaptic transmission (GO:0007270)	7	19.98	6.70E-04	Dnml, Grin1, Tmod2, Slc17a7, Dlgap2, Napb, Gria1
	regulation of neuronal synaptic plasticity (GO:0048168)	11	30.53	1.28E-09	Bcan, Ncdn, Dlg4, Syp, Grin1, Slc8a2, Rab3a, Rims1, Grin2b, Camk2b, Camk2a
	regulation of long-term neuronal synaptic plasticity (GO:0048169)	6	34.26	2.55E-04	Dlg4, Syp, Grin1, Rims1, Grin2b, Camk2b
	long-term synaptic potentiation (GO:0060291)	8	31.97	2.03E-06	Gfap, Syt12, Slc8a2, Rims1, Grin2b, Tnr, Camk2b, Snap25
	long-term memory (GO:0007616)	6	33.31	3.01E-04	Grin1, Slc17a7, Grin2b, Shank1, Snap25, Gria1

Biological Process	GO term	Nr. proteins	Fold enrichment (%)	p-value	Associated proteins
Learning or memory (GO:0007611)	memory (GO:0007613)	8	12.02	3.60E-03	Atp1a3, Grin1, Slc8a2, Slc17a7, Grin2b, Shank1, Snap25, Gria1
	associative learning (GO:0008306)	7	14.57	5.49E-03	Atp1a3, Grin1, Grin2b, Atp1a2, Tnr, Shank1, Snap25
	learning (GO:0007612)	10	12.26	1.03E-04	Atp1a3, Grin1, Slc12a5, Slc8a2, Amph, Grin2b, Atp1a2, Tnr, Shank1, Snap25
Synaptic vesicle cycle (GO:0099504)	vesicle-mediated transport in synapse (GO:0099003)	15	26.76	2.71E-13	Pclo, Syt1, Syt12, Stx1b, Syt2, Cadps, Rab3a, Rims1, Amph, Stx1a, Sh3gl2, Cplx1, Sptbn2, Rph3a, Snap25
	neurotransmitter uptake (GO:0001504)	4	57.10	7.53E-03	Slc17a6, Atp1a2, Sv2a, Sv2b
	neurotransmitter transport (GO:0006836)	27	36.71	4.53E-30	Slc17a6, Pclo, Stxbp1, Syt1, Syt12, Slc32a1, Stx1b, Syt2, Cadps, Rab3a, Rims1, Stx1a, Slc17a7, Cplx1, Atp1a2, Sptbn2, Sv2a, Sv2b, Slc1a2, Slc1a3, Syn1, Nsf, Snap91, Rph3a, Snap25, Syn2, Slc6a11
	import into cell (GO:0098657)	5	21.72	3.43E-02	Slc17a6, Slc8a2, Atp1a2, Sv2a, Sv2b
	vesicle docking (GO:0048278)	6	23.51	2.29E-03	Stxbp1, Syt1, Stx1b, Stx1a, Sptbn2, Nsf
	membrane docking (GO:0022406)	6	17.90	1.10E-02	Stxbp1, Syt1, Stx1b, Stx1a, Sptbn2, Nsf
	regulation of synaptic vesicle priming (GO:0010807)	5	> 100	3.27E-06	Stxbp1, Stx1b, Rims1, Stx1a, Napb
	regulation of protein complex assembly (GO:0043254)	11	6.16	1.73E-02	Add2, Stxbp1, Stx1b, Gda, Map1b, Rims1, Tmod2, Ncaml, Stx1a, Sptbn2, Napb
	vesicle fusion (GO:0006906)	7	15.54	3.58E-03	Syt12, Stx1b, Syt2, Stx1a, Nsf, Rph3a, Snap25
	organelle membrane fusion (GO:0090174)	7	15.21	4.15E-03	Syt12, Stx1b, Syt2, Stx1a, Nsf, Rph3a, Snap25
	single-organism organelle organization (GO:1902589)	28	3.86	4.44E-06	Map1a, Gfap, Add2, Crmp1, Ehd3, Stxbp1, Syt12, Nefm, Dlg4, Cnp, Stx1b, Map6, Nefl, Syt2, Map1b, Rab3a, Tmod2, Klc1, Map2, Stx1a, Slc17a7, Shank1, Ina, Slc1a3, Nsf, Rph3a, Snap25, Camk2a
	vesicle organization (GO:0016050)	13	10.82	2.71E-06	Dnml, Stxbp1, Syt12, Dlg4, Stx1b, Syt2, Cadps, Rab3a, Stx1a, Slc17a7, Nsf, Rph3a, Snap25
	regulation of synaptic vesicle exocytosis (GO:2000300)	6	54.50	1.66E-05	Stxbp1, Stx1b, Rab3a, Rims1, Stx1a, Napb
	synaptic vesicle exocytosis (GO:0016079)	13	35.59	1.03E-12	Pclo, Syt1, Syt12, Stx1b, Syt2, Cadps, Rab3a, Rims1, Stx1a, Cplx1, Sptbn2, Rph3a, Snap25
	calcium ion-regulated exocytosis of neurotransmitter (GO:0048791)	7	35.87	1.27E-05	Syt1, Syt12, Stx1b, Syt2, Rims1, Rph3a, Snap25
	positive regulation of calcium ion-dependent exocytosis (GO:0045956)	6	54.50	1.66E-05	Scamp5, Stxbp1, Syt1, Cadps, Rims1, Stx1a
	positive regulation of regulated secretory pathway (GO:1903307)	7	28.55	6.02E-05	Scamp5, Stxbp1, Syt1, Cadps, Rab3a, Rims1, Stx1a
	protein localization to synapse (GO:0035418)	7	77.72	6.17E-08	Homer1, Pclo, Dlg4, Klc1, Shank1, Bsn, Dlgap1
	protein localization (GO:0008104)	28	3.58	2.30E-05	Scamp5, Ehd3, Homer1, Pclo, Dlg2, Stxbp1, Dlg4, Kif5c, Stx1b, Cadps, Rab3a, Rims1, Kif5a, Klc1, Cntnap1, Gria2, Stx1a, Kcna1, Cplx1, Grin2b, Shank1, Napb, Nsf, Snap91, Rph3a, Bsn, Rab3c, Dlgap1
	synaptic vesicle maturation (GO:0016188)	4	88.82	1.31E-03	Stxbp1, Dlg4, Rab3a, Slc17a7
	developmental maturation (GO:0021700)	10	9.25	1.38E-03	Plp1, Dlg2, Stxbp1, Dlg4, Grin1, Map1b, Rab3a, Cend1, Slc17a7, Shank1
	synaptic vesicle endocytosis (GO:0048488)	5	52.59	4.59E-04	Syt1, Syt12, Syt2, Amph, Sh3gl2

Biological Process	GO term	Nr. proteins	Fold enrichment (%)	p-value	Associated proteins
	clathrin-dependent endocytosis (GO:0072583)	6	38.68	1.25E-04	Dnml, Syt1, Syt12, Syt2, Amph, Sh3gl2
	synaptic vesicle recycling (GO:0036465)	6	47.96	3.53E-05	Rab3a, Syt1, Syt12, Syt2, Amph, Sh3gl2
Ion transport (GO:0006811)	inorganic cation transmembrane transport (GO:0098662)	13	5.42	7.99E-03	Atp1a3, Atp1b2, Grin1, Slc30a3, Slc12a5, Slc8a2, Atp2b2, Cacng2, Kcna1, Slc17a7, Atp1a2, Atp2b3, Snap25
	cation transport (GO:0006812)	19	4.81	1.36E-04	Atp1a3, Slc17a6, Slc32a1, Atp1b2, Grin1, Slc30a3, Slc12a5, Slc8a2, Atp2b2, Cacng2, Kcna1, Slc17a7, Grin2b, Atp1a2, Atp2b3, Nsf, Camk2b, Snap25, Camk2a
	metal ion transport (GO:0030001)	18	6.48	3.42E-06	Atp1a3, Slc17a6, Atp1b2, Grin1, Slc30a3, Slc12a5, Slc8a2, Atp2b2, Cacng2, Kcna1, Slc17a7, Grin2b, Atp1a2, Atp2b3, Nsf, Camk2b, Snap25, Camk2a
	regulation of ion transport (GO:0043269)	15	4.65	7.61E-03	Ehd3, Homer1, Syt1, Cntn1, Dlg4, Gnao1, Atp1b2, Grin1, Atp2b2, Cacng2, Kcna1, Grin2b, Atp1a2, Shank1, Camk2a
L-glutamate transport (GO:0015813)	L-glutamate transmembrane transport (GO:0089711)	4	72.67	2.90E-03	Slc17a6, Slc1a6, Slc1a2, Slc1a3
	L-glutamate transport (GO:0015813)	5	55.51	3.52E-04	Slc17a6, Slc1a6, Slc1a2, Slc1a3, Slc17a7
Glutamate receptor signalling pathway (GO:0007215)	ionotropic glutamate receptor signaling pathway (GO:0035235)	6	46.12	4.44E-05	Atp1a3, Grin1, Gria2, Grin2b, Gria1, Camk2a
	glutamate receptor signaling pathway (GO:0007215)	7	31.79	2.89E-05	Atp1a3, Grin1, Gria2, Grin2b, Gria1, Camk2a, Homer1
Neuromuscular process (GO:0050905)	neuromuscular process controlling balance (GO:0050885)	8	24.60	1.55E-05	Dlg4, Nefl, Atp2b2, Cntnap1, Tnr, Shank1, Slc1a3, Camk2b
	neuromuscular process (GO:0050905)	11	18.32	2.88E-07	Dlg4, Grin1, Nefl, Atp2b2, Cntnap1, Kcna1, Grin2b, Tnr, Shank1, Slc1a3, Camk2b
Behavior (GO:0007610)	locomotory behavior (GO:0007626)	12	10.61	1.68E-05	Atp1a3, Dnml, Dlg4, Cnp, Gnao1, Grin1, Atp2b2, Cend1, Lsamp, Atp1a2, Tnr, Snap25
	adult behavior (GO:0030534)	10	11.69	1.61E-04	Atp1a3, Dnml, Homer1, Cnp, Grin1, Cend1, Atp1a2, Sptbn2, Slc1a2, Shank1
Response to chemical (GO:0042221)	response to fungicide (GO:0060992)	4	39.97	3.06E-02	Grin1, Gria2, Grin2b, Gria1
	response to inorganic substance (GO:0010035)	15	4.65	7.46E-03	Homer1, Syt1, Gnao1, Grin1, Slc30a3, Nefl, Map1b, Mbp, Gria2, Ncaml, Kcna1, Grin2b, Slc1a3, Camk2b, Gria1
Others	microtubule-based process (GO:0007017)	14	4.98	8.14E-03	Map1a, Crmp1, Tubb2a, Tubb3, Nefm, Cnp, Kif5c, Map6, Nefl, Tubb2b, Map1b, Kif5a, Klc1, Map2
	cytoskeleton organization (GO:0007010)	20	4.42	2.15E-04	Map1a, Gfap, Add2, Crmp1, Tubb2a, Pclo, Tubb3, Nefm, Cnp, Map6, Nefl, Tubb2b, Map1b, Tmod2, Map2, Cntnap1, Sptbn2, Shank1, Ina, Bsn
	synapse organization (GO:0050808)	10	12.34	9.71E-05	Pclo, Dlg4, Map1b, Atp2b2, Rab3a, Cacng2, Sptbn2, Tnr, Shank1, Bsn
	sensory perception of mechanical stimulus (GO:0050954)	9	10.77	1.67E-03	Map1a, Dnml, Atp2b2, Rab3a, Mbp, Kcna1, Grin2b, Slc1a3, Crym
	negative regulation of cellular component organization (GO:0051129)	16	5.09	9.51E-04	Scamp5, Map1a, Gfap, Add2, Crmp1, Ntm, Stxbp1, Dlg4, Stx1b, Map1b, Mbp, Tmod2, Sptbn2, Mag, Tnr, Shank1

Table III.A.S 6 - Cellular component enrichment analysis of the brain specific BRI2 interactome using Panther online resource. Enriched categories are identified as those with p value <0.05, and GO terms presented correspond to the two most specific for each category retrieved in the analysis. Nr. Number.

GO term	Nr. proteins	Fold enrichment (%)	p-value	Associated proteins
synaptobrevin 2-SNAP-25-syntaxin-1a-complexin I complex (GO:0070032)	3	> 100	1.61E-03	Stx1a, Cplx1, Snap25
SNARE complex (GO:0031201)	8	31.35	3.57E-07	Scamp5, Syt1, Stx1b, Stx1a, Cplx1, Napb, Snap25, Syn2
synaptobrevin 2-SNAP-25-syntaxin-1a complex (GO:0070044)	3	> 100	3.14E-03	Stx1a, Napb, Snap25
neurofilament (GO:0005883)	4	79.94	3.00E-04	Nefm, Nefl, Dlgap2, Ina
polymeric cytoskeletal fiber (GO:0099513)	19	6.67	9.85E-08	Map1a, Gfap, Crmp1, Tubb2a, Dnml, Tubb3, Nefm, Cnp, Kif5c, Map6, Slc8a2, Nefl, Tubb2b, Map1b, Dcx, Kif5a, Klc1, Map2, Dlgap2, Ina
NMDA selective glutamate receptor complex (GO:0017146)	4	66.61	6.17E-04	Dlgap3, Grin1, Grin2b, Shank1
cation channel complex (GO:0034703)	11	12.63	2.06E-06	Dlgap3, Dlg2, Dlg4, Grin1, Cacng2, Cntnap1, Stx1a, Kcna1, Grin2b, Shank1, Snap25
ionotropic glutamate receptor complex (GO:0008328)	9	35.97	7.92E-09	Dlgap3, Dlg2, Dlg4, Grin1, Cacng2, Gria2, Grin2b, Shank1, Gria1
excitatory synapse (GO:0060076)	12	66.61	1.49E-15	Slc17a6, Ntm, Homer1, Syt1, Dlg4, Syp, Grin1, Stx1b, Slc17a7, Shank1, Bsn, Gria1
synapse (GO:0045202)	69	15.72	2.70E-63	Scamp5, Atp1a3, Map1a, Srcin1, Sgip1, Add2, Slc17a6, Dnml, Ntm, Bcan, Dlgap3, Homer1, Pclo, Dlg2, Stxbp1, Syt1, Anks1b, Syt12, Nefm, Dlg4, Prrt1, Syp, Slc32a1, Grin1, Gabbr2, Slc30a3, Dclk1, Stx1b, Slc8a2, Syt2, Sept5, Map1b, Atp2b2, Prkcg, Rab3a, Rims1, Map2, Amph, Gria2, Stx1a, Kcna1, Sh3gl2, Slc17a7, Cplx1, Grin2b, Atp1a2, Sptbn2, Sept3, Sv2a, Sv2b, Gap43, Slc1a2, Dlgap2, Shank1, Slc1a3, Syn1, Nsf, Snap91, Camk2b, Rph3a, Snap25, Bsn, Cnksr2, Gria1, Syn2, Camk2a, Rab3c, Dlgap1
juxtaparanode region of axon (GO:0044224)	3	66.61	1.80E-02	Dlg2, Dlg4, Kcna1
main axon (GO:0044304)	9	24.30	2.44E-07	Dnml, Dlg2, Dlg4, Map1b, Mbp, Cntnap1, Kcna1, Mag, Slc1a2
ciliary rootlet (GO:0035253)	3	59.95	2.47E-02	Kif5a, Kif5c, Klc1
sodium:potassium-exchanging ATPase complex (GO:0005890)	3	59.95	2.47E-02	Atp1a3, Atp1b2, Atp1a2
synaptic vesicle membrane (GO:0030672)	16	50.75	1.54E-19	Scamp5, Slc17a6, Syt1, Syt12, Syp, Slc30a3, Syt2, Amph, Gria2, Stx1a, Slc17a7, Sv2a, Sv2b, Syn1, Rph3a, Syn2
synaptic vesicle (GO:0008021)	29	37.15	1.47E-33	Scamp5, Slc17a6, Dnml, Syt1, Syt12, Dlg4, Syp, Slc32a1, Grin1, Slc30a3, Stx1b, Syt2, Sept5, Rab3a, Amph, Gria2, Stx1a, Slc17a7, Grin2b, Sptbn2, Sv2a, Sv2b, Syn1, Snap91, Rph3a, Snap25, Gria1, Syn2, Rab3c
presynaptic active zone (GO:0048786)	8	48.45	1.18E-08	Pclo, Syp, Slc32a1, Rims1, Slc17a7, Sv2a, Syn1, Bsn
presynaptic membrane (GO:0042734)	13	33.74	3.07E-13	Syt1, Syp, Stx1b, Rims1, Gria2, Stx1a, Kcna1, Grin2b, Sept3, Slc1a2, Snap91, Snap25, Camk2a
synaptic membrane (GO:0097060)	27	19.76	7.71E-24	Srcin1, Dlgap3, Homer1, Dlg2, Syt1, Anks1b, Dlg4, Syp, Grin1, Gabbr2, Stx1b, Prkcg, Rims1, Gria2, Stx1a, Kcna1, Grin2b, Sept3, Slc1a2, Dlgap2, Shank1, Snap91, Snap25, Cnksr2, Gria1, Camk2a, Dlgap1
terminal bouton (GO:0043195)	19	32.45	5.42E-20	Sgip1, Pclo, Stxbp1, Syt1, Syp, Grin1, Syt2, Sept5, Rab3a, Amph, Gria2, Cplx1, Grin2b, Sv2a, Sv2b, Syn1, Snap91, Snap25, Syn2
axon terminus (GO:0043679)	21	21.86	7.62E-19	Sgip1, Pclo, Stxbp1, Syt1, Syp, Slc32a1, Grin1, Syt2, Sept5, Rab3a, Amph, Gria2, Kcna1, Cplx1, Grin2b, Sv2a, Sv2b, Syn1, Snap91, Snap25, Syn2
AMPA glutamate receptor complex (GO:0032281)	4	26.65	2.25E-02	Dlg4, Cacng2, Gria2, Gria1

GO term	Nr. proteins	Fold enrichment (%)	p-value	Associated proteins
postsynaptic density (GO:0014069)	31	26.14	1.76E-31	Map1a, Srcin1, Add2, Dlgap3, Homer1, Pclo, Dlg2, Anks1b, Nefm, Dlg4, Grin1, Dclk1, Map1b, Prkcg, Rims1, Map2, Gria2, Grin2b, Gap43, Dlgap2, Shank1, Syn1, Nsf, Snap91, Camk2b, Bsn, Cnksr2, Gria1, Syn2, Camk2a, Dlgap1
postsynaptic specialization (GO:0099572)	31	26.14	1.76E-31	Map1a, Srcin1, Add2, Dlgap3, Homer1, Pclo, Dlg2, Anks1b, Nefm, Dlg4, Grin1, Dclk1, Map1b, Prkcg, Rims1, Map2, Gria2, Grin2b, Gap43, Dlgap2, Shank1, Syn1, Nsf, Snap91, Camk2b, Bsn, Cnksr2, Gria1, Syn2, Camk2a, Dlgap1
asymmetric synapse (GO:0032279)	31	25.60	3.30E-31	Map1a, Srcin1, Add2, Dlgap3, Homer1, Pclo, Dlg2, Anks1b, Nefm, Dlg4, Grin1, Dclk1, Map1b, Prkcg, Rims1, Map2, Gria2, Grin2b, Gap43, Dlgap2, Shank1, Syn1, Nsf, Snap91, Camk2b, Bsn, Cnksr2, Gria1, Syn2, Camk2a, Dlgap1
dendritic shaft (GO:0043198)	7	23.31	3.58E-05	Homer1, Slc12a5, Map2, Gria2, Slc1a2, Nsf, Gria1
dendrite (GO:0030425)	37	11.83	4.31E-26	Atp1a3, Srcin1, Crmp1, Bcan, Dlgap3, Homer1, Pclo, Tubb3, Dlg2, Anks1b, Ncdn, Dlg4, Gnao1, Slc32a1, Grin1, Slc12a5, Slc8a2, Map1b, Atp2b2, Prkcg, Dcx, Map2, Gnaz, Gria2, Kcna1, Cplx1, Grin2b, Atp1a2, Slc1a2, Dlgap2, Shank1, Slc1a3, Nsf, Camk2b, Bsn, Gria1, Camk2a
myelin sheath (GO:0043209)	23	22.10	5.60E-21	Atp1a3, Gfap, Ehd3, Plp1, Dnml, Stxbp1, Cntn1, Nefm, Cnp, Gnao1, Nefl, Mbp, Cntnap1, Ncaml, Atp1a2, Mag, Ina, Mog, Napb, Syn1, Nsf, Snap25, Syn2
dendritic spine (GO:0043197)	14	18.17	8.97E-11	Atp1a3,Dlgap3,Anks1b,Dlg4,Grin1,Slc8a2,Map1b,Gria2,Grin2b,Atp1a2,Slc1a2,Shank1, Slc1a3, Gria1
neuron spine (GO:0044309)	14	17.93	1.07E-10	Atp1a3,Dlgap3,Anks1b,Dlg4,Grin1,Slc8a2,Map1b,Gria2,Grin2b,Atp1a2,Slc1a2,Shank1, Slc1a3, Gria1
postsynaptic membrane (GO:0045211)	16	16.15	8.02E-12	Srcin1, Dlgap3,Homer1, Dlg2,Anks1b,Dlg4, Grin1,Gabbr2,Gria2, Grin2b,Dlgap2,Shank1, Snap91, Cnksr2, Gria1, Dlgap1
voltage-gated potassium channel complex (GO:0008076)	6	15.78	3.41E-03	Dlg2, Dlg4, Cntnap1, Stx1a, Kcna1, Snap25
potassium channel complex (GO:0034705)	6	14.45	5.62E-03	Dlg2, Dlg4, Cntnap1, Stx1a, Kcna1, Snap25
growth cone (GO:0030426)	11	12.42	2.46E-06	Crmp1, Pclo, Basp1, Nefl, Map1b, Tmod2, Klc1, Gria2, Ncaml, Gap43, Snap25
site of polarized growth (GO:0030427)	11	12.08	3.27E-06	Crmp1, Pclo, Basp1, Nefl, Map1b, Tmod2, Klc1, Gria2, Ncaml, Gap43, Snap25
perikaryon (GO:0043204)	7	9.58	1.27E-02	Nefm, Slc12a5, Slc8a2, Map1b, Gria2, Kcna1, Camk2b
neuronal cell body (GO:0043025)	30	9.46	9.35E-18	Srcin1, Crmp1, Dlgap3, Homer1, Pclo, Tubb3, Dlg2, Ncdn, Nefm, Grin1, Slc12a5, Slc8a2, Map1b, Atp2b2, Mbp, Kif5a, Klc1, Map2, Gria2, Ncaml, Kcna1, Cplx1, Sptbn2, Slc1a3, Camk2b, Snap25, Bsn, Cnksr2, Gria1, Camk2a
microtubule (GO:0005874)	13	7.97	1.53E-05	Map1a, Tubb2a, Dnml, Tubb3, Cnp, Kif5c, Map6, Slc8a2, Tubb2b, Map1b, Dcx, Kif5a, Klc1, Map2
cell junction (GO:0030054)	48	7.54	1.36E-26	Scamp5, Srcin1, Slc17a6, Ehd3, Dlgap3, Homer1, Pclo, Dlg2, Syt1, Basp1, Anks1b, Syt12, Dlg4, Prrt1, Syp, Grin1,Gabbr2, Slc30a3, Syt2, Map1b,Cadps, Atp2b2, Prkcg, Rims1,Amph, Gria2, Cadm4, Ncaml, Stx1a, Kcna1, Slc17a7, Grin2b, Sptbn2, Sept3, Sv2a, Sv2b, Gap43, Dlgap2, Shank1, Syn1, Rph3a, Snap25, Bsn, Gria1, Syn2, Camk2a, Dlgap1
Golgi apparatus (GO:0005794)	18	3.02	3.46E-02	Scamp5, Atp1a3, Itm2b, Dnml, Pclo, Syt1, Map6, Slc1a6, Amph, Atl1, Sptbn2, Atp2b3, Syn1, Nsf, Rph3a, Snap25, Bsn, Cnksr2

Table III.A.S 7 - Brain enriched/specific Nano-HPLC-MS/MS identified candidate BRI2 interacting proteins annotated with GO terms related to neuronal differentiation processes. Uniprot accession numbers and gene names are listed.

Uniprot Acession	Gene name	Uniprot Acession	Gene name
P21707	Syt1	Q63622	Dlg2
P29101	Syt2	P61765	Stxbp1
Q9JIR4	Rims1	O35095	Ncdn
Q5BJS7	Cpne9	P31016	Dlg4
Q9QXY2	Srcin1	P13233	Cnp
P47819	Gfap	P59215	Gnao1
Q62950	Crmp1	O08875	Dclk1
Q62718	Ntm	P56536	Kif5c
Q63198	Cntn1	Q63560	Map6
P12839	Nefm	Q63633	Slc12a5
P35439	Grin1	Q3KRE8	Tubb2b
P61265	Stx1b	P11506	Atp2b2
P19527	Nefl	P63012	Rab3a
P15205	Map1b	Q6QLM7	Kif5a
P02688	Mbp	P97846	Cntnap1
P15146	Map2	Q8CGU4	Agap2
P07722	Mag	P13596	Ncaml
Q05546	Tnr	Q6PST4	Atl1
Q9WV48	Shank1	P10499	Kcna1
P08413	Camk2b	Q64548	Rtn1
P60881	Snap25	P07936	Gap43
Q5FVI4	Cend1	P24942	Slc1a3
P60203	Plp1	Q05140	Snap91
Q62951	Dpysl4	P11275	Camk2a
Q4QRB4	Tubb3		

CHAPTER III.B - IDENTIFICATION OF NOVEL BRI3 INTERACTORS: CONSTRUCTION OF BRI3 INTERACTION NETWORK IN BRAIN

"The interactome of BRI3 reveals novel protein partners in brain tissue"

Filipa Martins[1], Thorsten Müller[2], Christina Loosse[2], Katharina Kolbe[2], Odete A.B. da Cruz e Silva[1] and Sandra Rebelo[1]

[1] Neuroscience and Signalling Laboratory, Department of Medical Sciences, Institute of Biomedicine-iBiMED, University of Aveiro, Portugal

[2] Leibniz-Institut für Analytische Wissenschaften -ISAS- e. V., Dortmund, Germany

Corresponding author: Sandra Rebelo, Neuroscience and Signalling Laboratory, Department of Medical Sciences, Institute of Biomedicine-iBiMED, University of Aveiro, 3810-193 Aveiro, Portugal, Tel: +351-924406306, E-mail: srebelo@ua.pt

Abstract

BRI3 is a type II integral membrane protein enriched in the CNS with unclear biological functions. Recent studies have established protein interactions for BRI3, namely with Amyloid precursor protein and protein phosphatase 1. Thus, like most proteins, BRI3 seems to function through interactions with a complex network of proteins, as well as with other molecules. Therefore, to further increase our understanding of BRI3 biology and role it seems essential to elucidate and characterize the BRI3 interactome. Here, we pursued the identification of BRI3 interactome in rat brain tissue lysates by co-immunoprecipitating BRI3 followed by mass-spectrometry identification. Bioinformatic analysis of the identified BRI3 interactome allows us to analyze the biological processes, localization and signaling pathways in which they are involved in order to identify potentially novel BRI3 functional relationships. We identified 274 different proteins as potential BRI3 interactors, which are mainly cytoskeletal proteins, transporters, and membrane traffic proteins. These were involved in several biological processes, which in turn suggests a role for BRI3 at the nerve terminals namely in synaptic signaling, transmission, and plasticity, as well as in neuronal trafficking and neuronal differentiation. Moreover, a strong connection of the BRI3 interactome with some nervous system diseases, including Alzheimer´s disease and cerebrovascular accident, was suggested.

Taken together, the results here presented provide novel insights provides a valuable list of BRI3 interacting proteins for further studies to investigate their potential roles in BRI3 biology and the underlying molecular and mechanisms, as well as in its associated pathologies.

III.B.1 Introduction

BRI3, also known as ITM2C (integral membrane protein 2C) is a type II integral membrane protein that belongs to an evolutionarily conserved multigene family of integral membrane proteins containing two additional members, BRI1 (ITM2A) and BRI2 (ITM2B). It is found in a variety of tissues but is enriched in the central nervous system (CNS) where presents highest levels of expression in cerebral cortex, medulla oblongata, amygdala, hippocampus, thalamus, striatum, caudate nucleus and spinal cord (Vidal *et al*. 2001; Choi *et al*. 2001). The biological function of BRI3 remains largely unclear, although it has been suggested that it may play a role in neuronal differentiation (Gong *et al*. 2008). Stathmin-2, a neuron-specific microtubule-destabilizing protein, was identified in a yeast two-hybrid screen as a BRI3 interacting partner. While overexpression of stathmin-2 seems to promote neurite outgrowth in NGF-treated PC12 cells, BRI3 overexpression slightly decreases neurite outgrowth. However, the overexpression of both proteins attenuates the stathmin-2 induced microtubule disassembly and outgrowth of neurites. Hence, it is possible to assume that BRI3 may inhibit neurite outgrowth through interaction with stathmin-2 by decreasing the dynamic instability of microtubules (Gong *et al*. 2008). Moreover, BRI3 was proposed as a negative regulator of Aβ production by interacting and regulating the processing of the amyloid precursor protein (APP) by masking the access of α- and β-secretases (Matsuda *et al*. 2009). Recently, it was also described protein phosphatase 1 (PP1) as a novel BRI3 interacting partner which is able to dephosphorylate the latter. Hence, BRI3 was described as a phosphoprotein although the physiological relevance of protein phosphorylation in its biology was not elucidated (Martins *et al*. 2016).

Therefore, to increase our understanding regarding the brain-enriched BRI3 it seems necessary to elucidate and characterize its brain interactome which could lead to the discovery of its neuronal physiological role, as well as its association with nervous system diseases. Interactomes are characterized by the molecular interactions that take place in a particular biological context, creating a network that promotes and regulates its trafficking, processing, activity and signaling effects (De Las Rivas and Fontanillo 2010; Mehta and Trinkle-Mulcahy 2016). Consequently, the identification and study of protein interactomes provide many insights into the biological processes of a particular network which might offer valuable information underlying protein cellular functions.

Here, we have attempted to elucidate the BRI3 protein interactome in rat brain using a combined immunoprecipitation and mass spectrometry (MS) approach. Given the described expression distribution of BRI3 in the brain, three different brain regions were analyzed in this work: cortex, hippocampus, and striatum. Moreover, bioinformatic tools were applied to analyze both the entire and the region-specific BRI3 interactome datasets to uncover the organization of BRI3 interacting

protein networks in the mammalian brain and consequently identify potentially novel BRI3 functional relationships.

III.B.2 Materials and Methods

III.B.2.1 Preparation of rat brain lysates

Wistar Hannover rats (9-12 weeks) were obtained from Harlan Interfaune Ibérica, SL, and all experimental procedures were conducted in accordance with the European legislation for animal experimentation (2010/63/EU). No specific ethics approval under EU guidelines was required for this project, since the rats were euthanized, by cervical stretching followed by decapitation, for brain removal. This is within the European law (Council Directive 86/609/EEC) and the number and suffering of the animals possible were minimized. The procedures were approved and supervised by our Institutional Animal Care and Use Committee (IACUC): Comissão Responsável pela Experimentação e Bem-Estar Animal (CREBEA). Briefly, animals were sacrificed by cervical stretching followed by decapitation and cortex, hippocampus and striatum were dissected out on ice. Tissues were further weighed and homogenized on ice with a Potter-Elvehjem tissue homogenizer with 10-15 pulses at 650-750 rpm, in non-denaturating lysis buffer (50 mM Tris-HCl pH 8.0, 120 mM NaCl and 4% CHAPS) containing protease inhibitors (1 mM PMSF, 10 mM Benzamidine, 2 μM Leupeptin, 1.5 μM Aprotinin and 5 μM Pepstatin A) (Santos *et al*. 2014) and used for immunoprecipitation analysis as described below.

III.B.2.2 Co-immunoprecipitation

Rat cortex, hippocampus and striatum extracts were divided into three equal parts each and pre-cleared separately using Dynabeads Protein G (Life Technologies). A direct immunoprecipitation approach was performed using the rabbit anti-BRI3 antibody (1:150; ab101389, Abcam), pre-incubated with Dynabeads Protein G for 1 hour at 4°C with rotation. After, the pre-cleared extracts were applied to antibody-Dynabeads and incubated overnight at 4°C with rotation. The immunoprecipitates were washed three times with PBS in 3% BSA for 10 min at 4°C with rotation and beads were re-suspended in 1% SDS. As negative controls were used extracts incubated with only dynabeads protein G or with dynabeads protein G coupled with rabbit IgGs (mock IPs).

III.B.2.3 In-gel protein digestion, nano-HPLC and Mass spectrometry

The eluted fractions from the brain BRI3 co-IP assays were separated by SDS-PAGE on a 12% Bis-Tris gel for HPLC analysis. Each lane of the gel was cut into 10 pieces, and the resulting gel pieces were washed alternately with 10 mM ammonium hydrogen carbonate (NH_4HCO_3) and 50% (v/v)

10 mM ammonium hydrogen carbonate, 50% (v/v) acetonitrile (ACN) and afterward were digested with trypsin in 10 mM HCl and 50 mM ammonium hydrogen carbonate at 37 °C overnight. The resulting peptides were extracted from the gel slices twice by means of sonication in 50% (v/v) ACN, 50% (v/v) 0.1% trifluoroacetic acid (TFA). After the extracts were merged, the ACN was removed in a centrifugal vacuum concentrator. The final sample volumes were adjusted to 40 µl with 0.1% TFA. Nano-HPLC-MS/MS was carried out on an UltiMate 3000 RSLCnano LC system (Dionex Sunnyvale, CA). After the samples had been loaded on a trap column (75 µm X 2 cm, particle size = 3 µm, pore size = 100 Å; Dionex) and washed with 0.1% TFA (flow rate: 10 µl/min), the trap column was connected with an analytical C18 column (75 µm X 25 cm, particle size = 2 µm, pore size = 100 Å; Dionex). The following system of solvents was used for separating the peptides with a flow rate of 400 nl/min: 95% ACN, 0.1% formic acid (A); and 80% ACN, 0.1% formic acid (B). First, a gradient from 0% to 40% B (95 min) was performed, followed by a second gradient from 40% to 95% B within 2 min. Finally, 95% B was used for 5 min, followed by equilibration with buffer A. The HPLC system was connected to a nanoelectrospray ionization source (Thermo Fisher Scientific). Electrospray ionization MS/MS was performed on an LTQ Orbitrap Velos (Thermo Fisher Scientific). MS spectra were scanned between 300 and 2000 m/z with a resolution of 30,000 and a maximal acquisition time of 500 ms. The m/z values initiating MS/MS were set on a dynamic exclusion list for 35 s. Lock mass polydimethylcyclosiloxane (m/z 445.120) was used for internal recalibration. The 20 most intensive ions (charge _ 1) were selected for MS/MS fragmentation in the ion trap. Fragments were generated via low-energy collision induced dissociation on isolated ions with a collision energy of 35% and a maximal acquisition time of 50 ms. Raw files were transformed to *.mgf files using ProteomeDiscoverer 1.3 software (Thermo Fisher Scientific). Mascot generic files were imported into ProteinScape™ 2.1 (Bruker Daltonics, Bremen, Germany) and analyzed using MASCOT (version 2.2.0, Matrix Science, London, UK) with a peptide mass tolerance of 10 ppm and a fragment mass tolerance of 0.5 Da. One missed cleavage site after tryptic digestion was allowed in the database search. Carbamidomethylation (C), oxidation (M), and phosphorylation (S, T, Y) were regarded as variable modifications. All data were searched against the UniProt/ Swiss-Prot database (downloaded on June 1, 2011; containing 529,056 entries, plus one shuffled decoy entry for each target entry for false discovery rate estimation with taxonomy restriction for human (resulting in 40,620 target and decoy entries).

Two mock IPs for each sample condition (i.e. for each specific brain region) were used as negative controls. Therefore, the proteins identified in the mock IPs were excluded from the list of the proteins identified in the BRI3 co-IPs, with one exception: the ratio between the number of peptide-spectrum matches (PSM) for a given protein in a BRI3 co-IP sample and the PSM in the mock IPs, of the same brain region, were equal or higher than 2.0. In addition, were excluded well described common

contaminants as presented in (Hodge *et al*. 2013), and proteins characteristic of hair, skin/epidermis, tongue and gums (KRT33A, KRT78, KRT85, KRT14, KRT5, KRT3, KRT31, KRT32, KRT33B, KRT35, KRT36, KRT4, KRT77, KRT8, KRT17) which are also highly probable contaminants.

III.B.2.4 Bioinformatic data analysis

Experimentally detected BRI3 protein-protein interactions documented in the literature were mapped using the PSIQUIC View web service (del-Toro *et al*. 2013) (version 1.4.5, downloaded October 03, 2016) which enabled access to multiple PSI-MI compliant resources. Moreover, two BRI3 protein interactors previously identified and validated recently in our laboratory, protein phosphatase 1 alpha (PPP1CA) and protein phosphatase 1 gamma (PPP1CC), were manually added to the list.

Tissue-expression analysis was performed using the following databases: Human Protein Atlas (HPA), (Uhlen *et al*. 2005; Uhlen *et al*. 2010; Uhlén *et al*. 2015) which also retrieves information from the Genotype-Tissue Expression (GTEx) portal (Carithers *et al*. 2015) and FANTOM5 (Functional Annotation of the Mammalian Genome) (Kawai *et al*. 2001); TiGER (Liu *et al*. 2008); and UniGene (Wheeler *et al*. 2003). The HPA was searched for proteins strongly expressed in the brain and a list of proteins within the brain 'Tissue enriched', 'Tissue enhanced' and 'Group enriched' categories was obtained. Annotated protein expression is a manually curated score based on IHC staining patterns in normal tissues from two or more paired antibodies binding to different epitopes of the same protein, which describes the distribution and strength of expression of each protein in cells. The TiGER database was searched for proteins preferentially expressed in brain based on ESTs by searching 'Brain' in 'Tissue View'. The UniGene database was searched for brain-restricted genes by using the following search criteria: [brain][restricted].

Functional enrichment analysis of Gene Ontology (GO) categories (Biological Process and Cellular Component) and KEGG pathways was performed using ClueGO plugin version 2.2.6 (Bindea *et al*. 2009) of the Cytoscape software version 3.4.0, freely available online (Shannon *et al*. 2003), whereas analysis of the Protein Class was performed using PANTHER v.10 (Protein Annotation Through Evolutionary Relationship) online resource (Mi et al. 2013; Mi et al. 2016). Of note, only enriched annotations with a p-value <0.05 were considered.

Protein-protein interaction (PPI) network construction was achieved using Cytoscape software, and topological analysis using the NetworkAnalyzer plugin. Network augmentation was performed by retrieving protein-protein data only from the International Molecular Exchange (IMEx) consortium partners. Given the lacking information for *Rattus norvergicus* in these databases, the lists of proteins were extrapolated by homology to human. Rat UniProt accession numbers were converted to human using the Uniprot tool available online – Uniprot Retrieve/ID mapping (http://www.uniprot.org/uploadlists/).

Genes that share diseases with BRI3 protein were retrieved using the DisGeNET database (consulted on March 17, 2017), which integrates human gene-disease associations from various expert-curated databases and text-mining derived associations (Piñero *et al*. 2017).

III.B.3 Results

III.B.3.1 Identification of BRI3 brain interactome

The central goal of this study was the identification of novel BRI3 interacting proteins in the brain. Rat brain represents a valuable tool for the study of protein expression and brain function in mammals and was used as the protein pool for co-IP of BRI3 protein using a specific antibody. These co-IPs were further analyzed Nano HPLC-MS/MS. Given the BRI3 expression distribution, three different brain regions were analyzed in this study: cortex, hippocampus, and striatum. The applied workflow is presented in Figure III.B.1. Of note, the data obtained were first 'filtered' to remove known contaminants and taking into account the negative controls (mock IPs), as mentioned in the materials and methods section.

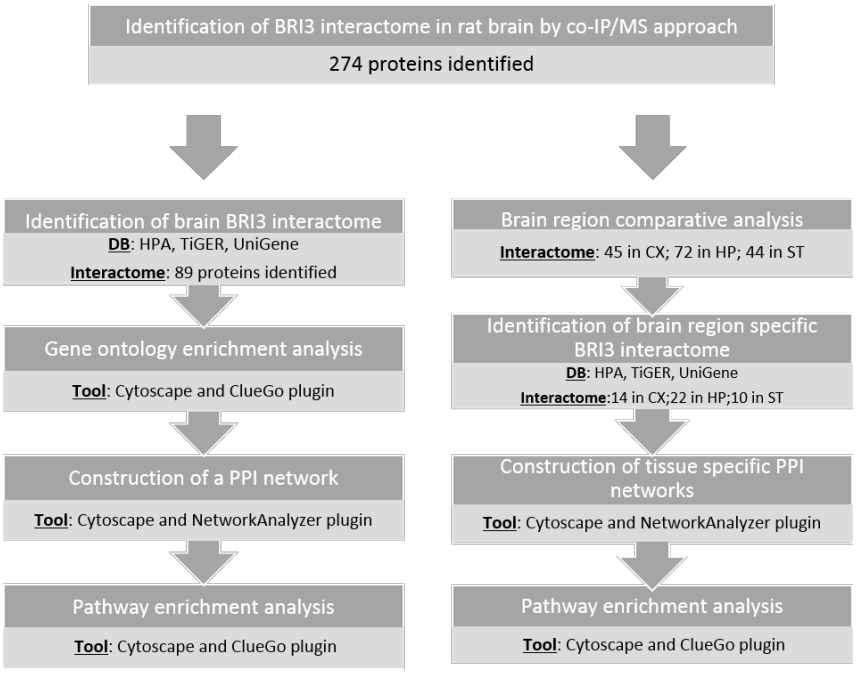

Figure III.B 1- Workflow for the identification of novel brain BRI3 interacting proteins using rat brain tissue lysates. Co-IP, co-immunoprecipitation; MS, mass spectrometry; DB, database; CX, cerebral cortex; HP, hippocampus; ST, striatum.

As a result, we were able to identify 108 proteins in the cortex, 173 in the hippocampus, and 141 in the striatum. In total, we identified 274 different proteins, including BRI3, as potential candidates for BRI3 interacting proteins (Supplementary Table III.B.S1). It is important to point out that from this list of BRI3 brain interactors two were previously described as BRI3 interacting proteins: APP and DLG4 (also known as PSD-95), from a list of 18 proteins (Supplementary Table III.B.S2).

Next, we assessed the protein class of BRI3 interactors using the PANTHER protein class system. As shown in Figure III.B.2 and Supplementary Table III.B.S3, BRI3 protein interactors are mainly cytoskeletal proteins (32%; half of which belong to actin family), transporters (16%), G-proteins (7%), transmembrane receptor regulatory/adaptor proteins (4%), membrane traffic proteins (12%), structural proteins (6%) and chaperones (6%).

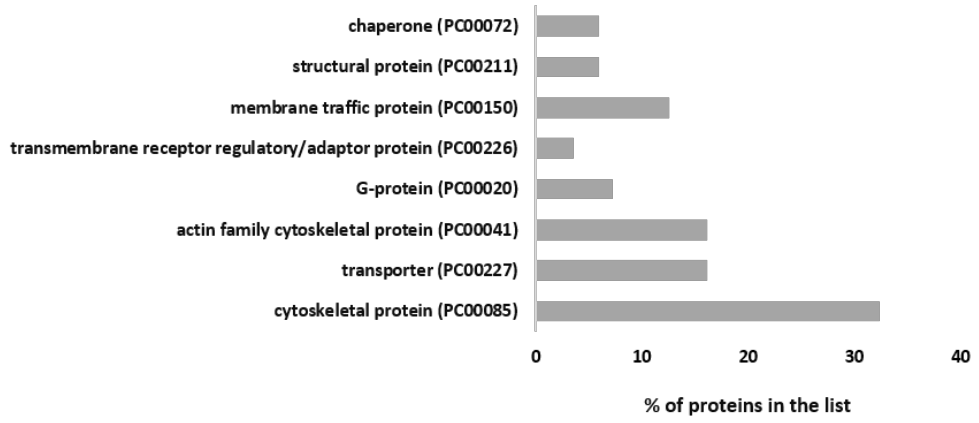

Figure III.B 2- Panther Protein class of the identified BRI3 interactome using the PANTHER online resource. The percentage of the BRI3 interacting proteins in each category was calculated and plotted.

Several proteins are known to be expressed in a tissue-specific manner and as a result, the signaling mechanisms in which they are involved are diverse, reflecting the specific biological roles of each individual tissue (Uhlén *et al*. 2015). Thus, given that BRI3 is a brain enriched protein, to further explore its potential associations to specific cellular mechanisms and signaling pathways in the brain, we have constructed a brain-enriched/specific network approach. Tissue-expression analysis of the 274 BRI3 interacting protein candidates resulted in the identification of 89 proteins specific or highly enriched in brain (Table III.B.1), the BRI3 brain-enriched/specific interactome (BRI3 brain ES interactome).

Table III.B 1- Novel candidate BRI3 interacting proteins highly enriched or specific for the brain tissue. Uniprot accession numbers, gene and protein names, are listed, as well as the rat brain tissues in where the proteins were found. CX, cerebral cortex; HP, hippocampus; ST, striatum.

Uniprot accession	Gene name	Protein name	Brain regions
P13233	***Cnp***	2',3'-cyclic-nucleotide 3'-phosphodiesterase	CX, HP, ST

Uniprot accession	Gene name	Protein name	Brain regions
P23565	***Ina***	Alpha-internexin	HP, ST
P0C6S7	***Anks1b***	Ankyrin repeat and sterile alpha motif domain-containing protein 1B	CX, HP
Q8CGU4	***Agap2***	Arf-GAP with GTPase, ANK repeat and PH domain-containing protein 2	HP
P85969	***Napb***	Beta-soluble NSF attachment protein	CX
Q05175	***Basp1***	Brain acid soluble protein 1	HP
P11275	***Camk2a***	Calcium/calmodulin-dependent protein kinase type II subunit alpha	ST
P08413	***Camk2b***	Calcium/calmodulin-dependent protein kinase type II subunit beta	CX, HP, ST
P68182	***Prkacb***	cAMP-dependent protein kinase catalytic subunit beta	HP, ST
O55156	***Clip2***	CAP-Gly domain-containing linker protein 2	ST
Q8VHK2	***Caskin1***	Caskin-1	CX
Q5FVI4	***Cend1***	Cell cycle exit and neuronal differentiation protein 1	CX
Q05140	***Snap91***	Clathrin coat assembly protein AP180	HP
Q99P82	***Cldn11***	Claudin-11	CX, HP, ST
Q99JD4	***Clasp2***	CLIP-associating protein 2	CX
Q9Z1T4	***Cnksr2***	Connector enhancer of kinase suppressor of ras 2	HP
Q63198	***Cntn1***	Contactin-1	CX, HP, ST
Q5BJS7	***Cpne9***	Copine-9	HP
Q62950	***Crmp1***	Dihydropyrimidinase-related protein 1	CX, HP, ST
Q63622	***Dlg2***	Disks large homolog 2	CX, HP, ST
P31016	***Dlg4***	Disks large homolog 4	CX, HP, ST
P97838	***Dlgap3***	Disks large-associated protein 3	CX
P21575	***Dnm1***	Dynamin-1	HP, ST
O35179	***Sh3gl2***	Endophilin-A1	CX
Q8K3M6	***Erc2***	ERC protein 2	ST
P24942	***Slc1a3***	Excitatory amino acid transporter 1	HP, ST
P31596	***Slc1a2***	Excitatory amino acid transporter 2	HP, ST
P47819	***Gfap***	Glial fibrillary acidic protein	CX, ST
P19491	***Gria2***	Glutamate receptor 2	HP
P35439	***Grin1***	Glutamate receptor ionotropic, NMDA 1	HP
Q00960	***Grin2b***	Glutamate receptor ionotropic, NMDA 2B	HP
Q9WTT6	***Gda***	Guanine deaminase	HP
P59215	***Gnao1***	Guanine nucleotide-binding protein G	HP
P19627	***Gnaz***	Guanine nucleotide-binding protein G	HP
Q9Z214	***Homer1***	Homer protein homolog 1	CX, ST
P17105	***Itpka***	Inositol-trisphosphate 3-kinase A	HP
Q9QYU4	***Crym***	Ketimine reductase mu-crystallin	CX, HP, ST
Q8K4Y5	***Lgi1***	Leucine-rich glioma-inactivated protein 1	CX
P34926	***Map1a***	Microtubule-associated protein 1A	HP
P15205	***Map1b***	Microtubule-associated protein 1B	CX, HP, ST
P15146	***Map2***	Microtubule-associated protein 2	CX, ST
Q63560	***Map6***	Microtubule-associated protein 6	CX, HP
P19332	***Mapt***	Microtubule-associated protein tau	CX, ST

Uniprot accession	Gene name	Protein name	Brain regions
Q505J6	***Slc25a18***	Mitochondrial glutamate carrier 2	CX, HP
P02688	***Mbp***	Myelin basic protein	ST
P60203	***Plp1***	Myelin proteolipid protein	ST
Q63345	***Mog***	Myelin-oligodendrocyte glycoprotein	CX, HP, ST
P55067	***Ncan***	Neurocan core protein	ST
P97685	***Nfasc***	Neurofascin	HP
P19527	***Nefl***	Neurofilament light polypeptide	ST
P12839	***Nefm***	Neurofilament medium polypeptide	CX, ST
Q04940	***Nrgn***	Neurogranin	CX
P07936	***Gap43***	Neuromodulin	CX
Q9ESI7	***Dcx***	Neuronal migration protein doublecortin	HP
P32736	***Opcml***	Opioid-binding protein/cell adhesion molecule	CX
P62024	***Phactr1***	Phosphatase and actin regulator 1	ST
P11506	***Atp2b2***	Plasma membrane calcium-transporting ATPase 2	CX
O88778	***Bsn***	Protein bassoon	CX, HP
Q9Z0W5	***Pacsin1***	Protein kinase C and casein kinase substrate in neurons protein 1	CX
P63319	***Prkcg***	Protein kinase C gamma type	CX, HP, ST
Q9JKS6	***Pclo***	Protein piccolo	ST
P63012	***Rab3a***	Ras-related protein Rab-3A	CX, ST
Q63941	***Rab3b***	Ras-related protein Rab-3B	ST
P62824	***Rab3c***	Ras-related protein Rab-3C	HP, ST
Q9JIR4	***Rims1***	Regulating synaptic membrane exocytosis protein 1	HP
Q64548	***Rtn1***	Reticulon-1	CX
Q9JJM9	***Sept5***	Septin-5	CX, HP
Q5MPA9	***Dclk2***	Serine/threonine-protein kinase DCLK2	HP
Q9WV48	***Shank1***	SH3 and multiple ankyrin repeat domains protein 1	HP
Q9QX74	***Shank2***	SH3 and multiple ankyrin repeat domains protein 2	CX, HP
Q8CFD0	***Sfxn5***	Sideroflexin-5	HP
P48768	***Slc8a2***	Sodium/calcium exchanger 2	HP
P06687	***Atp1a3***	Sodium/potassium-transporting ATPase subunit alpha-3	CX, HP, ST
Q9QWN8	***Sptbn2***	Spectrin beta chain, non-erythrocytic 2	CX, HP, ST
Q9QXY2	***Srcin1***	SRC kinase signaling inhibitor 1	CX, HP, ST
P09951	***Syn1***	Synapsin-1	CX, HP, ST
Q63537	***Syn2***	Synapsin-2	HP
P07825	***Syp***	Synaptophysin	CX, HP, ST
P60881	***Snap25***	Synaptosomal-associated protein 25	CX, HP
P21707	***Syt1***	Synaptotagmin-1	CX, HP, ST
P61265	***Stx1b***	Syntaxin-1B	CX, HP, ST
P61765	***Stxbp1***	Syntaxin-binding protein 1	CX, HP, ST
Q05546	***Tnr***	Tenascin-R	HP
P01830	***Thy1***	Thy-1 membrane glycoprotein	CX
Q6AY56	***Tuba8***	Tubulin alpha-8 chain	HP

Uniprot accession	Gene name	Protein name	Brain regions
P85108	***Tubb2a***	Tubulin beta-2A chain	HP, ST
Q3KRE8	***Tubb2b***	Tubulin beta-2B chain	HP, ST
Q4QRB4	***Tubb3***	Tubulin beta-3 chain	HP, ST
Q9QUL6	***Nsf***	Vesicle-fusing ATPase	HP, ST

Biological process and cellular component of the BRI3 brain ES interacting proteins were annotated according to GO annotation categories using the ClueGO plugin of the Cytoscape software (Bindea *et al*. 2009). The results suggest that BRI3 brain ES interactors mainly participated in exocytosis, synaptic signaling, synaptic transmission, vesicle-mediated transport, synaptic vesicle cycle, and in the establishment of synaptic vesicle localization (Table III.B.2). Of note, other biological process categories such as 'cytoskeleton organization', 'synapse organization' and 'glutamate receptor signaling pathway' were also evidenced (Table III.B.2). In addition, GO analysis demonstrates that BRI3 brain ES interactors are located in different areas within the cell, such as neuron projection, axon, growth cone, dendrite, presynapse, postsynapse, and synaptic vesicle (Table III.B.3). Remarkably, were also found proteins associated with the cytoskeleton and the ionotropic glutamate receptor complex (Table III.B.3).

Table III.B2- Biological process enrichment analysis of the brain specific/enriched BRI3 interactome using ClueGo plugin of the Cytoscape software. Enriched categories are identified as those with p-value <0.05. Nr. Number.

GO term	GO ID	Nr. proteins	% associated proteins	p-value	Associated proteins
exocytosis	GO:0006887	9.0	12.5	1.20E-04	Nsf, Rab3a, Rims1, Sept5, Snap25, Sptbn2, Stx1b, Stxbp1, Syt1
synaptic signaling	GO:0099536	15.0	6.4	1.70E-04	Camk2b, Dlg4, Dnml, Gria2, Grin1, Grin2b, Lgi1, Map1b, Mapt, Nrgn, Rab3a, Rims1, Snap25, Sptbn2, Stxbp1
trans-synaptic signaling	GO:0099537	15.0	6.4	1.70E-04	Camk2b, Dlg4, Dnml, Gria2, Grin1, Grin2b, Lgi1, Map1b, Mapt, Nrgn, Rab3a, Rims1, Snap25, Sptbn2, Stxbp1
synaptic transmission	GO:0007268	15.0	6.4	1.70E-04	Camk2b, Dlg4, Dnml, Gria2, Grin1, Grin2b, Lgi1, Map1b, Mapt, Nrgn, Rab3a, Rims1, Snap25, Sptbn2, Stxbp1
vesicle-mediated transport	GO:0016192	14.0	6.7	2.70E-04	Dlg4, Dnml, Gria2, Nsf, Rab3a, Rims1, Sept5, Snap25, Snap91, Sptbn2, Stx1b, Stxbp1, Syp, Syt1
synaptic vesicle cycle	GO:0099504	6.0	20.7	4.00E-04	Dnml, Rab3a, Rims1, Snap25, Sptbn2, Stxbp1
synaptic vesicle transport	GO:0048489	6.0	20.7	4.00E-04	Dnml, Rab3a, Rims1, Snap25, Sptbn2, Stxbp1
establishment of synaptic vesicle localization	GO:0097480	6.0	20.7	4.00E-04	Dnml, Rab3a, Rims1, Snap25, Sptbn2, Stxbp1
synaptic vesicle localization	GO:0097479	6.0	20.0	4.90E-04	Dnml, Rab3a, Rims1, Snap25, Sptbn2, Stxbp1
positive regulation of synaptic transmission	GO:0050806	9.0	10.3	5.90E-04	Camk2b, Dlg4, Dnml, Gria2, Grin1, Grin2b, Lgi1, Nrgn, Rims1
synaptic vesicle exocytosis	GO:0016079	5.0	26.3	7.50E-04	Rab3a, Rims1, Snap25, Sptbn2, Stxbp1
calcium ion regulated exocytosis	GO:0017156	6.0	17.1	1.20E-03	Rab3a, Rims1, Snap25, Sptbn2, Stxbp1, Syt1
modulation of synaptic transmission	GO:0050804	12.0	6.5	1.80E-03	Camk2b, Dlg4, Dnml, Gria2, Grin1, Grin2b, Lgi1, Map1b, Mapt, Nrgn, Rims1, Stxbp1
establishment of vesicle localization	GO:0051650	6.0	15.4	2.30E-03	Dnml, Rab3a, Rims1, Snap25, Sptbn2, Stxbp1
regulation of vesicle-mediated transport	GO:0060627	9.0	8.6	2.60E-03	Dlg4, Dnml, Nsf, Rims1, Sept5, Snap91, Stx1b, Stxbp1, Syt1
cytoskeleton organization	GO:0007010	10.0	7.5	3.00E-03	Clasp2, Cnp, Gda, Itpka, Map1a, Map1b, Nefl, Nefm, Pacsin1, Thy1
vesicle localization	GO:0051648	6.0	14.6	3.00E-03	Dnml, Rab3a, Rims1, Snap25, Sptbn2, Stxbp1
single-organism cellular localization	GO:1902580	11.0	6.7	3.30E-03	Dlg2, Dlg4, Dnml, Grin2b, Nfasc, Pacsin1, Rab3a, Rims1, Snap25, Sptbn2, Stxbp1
microtubule cytoskeleton organization	GO:0000226	5.0	17.2	6.20E-03	Clasp2, Cnp, Gda, Map1a, Map1b
negative regulation of microtubule depolymerization	GO:0007026	3.0	50.0	6.20E-03	Clasp2, Map1a, Map1b
regulation of exocytosis	GO:0017157	6.0	12.8	6.40E-03	Nsf, Rims1, Sept5, Stx1b, Stxbp1, Syt1
regulation of microtubule polymerization or depolymerization	GO:0031110	4.0	25.0	7.30E-03	Clasp2, Gda, Map1a, Map1b
microtubule polymerization or depolymerization	GO:0031109	4.0	23.5	9.40E-03	Clasp2, Gda, Map1a, Map1b
regulated exocytosis	GO:0045055	6.0	11.1	1.30E-02	Rab3a, Rims1, Snap25, Sptbn2, Stxbp1, Syt1
glutamate receptor signaling pathway	GO:0007215	5.0	14.3	1.40E-02	Camk2a, Dlg4, Grin1, Grin2b, Homer1

GO term	GO ID	Nr. proteins	% associated proteins	p-value	Associated proteins
regulation of microtubule cytoskeleton organization	GO:0070507	4.0	21.1	1.40E-02	Clasp2, Gda, Map1a, Map1b
negative regulation of protein complex disassembly	GO:0043242	3.0	37.5	1.50E-02	Clasp2, Map1a, Map1b
negative regulation of protein depolymerization	GO:1901880	3.0	37.5	1.50E-02	Clasp2, Map1a, Map1b
regulation of microtubule depolymerization	GO:0031114	3.0	37.5	1.50E-02	Clasp2, Map1a, Map1b
single-organism intracellular transport	GO:1902582	12.0	5.2	1.50E-02	Cnp, Crym, Dnml, Nfasc, Rab3a, Rims1, Slc1a3, Slc8a2, Snap25, Sptbn2, Stxbp1, Thy1
synapse organization	GO:0050808	6.0	10.5	1.70E-02	Camk2b, Dlg4, Erc2, Map1b, Shank1, Snap25
regulation of microtubule-based process	GO:0032886	4.0	20.0	1.70E-02	Clasp2, Gda, Map1a, Map1b
presynaptic process involved in synaptic transmission	GO:0099531	5.0	13.5	1.80E-02	Rab3a, Rims1, Snap25, Sptbn2, Stxbp1
neurotransmitter secretion	GO:0007269	5.0	13.5	1.80E-02	Rab3a, Rims1, Snap25, Sptbn2, Stxbp1
signal release from synapse	GO:0099643	5.0	13.5	1.80E-02	Rab3a, Rims1, Snap25, Sptbn2, Stxbp1
cell-cell signaling	GO:0007267	15.0	4.2	1.90E-02	Camk2b, Dlg4, Dnml, Gria2, Grin1, Grin2b, Lgi1, Map1b, Mapt, Nrgn, Rab3a, Rims1, Snap25, Sptbn2, Stxbp1
establishment of organelle localization	GO:0051656	6.0	10.2	2.00E-02	Dnml, Rab3a, Rims1, Snap25, Sptbn2, Stxbp1
microtubule depolymerization	GO:0007019	3.0	33.3	2.10E-02	Clasp2, Map1a, Map1b
negative regulation of microtubule polymerization or depolymerization	GO:0031111	3.0	33.3	2.10E-02	Clasp2, Map1a, Map1b
protein localization to synapse	GO:0035418	3.0	30.0	2.90E-02	Anks1b, Dlg4, Homer1
ionotropic glutamate receptor signaling pathway	GO:0035235	3.0	30.0	2.90E-02	Camk2a, Grin1, Grin2b
intracellular transport	GO:0046907	12.0	4.8	2.90E-02	Cnp, Crym, Dnml, Nfasc, Rab3a, Rims1, Slc1a3, Slc8a2, Snap25, Sptbn2, Stxbp1, Thy1
microtubule-based process	GO:0007017	5.0	11.6	3.40E-02	Clasp2, Cnp, Gda, Map1a, Map1b
neuron projection morphogenesis	GO:0048812	9.0	5.9	3.50E-02	Camk2b, Dlg4, Itpka, Map1b, Mbp, Pacsin1, Snap25, Snap91, Thy1
regulation of protein depolymerization	GO:1901879	3.0	27.3	3.70E-02	Clasp2, Map1a, Map1b
neurotransmitter transport	GO:0006836	5.0	11.4	3.70E-02	Rab3a, Rims1, Snap25, Sptbn2, Stxbp1
regulation of synaptic vesicle transport	GO:1902803	3.0	27.3	3.70E-02	Dnml, Rims1, Stxbp1
cell part morphogenesis	GO:0032990	9.0	5.8	3.90E-02	Camk2b, Dlg4, Itpka, Map1b, Mbp, Pacsin1, Snap25, Snap91, Thy1
cell projection morphogenesis	GO:0048858	9.0	5.8	3.90E-02	Camk2b, Dlg4, Itpka, Map1b, Mbp, Pacsin1, Snap25, Snap91, Thy1
regulation of neurotransmitter levels	GO:0001505	5.0	11.1	3.90E-02	Rab3a, Rims1, Snap25, Sptbn2, Stxbp1
organelle localization	GO:0051640	6.0	8.8	3.90E-02	Dnml, Rab3a, Rims1, Snap25, Sptbn2, Stxbp1
cytosolic transport	GO:0016482	7.0	7.3	4.10E-02	Dnml, Rab3a, Rims1, Snap25, Sptbn2, Stxbp1, Thy1

GO term	GO ID	Nr. proteins	% associated proteins	p-value	Associated proteins
regulation of protein complex disassembly	GO:0043244	3.0	25.0	4.50E-02	Clasp2, Map1a, Map1b
single-organism membrane organization	GO:0044802	7.0	7.1	4.50E-02	Cnp, Dlg2, Dlg4, Grin2b, Nfasc, Pacsin1, Syt1
developmental maturation	GO:0021700	4.0	14.8	4.60E-02	Camk2b, Dlg2, Map1b, Shank1
positive regulation of exocytosis	GO:0045921	4.0	14.8	4.60E-02	Rims1, Sept5, Stxbp1, Syt1

Table III.B3 - Cellular component enrichment analysis of the brain specific/enriched BRI3 interactome using ClueGo plugin of the Cytoscape software. Enriched categories are identified as those with p-value <0.05. Nr. Number

GO term	GO ID	Nr. genes	% associated genes	p-value	Associated genes
neuron projection	GO:0043005	46.00	5.79	2.50E-14	Atp1a3, Atp2b2, Camk2a, Camk2b, Clip2, Cnksr2, Dcx, Dlg2, Dlg4, Dlgap3, Dnml, Erc2, Gnao1, Gria2, Grin1, Grin2b, Homer1, Itpka, Map1b, Map2, Mapt, Nefl, Nefm, Nfasc, Nrgn, Nsf, Pacsin1, Pclo, Prkcg, Rab3a, Sept5, Shank1, Shank2, Slc1a2, Slc1a3, Slc8a2, Snap25, Snap91, Srcin1, Stxbp1, Syn1, Syn2, Syp, Syt1, Thy1, Tubb3
neuron part	GO:0097458	49.00	5.31	3.60E-14	Atp1a3, Atp2b2, Bsn, Camk2a, Camk2b, Clip2, Cnksr2, Dcx, Dlg2, Dlg4, Dlgap3, Dnml, Erc2, Gnao1, Gria2, Grin1, Grin2b, Homer1, Itpka, Map1b, Map2, Mapt, Nefl, Nefm, Nfasc, Nrgn, Nsf, Pacsin1, Pclo, Prkcg, Rab3a, Rims1, Sept5, Shank1, Shank2, Slc1a2, Slc1a3, Slc8a2, Snap25, Snap91, Sptbn2, Srcin1, Stxbp1, Syn1, Syn2, Syp, Syt1, Thy1, Tubb3
cell projection	GO:0042995	48.00	5.08	6.30E-13	Atp1a3, Atp2b2, Camk2a, Camk2b, Clip2, Cnksr2, Cnp, Dcx, Dlg2, Dlg4, Dlgap3, Dnml, Erc2, Gfap, Gnao1, Gria2, Grin1, Grin2b, Homer1, Itpka, Map1b, Map2, Mapt, Nefl, Nefm, Nfasc, Nrgn, Nsf, Pacsin1, Pclo, Prkcg, Rab3a, Sept5, Shank1, Shank2, Slc1a2, Slc1a3, Slc8a2, Snap25, Snap91, Srcin1, Stxbp1, Syn1, Syn2, Syp, Syt1, Thy1, Tubb3
presynapse	GO:0098793	22.00	11.70	3.10E-11	Bsn, Dnml, Erc2, Gria2, Grin1, Grin2b, Nsf, Pacsin1, Pclo, Rab3a, Rims1, Sept5, Shank2, Slc1a2, Snap25, Snap91, Sptbn2, Stxbp1, Syn1, Syn2, Syp, Syt1
axon	GO:0030424	29.00	7.82	8.70E-11	Atp1a3, Camk2a, Dlg2, Dlg4, Dnml, Erc2, Gria2, Grin1, Grin2b, Map1b, Mapt, Nefl, Nefm, Nfasc, Nrgn, Nsf, Pacsin1, Pclo, Rab3a, Sept5, Snap25, Snap91, Srcin1, Stxbp1, Syn1, Syn2, Syp, Syt1, Tubb3
postsynapse	GO:0098794	22.00	10.53	2.60E-10	Atp1a3, Camk2a, Camk2b, Cnksr2, Dlg4, Dlgap3, Erc2, Gria2, Grin1, Grin2b, Homer1, Itpka, Map1b, Nrgn, Nsf, Shank1, Shank2, Slc1a2, Slc1a3, Slc8a2, Snap91, Srcin1
terminal bouton	GO:0043195	16.00	16.00	5.80E-10	Erc2, Gria2, Grin1, Grin2b, Nsf, Pacsin1, Pclo, Rab3a, Sept5, Snap25, Snap91, Stxbp1, Syn1, Syn2, Syp, Syt1
dendrite	GO:0030425	26.00	6.37	1.70E-07	Atp1a3, Atp2b2, Camk2a, Camk2b, Clip2, Dcx, Dlg2, Dlg4, Dlgap3, Gria2, Grin1, Grin2b, Homer1, Itpka, Map1b, Map2, Nrgn, Nsf, Pclo, Prkcg, Shank1, Slc1a2, Slc1a3, Slc8a2, Srcin1, Syn1
somatodendritic compartment	GO:0036477	32.00	5.20	2.00E-07	Atp1a3, Atp2b2, Bsn, Camk2a, Camk2b, Clip2, Cnksr2, Dcx, Dlg2, Dlg4, Dlgap3, Erc2, Gria2, Grin1, Grin2b, Homer1, Itpka, Map1b, Map2, Nefm, Nrgn, Nsf, Pclo, Prkcg, Shank1, Shank2, Slc1a2, Slc1a3, Slc8a2, Snap25, Srcin1, Syn1
axon terminus	GO:0043679	16.00	9.82	9.20E-07	Erc2, Gria2, Grin1, Grin2b, Nsf, Pacsin1, Pclo, Rab3a, Sept5, Snap25, Snap91, Stxbp1, Syn1, Syn2, Syp, Syt1
transport vesicle	GO:0030133	13.00	12.38	1.40E-06	Dnml, Gria2, Nrgn, Pclo, Rab3a, Sept5, Snap91, Sptbn2, Stx1b, Syn1, Syn2, Syp, Syt1
postsynaptic specialization	GO:0099572	14.00	11.11	1.50E-06	Camk2a, Camk2b, Dlg4, Erc2, Gria2, Grin1, Grin2b, Homer1, Map1b, Nrgn, Nsf, Shank2, Snap91, Srcin1
postsynaptic density	GO:0014069	14.00	11.11	1.50E-06	Camk2a, Camk2b, Dlg4, Erc2, Gria2, Grin1, Grin2b, Homer1, Map1b, Nrgn, Nsf, Shank2, Snap91, Srcin1

GO term	GO ID	Nr. genes	% associated genes	p-value	Associated genes
synaptic vesicle	GO:0008021	10.00	12.20	7.10E-05	Dnml, Gria2, Rab3a, Sept5, Snap91, Sptbn2, Syn1, Syn2, Syp, Syt1
dendritic spine	GO:0043197	11.00	10.58	8.50E-05	Atp1a3, Dlgap3, Gria2, Grin1, Grin2b, Itpka, Nrgn, Shank1, Slc1a2, Slc1a3, Slc8a2
neuron spine	GO:0044309	11.00	10.58	8.50E-05	Atp1a3, Dlgap3, Gria2, Grin1, Grin2b, Itpka, Nrgn, Shank1, Slc1a2, Slc1a3, Slc8a2
exocytic vesicle	GO:0070382	10.00	11.76	9.50E-05	Dnml, Gria2, Rab3a, Sept5, Snap91, Sptbn2, Syn1, Syn2, Syp, Syt1
presynaptic active zone	GO:0048786	5.00	29.41	3.70E-04	Bsn, Pclo, Shank2, Syn1, Syp
myelin sheath	GO:0043209	6.00	17.14	1.10E-03	Atp1a3, Cnp, Gnao1, Mbp, Mog, Plp1
presynaptic membrane	GO:0042734	6.00	17.14	1.10E-03	Erc2, Gria2, Grin2b, Rims1, Slc1a2, Snap91
NMDA selective glutamate receptor complex	GO:0017146	4.00	36.36	1.10E-03	Dlgap3, Grin1, Grin2b, Shank1
synaptic membrane	GO:0097060	9.00	9.47	1.60E-03	Cnksr2, Dlg4, Erc2, Gria2, Grin2b, Rims1, Shank1, Slc1a2, Snap91
cytoskeleton	GO:0005856	13.00	6.22	2.80E-03	Bsn, Clasp2, Clip2, Map1a, Map1b, Mapt, Nefl, Nefm, Pclo, Sept5, Slc8a2, Snap25, Srcin1
ionotropic glutamate receptor complex	GO:0008328	5.00	19.23	2.90E-03	Dlgap3, Gria2, Grin1, Grin2b, Shank1
growth cone	GO:0030426	9.00	8.11	5.10E-03	Erc2, Gria2, Map1b, Mapt, Nefl, Pclo, Shank2, Snap25, Thy1
transmembrane transporter complex	GO:1902495	9.00	7.96	5.50E-03	Atp1a3, Dlg2, Dlg4, Dlgap3, Gria2, Grin1, Grin2b, Shank1, Snap25
neuronal cell body	GO:0043025	20.00	4.22	8.60E-03	Atp2b2, Bsn, Camk2a, Camk2b, Cnksr2, Dlg2, Dlgap3, Erc2, Gria2, Grin1, Homer1, Map1b, Map2, Nefm, Nrgn, Pclo, Shank2, Slc8a2, Snap25, Srcin1
ion channel complex	GO:0034702	8.00	8.00	1.10E-02	Dlg2, Dlg4, Dlgap3, Gria2, Grin1, Grin2b, Shank1, Snap25
membrane-bounded vesicle	GO:0031988	14.00	4.62	2.40E-02	Clip2, Dnml, Gria2, Nrgn, Pclo, Rab3a, Sept5, Snap91, Sptbn2, Stx1b, Syn1, Syn2, Syp, Syt1
plasma membrane protein complex	GO:0098797	9.00	6.25	2.60E-02	Atp1a3, Dlg2, Dlg4, Dlgap3, Gria2, Grin1, Grin2b, Shank1, Snap25
secretory vesicle	GO:0099503	11.00	5.14	3.30E-02	Clip2, Dnml, Gria2, Rab3a, Sept5, Snap91, Sptbn2, Syn1, Syn2, Syp, Syt1
integral component of plasma membrane	GO:0005887	9.00	5.81	3.60E-02	Atp1a3, Dlg2, Dlg4, Dlgap3, Gria2, Grin1, Grin2b, Shank1, Snap25
polymeric cytoskeletal fiber	GO:0099513	6.00	8.22	3.70E-02	Clasp2, Clip2, Mapt, Nefl, Nefm, Slc8a2

Further, using the Cytoscape software, we constructed a PPI network (see materials and methods section). This approach allows to infer other proteins that may be involved in BRI3 interactome by deciphering their relationships and potential functional protein complexes. BRI3 PPI network is presented in Figure 3, summing up previously known and experimentally evidenced interactions. Further, in the network the grey nodes correspond to PPI added by the Cytoscape analysis, the colorful nodes to the proteins identified in our study and the node size correspond to its degree (k; the number of edges linked to it) (Figure III.B.3). This network consists of 244 nodes, including BRI3, and 543 interactions (Figure III.B.3). The average connectivity, i.e. the average number of neighbors of a node in the network, is 4.451, and the mean clustering coefficient is 0.083. The mean clustering coefficient of the network which characterizes how nearest neighboring nodes of a node are connected to each other is about 4 times larger than the clustering coefficient expected for a sparse random uncorrelated network (0.02) (Doncheva *et al.* 2012; Newman 2006). Moreover, the results from topological network analysis showed that besides BRI3 which accounted for 92 interactions, TUBB3 (k =38), TUBB2A (k =28), CRMP1 (k =20), NSF (k =16), MAPT (k =15), CAMK2A (k =15), and MAP1B (k =14) were the most connected hub proteins in the network (Figure III.B.3).

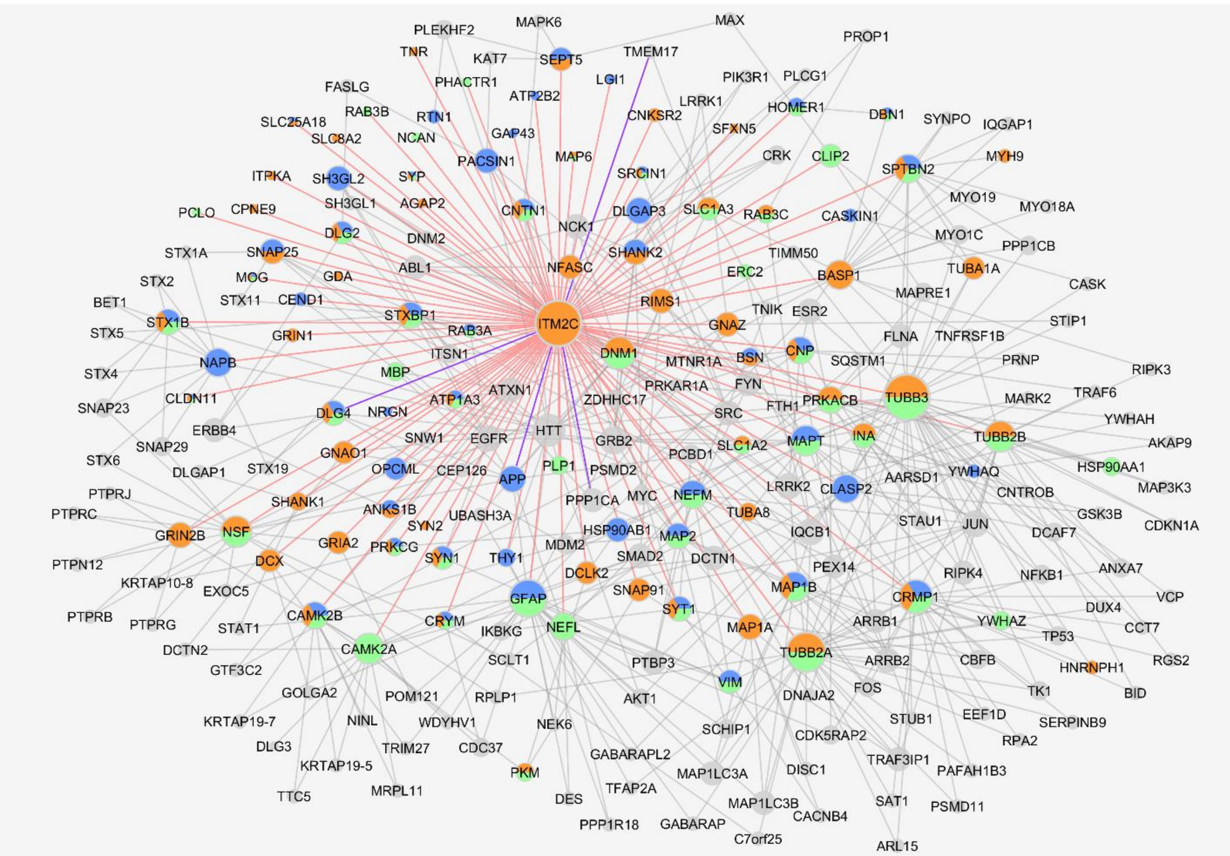

Figure III.B 3- BRI3 brain ES sub-network. Node colors represent the source: blue nodes correspond to proteins identified in this study in the cerebral cortex, orange nodes correspond to proteins identified in this study in the hippocampus, green nodes correspond to proteins identified in this study in the striatum, and grey nodes are proteins added by network annotation. Node size according to the degree in the network. Edge color represents the source of interaction: light red edges correspond to connections between proteins identified in this study, purple edges correspond to connections between proteins that was manually added to the network (correspond to interactions already described in the literature but not identified in the iMEX consortium databases), and grey edges correspond to connections between proteins added by network annotation.

Further, integrated metabolic KEGG pathway analysis, using the ClueGo plugin of the Cytoscape software (Bindea *et al*. 2009), was performed to identify the pathways that BRI3 brain ES network is involved in. The results shown that the network is mainly involved in the ErbB signaling pathway, SNARE interaction in vesicular transport, neurotrophin signaling pathway, MAPK signaling pathway, glutamatergic synapse, synaptic vesicle cycle, estrogen signaling pathway, dopaminergic synapse, oxytocin signaling pathway and long-term potentiation were the most represented pathways (Table III.B.4). Of note, signaling pathways related to gap junction, focal adhesion, adherens junction, and apoptosis were also evidenced (Table III.B.4).

Table III.B 4- KEGG categories enrichment analysis of the brain specific/enriched BRI3 interactome using ClueGo plugin of the Cytoscape software. Enriched categories are identified as those with p-value <0.05. Nr., number.

KEGG Term	KEGG ID	Nr. Genes	% Associated Genes	pValue	Associated Genes Found
ErbB signaling pathway	KEGG:04012	17	19.32	3.37E-11	ABL1, AKT1, CAMK2A, CAMK2B, CDKN1A, CRK, EGFR, ERBB4, GRB2, GSK3B, JUN, MYC, NCK1, PIK3R1, PLCG1, PRKCG, SRC
Proteoglycans in cancer	KEGG:05205	21	10.24	1.58E-08	AKT1, CAMK2A, CAMK2B, CDKN1A, EGFR, ERBB4, FASLG, FLNA, GRB2, IQGAP1, MDM2, MYC, PIK3R1, PLCG1, PPP1CA, PPP1CB, PRKACB, PRKCG, SMAD2, SRC, TP53
SNARE interactions in vesicular transport	KEGG:04130	10	29.41	3.82E-08	BET1, SNAP23, SNAP29, STX11, STX19, STX1A, STX1B, STX4, STX5, STX6
Epstein-Barr virus infection	KEGG:05169	20	9.80	9.84E-08	AKT1, CDKN1A, GSK3B, IKBKG, JUN, MDM2, MYC, NFKB1, PIK3R1, PLCG1, PRKACB, PSMD11, PSMD2, SNW1, TP53, TRAF6, VIM, YWHAH, YWHAQ, YWHAZ
Amphetamine addiction	KEGG:05031	12	17.65	3.71E-07	CAMK2A, CAMK2B, FOS, GRIA2, GRIN1, GRIN2B, JUN, PPP1CA, PPP1CB, PRKACB, PRKCG, STX1A
Neurotrophin signaling pathway	KEGG:04722	15	12.40	5.97E-07	ABL1, AKT1, CAMK2A, CAMK2B, CRK, FASLG, GRB2, GSK3B, JUN, MAP3K3, NFKB1, PIK3R1, PLCG1, TP53, TRAF6
Hepatitis B	KEGG:05161	16	10.96	1.09E-06	AKT1, CDKN1A, FASLG, FOS, GRB2, IKBKG, JUN, MYC, NFKB1, PIK3R1, PRKCG, SRC, STAT1, TP53, YWHAQ, YWHAZ
Pathways in cancer	KEGG:05200	26	6.55	1.45E-06	ABL1, AKT1, BID, CDKN1A, CRK, EGFR, FASLG, FOS, GRB2, GSK3B, HSP90AA1, HSP90AB1, IKBKG, JUN, MAX, MDM2, MYC, NFKB1, PIK3R1, PLCG1, PRKACB, PRKCG, SMAD2, STAT1, TP53, TRAF6
Glioma	KEGG:05214	11	16.67	3.13E-06	AKT1, CAMK2A, CAMK2B, CDKN1A, EGFR, GRB2, MDM2, PIK3R1, PLCG1, PRKCG, TP53
MAPK signaling pathway	KEGG:04010	20	7.84	4.47E-06	AKT1, ARRB1, ARRB2, CRK, EGFR, FASLG, FLNA, FOS, GRB2, IKBKG, JUN, MAP3K3, MAPT, MAX, MYC, NFKB1, PRKACB, PRKCG, TP53, TRAF6
Pathogenic Escherichia coli infection	KEGG:05130	10	18.18	5.70E-06	ABL1, FYN, NCK1, TUBA1A, TUBA8, TUBB2A, TUBB2B, TUBB3, YWHAQ, YWHAZ
Prostate cancer	KEGG:05215	12	13.48	8.15E-06	AKT1, CDKN1A, EGFR, GRB2, GSK3B, HSP90AA1, HSP90AB1, IKBKG, MDM2, NFKB1, PIK3R1, TP53
Chronic myeloid leukemia	KEGG:05220	11	15.07	8.97E-06	ABL1, AKT1, CDKN1A, CRK, GRB2, IKBKG, MDM2, MYC, NFKB1, PIK3R1, TP53
Glutamatergic synapse	KEGG:04724	13	11.40	1.70E-05	DLG4, DLGAP1, GNAO1, GRIA2, GRIN1, GRIN2B, HOMER1, PRKACB, PRKCG, SHANK1, SHANK2, SLC1A2, SLC1A3
Synaptic vesicle cycle	KEGG:04721	10	15.87	2.12E-05	DNM1, DNM2, NSF, RAB3A, RIMS1, SNAP25, STX1A, STX1B, STXBP1, SYT1
Estrogen signaling pathway	KEGG:04915	12	12.00	2.92E-05	AKT1, EGFR, ESR2, FOS, GNAO1, GRB2, HSP90AA1, HSP90AB1, JUN, PIK3R1, PRKACB, SRC
Amyotrophic lateral sclerosis (ALS)	KEGG:05014	9	17.65	3.39E-05	BID, GRIA2, GRIN1, GRIN2B, NEFL, NEFM, SLC1A2, TNFRSF1B, TP53
T cell receptor signaling pathway	KEGG:04660	12	11.43	4.92E-05	AKT1, FOS, FYN, GRB2, GSK3B, IKBKG, JUN, NCK1, NFKB1, PIK3R1, PLCG1, PTPRC
Dopaminergic synapse	KEGG:04728	13	10.00	7.60E-05	AKT1, ARRB2, CAMK2A, CAMK2B, FOS, GNAO1, GRIA2, GRIN2B, GSK3B, PPP1CA, PPP1CB, PRKACB, PRKCG
Oxytocin signaling pathway	KEGG:04921	14	8.81	1.31E-04	CAMK2A, CAMK2B, CDKN1A, EGFR, FOS, GNAO1, JUN, PIK3R1, PPP1CA, PPP1CB, PRKACB, PRKCG, RGS2, SRC

Thyroid hormone signaling pathway	KEGG:04919	12	10.17	1.70E-04	AKT1, ATP1A3, GSK3B, MDM2, MYC, PIK3R1, PLCG1, PRKACB, PRKCG, SRC, STAT1, TP53
Long-term potentiation	KEGG:04720	9	13.43	3.52E-04	CAMK2A, CAMK2B, GRIA2, GRIN1, GRIN2B, PPP1CA, PPP1CB, PRKACB, PRKCG
cAMP signaling pathway	KEGG:04024	15	7.50	3.97E-04	AKT1, ATP1A3, ATP2B2, CAMK2A, CAMK2B, FOS, GRIA2, GRIN1, GRIN2B, JUN, NFKB1, PIK3R1, PPP1CA, PPP1CB, PRKACB
Gap junction	KEGG:04540	10	11.36	4.61E-04	EGFR, GRB2, PRKACB, PRKCG, SRC, TUBA1A, TUBA8, TUBB2A, TUBB2B, TUBB3
Prolactin signaling pathway	KEGG:04917	9	12.50	6.23E-04	AKT1, ESR2, FOS, GRB2, GSK3B, NFKB1, PIK3R1, SRC, STAT1
FoxO signaling pathway	KEGG:04068	12	8.96	6.26E-04	AGAP2, AKT1, CDKN1A, EGFR, FASLG, GABARAP, GABARAPL2, GRB2, HOMER1, MDM2, PIK3R1, SMAD2
Circadian entrainment	KEGG:04713	10	10.42	9.84E-04	CAMK2A, CAMK2B, FOS, GNAO1, GRIA2, GRIN1, GRIN2B, MTNR1A, PRKACB, PRKCG
Colorectal cancer	KEGG:05210	8	12.90	1.60E-03	AKT1, FOS, GSK3B, JUN, MYC, PIK3R1, SMAD2, TP53
Chagas disease (American trypanosomiasis)	KEGG:05142	10	9.62	1.97E-03	AKT1, FASLG, FOS, GNAO1, IKBKG, JUN, NFKB1, PIK3R1, SMAD2, TRAF6
Viral carcinogenesis	KEGG:05203	14	6.83	2.29E-03	CDKN1A, GRB2, IKBKG, JUN, MDM2, NFKB1, PIK3R1, PRKACB, SNW1, SRC, TP53, YWHAH, YWHAQ, YWHAZ
Pancreatic cancer	KEGG:05212	8	12.12	2.47E-03	AKT1, EGFR, IKBKG, NFKB1, PIK3R1, SMAD2, STAT1, TP53
Cocaine addiction	KEGG:05030	7	14.29	2.67E-03	DLG4, GRIA2, GRIN1, GRIN2B, JUN, NFKB1, PRKACB
Osteoclast differentiation	KEGG:04380	11	8.33	2.80E-03	AKT1, FOS, FYN, GRB2, IKBKG, JUN, NFKB1, PIK3R1, SQSTM1, STAT1, TRAF6
Hepatitis C	KEGG:05160	11	8.27	2.97E-03	AKT1, CDKN1A, EGFR, GRB2, GSK3B, IKBKG, NFKB1, PIK3R1, STAT1, TP53, TRAF6
Endometrial cancer	KEGG:05213	7	13.46	3.84E-03	AKT1, EGFR, GRB2, GSK3B, MYC, PIK3R1, TP53
Apoptosis	KEGG:04210	11	7.86	4.67E-03	AKT1, BID, FASLG, FOS, IKBKG, JUN, NFKB1, PIK3R1, TP53, TUBA1A, TUBA8
PI3K-Akt signaling pathway	KEGG:04151	18	5.28	4.69E-03	AKT1, CDC37, CDKN1A, EGFR, FASLG, GRB2, GSK3B, HSP90AA1, HSP90AB1, IKBKG, MDM2, MYC, NFKB1, PIK3R1, TP53, YWHAH, YWHAQ, YWHAZ
B cell receptor signaling pathway	KEGG:04662	8	10.96	4.79E-03	AKT1, FOS, GRB2, GSK3B, IKBKG, JUN, NFKB1, PIK3R1
Non-small cell lung cancer	KEGG:05223	7	12.50	5.97E-03	AKT1, EGFR, GRB2, PIK3R1, PLCG1, PRKCG, TP53
Breast cancer	KEGG:05224	11	7.53	6.54E-03	AKT1, CDKN1A, EGFR, ESR2, FOS, GRB2, GSK3B, JUN, MYC, PIK3R1, TP53
Inflammatory mediator regulation of TRP channels	KEGG:04750	9	9.09	6.99E-03	CAMK2A, CAMK2B, PIK3R1, PLCG1, PPP1CA, PPP1CB, PRKACB, PRKCG, SRC
Cell cycle	KEGG:04110	10	8.06	7.62E-03	ABL1, CDKN1A, GSK3B, MDM2, MYC, SMAD2, TP53, YWHAH, YWHAQ, YWHAZ
Bladder cancer	KEGG:05219	6	14.63	7.65E-03	CDKN1A, EGFR, MDM2, MYC, SRC, TP53
Focal adhesion	KEGG:04510	13	6.40	7.66E-03	AKT1, CRK, EGFR, FLNA, FYN, GRB2, GSK3B, JUN, PIK3R1, PPP1CA, PPP1CB, PRKCG, SRC
HIF-1 signaling pathway	KEGG:04066	9	8.74	9.05E-03	AKT1, CAMK2A, CAMK2B, CDKN1A, EGFR, NFKB1, PIK3R1, PLCG1, PRKCG
Hippo signaling pathway	KEGG:04390	11	7.14	9.80E-03	DLG2, DLG3, DLG4, GSK3B, MYC, PPP1CA, PPP1CB, SMAD2, YWHAH, YWHAQ, YWHAZ

Insulin secretion	KEGG:04911	8	9.41	1.27E-02	ATP1A3, CAMK2A, CAMK2B, PRKACB, PRKCG, RAB3A, SNAP25, STX1A
Chemokine signaling pathway	KEGG:04062	12	6.42	1.30E-02	AKT1, ARRB1, ARRB2, CRK, GRB2, GSK3B, IKBKG, NFKB1, PIK3R1, PRKACB, SRC, STAT1
Small cell lung cancer	KEGG:05222	8	9.30	1.34E-02	AKT1, IKBKG, MAX, MYC, NFKB1, PIK3R1, TP53, TRAF6
Cholinergic synapse	KEGG:04725	9	8.11	1.50E-02	AKT1, CAMK2A, CAMK2B, FOS, FYN, GNAO1, PIK3R1, PRKACB, PRKCG
GnRH signaling pathway	KEGG:04912	8	8.70	2.08E-02	CAMK2A, CAMK2B, EGFR, GRB2, JUN, MAP3K3, PRKACB, SRC
Ras signaling pathway	KEGG:04014	13	5.68	2.23E-02	ABL1, AKT1, EGFR, FASLG, GRB2, GRIN1, GRIN2B, IKBKG, NFKB1, PIK3R1, PLCG1, PRKACB, PRKCG
Adherens junction	KEGG:04520	7	9.46	2.92E-02	EGFR, FYN, IQGAP1, PTPRB, PTPRJ, SMAD2, SRC
Choline metabolism in cancer	KEGG:05231	8	7.92	3.77E-02	AKT1, EGFR, FOS, GRB2, JUN, PIK3R1, PLCG1, PRKCG
Acute myeloid leukemia	KEGG:05221	6	10.53	4.16E-02	AKT1, GRB2, IKBKG, MYC, NFKB1, PIK3R1
Herpes simplex infection	KEGG:05168	11	5.95	4.18E-02	EEF1D, FASLG, FOS, IKBKG, JUN, NFKB1, PPP1CA, PPP1CB, STAT1, TP53, TRAF6
Toll-like receptor signaling pathway	KEGG:04620	8	7.55	4.97E-02	AKT1, FOS, IKBKG, JUN, NFKB1, PIK3R1, STAT1, TRAF6

III.B.3.2 BRI3 brain region specific interactome

The analysis of interactome from the different brain regions may reveal possible differences that could provide insight into selective brain region-dependent processes, and thus here we attempt to identify specific BRI3 interactors from three different rat brain region: cortex, hippocampus, and striatum. Comparative analysis of all of the candidate BRI3 interactors identified in our study (Figure III.B.4) indicates that 45 proteins were specifically identified in the cortex, 72 in the hippocampus and 44 in the striatum (Figure III.B.4A). Moreover, tissue-expression analysis of those proteins resulted in the identification of 14 BRI3 interactors brain enriched/specific in the cortex, 22 in the hippocampus, and 10 in the striatum (Figure III.B.4B).

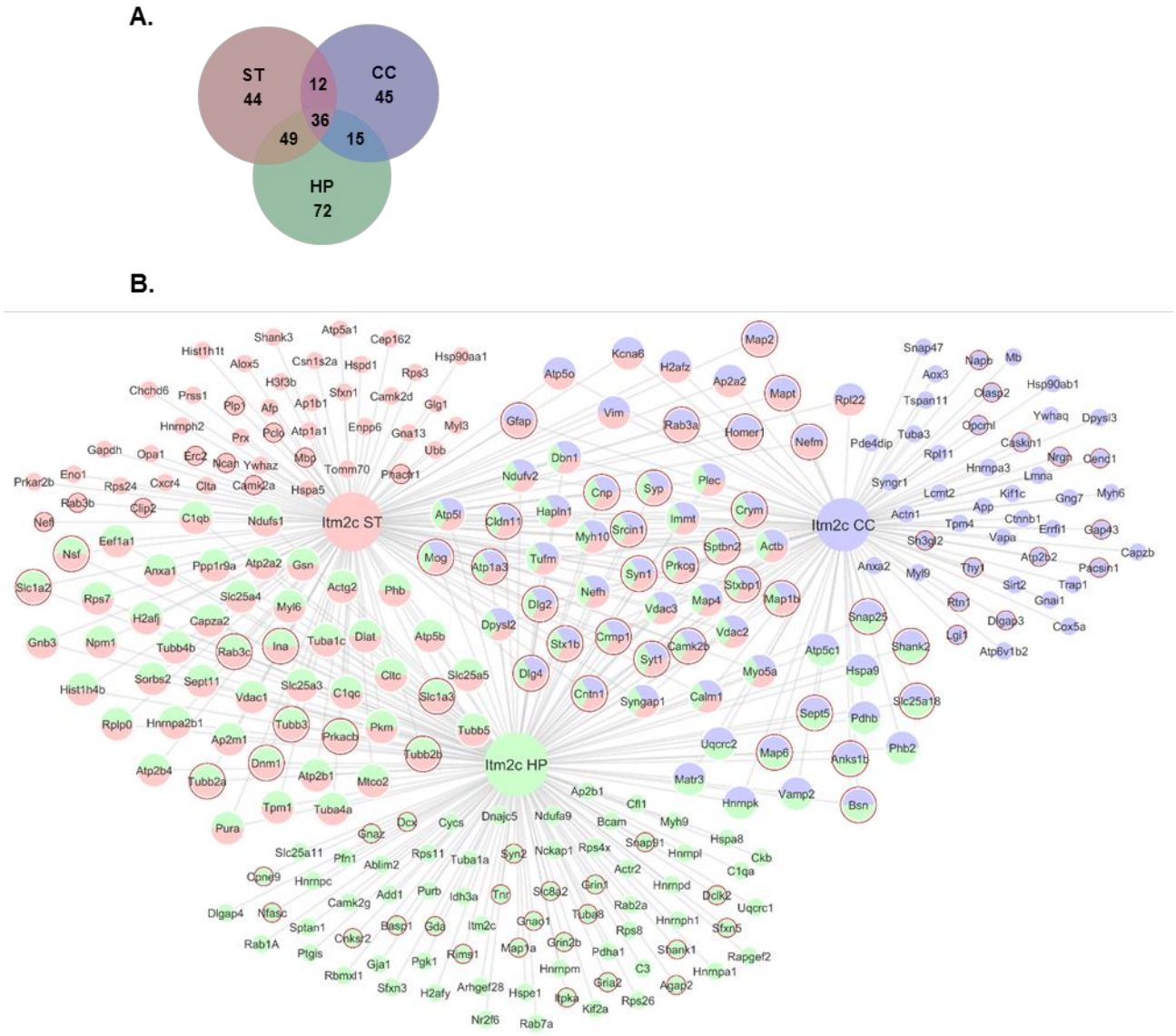

Figure III.B 4 - Brain region specific protein interactions in the BRI3 interactome. A- Venn diagram comparison of the brain region (cerebral cortex, hippocampus and striatum) specific BRI3 protein interactions identified in this study. **B-** BRI3 interactome identified in this study. Node size according to the degree in the network. Node color represents the source of interaction: blue nodes correspond to the BRI3 interactors identified in the cerebral cortex, green nodes correspond to the BRI3 interactors identified in the hippocampus, and light red nodes correspond to the BRI3 interactors identified in the striatum. Nodes with red border correspond to BRI3 interactors highly enriched or brain specific. CX, cerebral cortex; HP, hippocampus; ST, striatum.

Further, network augmentation was performed for the brain enriched/specific BRI3 candidate interactors specific for each brain tissue (Supplementary Figure III.B.S1). This approach was performed in order to increase our PPI network and enhance our experimental data with additional known and experimentally validated protein partners which then allow us to asses if the BRI3 interactome could be assigned to selective brain regional-dependent pathways. For the cortex, specific PPI network (Supplementary Figure III.B.S1A) were mapped a total of 141 proteins with 146 connections between them. Moreover, the network presented an average number of neighbors of 2.071. The hippocampus specific PPI network possessed 127 proteins connected with 141 edges, and an average number of neighbors of 2.169 (Supplementary Figure III.B.S1B). Striatum specific PPI network resulted in the mapping of 106 proteins connected by 106 edges and presented an average number of neighbors of 2.019 (Supplementary Figure III.B.S1C). Cluster comparison functional analysis regarding KEGG pathways was performed using the ClueGO plugin from Cytoscape between the cortex, hippocampus, and striatum-specific PPI networks (Supplementary Table III.B.S4). Noticeably, the analysis revealed that the majority of pathways are in fact common between the three specific BRI3 interactomes, and essentially corresponds to pathways already highlighted in the analysis of the total BRI3 brain ES interactome: ErbB signaling pathway, neurotrophin signaling pathway, dopaminergic synapse, estrogen signaling pathway, long-term potentiation, adherens junction, and focal adhesion (Supplementary Table III.B.S4). Nevertheless, some pathways seem to be more associated to the cortex specific PPI network: SNARE interactions in vesicular transport, and synaptic vesicle cycle (Supplementary Table III.B.S4).

III.B.3.3 Evidence for BRI3 association with nervous system diseases

Additionally, the significance of BRI3 interactome can be supported by its involvement with human nervous system diseases. Therefore, to address this issue DisGeNET database was used (see materials and methods section) and a list of all genes that are together with BRI3 are associated with brain disease, which was further crossed with the list of BRI3 interactors was identified. This analysis resulted in a list of 73 BRI3 protein interactors and its associated diseases which was further represented as a network (Figure III.B.5). In fact, almost 30% (73 out of 274 proteins) of the identified BRI3 interactors share diseases with BRI3, suggesting a complex functional connection

between the proteins. The disease associated with the highest number of BRI3 protein interactors was Alzheimer´s Disease (AD; linked to 64 BRI3 interactors) (Figure III.B.5). Other diseases included Cerebrovascular Accident, Cerebral Hemorrhage, Subarachnoid Hemorrhage, Intracranial Hemorrhage and Neuritis (Figure III.B.5).

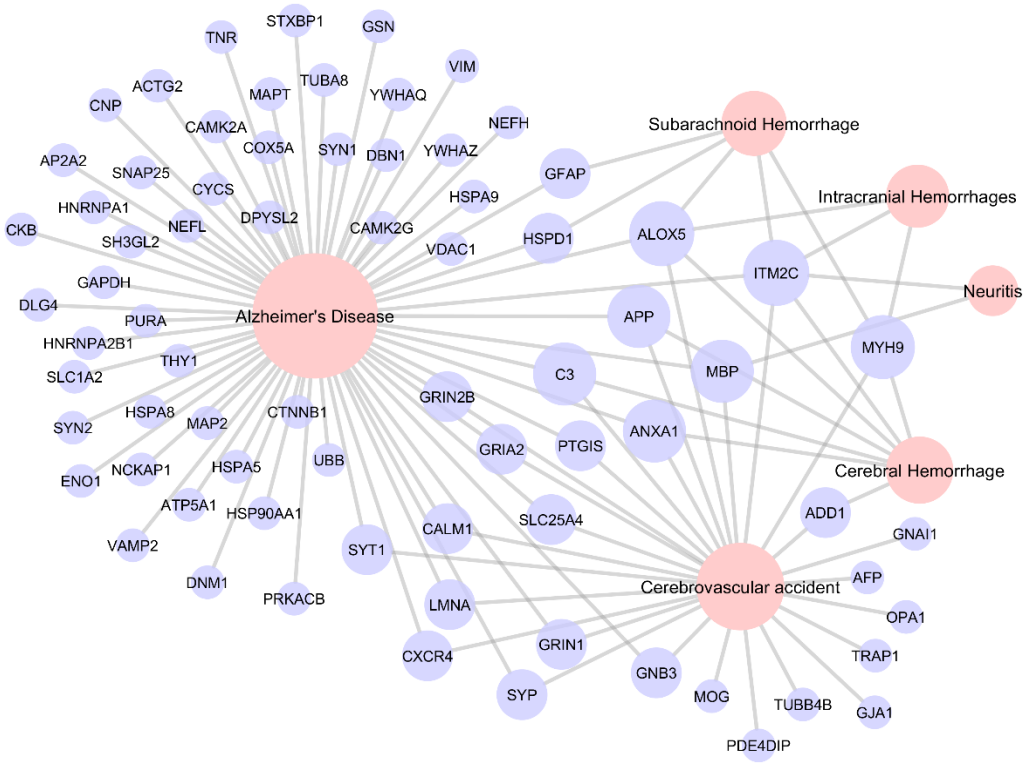

Figure III.B 5 - Diseases network shared by BRI3 and its identified protein interactors. The complete list of diseases shared by BRI3 and other genes was retrieved from the DisGeNET database. The identified BRI3 protein interactors were searched in the obtained list, to create a network of diseases shared between them. Diseases are represented in red circular nodes. Proteins are identified by their gene names represented in blue circular nodes. Network nodes are configured by size accordingly to node degree (low values to small sizes).

.

III.B.4 Discussion

BRI3 is a brain-enriched protein whose biological function remains elusive. In the present study, we focused on the identification and BRI3 interacting proteins in the brain and its characterization in order to further understand the biological roles of BRI3. Hence, BRI3 was co-IPed from three rat brain regions (cerebral cortex, hippocampus, and striatum). In total, we were able to identify 274 proteins as potential BRI3 interactors, from which two were already described in the literature: APP and PSD-95. Remarkably, 89 out of the 274 proteins were found to be specific or strongly expressed in the brain. Based on the bioinformatic analysis, the BRI3 candidate interactors were found to be involved in a variety of biological processes relevant to CNS development and function and could form a complex interaction network. Protein class analysis allows us to conclude that BRI3 mainly interacts with cytoskeletal proteins, transporters, and membrane traffic proteins (Figure 2). Moreover, the cellular component annotation analysis of the BRI3 ES brain interactors suggested a subcellular localization for BRI3 in neuron projections, at synapses, both presynapse and postsynapse, and associated with synaptic vesicles and cytoskeleton (Table 3), which in turn suggests a role for BRI3 at the nerve terminals.

Several proteins here identified to be associated with BRI3 protein, participate in the synaptic vesicle cycle, namely in synaptic vesicle transport and exocytosis (Table 2 and Table 4) which implies a role for BRI3 in synaptic vesicle function. Among the BRI3 interacting protein candidates, we identified several key proteins for synaptic vesicle fusion, namely the synaptosomal-associated protein 25 (Snap-25), syntaxin-1b (Stx1b), Vesicle-fusing ATPase (NSF), the SNARE complex protein Vamp2 (Vesicle-associated membrane protein 2) and Rab3 (Rab3a, Rab3b, Rab3c) (Jahn and Fasshauer 2012; Augustine *et al*. 1999). Moreover, we identified proteins involved in the endocytosis of synaptic vesicles from the membrane, including Dynamin-1 (Dnm1) and Endophilin-A1 (Sh3gl2) (Saheki and De Camilli 2012). Other synaptic vesicle-associated proteins such as synaptotagmin 1 (Syt1), and synapsin-1 and -2 (Syn1 and Syn2) were also identified.

The present work also resulted in the identification of cytoplasmic kinesin motor proteins Kif1c and Kif2a, members of the AP-1 and AP-2 complex (Ap1b1, Ap2a2, Ap2b1, Ap2m1) and Arf GAP with GTPAse domain, Ankyrin repeat and PH domain 2 protein (Agap2), myosin subunits (Myl3, Myl6, Myl9, Myh6, Myh9, Myh10) as well as other proteins involved in vesicle trafficking, such as clathrins (Clta, Cltc) and its adaptor protein Snap91. All these proteins are involved in neuronal trafficking along the cytoskeleton, a key process in the formation and dynamics of synapses (Maeder *et al*. 2014; Lasiecka and Winckler 2011). Hence, the association of the BRI3 protein with these novel potential interactors suggest either a role for BRI3 in axonal and dendritic trafficking or that the proper BRI3 protein is transported within axons and dendrites to the nerve terminals where it might be functionally required. In fact, the results here presented suggest that BRI3 is expressed both

pre- and post-synaptically (Table 3) which strongly suggest a role for BRI3 at the synapse, namely in synapse formation. For instance, BRI3 may contribute to the adhesion of synapses, in a process involving trans-synaptic interactions between pre- and postsynaptic BRI3. Additionally, given the biological functions attributed to the identified BRI3 brain ES interactors (Table 2) it is also plausible to assume that the synapse, BRI3 might be directly involved in synaptic signaling and transmission. In fact, we identified several proteins in the BRI3 interactome known to be involved in synaptic transmission, namely the calcium/calmodulin-dependent protein kinase type II subunit beta (Camk2b), Dlg4 (PSD-95), glutamate receptor 2 (Gria2/ GluR2), glutamate receptor ionotropic, NMDA 1 (Grin1/NMDAR1), glutamate receptor ionotropic, NMDA 2B (Grin2b/NMDAR2B). Remarkably, it is already described for APP, a well-established BRI3 interactor, a role in excitatory synaptic transmission by altering AMPA receptor (AMPAR) and NMDA (NMDAR) receptor trafficking. For example, APP is able to increase the cell surface levels of the GluR2 subunit of AMPARs which potentially enhance excitatory synaptic transmission (Spires *et al*. 2005; Isaac *et al*. 2007). APP also facilitates NMDAR function by increasing cell surface levels of NMDAR1 and NMDAR2B subunits (Hoe *et al*. 2009). However, several evidences suggest a relationship between Aβ (a peptide derived from sequential cleavage of APP by β- and γ-secretase) accumulation and synaptic dysfunction. Actually, in cultured neurons it was demonstrated that Aβ: (1) leads to decrease in PSD-95, a protein involved in recruiting and anchoring glutamate receptor subunits to the post-synaptic density, and also reduction in surface expression of glutamate receptor subunit GluR1 (Almeida *et al*. 2005); (2) promotes endocytosis of NMDA receptors (Snyder *et al*. 2005). Hence, given the nature of BRI3:APP interaction (Matsuda *et al*. 2009) (BRI3 is a negative regulator of Aβ production) it is possible to hypothesize a role for BRI3 in synaptic transmission and plasticity, namely in the regulation of the AMPARs and NMDARs receptors trafficking.

Of note, a high number of proteins of BRI3 brain interactome are cytoskeletal and cytoskeletal binding proteins involved in its organization, namely tubulin [tubulin beta-3 chain (Tubb3), tubulin beta-2A chain (Tubb2a)], microtubule-associated protein 1b (Map1b), microtubule-associated protein tau (Mapt), doublecortin (Dcx), collapsing response mediator protein-2 (Crmp2), CLIP-associating protein 2 (Clasp2), cofilin-1 (Cfl1), F-actin-capping protein Capz [subunit alpha-2 (Capza2), subunit beta (Capzb)], and spectrin beta chain (Sptbn2), which translated into an overrepresentation of functions like cytoskeleton organization, regulation of microtubule polymerization and depolymerization in the BRI3 interactome. Remarkably, the establishment and maintenance of neuronal polarity is coordinated by rearrangements of the cytoskeletal architecture and depends on the ability of the growth cone to sense extracellular guidance cues (Mattson 1999; Tahirovic and Bradke 2009). This fact together with the suggested localization of BRI3 in neuron projections and neuronal growth cones (Table 3) is consistent with a BRI3 role in neurite outgrowth,

as previously proposed (Gong *et al*. 2008), by mediating cytoskeleton stability. In concordance with this, BRI3 brain ES interactome was strongly associated with signaling pathways with well-established roles in CNS development and function, namely in several neuronal differentiation related events: neurotrophin signaling pathway (Reichardt 2006), ErbB signaling pathway (Iwakura and Nawa 2013; Mei and Nave 2014), estrogen signaling pathway (Wang *et al*. 2003) and MAPK signaling pathway (Perron and Bixby 1999; Takeda and Ichijo 2002). Therefore, an association of BRI3 with these signaling pathways deserve further investigations.

Moreover, a comparative analysis of the BRI3 interactome in the three brain regions evidenced that 14 brain ES proteins were identified specifically in the cortex, 22 in the hippocampus, and 10 in the striatum (Figure 5). Of note, no particular event seems to be exclusively associated a particular brain region which supports the sight that the majority of the proteins of the BRI3 interactome are in fact relatively stable across the three brain regions.

Limitations of the present study include the possibility of poor recovery of the membrane and nuclear proteins and the lack of detection of proteins which interact only transiently with BRI3 interactome. Remarkably, although the BRI3 interactors here identified does not present higher overlap with the other previously reported in the literature (2 out of 274), many were functionally related. In fact, some genes encoding BRI3 protein interactors here identified are closely interconnected with *BRI3* gene with respect to diseases in each they were found associated (Fig. 3). Interestingly, BRI3 interactome seems to be strongly associated with AD. Strong evidences suggest imbalanced activities of protein kinases and phosphatases (including PP1) in AD thus affecting the phosphorylation state of AD-related proteins, such as APP and tau (Oliveira *et al*. 2015). Recently, we have shown that BRI3 is, in fact, a phosphoprotein that can be dephosphorylated by PP1 (Martins *et al*. 2016). However, the relevance and impact of protein phosphorylation in its biology was not elucidated. Given the described influence of BRI3 on Aβ production, further studies should investigate its function/dysfunction in AD, namely its phosphorylation state, which may provide novel and important insights on the pathology mechanisms.

In conclusion, several novel BRI3 candidate interacting proteins were identified and the bioinformatic study of its characteristics revealed a strong association of BRI3 with proteins related to several related synaptic functions (synaptic vesicle cycle, synapse formation, synaptic signaling, and transmission), neuronal trafficking and neuronal differentiation. Therefore, the findings suggest that further studies of BRI3 should address these potential roles and the underlying mechanism, as well as its association with nervous system pathologies.

References

Almeida C. G., Tampellini D., Takahashi R. H., Greengard P., Lin M. T., Snyder E. M., Gouras G. K. (2005) Beta-amyloid accumulation in APP mutant neurons reduces PSD-95 and GluR1 in synapses. *Neurobiol. Dis.* **20**, 187–198.

Arbuckle M. I., Komiyama N. H., Delaney A., Coba M., Garry E. M., Rosie R., Allchorne A. J., et al. (2010) The SH3 domain of postsynaptic density 95 mediates inflammatory pain through phosphatidylinositol-3-kinase recruitment. *EMBO Rep.* **11**, 473–8.

Augustine G. J., Burns M. E., DeBello W. M., Hilfiker S., Morgan J. R., Schweizer F. E., Tokumaru H., Umayahara K. (1999) Proteins involved in synaptic vesicle trafficking. *J. Physiol.* **520 Pt 1**, 33–41.

Berndt J. D., Aoyagi A., Yang P., Anastas J. N., Tang L., Moon R. T. (2011) Mindbomb 1, an E3 ubiquitin ligase, forms a complex with RYK to activate Wnt/β-catenin signaling. *J. Cell Biol.* **194**, 737–50.

Bindea G., Mlecnik B., Hackl H., Charoentong P., Tosolini M., Kirilovsky A., Fridman W.-H., Pagès F., Trajanoski Z., Galon J. (2009) ClueGO: a Cytoscape plug-in to decipher functionally grouped gene ontology and pathway annotation networks. *Bioinformatics* **25**, 1091–3.

Carithers L. J., Ardlie K., Barcus M., Branton P. A., Britton A., Buia S. A., Compton C. C., et al. (2015) A Novel Approach to High-Quality Postmortem Tissue Procurement: The GTEx Project. *Biopreserv. Biobank.* **13**, 311–319.

Choi S. C., Kim J., Kim T. H., Cho S. Y., Park S. S., Kim K. D., Lee S. H. (2001) Cloning and characterization of a type II integral transmembrane protein gene, Itm2c, that is highly expressed in the mouse brain. *Mol. Cells* **12**, 391–7.

Daulat A. M., Maurice P., Froment C., Guillaume J.-L., Broussard C., Monsarrat B., Delagrange P., Jockers R. (2007) Purification and identification of G protein-coupled receptor protein complexes under native conditions. *Mol. Cell. Proteomics* **6**, 835–44.

del-Toro N., Dumousseau M., Orchard S., Jimenez R. C., Galeota E., Launay G., Goll J., et al. (2013) A new reference implementation of the PSICQUIC web service. *Nucleic Acids Res.* **41**, W601-6.

Doncheva N. T., Assenov Y., Domingues F. S., Albrecht M. (2012) Topological analysis and interactive visualization of biological networks and protein structures. *Nat. Protoc.* **7**, 670–685.

Esteves S. L. C., Korrodi-Gregório L., Cotrim C. Z., Kleeff P. J. M. van, Domingues S. C., Cruz e Silva O. A. B. da, Fardilha M., Cruz e Silva E. F. da (2013) Protein phosphatase 1γ isoforms linked interactions in the brain. *J. Mol. Neurosci.* **50**, 179–97.

Gong Y., Wu J., Qiang H., Liu B., Chi Z., Chen T., Yin B., Peng X., Yuan J. (2008) BRI3 associates with SCG10 and attenuates NGF-induced neurite outgrowth in PC12 cells. *BMB Rep.* **41**, 287–93.

Gupta G. D., Coyaud É., Gonçalves J., Mojarad B. A., Liu Y., Wu Q., Gheiratmand L., et al. (2015) A Dynamic Protein Interaction Landscape of the Human Centrosome-Cilium Interface. *Cell* **163**, 1484–99.

Hanson D., Stevens A., Murray P. G., Black G. C. M., Clayton P. E. (2014) Identifying biological pathways that underlie primordial short stature using network analysis. *J. Mol. Endocrinol.* **52**, 333–44.

Hodge K., Have S., Hutton L., Lamond A. (2013) Cleaning up the masses: Exclusion lists to reduce contamination with HPLC-MS/MS. *J. Proteomics* **88**, 92–103.

Hoe H.-S., Fu Z., Makarova A., Lee J.-Y., Lu C., Feng L., Pajoohesh-Ganji A., et al. (2009) The Effects of Amyloid Precursor Protein on Postsynaptic Composition and Activity. *J. Biol. Chem.* **284**, 8495–8506.

Huttlin E. L., Ting L., Bruckner R. J., Gebreab F., Gygi M. P., Szpyt J., Tam S., et al. (2015) The BioPlex Network: A Systematic Exploration of the Human Interactome. *Cell* **162**, 425–40.

Isaac J. T. R., Ashby M. C., McBain C. J., Biagini G., Agnati L. F., Muller R. U., Roder J. C., et al. (2007) The role of the GluR2 subunit in AMPA receptor function and synaptic plasticity. *Neuron* **54**, 859–71.

Iwakura Y., Nawa H. (2013) ErbB1-4-dependent EGF/neuregulin signals and their cross talk in the central nervous system: pathological implications in schizophrenia and Parkinson's disease. *Front. Cell. Neurosci.* **7**, 4.

Jahn R., Fasshauer D. (2012) Molecular machines governing exocytosis of synaptic vesicles. *Nature* **490**, 201–207.

Kawai J., Shinagawa A., Shibata K., Yoshino M., Itoh M., Ishii Y., Arakawa T., et al. (2001) Gateways to the FANTOM5 promoter level mammalian expression atlas. *Nature* **409**, 685–690.

Las Rivas J. De, Fontanillo C. (2010) Protein-protein interactions essentials: key concepts to building and analyzing interactome networks. *PLoS Comput. Biol.* **6**, e1000807.

Lasiecka Z. M., Winckler B. (2011) Mechanisms of polarized membrane trafficking in neurons — Focusing in on endosomes. *Mol. Cell. Neurosci.* **48**, 278–287.

Liu X., Yu X., Zack D. J., Zhu H., Qian J. (2008) TiGER: a database for tissue-specific gene expression and regulation. *BMC Bioinformatics* **9**, 271.

Maeder C. I., Shen K., Hoogenraad C. C. (2014) Axon and dendritic trafficking. *Curr. Opin. Neurobiol.* **27**, 165–170.

Martins F., Rebelo S., Santos M., Cotrim C. Z., Cruz E Silva E. F. da, Cruz E Silva O. A. B. da (2016) BRI2 and BRI3 are functionally distinct phosphoproteins. *Cell. Signal.* **28**, 130–44.

Matsuda S., Matsuda Y., D'Adamio L. (2009) BRI3 inhibits amyloid precursor protein processing in a mechanistically distinct manner from its homologue dementia gene BRI2. *J. Biol. Chem.* **284**, 15815–25.

Mattson M. P. (1999) Establishment and plasticity of neuronal polarity. *J. Neurosci. Res.* **57**, 577–89.

Mehta V., Trinkle-Mulcahy L. (2016) Recent advances in large-scale protein interactome mapping. *F1000Research* **5**, 782.

Mei L., Nave K.-A. (2014) Neuregulin-ERBB signaling in the nervous system and neuropsychiatric diseases. *Neuron* **83**, 27–49.

Mi H., Muruganujan A., Casagrande J. T., Thomas P. D. (2013) Large-scale gene function analysis with the PANTHER classification system. *Nat. Protoc.* **8**, 1551–1566.

Mi H., Poudel S., Muruganujan A., Casagrande J. T., Thomas P. D. (2016) PANTHER version 10: expanded protein families and functions, and analysis tools. *Nucleic Acids Res.* **44**, D336–D342.

Na C. H., Jones D. R., Yang Y., Wang X., Xu Y., Peng J. (2012) Synaptic protein ubiquitination in rat brain revealed by antibody-based ubiquitome analysis. *J. Proteome Res.* **11**, 4722–32.

Newman M. E. J. (2006) Modularity and community structure in networks. *Proc. Natl. Acad. Sci. U. S. A.* **103**, 8577–82.

Oliveira J. M., Henriques A. G., Martins F., Rebelo S., Cruz E Silva O. A. B. da (2015) Amyloid-β Modulates Both AβPP and Tau Phosphorylation. *J. Alzheimers. Dis.*

Perron J. C., Bixby J. L. (1999) Distinct Neurite Outgrowth Signaling Pathways Converge on ERK Activation. *Mol. Cell. Neurosci.* **13**, 362–378.

Piñero J., Bravo À., Queralt-Rosinach N., Gutiérrez-Sacristán A., Deu-Pons J., Centeno E., García-García J., Sanz F., Furlong L. I. (2017) DisGeNET: a comprehensive platform integrating information on human disease-associated genes and variants. *Nucleic Acids Res.* **45**, D833–D839.

Reichardt L. F. (2006) Neurotrophin-regulated signalling pathways. *Philos. Trans. R. Soc. Lond. B. Biol. Sci.* **361**, 1545–64.

Rual J.-F., Venkatesan K., Hao T., Hirozane-Kishikawa T., Dricot A., Li N., Berriz G. F., et al. (2005) Towards

a proteome-scale map of the human protein-protein interaction network. *Nature* **437**, 1173–8.

Saheki Y., Camilli P. De (2012) Synaptic Vesicle Endocytosis. *Cold Spring Harb. Perspect. Biol.* **4**, a005645–a005645.

Santos M., Domingues S. C., Costa P., Muller T., Galozzi S., Marcus K., Cruz E Silva E. F. da, Cruz E Silva O. A. da, Rebelo S. (2014) Identification of a Novel Human LAP1 Isoform That Is Regulated by Protein Phosphorylation. *PLoS One* **9**, e113732.

Shannon P., Markiel A., Ozier O., Baliga N. S., Wang J. T., Ramage D., Amin N., Schwikowski B., Ideker T. (2003) Cytoscape: A Software Environment for Integrated Models of Biomolecular Interaction Networks. *Genome Res.* **13**, 2498–2504.

Snyder E. M., Nong Y., Almeida C. G., Paul S., Moran T., Choi E. Y., Nairn A. C., et al. (2005) Regulation of NMDA receptor trafficking by amyloid-β. *Nat. Neurosci.* **8**, 1051–1058.

Spires T. L., Meyer-Luehmann M., Stern E. A., McLean P. J., Skoch J., Nguyen P. T., Bacskai B. J., Hyman B. T. (2005) Dendritic Spine Abnormalities in Amyloid Precursor Protein Transgenic Mice Demonstrated by Gene Transfer and Intravital Multiphoton Microscopy. *J. Neurosci.* **25**, 7278–7287.

Stelzl U., Worm U., Lalowski M., Haenig C., Brembeck F. H., Goehler H., Stroedicke M., et al. (2005) A human protein-protein interaction network: a resource for annotating the proteome. *Cell* **122**, 957–68.

Tahirovic S., Bradke F. (2009) Neuronal Polarity. *Cold Spring Harb. Perspect. Biol.* **1**, a001644–a001644.

Takeda K., Ichijo H. (2002) Neuronal p38 MAPK signalling: an emerging regulator of cell fate and function in the nervous system. *Genes to Cells* **7**, 1099–1111.

Uhlen M., Björling E., Agaton C., Szigyarto C. A.-K., Amini B., Andersen E., Andersson A.-C., et al. (2005) A Human Protein Atlas for Normal and Cancer Tissues Based on Antibody Proteomics. *Mol. Cell. Proteomics* **4**, 1920–1932.

Uhlén M., Fagerberg L., Hallström B. M., Lindskog C., Oksvold P., Mardinoglu A., Sivertsson Å., et al. (2015) Tissue-based map of the human proteome. *Science (80-.).* **347**.

Uhlen M., Oksvold P., Fagerberg L., Lundberg E., Jonasson K., Forsberg M., Zwahlen M., et al. (2010) Towards a knowledge-based Human Protein Atlas. *Nat. Biotechnol.* **28**, 1248–1250.

Vidal R., Calero M., Révész T., Plant G., Ghiso J., Frangione B. (2001) Sequence, genomic structure and tissue expression of Human BRI3, a member of the BRI gene family. *Gene* **266**, 95–102.

Wang L., Andersson S., Warner M., Gustafsson J.-A. (2003) Estrogen receptor (ER) knockout mice reveal a role for ER in migration of cortical neurons in the developing brain. *Proc. Natl. Acad. Sci.* **100**, 703–708.

Wheeler D. L., Church D. M., Federhen S., Lash A. E., Madden T. L., Pontius J. U., Schuler G. D., et al. (2003) Database resources of the National Center for Biotechnology. *Nucleic Acids Res.* **31**, 28–33.

Wickham L., Benjannet S., Marcinkiewicz E., Chretien M., Seidah N. G. (2005) Beta-amyloid protein converting enzyme 1 and brain-specific type II membrane protein BRI3: binding partners processed by furin. *J. Neurochem.* **92**, 93–102.

Supplementary Data

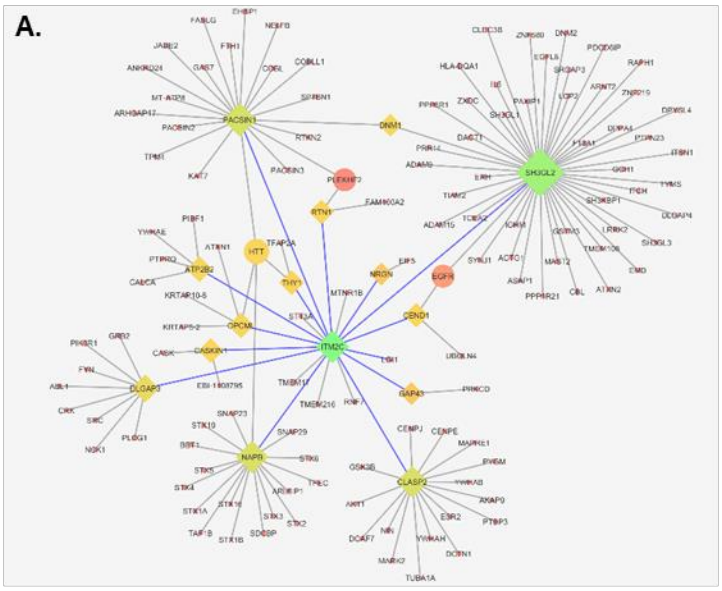
A.
PACSIN1
SH3GL2
ITM2C
NAP1
CLASP2
DLGAP3
BASP1
HTT
DNM1
RTN1
TRAF3IP1
CENDI
EGFR
GRIA2
DCX
B.
C.
CAMK2A
ITM2C
SH3GL2
NEFL
MBP
ERC2
CLIP2
APP
CHD3
PRG2

Figure III.B.S 1 - BRI3 ES-based region specific sub-networks for the cerebral cortex (A), hippocampus (B) and striatum (C). Diamond nodes represent the proteins identified in this study. Node colors are represented according to the betweenness-centrality, in which green corresponds to higher betweenness-centrality and red to lower betweenness-centrality. Node size according to the degree in the network. Edge color represent the source of interaction: blue edges correspond to connections between proteins identified in this study in the cortex, and grey edges correspond to connections between proteins added by network annotation.

Table III.B.S 1- Novel BRI3 interacting protein candidates. Uniprot accession numbers, gene and protein names, are listed, as well as the rat brain tissues in where the proteins were found. CX, cortex; HP, hippocampus; ST, striatum.

Uniprot accession	Gene name	Protein name	Brain regions
P26772	**Hspe1**	10 kDa heat shock protein, mitochondrial	HP
P68255	**Ywhaq**	14-3-3 protein theta	CX
P63102	**Ywhaz**	14-3-3 protein zeta/delta	ST
P13233	**Cnp**	2',3'-cyclic-nucleotide 3'-phosphodiesterase	CX, HP, ST
P62282	**Rps11**	40S ribosomal protein S11	HP
P62850	**Rps24**	40S ribosomal protein S24	ST
P62856	**Rps26**	40S ribosomal protein S26	HP
P62909	**Rps3**	40S ribosomal protein S3	ST
P62703	**Rps4x**	40S ribosomal protein S4, X isoform	HP
P62083	**Rps7**	40S ribosomal protein S7	HP, ST
P62243	**Rps8**	40S ribosomal protein S8	HP
P63039	**Hspd1**	60 kDa heat shock protein, mitochondrial	ST
P19945	**Rplp0**	60S acidic ribosomal protein P0	HP, ST
P62914	**Rpl11**	60S ribosomal protein L11	CX
P47198	**Rpl22**	60S ribosomal protein L22	CX, ST
P06761	**Hspa5**	78 kDa glucose-regulated protein	ST
P60711	**Actb**	Actin, cytoplasmic 1	CX, HP, ST
P63269	**Actg2**	Actin, gamma-enteric smooth muscle	HP, ST
Q6KC51	**Ablim2**	Actin-binding LIM protein 2	HP
Q5M7U6	**Actr2**	Actin-related protein 2	HP
Q05962	**Slc25a4**	ADP/ATP translocase 1	HP, ST
Q09073	**Slc25a5**	ADP/ATP translocase 2	HP, ST
Q5QE80	**Aox3**	Aldehyde oxidase 3	CX
Q9Z1P2	**Actn1**	Alpha-actinin-1	CX
Q63028	**Add1**	Alpha-adducin	HP
P04764	**Eno1**	Alpha-enolase	ST
P02773	**Afp**	Alpha-fetoprotein	ST
P23565	**Ina**	Alpha-internexin	HP, ST
P02667	**Csn1s2a**	Alpha-S2-casein-like A	ST
P08592	**App**	Amyloid beta A4 protein	CX
P00762	**Prss1**	Anionic trypsin-1	ST
P0C6S7	**Anks1b**	Ankyrin repeat and sterile alpha motif domain-containing protein 1B	CX, HP
P07150	**Anxa1**	Annexin A1	HP, ST
Q07936	**Anxa2**	Annexin A2	CX

Uniprot accession	Gene name	Protein name	Brain regions
P52303	**Ap1b1**	AP-1 complex subunit beta-1	ST
P18484	**Ap2a2**	AP-2 complex subunit alpha-2	CX, ST
P62944	**Ap2b1**	AP-2 complex subunit beta	HP
P84092	**Ap2m1**	AP-2 complex subunit mu	HP, ST
P12527	**Alox5**	Arachidonate 5-lipoxygenase	ST
Q8CGU4	**Agap2**	Arf-GAP with GTPase, ANK repeat and PH domain-containing protein 2	HP
P15999	**Atp5a1**	ATP synthase subunit alpha, mitochondrial	ST
P10719	**Atp5b**	ATP synthase subunit beta, mitochondrial	HP, ST
Q6PDU7	**Atp5l**	ATP synthase subunit g, mitochondrial	CX, HP, ST
P35435	**Atp5c1**	ATP synthase subunit gamma, mitochondrial	CX, HP
Q06647	**Atp5o**	ATP synthase subunit O, mitochondrial	CX, ST
Q9ESS6	**Bcam**	Basal cell adhesion molecule	HP
P85969	**Napb**	Beta-soluble NSF attachment protein	CX
Q05175	**Basp1**	Brain acid soluble protein 1	HP
P11275	**Camk2a**	Calcium/calmodulin-dependent protein kinase type II subunit alpha	ST
P08413	**Camk2b**	Calcium/calmodulin-dependent protein kinase type II subunit beta	CX, HP, ST
P15791	**Camk2d**	Calcium/calmodulin-dependent protein kinase type II subunit delta	ST
P11730	**Camk2g**	Calcium/calmodulin-dependent protein kinase type II subunit gamma	HP
P62161	**Calm1**	Calmodulin	CX, HP, ST
P68182	**Prkacb**	cAMP-dependent protein kinase catalytic subunit beta	HP, ST
P12369	**Prkar2b**	cAMP-dependent protein kinase type II-beta regulatory subunit	ST
O55156	**Clip2**	CAP-Gly domain-containing linker protein 2	ST
Q8VHK2	**Caskin1**	Caskin-1	CX
Q9WU82	**Ctnnb1**	Catenin beta-1	CX
Q5FVI4	**Cend1**	Cell cycle exit and neuronal differentiation protein 1	CX
Q4KLH6	**Cep162**	Centrosomal protein of 162 kDa	ST
Q05140	**Snap91**	Clathrin coat assembly protein AP180	HP
P11442	**Cltc**	Clathrin heavy chain 1	HP, ST
P08081	**Clta**	Clathrin light chain A	ST
Q99P82	**Cldn11**	Claudin-11	CX, HP, ST
Q99JD4	**Clasp2**	CLIP-associating protein 2	CX
P45592	**Cfl1**	Cofilin-1	HP
P31720	**C1qa**	Complement C1q subcomponent subunit A	HP
P31721	**C1qb**	Complement C1q subcomponent subunit B	HP, ST
P31722	**C1qc**	Complement C1q subcomponent subunit C	HP, ST
P01026	**C3**	Complement C3	HP
Q9Z1T4	**Cnksr2**	Connector enhancer of kinase suppressor of ras 2	HP
Q63198	**Cntn1**	Contactin-1	CX, HP, ST
Q5BJS7	**Cpne9**	Copine-9	HP
Q02874	**H2afy**	Core histone macro-H2A.1	HP
P07335	**Ckb**	Creatine kinase B-type	HP
O08565	**Cxcr4**	C-X-C chemokine receptor type 4	ST

Uniprot accession	Gene name	Protein name	Brain regions
Q68FY0	**Uqcrc1**	Cytochrome b-c1 complex subunit 1, mitochondrial	HP
P32551	**Uqcrc2**	Cytochrome b-c1 complex subunit 2, mitochondrial	CX, HP
P00406	**Mtco2**	Cytochrome c oxidase subunit 2	HP, ST
P11240	**Cox5a**	Cytochrome c oxidase subunit 5A, mitochondrial	CX
P62898	**Cycs**	Cytochrome c, somatic	HP
P08461	**Dlat**	Dihydrolipoyllysine-residue acetyltransferase component of pyruvate dehydrogenase complex, mitochondrial	HP, ST
Q62950	**Crmp1**	Dihydropyrimidinase-related protein 1	CX, HP, ST
P47942	**Dpysl2**	Dihydropyrimidinase-related protein 2	CX, HP, ST
Q62952	**Dpysl3**	Dihydropyrimidinase-related protein 3	CX
Q63622	**Dlg2**	Disks large homolog 2	CX, HP, ST
P31016	**Dlg4**	Disks large homolog 4	CX, HP, ST
P97838	**Dlgap3**	Disks large-associated protein 3	CX
P97839	**Dlgap4**	Disks large-associated protein 4	HP
P60905	**Dnajc5**	DnaJ homolog subfamily C member 5	HP
Q07266	**Dbn1**	Drebrin	CX, HP, ST
P21575	**Dnm1**	Dynamin-1	HP, ST
Q2TA68	**Opa1**	Dynamin-like 120 kDa protein, mitochondrial	ST
B0BND0	**Enpp6**	Ectonucleotide pyrophosphatase/phosphodiesterase family member 6	ST
P62630	**Eef1a1**	Elongation factor 1-alpha 1	HP, ST
P85834	**Tufm**	Elongation factor Tu, mitochondrial	CX, HP, ST
O35179	**Sh3gl2**	Endophilin-A1	CX
P05432	**Errfi1**	ERBB receptor feedback inhibitor 1	CX
Q8K3M6	**Erc2**	ERC protein 2	ST
P24942	**Slc1a3**	Excitatory amino acid transporter 1	HP, ST
P31596	**Slc1a2**	Excitatory amino acid transporter 2	HP, ST
Q3T1K5	**Capza2**	F-actin-capping protein subunit alpha-2	HP, ST
Q5XI32	**Capzb**	F-actin-capping protein subunit beta	CX
P08050	**Gja1**	Gap junction alpha-1 protein	HP
Q68FP1	**Gsn**	Gelsolin	HP, ST
P47819	**Gfap**	Glial fibrillary acidic protein	CX, ST
P19491	**Gria2**	Glutamate receptor 2	HP
P35439	**Grin1**	Glutamate receptor ionotropic, NMDA 1	HP
Q00960	**Grin2b**	Glutamate receptor ionotropic, NMDA 2B	HP
P04797	**Gapdh**	Glyceraldehyde-3-phosphate dehydrogenase	ST
Q62638	**Glg1**	Golgi apparatus protein 1	ST
Q9WTT6	**Gda**	Guanine deaminase	HP
P43425	**Gng7**	Guanine nucleotide-binding protein G	CX
P10824	**Gnai1**	Guanine nucleotide-binding protein G	CX
P59215	**Gnao1**	Guanine nucleotide-binding protein G	HP
P19627	**Gnaz**	Guanine nucleotide-binding protein G	HP
P52287	**Gnb3**	Guanine nucleotide-binding protein G	HP, ST
Q6Q7Y5	**Gna13**	Guanine nucleotide-binding protein subunit alpha-13	ST

Uniprot accession	Gene name	Protein name	Brain regions
P63018	**Hspa8**	Heat shock cognate 71 kDa protein	HP
Q5XHZ0	**Trap1**	Heat shock protein 75 kDa, mitochondrial	CX
P82995	**Hsp90aa1**	Heat shock protein HSP 90-alpha	ST
P34058	**Hsp90ab1**	Heat shock protein HSP 90-beta	CX
P04256	**Hnrnpa1**	Heterogeneous nuclear ribonucleoprotein A1	HP
Q6URK4	**Hnrnpa3**	Heterogeneous nuclear ribonucleoprotein A3	CX
G3V9R8	**Hnrnpc**	Heterogeneous nuclear ribonucleoprotein C	HP
Q9JJ54	**Hnrnpd**	Heterogeneous nuclear ribonucleoprotein D0	HP
Q8VHV7	**Hnrnph1**	Heterogeneous nuclear ribonucleoprotein H	HP
Q6AY09	**Hnrnph2**	Heterogeneous nuclear ribonucleoprotein H2	ST
P61980	**Hnrnpk**	Heterogeneous nuclear ribonucleoprotein K	CX, HP
F1LQ48	**Hnrnpl**	Heterogeneous nuclear ribonucleoprotein L	HP
Q62826	**Hnrnpm**	Heterogeneous nuclear ribonucleoprotein M	HP
A7VJC2	**Hnrnpa2b1**	Heterogeneous nuclear ribonucleoproteins A2/B1	HP, ST
P06349	**Hist1h1t**	Histone H1t	ST
A9UMV8	**H2afj**	Histone H2A.J	HP, ST
P0C0S7	**H2afz**	Histone H2A.Z	CX, ST
P84245	**H3f3b**	Histone H3.3	ST
P62804	**Hist1h4b**	Histone H4	HP, ST
Q9Z214	**Homer1**	Homer protein homolog 1	CX, ST
P03994	**Hapln1**	Hyaluronan and proteoglycan link protein 1	CX, HP, ST
P17105	**Itpka**	Inositol-trisphosphate 3-kinase A	HP
Q5PQL7	**Itm2c**	Integral membrane protein 2C	HP
Q99NA5	**Idh3a**	Isocitrate dehydrogenase [NAD] subunit alpha, mitochondrial	HP
Q9QYU4	**Crym**	Ketimine reductase mu-crystallin	CX, HP, ST
O35787	**Kif1c**	Kinesin-like protein KIF1C	CX
Q9WV63	**Kif2a**	Kinesin-like protein KIF2A	HP
Q8K4Y5	**Lgi1**	Leucine-rich glioma-inactivated protein 1	CX
P43244	**Matr3**	Matrin-3	CX, HP
D4A7N1	**Chchd6**	MICOS complex subunit Mic25	ST
Q3KR86	**Immt**	MICOS complex subunit Mic60	CX, HP, ST
P34926	**Map1a**	Microtubule-associated protein 1A	HP
P15205	**Map1b**	Microtubule-associated protein 1B	CX, HP, ST
P15146	**Map2**	Microtubule-associated protein 2	CX, ST
Q5M7W5	**Map4**	Microtubule-associated protein 4	CX, HP, ST
Q63560	**Map6**	Microtubule-associated protein 6	CX, HP
P19332	**Mapt**	Microtubule-associated protein tau	CX, ST
P97700	**Slc25a11**	Mitochondrial 2-oxoglutarate/malate carrier protein	HP
Q505J6	**Slc25a18**	Mitochondrial glutamate carrier 2	CX, HP
Q75Q39	**Tomm70**	Mitochondrial import receptor subunit TOM70	ST
P02688	**Mbp**	Myelin basic protein	ST
P60203	**Plp1**	Myelin proteolipid protein	ST

Uniprot accession	Gene name	Protein name	Brain regions
Q63345	**Mog**	Myelin-oligodendrocyte glycoprotein	CX, HP, ST
Q9QZ76	**Mb**	Myoglobin	CX
Q9WUJ3	**Pde4dip**	Myomegalin	CX
P16409	**Myl3**	Myosin light chain 3	ST
Q64119	**Myl6**	Myosin light polypeptide 6	HP, ST
Q64122	**Myl9**	Myosin regulatory light polypeptide 9	CX
Q9JLT0	**Myh10**	Myosin-10	CX, HP, ST
P02563	**Myh6**	Myosin-6	CX
Q62812	**Myh9**	Myosin-9	HP
Q5RJQ4	**Sirt2**	NAD-dependent protein deacetylase sirtuin-2	CX
P19234	**Ndufv2**	NADH dehydrogenase [ubiquinone] flavoprotein 2, mitochondrial	CX, HP, ST
Q5BK63	**Ndufa9**	NADH dehydrogenase 1 alpha subcomplex subunit 9, mitochondrial	HP
Q66HF1	**Ndufs1**	NADH-ubiquinone oxidoreductase 75 kDa subunit, mitochondrial	HP, ST
P55161	**Nckap1**	Nck-associated protein 1	HP
O35867	**Ppp1r9a**	Neurabin-1	HP, ST
P55067	**Ncan**	Neurocan core protein	ST
P97685	**Nfasc**	Neurofascin	HP
P16884	**Nefh**	Neurofilament heavy polypeptide	CX, HP, ST
P19527	**Nefl**	Neurofilament light polypeptide	ST
P12839	**Nefm**	Neurofilament medium polypeptide	CX, ST
Q04940	**Nrgn**	Neurogranin	CX
P07936	**Gap43**	Neuromodulin	CX
Q9ESI7	**Dcx**	Neuronal migration protein doublecortin	HP
O09017	**Nr2f6**	Nuclear receptor subfamily 2 group F member 6	HP
P13084	**Npm1**	Nucleophosmin	HP, ST
P32736	**Opcml**	Opioid-binding protein/cell adhesion molecule	CX
Q63425	**Prx**	Periaxin	ST
P62024	**Phactr1**	Phosphatase and actin regulator 1	ST
P16036	**Slc25a3**	Phosphate carrier protein, mitochondrial	HP, ST
P16617	**Pgk1**	Phosphoglycerate kinase 1	HP
P11505	**Atp2b1**	Plasma membrane calcium-transporting ATPase 1	HP, ST
P11506	**Atp2b2**	Plasma membrane calcium-transporting ATPase 2	CX
Q64542	**Atp2b4**	Plasma membrane calcium-transporting ATPase 4	HP, ST
P30427	**Plec**	Plectin	CX, HP, ST
P0CG51	**Ubb**	Polyubiquitin-B	ST
P17659	**Kcna6**	Potassium voltage-gated channel subfamily A member 6	CX, ST
P48679	**Lmna**	Prelamin-A/C	CX
P62963	**Pfn1**	Profilin-1	HP
P67779	**Phb**	Prohibitin	HP, ST
Q5XIH7	**Phb2**	Prohibitin-2	CX, HP
Q62969	**Ptgis**	Prostacyclin synthase	HP
O88778	**Bsn**	Protein bassoon	CX, HP

Uniprot accession	Gene name	Protein name	Brain regions
Q9Z0W5	**Pacsin1**	Protein kinase C and casein kinase substrate in neurons protein 1	CX
P63319	**Prkcg**	Protein kinase C gamma type	CX, HP, ST
Q9JKS6	**Pclo**	Protein piccolo	ST
P26284	**Pdha1**	Pyruvate dehydrogenase E1 component subunit alpha, somatic form, mitochondrial	HP
P49432	**Pdhb**	Pyruvate dehydrogenase E1 component subunit beta, mitochondrial	CX, HP
P11980	**Pkm**	Pyruvate kinase PKM	HP, ST
F1M386	**Rapgef2**	Rap guanine nucleotide exchange factor 2	HP
Q9QUH6	**Syngap1**	Ras/Rap GTPase-activating protein SynGAP	CX, HP, ST
Q6NYB7	**Rab1A**	Ras-related protein Rab-1A	HP
P05712	**Rab2a**	Ras-related protein Rab-2A	HP
P63012	**Rab3a**	Ras-related protein Rab-3A	CX, ST
Q63941	**Rab3b**	Ras-related protein Rab-3B	ST
P62824	**Rab3c**	Ras-related protein Rab-3C	HP, ST
P09527	**Rab7a**	Ras-related protein Rab-7a	HP
Q9JIR4	**Rims1**	Regulating synaptic membrane exocytosis protein 1	HP
Q64548	**Rtn1**	Reticulon-1	CX
P0C6P5	**Arhgef28**	Rho guanine nucleotide exchange factor 28	HP
D4AE41	**Rbmxl1**	RNA binding motif protein, X-linked-like-1	HP
P11507	**Atp2a2**	Sarcoplasmic/endoplasmic reticulum calcium ATPase 2	HP, ST
B3GNI6	**Sept11**	Septin-11	HP, ST
Q9JJM9	**Sept5**	Septin-5	CX, HP
Q5MPA9	**Dclk2**	Serine/threonine-protein kinase DCLK2	HP
Q9WV48	**Shank1**	SH3 and multiple ankyrin repeat domains protein 1	HP
Q9QX74	**Shank2**	SH3 and multiple ankyrin repeat domains protein 2	CX, HP
Q9JLU4	**Shank3**	SH3 and multiple ankyrin repeat domains protein 3	ST
Q63965	**Sfxn1**	Sideroflexin-1	ST
Q9JHY2	**Sfxn3**	Sideroflexin-3	HP
Q8CFD0	**Sfxn5**	Sideroflexin-5	HP
P48768	**Slc8a2**	Sodium/calcium exchanger 2	HP
P06685	**Atp1a1**	Sodium/potassium-transporting ATPase subunit alpha-1	ST
P06687	**Atp1a3**	Sodium/potassium-transporting ATPase subunit alpha-3	CX, HP, ST
O35413	**Sorbs2**	Sorbin and SH3 domain-containing protein 2	HP, ST
P16086	**Sptan1**	Spectrin alpha chain, non-erythrocytic 1	HP
Q9QWN8	**Sptbn2**	Spectrin beta chain, non-erythrocytic 2	CX, HP, ST
Q9QXY2	**Srcin1**	SRC kinase signaling inhibitor 1	CX, HP, ST
P48721	**Hspa9**	Stress-70 protein, mitochondrial	CX, HP
P09951	**Syn1**	Synapsin-1	CX, HP, ST
Q63537	**Syn2**	Synapsin-2	HP
Q62876	**Syngr1**	Synaptogyrin-1	CX
P07825	**Syp**	Synaptophysin	CX, HP, ST
P60881	**Snap25**	Synaptosomal-associated protein 25	CX, HP
Q6P6S0	**Snap47**	Synaptosomal-associated protein 47	CX

Uniprot accession	Gene name	Protein name	Brain regions
P21707	**Syt1**	Synaptotagmin-1	CX, HP, ST
P61265	**Stx1b**	Syntaxin-1B	CX, HP, ST
P61765	**Stxbp1**	Syntaxin-binding protein 1	CX, HP, ST
Q05546	**Tnr**	Tenascin-R	HP
Q568Y5	**Tspan11**	Tetraspanin-11	CX
P01830	**Thy1**	Thy-1 membrane glycoprotein	CX
P86252	**Pura**	Transcriptional activator protein Pur-alpha	HP, ST
Q68A21	**Purb**	Transcriptional activator protein Pur-beta	HP
Q5XIA3	**Lcmt2**	tRNA wybutosine-synthesizing protein 4	CX
P04692	**Tpm1**	Tropomyosin alpha-1 chain	HP, ST
P09495	**Tpm4**	Tropomyosin alpha-4 chain	CX
P68370	**Tuba1a**	Tubulin alpha-1A chain	HP
Q6AYZ1	**Tuba1c**	Tubulin alpha-1C chain	HP, ST
Q68FR8	**Tuba3**	Tubulin alpha-3 chain	CX
Q5XIF6	**Tuba4a**	Tubulin alpha-4A chain	HP, ST
Q6AY56	**Tuba8**	Tubulin alpha-8 chain	HP
P85108	**Tubb2a**	Tubulin beta-2A chain	HP, ST
Q3KRE8	**Tubb2b**	Tubulin beta-2B chain	HP, ST
Q4QRB4	**Tubb3**	Tubulin beta-3 chain	HP, ST
Q6P9T8	**Tubb4b**	Tubulin beta-4B chain	HP, ST
P69897	**Tubb5**	Tubulin beta-5 chain	HP, ST
Q9QYF3	**Myo5a**	Unconventional myosin-Va	CX, HP, ST
P63045	**Vamp2**	Vesicle-associated membrane protein 2	CX, HP
Q9Z270	**Vapa**	Vesicle-associated membrane protein-associated protein A	CX
Q9QUL6	**Nsf**	Vesicle-fusing ATPase	HP, ST
P31000	**Vim**	Vimentin	CX, ST
Q9Z2L0	**Vdac1**	Voltage-dependent anion-selective channel protein 1	HP, ST
P81155	**Vdac2**	Voltage-dependent anion-selective channel protein 2	CX, HP, ST
Q9R1Z0	**Vdac3**	Voltage-dependent anion-selective channel protein 3	CX, HP, ST
P62815	**Atp6v1b2**	V-type proton ATPase subunit B, brain isoform	CX

Table III.B.S 2 – BRI3 protein interactors obtained from online databases. Information about the identified BRI3 interactors, as well as, the UniProt accession number, the species and the experimental evidence supporting the interactions, as well as the cell line or tissue where was detected.

Gene	Protein	Uniprot accession number	Species	Experimental evidence	Cell line/Tissue	References
APP	Amyloid beta A4 protein	P05067	*Homo sapiens*	Two-hybrid Co-IP	HeLa cells co-transfected with BRI3 and APP cDNAs	(Matsuda *et al.* 2009)
BACE1	β-secretase β-amyloid protein converting enzyme 1	P56817	*Homo sapiens*	Two-hybrid Co-IP	HEK293 cells co-transfected with BRI3 and BACE1 cDNAs	(Wickham *et al.* 2005)
CUL7	Cullin-7	Q14999	*Homo sapiens*	Affinity Capture-MS	HEK293 cells transfected with CUL7 cDNA	(Hanson *et al.* 2014)
Dlg4	Disks large homolog 4	P31016	BRI3 *Hs* – Dlg4 *Rat*	Peptide array assay	----	(Arbuckle *et al.* 2010)
		Q62108	BRI3 *Hs* – Dlg4 *Ms*	Peptide array assay	----	(Arbuckle *et al.* 2010)
FURIN	Furin	P09958	*Homo sapiens*	*in vivo* assay	CHO-FD11 cells	(Wickham *et al.* 2005)
LLGL2	Lethal(2) giant larvae protein homolog 2	Q6P1M3	*Homo sapiens*	Peptide array assay	----	(Arbuckle *et al.* 2010)
MTNR1B	Melatonin receptor type 1B	P49286	*Homo sapiens*	Tandem affinity purification- MS	HEK293 cells	(Daulat *et al.* 2007)
MVB12B	Multivesicular body subunit 12B	Q9H7P6	*Homo sapiens*	Affinity Capture-MS	HEK293 cells	(Huttlin *et al.* 2015)
PPP1CA/Ppp1ca	Serine/threonine-protein phosphatase PP1-alpha catalytic subunit	P62136	Homo sapiens	Co-IP	SH-SY5Y cells transfected BRI3 cDNA	(Martins *et al.* 2016)
		P62138	*Homo sapiens*	Co-IP	Rat primary cortical and hippocampal cultures	
PPP1CC/Ppp1cc	Serine/threonine-protein phosphatase PP1-gamma catalytic subunit	P36873	*Homo sapiens*	Two-hybrid Co-IP	SH-SY5Y cells transfected BRI3 cDNA	(Esteves *et al.* 2013; Martins *et al.* 2016)
		P63088	*Rattus norvergicus*	Co-IP	Rat primary cortical and hippocampal cultures	(Martins *et al.* 2016)
RNF7	RING-box protein 2	Q9UBF6	*Homo sapiens*	Two-hybrid	----	(Rual *et al.* 2005)
RYK	Tyrosine-protein kinase RYK	P34925	*Homo sapiens*	Tandem affinity purification- MS	HEK293 cells	(Berndt *et al.* 2011)
STMN2	Stathmin-2	Q93045	*Homo sapiens*	Co-IP	PC12 cells	(Gong *et al.* 2008)
STT3A	Dolichyl-diphosphooligosaccharide--protein glycosyltransferase subunit STT3A	P46977	*Homo sapiens*	Two-hybrid	----	(Stelzl *et al.* 2005)
TMEM17	Transmembrane protein 17	Q86X19	*Homo sapiens*	Proximity labeling technology	293 Flp-In T-REx cells	(Gupta *et al.* 2015)
TMEM216	Transmembrane protein 216	Q86X19	*Homo sapiens*	Proximity labeling technology	293 Flp-In T-REx cells	(Gupta *et al.* 2015)
Ubc	Polyubiquitin-C	Q63429	*Rattus norvergicus*	Affinity Capture-MS	Rat brain	(Na *et al.* 2012)

Co-IP, co-immunoprecipitation; MS, mass spectrometry; *Hs, Homo sapiens; Ms, Mus musculus; Rat, Rattus norvergicus.*

Table III.B.S 3 - Protein class enrichment analysis of the brain specific BRI2 interactome using Panther online resource. Enriched categories are identified as those with a p-value <0.05. Nr. Number.

GO term	Nr. proteins	Fold enrichment (%)	p-value	Associated proteins
tubulin (PC00228)	11	40.91	1.74E-12	Tubb2a,Tubb3,Tubb4b,Tuba3a,Tuba8,Tuba4a,Tubb2b,Tuba1a,Tubb5,Tuba1c,Tuba3a
microtubule family cytoskeletal protein (PC00157)	18	7.00	4.45E-08	Map1a,Kif2a,Tubb2a,Dnml,Tubb3,Clip2,Tubb4b,Kifl c,Tuba3a,Tuba8,Tuba4a,Tubb2b,Map1b,Tu ba1a,Tubb5,Opa1,Tuba1c,Tuba3a
cytoskeletal protein (PC00085)	54	5.83	3.44E-23	Map1a,Myh6,Sorbs2,Kif2a,Gfap,Sept11,Actg2,Tpm4,Myo5a,Cfl1,Tpml,Tubb2a,Dnml,Myl9,Tub b3,Clip2,Tubb4b,Nefm,Myl6,Capza2,Kifl c,Capzb,Pde4dip,Actn1,Vim,Myl3,Tuba3a,Nefl,Tuba8,T uba4a,Sept5,Tubb2b,Map1b,Plec,Sptan1,Myh10,Ctnnb1,Tuba1a,Tubb5,Dbn1,Lmna,Gsn,Sptbn2,A blim2,Opa1,Actb,Pacsin1,Myh9,Ina,Add1,Tuba1c,Syn1,Tuba3a,Syn2
anion channel (PC00049)	6	14.66	8.85E-04	Atp5a1,Vdac2,Vdac3,Atp6v1b2,Atp5b,Vdac1
ion channel (PC00133)	14	3.41	1.69E-02	Atp5a1,Atp1a3,Vdac2,Atp2a2,Atp2b1,Atp1a1,Vdac3,Atp2b2,Atp6v1b2,Gria2,Atp2b4,Grin2b,Atp 5b,Vdac1
transporter (PC00227)	27	2.26	1.62E-02	Atp5a1,Atp1a3,Atp5o,Slc25a11,Vdac2,Slc25a4,Slc25a18,Sfxn3,Stxbp1,Atp2a2,Atp2b1,Sfxn1,Atp 1a1,Slc8a2,Vdac3,Atp2b2,Sfxn5,Atp6v1b2,Gria2,Atp2b4,Grin2b,Slc1a2,Atp5b,Slc1a3,Slc25a5,Vd ac1,Slc25a3
actin binding motor protein (PC00040)	7	11.30	7.69E-04	Myh6,Tpm4,Myo5a,Tpml,Pde4dip,Myh10,Myh9
actin family cytoskeletal protein (PC00041)	27	5.80	9.14E-11	Myh6,Sorbs2,Actg2,Tpm4,Myo5a,Cfl1,Tpml,Myl9,Myl6,Capza2,Capzb,Pde4dip,Actn1,Myl3,Ple c,Sptan1,Myh10,Dbn1,Gsn,Sptbn2,Ablim2,Actb,Pacsin1,Myh9,Add1,Syn1,Syn2
heterotrimeric G-protein (PC00117)	6	10.06	7.25E-03	Gna13,Gnai1,Gnao1,Gnaz,Gng7,Gnb3
G-protein (PC00020)	12	4.41	5.03E-03	Sept11,Gna13,Eefl a1,Dnml,Gnai1,Gnao1,Sept5,Gnaz,Tufm,Gng7,Opa1,Gnb3
transmembrane receptor regulatory/adaptor protein (PC00226)	6	9.17	1.21E-02	Dlgap3,Anks1b,Dlg4,Ap2a2,Dlgap4,Caskin1
cation transporter (PC00068)	16	6.19	2.48E-06	Atp5a1,Atp1a3,Atp5o,Sfxn3,Atp2a2,Atp2b1,Sfxn1,Atp1a1,Slc8a2,Atp2b2,Sfxn5,Atp6v1b2,Atp2b 4,Slc1a2,Atp5b,Slc1a3
membrane trafficking regulatory protein (PC00151)	8	5.90	1.62E-02	Stxbp1,Syt1,Syp,Pacsin1,Syn1,Vapa,Syngr1,Syn2
membrane traffic protein (PC00150)	21	5.10	3.81E-07	Stxbp1,Syt1,Syp,Clta,Cltc,Stx1b,Ap1b1,Erc2,Rtn1,Ap2b1,Snap47,Pacsin1,Napb,Syn1,Cpne9,Vam p2,Vapa,Snap91,Snap25,Syngr1,Syn2
structural protein (PC00211)	10	5.35	4.84E-03	Clasp2,Gfap,Plp1,Nefm,Vim,Nefl,Mbp,Lmna,Ablim2,Ina
non-motor actin binding protein (PC00165)	12	5.21	9.70E-04	Cfl1,Capza2,Capzb,Actn1,Plec,Sptan1,Dbn1,Gsn,Sptbn2,Add1,Syn1,Syn2
chaperone (PC00072)	10	4.34	2.66E-02	Ywhaq,Hsp90aa1,Tomm70a,Hspe1,Clip2,Hsp90ab1,Ywhaz,Trap1,Hspd1,Npml

Table III.B.S 4 - KEGG pathway cluster analysis of the individual specific BRI3 interactors in cortex, hippocampus and striatum using the ClueGo plugin of the Cytoscape software. Enriched categories are identified as those with p-value <0.05.

KEGG term ID	KEGG Term	Nr. Genes	% Associated Genes	Term pValue	Genes Cluster #1 (cortex specific BRI3 interactors)	Genes Cluster #2 (hippocampus specific BRI3 interactors)	Genes Cluster #3 (striatum specific BRI3 interactors)
KEGG:0004012	ErbB signaling pathway	18.00	20.45	1.80E-11	ABL1, AKT1, CBL, CRK, EGFR, GRB2, GSK3B, NCK1, PIK3R1, PLCG1, SRC	ABL1, CAMK2A, CRK, ERBB4, GRB2, JUN, MYC, NCK1	CAMK2A, CAMK2B, CAMK2D, CAMK2G
KEGG:0004130	SNARE interactions in vesicular transport	11.00	32.35	4.50E-09	BET1, SNAP23, SNAP29, STX16, STX19, STX1A, STX1B, STX3, STX4, STX5, STX6		
KEGG:0004722	Neurotrophin signaling pathway	16.00	13.22	3.70E-07	ABL1, AKT1, CRK, FASLG, GRB2, GSK3B, PIK3R1, PLCG1, PRKCD, YWHAE	ABL1, CAMK2A, CRK, GRB2, JUN	CALM1, CAMK2A, CAMK2B, CAMK2D, CAMK2G
KEGG:0005205	Proteoglycans in cancer	20.00	9.76	8.90E-07	ACTG1, AKT1, CBL, EGFR, FASLG, GRB2, PIK3R1, PLCG1, SRC	CAMK2A, ERBB4, FLNA, GRB2, IQGAP1, MYC, PPP1CB, SMAD2	CAMK2A, CAMK2B, CAMK2D, CAMK2G, SMAD2, TNF
KEGG:0004660	T cell receptor signaling pathway	14.00	13.33	3.10E-06	AKT1, CBL, FYN, GRB2, GSK3B, LCP2, NCK1, PIK3R1, PLCG1	DLG1, FYN, GRB2, IKBKG, JUN, NCK1, PTPRC	TNF
KEGG:0004728	Dopaminergic synapse	15.00	11.54	7.10E-06	AKT1, GSK3B	ARRB2, ATF2, CAMK2A, GNAO1, GRIA2, GRIN2B, PLCB4, PPP1CB	CALM1, CAMK2A, CAMK2B, CAMK2D, CAMK2G, GRIA4, GRIN2B
KEGG:0005214	Glioma	11.00	16.67	8.70E-06	AKT1, EGFR, GRB2, PIK3R1, PLCG1	CAMK2A, GRB2	CALM1, CAMK2A, CAMK2B, CAMK2D, CAMK2G, E2F3
KEGG:0004915	Estrogen signaling pathway	13.00	13.00	1.20E-05	AKT1, EGFR, ESR2, GRB2, PIK3R1, PRKCD, SRC	ATF2, GNAO1, GRB2, HSP90AB1, JUN, PLCB4	CALM1, HSP90AB1
KEGG:0005161	Hepatitis B	15.00	10.27	3.10E-05	AKT1, FASLG, GRB2, IL6, PIK3R1, SRC, YWHAB	ATF2, CDK2, GRB2, IKBKG, JUN, MYC, STAT1	E2F3, TNF
KEGG:0004713	Circadian entrainment	12.00	12.50	5.70E-05	MTNR1B	CAMK2A, GNAO1, GRIA2, GRIN1, GRIN2B, MTNR1B, PLCB4	CALM1, CAMK2A, CAMK2B, CAMK2D, CAMK2G, GRIA4, GRIN2B, MTNR1B
KEGG:0004720	Long-term potentiation	10.00	14.93	9.10E-05		CAMK2A, GRIA2, GRIN1, GRIN2B, PLCB4, PPP1CB	CALM1, CAMK2A, CAMK2B, CAMK2D, CAMK2G, GRIN2B
KEGG:0004520	Adherens junction	10.00	13.51	2.20E-04	ACTG1, EGFR, FYN, SRC	FYN, INSR, IQGAP1, PTPRB, PTPRJ, SMAD2	ACTN1, SMAD2
KEGG:0004912	GnRH signaling pathway	11.00	11.96	2.40E-04	EGFR, GRB2, PRKCD, SRC	CAMK2A, GRB2, JUN, PLCB4	CALM1, CAMK2A, CAMK2B, CAMK2D, CAMK2G
KEGG:0004750	Inflammatory mediator regulation of TRP channels	11.00	11.11	5.00E-04	PIK3R1, PLCG1, PRKCD, SRC	CAMK2A, PLCB4, PPP1CB	CALM1, CAMK2A, CAMK2B, CAMK2D, CAMK2G
KEGG:0005220	Chronic myeloid leukemia	9.00	12.33	1.40E-03	ABL1, AKT1, CBL, CRK, GRB2, PIK3R1	ABL1, CRK, GRB2, IKBKG, MYC	E2F3
KEGG:0004144	Endocytosis	17.00	6.54	2.40E-03	ASAP1, CBL, DNM1, DNM2, EGFR, ITCH, PDCD6IP, SH3GL1, SH3GL2, SH3GL3, SH3KBP1, SRC	AGAP2, ARRB2, ERBB4, SMAD2	CHMP5, SMAD2

KEGG:0004933	AGE-RAGE signaling pathway in diabetic complications	10.00	9.90	3.40E-03	AKT1, IL6, PIK3R1, PLCG1, PRKCD	JUN, PLCB4, SMAD2, STAT1	SMAD2, TNF
KEGG:0005321	Inflammatory bowel disease (IBD)	8.00	12.31	3.80E-03	HLA-DQA1, IL6	JUN, SMAD2, STAT1	HLA-DMA, HLA-DRB1, SMAD2, TNF
KEGG:0004066	HIF-1 signaling pathway	10.00	9.71	3.90E-03	AKT1, EGFR, IL6, PIK3R1, PLCG1	CAMK2A, INSR	CAMK2A, CAMK2B, CAMK2D, CAMK2G
KEGG:0004114	Oocyte meiosis	11.00	8.87	3.90E-03	YWHAB, YWHAE, YWHAH	CAMK2A, CDK2, PPP1CB	CALM1, CAMK2A, CAMK2B, CAMK2D, CAMK2G, YWHAG
KEGG:0005142	Chagas disease (American trypanosomiasis)	10.00	9.62	4.10E-03	AKT1, FASLG, IL6, PIK3R1	GNAO1, IKBKG, JUN, PLCB4, SMAD2	SMAD2, TNF
KEGG:0005164	Influenza A	13.00	7.43	5.10E-03	ACTG1, AKT1, FASLG, GSK3B, HLA-DQA1, IL6, PIK3R1	ATF2, JUN, STAT1	HLA-DMA, HLA-DRB1, TNF
KEGG:0004510	Focal adhesion	14.00	6.90	6.00E-03	ACTG1, AKT1, CRK, EGFR, FYN, GRB2, GSK3B, PIK3R1, SRC	CRK, FLNA, FYN, GRB2, JUN, PPP1CB, TNR	ACTN1
KEGG:0005215	Prostate cancer	9.00	10.11	6.00E-03	AKT1, EGFR, GRB2, GSK3B, PIK3R1	CDK2, GRB2, HSP90AB1, IKBKG	E2F3, HSP90AB1
KEGG:0005152	Tuberculosis	13.00	7.26	6.10E-03	AKT1, HLA-DQA1, IL6, SRC	CAMK2A, STAT1	CALM1, CAMK2A, CAMK2B, CAMK2D, CAMK2G, HLA-DMA, HLA-DRB1, TNF
KEGG:0004724	Glutamatergic synapse	10.00	8.77	8.00E-03		DLG4, DLGAP1, GNAO1, GRIA2, GRIN1, GRIN2B, PLCB4, SHANK1, SLC38A1	GRIA4, GRIN2B
KEGG:0005223	Non-small cell lung cancer	7.00	12.50	8.80E-03	AKT1, EGFR, GRB2, PIK3R1, PLCG1	GRB2	E2F3, RXRB
KEGG:0004919	Thyroid hormone signaling pathway	10.00	8.47	1.00E-02	ACTG1, AKT1, GSK3B, PIK3R1, PLCG1, SRC	MYC, PLCB4, STAT1	RXRB
KEGG:0005332	Graft-versus-host disease	6.00	14.63	1.00E-02	FASLG, HLA-DQA1, IL6		HLA-DMA, HLA-DRB1, TNF
KEGG:0004110	Cell cycle	10.00	8.06	1.40E-02	ABL1, GSK3B, YWHAB, YWHAE, YWHAH	ABL1, CDK2, MYC, SMAD2	E2F3, SMAD2, YWHAG
KEGG:0004721	Synaptic vesicle cycle	7.00	11.11	1.60E-02	DNM1, DNM2, STX1A, STX1B, STX3	NSF, RIMS1	
KEGG:0004360	Axon guidance	12.00	6.82	1.60E-02	ABL1, FYN, GSK3B, NCK1, PIK3R1, PLCG1, SRC, SRGAP3	ABL1, CAMK2A, FYN, NCK1	CAMK2A, CAMK2B, CAMK2D, CAMK2G
KEGG:0004922	Glucagon signaling pathway	9.00	8.74	1.60E-02	AKT1, PYGM	ATF2, CAMK2A, PLCB4	CALM1, CAMK2A, CAMK2B, CAMK2D, CAMK2G
KEGG:0004911	Insulin secretion	8.00	9.41	1.90E-02	STX1A	ATF2, CAMK2A, PLCB4	CAMK2A, CAMK2B, CAMK2D, CAMK2G, PCLO
KEGG:0005310	Asthma	5.00	16.13	1.90E-02	HLA-DQA1		HLA-DMA, HLA-DRB1, PRG2, TNF
KEGG:0005212	Pancreatic cancer	7.00	10.61	2.00E-02	AKT1, EGFR, PIK3R1	IKBKG, SMAD2, STAT1	E2F3, SMAD2
KEGG:0004931	Insulin resistance	9.00	8.26	2.10E-02	AKT1, GSK3B, IL6, PIK3R1, PRKCD, PYGM	INSR, PPP1CB	TNF
KEGG:0004068	FoxO signaling pathway	10.00	7.46	2.20E-02	AKT1, EGFR, FASLG, GRB2, IL6, PIK3R1	AGAP2, CDK2, GRB2, INSR, SMAD2	SMAD2

CHAPTER IV - DISCUSSION AND CONCLUDING REMARKS

IV.1 Overview

BRI2 and BRI3 are two type II transmembrane proteins with unclear functions. While BRI3 is mainly expressed in the CNS, BRI2 is an ubiquitously expressed protein. However, several lines of evidence suggest an important role for BRI2 in the CNS:

- BRI2 is a central protein of the FBD and FDD pathogenesis since mutated forms of this protein appear in FBD and FDD patients. Mutations of the stop codon in the *BRI2* gene are responsible for the generation of a longer open reading frame causing the release of a longer propeptide by furin-mediated proteolysis, the ABri and ADan which tend to aggregate in amyloid deposits in the brain and cause FBD and FDD, respectively (Vidal *et al*. 1999; Vidal *et al*. 2000);
- BRI2 was found deposited in the hippocampus of early stages of AD cases, associated with Aβ plaques (Del Campo *et al*. 2014);
- BRI2 RIP in the cis- or medial-Golgi results in the formation of several secreted peptides. The first cleavage by furin and related proteases within its ectodomain leads to the release of a 3 kDa C-terminal propeptide (Choi *et al*. 2004). BRI2 staining in dystrophic neurites in some neurodegenerative disorders and its distribution within neuronal cell bodies and axons suggests that BRI2 is transported along neuronal processes and potentially a role at the nerve terminals;
- *Bri2* $^{+/-}$ mice exhibit synaptic and memory deficits (Tamayev *et al*. 2010b).

Most proteins function as part of complexes rather than as individuals, this is essential for proper protein function. The study of protein-protein interactions contributes to understanding the protein´s normal functions and the information obtained can help one to predict biological processes and signaling pathways that a protein is involved.

Previous work from our laboratory identified BRI3 protein in a Yeast Two-Hybrid screen of a human brain cDNA library using PP1γ2 as bait (Esteves *et al*. 2013). Although BRI2 was not identified in this screen it was also explored as a possible PP1 interactor.

IV.2 BRI2 protein

In the work here presented BRI2 was described as a novel PP1 interacting protein. The interaction of BRI2 with both PP1α and PP1γ isoforms was validated using different techniques which permitted concluding that BRI2 interacts directly with PP1 both *in vitro* and *ex vivo*. BRI2 interacts with PP1 through a conserved RVxF motif located in its intracellular N-terminal domain. Although some phosphorylatable residues for BRI2 were recently described using high-throughput techniques this is the first report identifying BRI2 as a phosphoprotein which can be dephosphorylated by PP1. In fact, when BRI2:PP1 interaction is abolished BRI2 phosphorylation levels greatly increase.

However, the BRI2 residues altered by PP1 dephosphorylation were not identified and this deserves further investigation, as well as the identification of the BRI2 protein kinases.

The identification of the BRI2/PP1 was of paramount importance since it opened new perspectives for the study of protein phosphorylation as a key regulatory mechanism for the biological function of BRI2. It was already demonstrated that BRI2 N-glycosylation at Asn170 is essential for its proper trafficking through the membrane compartments to the cell surface (Tsachaki *et al*. 2011), however, there was no previous evidence suggesting a role for post-translational modifications on BRI2 processing. The involvement of protein phosphorylation on BRI2 processing was reported for the first time during the work here described. Dephosphorylation of BRI2 by PP1 is able to increase its processing by ADAM10 resulting in increased production of the membrane-bound NTF, which is further subjected to intramembrane regulated proteolysis by SPPLa/b to release the intracellular domain of BRI2. The underlying regulatory mechanisms responsible for favoring BRI2 processing by phosphorylation should be addressed. For instance, BRI2 phosphorylation/dephosphorylation may control its affinity to specific interacting proteins, such as ADAM10 and SPPL2a/b, by inducing conformational changes and these should be explored. It is also possible that phosphorylation/dephosphorylation affects BRI2 interaction with proteins responsible for its targeting to the subcellular compartments where processing occurs. The results here presented suggest that BRI2 trafficking is not altered by PP1 dephosphorylation since a normal distribution vesicle-structures covering the whole cytoplasm and the cell membrane is observed, and it does not accumulate in intracellular compartments. However, this issue was not addressed in this study and further studies such as biotinylation studies to evaluate BRI2 levels at the cell surface, and by inhibiting 'de novo' protein synthesis (for instance with cycloheximide) (Rebelo *et al*. 2008), thus allowing the monitoring of BRI2 protein pool in a time-dependent manner.

IV.2.1. BRI2 neuritogenic role

Moreover, a role for BRI2:PP1 complex was established in the dynamic regulation of neuritogenesis, since BRI2 phosphorylation is able to promote neurite outgrowth. Significantly, the impact of BRI2 phosphorylation on its neuritogenic role was well correlated with its processing. Indeed, by modulating BRI2 processing using the ADAM10 specific inhibitor, GI254023X, it was possible to unravel a dual role for BRI2 in neuritogenesis: phosphorylation of full-length protein promotes the emergence of neurites whereas the increased BRI2 NTFs play a relevant role in neurites' elongation and stabilization. The results here presented regarding the BRI2 neuritogenic role were accomplished with BRI2 overexpression; however BRI2 knockdown experiments will likely prove to be useful. The SH-SY5Y neuroblastoma cell line was largely used in this work since it is a widely used neuronal differentiation model (Agholme *et al*. 2010; da Rocha *et al*. 2015). However, to further address the

BRI2 neuritogenic role primary neuronal cultures which are physiologically more relevant should be used as cell model in the future. This will allow us to further evaluate BRI2 role on both axonal and dendritic growth as well as branching. In addition, to elucidate BRI2 contributions to neurite outgrowth for full-length BRI2 and its fragments, cultured neurons from BRI2 knockout (KO) and phosphorylation mutants should be worthwhile.

Given our results and the previously published results, it is clear the involvement of BRI2 in neuritogenesis, however, the underlying mechanisms and signaling pathways have not been elucidated. Hence, the BRI2 interactome was identified in order to uncover the signaling mechanisms responsible for the BRI2 role in neuritogenesis, and also to explore potential novel cellular functions for BRI2 in the CNS.

Bioinformatic analysis of the BRI2 interactome identified almost 50% of the novel BRI2 candidate interacting proteins as cytoskeletal proteins, which translated in an overrepresentation of functions like cytoskeleton organization and microtubule-based processes, strengthening the proposed role of this protein in neuronal differentiation. Therefore, it is feasible to propose that a mechanism by which BRI2 is able to induce neurite outgrowth relies on the modulation of different signaling pathways that converge on changes in the cytoskeleton. BRI2 is able to form homodimers linked by disulfide bonds that appear at the cell surface resembling the structure of a cell-surface receptor (Tsachaki *et al*. 2010). By acting as a cell receptor BRI2 may initiate intracellular signal transduction in response to extracellular signaling molecules (Figure IV.1). Moreover, the soluble ectodomain products resulting from BRI2 cleavage could also be implicated in neurite outgrowth by binding to a growth factor receptor (Figure IV.1). Taking into consideration the results here presented, these points to protein phosphorylation as a key regulator of BRI2 mediated neurite outgrowth it is possible that: (1) BRI2 full-length phosphorylation induces conformational changes in the protein affecting the binding specificity and affinity for the protein partners thus regulating its receptor activity; (2) by increasing BRI2 processing, phosphorylation increases the levels of the secreted fragments that can further act as a neuritogenic ligand that binds to and activates a growth factor receptor; (3) by increasing BRI2 processing, phosphorylation leads to increased generation of the BRI2 intracellular domain (BRI2ICD) that can translocate to the nucleus (Mentrup *et al*. 2015) where it may promote gene transcription (Figure IV.1).

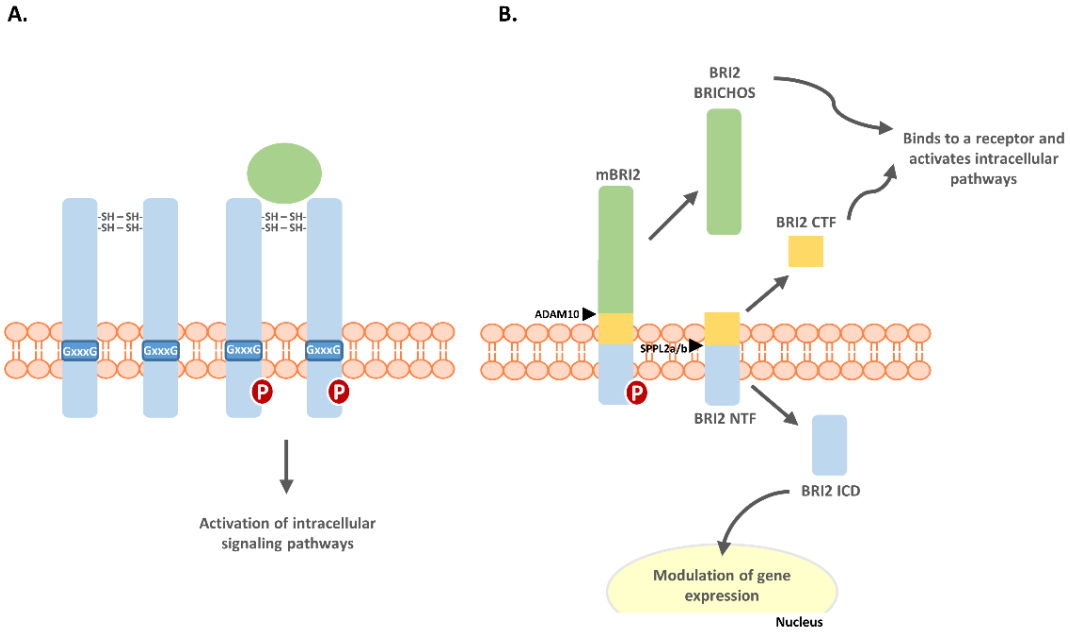

Figure IV. 1 - Schematic representation of the proposed mechanisms for BRI2 phosphorylation-mediated neurite outgrowth. A – BRI2 may act as a receptor initiating intracellular signal transduction in response to extracellular signaling molecules. BRI2 forms homodimers linked by disulfide bonds that appear at the cell surface, resembling the structure of a cell-surface receptor. BRI2 contains two extracellular cysteines at the C-terminus that most likely are capable of forming an intramolecular disulfide bond. In addition, BRI2 contains within its transmembrane domain, the GXXXG motif that has been found to contribute to protein homo- and hetero-association. BRI2 full-length phosphorylation may induce conformational changes in the protein affecting the binding specificity and affinity for the extracellular signaling molecules thus regulating its receptor activity. **B – BRI2 proteolytic processing fragments induced neurite outgrowth.** BRI2 phosphorylation promotes BRI2 processing increasing the levels of the proteolytic processing fragments that can further act as neuritogenic molecules. The soluble secreted fragments BRI2 BRICHOS and BRI2 CTF may function as ligands by binding to and activating growth factor receptors; BRI2ICD can translocate to the nucleus where it may promote gene transcription.

In conclusion, with the work here presented we gathered a wide range of evidences suggesting a role for BRI2 in neurite outgrowth and several underlying mechanisms were proposed which might be pursued in a near future. Moreover, the study of BRI2 and its potential value in neuritogenic therapeutic applications seems to be very promising.

IV.2.2 Potential novel roles for BRI2 in the CNS

In addition, by further analyzing the BRI2 brain interactome here identified, novel potential roles for BRI2 emerged, namely with roles in synapse formation and activity.

Remarkably, the results lead us to propose other roles for BRI2 in neuronal differentiation, namely in synapse formation. Several proteins identified as candidate BRI2 interactors were found to be associated with microtubule transport machinery, as is the case for kinesin heavy chain isoforms 5a and 5c (Kif5a and kif5c, respectively), and kinesin light chain isoform 1 (Klc1). Kinesins are

important for trafficking in axons and dendrites (Rahman *et al*. 1998; Xia *et al*. 1998) that are crucial for the formation and dynamics of both presynaptic and postsynaptic structures. Thus, these results suggest that in neurons BRI2 is transported by anterograde axonal transport to the distal nerve terminals. The results also suggest the expression of BRI2 both in pre-and postsynapse and so one can propose a role for BRI2 in promoting synaptic formation via trans-synaptic interactions of its extracellular domains which may contribute to the adhesion of synapses (Figure IV.2). This point deserves further investigation in order to confirm the distribution of BRI2 in synapses.

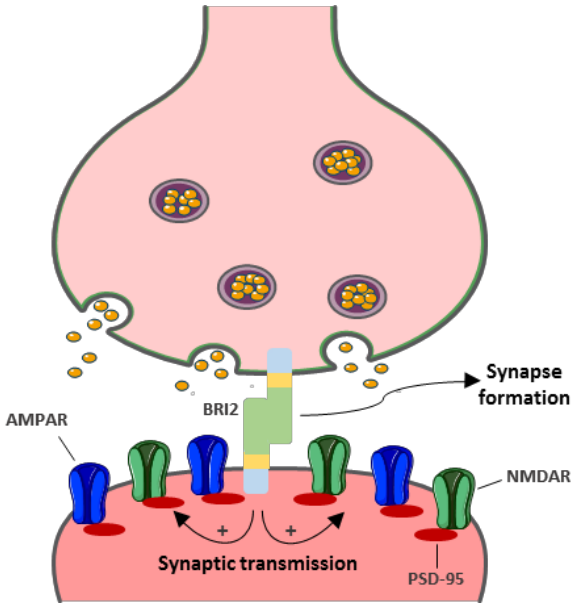

Figure IV. 2 - Schematic diagram of putative functions for BRI2 at synapses. BRI2 is suggested to be expressed both in pre- and postsynapse, and via trans-synaptic interactions of its extracellular domains could promote synapse formation. BRI2 protein via interaction with several interacting proteins could be involved in synaptic transmission and plasticity by enhancing AMPAR and NMDAR surface expression.

Furthermore, novel candidate BRI2 interactors subunits of the AMPARs and NMDARs, as well as PSD-95 were identified. PSD-95 interacts with both AMPARs and NMDARs through its PDZ (PSD-95/Dlg/ZO-1) domain and is able to regulate its expression at synapses (Béïque and Andrade 2003; El-Husseini *et al*. 2000; Niethammer *et al*. 1996; Kornau *et al*. 1995). Although no previous studies have identified PSD-95 as a BRI2 interactor, a functional evidence suggesting a relationship between those proteins were already pointed out: in a synaptosomal proteome characterization of the mouse model FDD_{KI}, PSD-95 expression was found decreased (Vitale *et al*. 2012). Hence, we hypothesize a role for BRI2 in the postsynaptic compartment in which it may be involved in synaptic transmission and plasticity by altering the AMPA and NMDA receptors trafficking (Figure IV.2). Consistent with

this proposed role for BRI2 is the already mentioned phenotype observed in *Itm2b* (+/-) mice (synaptic and memory deficits). Remarkably, PSD-95 knockout mice display phenotypic similarities, such as abnormal synaptic plasticity as well as abnormal memory and learning (Feyder *et al*. 2010). In essence, it seems important to further explore the novel proposed roles for BRI2 since the understanding of its normal function will provide novel insights into its dysfunctions that contribute to the development of the neurodegenerative disorders FBD, FDD, and AD.

IV.2.3. Relevance of BRI2 in neurodegenerative diseases

FBD and FDD, respectively, as discussed, are two rare early-onset forms of dementia, caused by different autosomal dominant mutations in the *BRI2* gene. These diseases share clinical symptoms such as progressive cognitive impairment, cerebellar ataxia, and spasticity (Tsachaki *et al*. 2008). Similar to wild-type BRI2, mutant forms undergo proteolytic processing by furin leading to the secretion of the propetides, ABri in FBD and ADan in FDD. In the brain of patients these peptides were found in amyloid deposits, and as soluble monomeric forms in plasma (Vidal *et al*. 1999; Vidal *et al*. 2000; Ghiso *et al*. 2001; Tomidokoro *et al*. 2005). For several years the production and deposition of these peptides were acknowledged as being responsible for the pathologies of FBD and FDD. However, recent studies using knock-in mouse models of FDD and FBD, FDD_{KI} and FBD_{KI} respectively, proposed the loss of BRI2 function as the mechanism responsible for the synaptic and memory deficits in these diseases rather than amyloidosis, since a significant reduction of mature BRI2 levels is observed (Tamayev *et al*. 2010b; Tamayev *et al*. 2010a). In fact, a recent study reported that the cleavage of BRI2 by proprotein convertases is more efficient for the wild-type BRI2 than for mutant BRI2 since the mutant sequences may interfere both with the proper folding of BRI2 and the enzymatic activity of proprotein convertases (Garringer *et al*. 2017). Therefore, given our results that suggest a regulation of BRI2 function and processing by protein phosphorylation, it seems critical to further evaluate the phosphorylation levels of BRI2 mutant forms in FBD and FDD, as well as the formation of complexes with PP1. Curiously, BRI2 affects APP processing and reduces Aβ production. Given that FBD and FDD share many neuropathological features with AD, it is possible that common cellular events result in neuronal loss in these diseases. Therefore, the study of FBD and FDD could also provide insights into the neurodegenerative mechanism underlying AD. Remarkably, BRI2 was also found to be deposited in the hippocampus of early stages of AD cases and clearly associated with Aβ plaques. In fact, in brain homogenates from AD patients the BRI2 binds to APP. Thus, BRI2 abnormal accumulation and its subcellular localization may prevent the formation of the BRI2-APP complex formation leading to an increase in APP processing and Aβ production (Del Campo *et al*. 2014). Interestingly, abnormal protein phosphorylation levels have been associated with several neuropathological disorders including AD due to abnormal protein

kinase and protein phosphatase activities (Chung 2009). Remarkably, BRI2 was also found to be deposited in the hippocampus of early stages of AD cases and clearly associated with Aβ plaques. In fact, in brain homogenates from AD patients the BRI2 binds to APP. Thus, BRI2 abnormal accumulation and its subcellular localization may prevent the formation of the BRI2-APP complex formation leading to an increase in APP processing and Aβ production.

IV.3. BRI3

BRI3 is a type II transmembrane protein mainly expressed in the brain. Given its distribution pattern it seems important in the CNS function, however, its biological function remains undisclosed.

Therefore the finding that BRI3 is a phosphoprotein that interacts directly with PP1 opens a new perspective in the study of BRI3 biology. BRI3 interacts with PP1 through a conserved RVxF motif located in its intracellular N-terminal domain. Furthermore, BRI3 is a substrate of PP1 being dephosphorylated by the later. However, the relevance of phosphorylation was not determined since no clear phenotype is observed when the BRI3:PP1 complex formation is impaired.

BRI3 is also processed by furin and other members of the pro-protein convertase family, however, in contrast to BRI2, it fails to undergo shedding by ADAM-10 as well as intramembrane proteolysis by SPPL2a/b (Martin *et al*. 2009). Therefore, the involvement of protein phosphorylation in its processing is unlikely. Although, it seems to be of paramount importance to explore the role of BRI3 phosphorylation, namely dephosphorylation by PP1 associated with its trafficking, as this modification may induce conformational changes which may affect the interaction with other protein partners.

The development of BRI3 loss- and gain-of-function models will further provide valuable insights into BRI3 physiological functions. In addition, knock-in models expressing BRI3 phosphorylation mutants would help us to study the impact of protein phosphorylation on BRI3 without protein overexpression.

IV.3.1. Potential roles for BRI3 in the CNS

Bioinformatic analysis of the BRI3 brain interactome provided hints regarding BRI3 biology and its physiological roles in the CNS. Given the localization of its interactors, one can hypothesize that BRI3 in neurons is localized at synapses, both presynapse and postsynapse, and associated with synaptic vesicles and the cytoskeleton.

The work here presented led to the identification of high number of candidate BRI3 interactors involved in neuronal trafficking along the cytoskeleton, namely kinesins, members of the AP complex and clathrins. This suggests that BRI3 protein is transported within axons and dendrites to the nerve terminals where it may be functionally required. Moreover, it is plausible that BRI3 is

expressed both in pre- and postsynapse and by trans-synaptic interactions and may have a role in synapse formation. Interactions for BRI2 with proteins involved in synaptic transmission were also detected, namely PSD-95, NMDAR1 and NMDAR2B suggesting an additional role for BRI2 in excitatory synaptic transmission by altering AMPARs and NMDARs trafficking, as is described for other transmembrane proteins (Spires *et al*. 2005; Isaac *et al*. 2007; Hoe *et al*. 2009). However, the underlying mechanisms deserve further investigations. Curiously, BRI3 is a negative regulator of Aβ production by interacting with APP (Matsuda *et al*. 2009). Since Aβ is able to induce synaptic dysfunction by either decreasing surface expression or by promoting endocytosis of the glutamate receptors (Almeida *et al*. 2005; Snyder *et al*. 2005). Therefore, we propose a novel role for BRI3:APP complex in synaptic transmission and plasticity by regulating AMPARs and NMDARs trafficking. Furthermore, a previous study suggested a possible role for BRI3 in neuronal differentiation. Briefly, BRI3 by interacting with the microtubule-destabilizing protein SCG10, attenuates the SCG10 mediated neurite outgrowth by preventing microtubule disassembly (Gong *et al*. 2008). The work here presented supports a role for BRI3 in neurite outgrowth by mediating cytoskeleton dynamics since a high number of proteins identified as BRI3 interactors are cytoskeletal and cytoskeletal binding proteins involved in its organization.

In summary, the involvement of BRI3 in the above mentioned biological processes should be further addressed, as well as other several issues regarding BRI3 biology, namely the localization and function of different BRI3 forms (ex. phosphorylated).

IV.3.2. BRI3 and nervous system diseases

Although no mutation has yet been reported for BRI3, as is described for BRI2, some associations for BRI3 with pathological conditions have been pointed out: (1) a polymorphism (A→G) of *BRI3* was associated with the prevalence of subarachnoid hemorrhage in Japanese individuals (Yoshida *et al*. 2010); (2) as a negative regulator of Aβ production, BRI3 could have a role in the pathogenesis of AD; however, so far no clear association has been established for BRI3 in the pathogenesis of AD. Remarkably, a high number of BRI3 protein interactors here identified were found to share with BRI3 the association to some nervous system disorders, particularly with AD. Therefore, it would be advantageous to study BRI3 dysfunction as a potential underlying mechanism in the pathogenesis of the disease. Evidences suggest imbalanced activities of protein kinases and phosphatases in AD which affect the phosphorylation state of AD-related proteins, such as APP and Tau (Oliveira *et al*. 2015). Consequently, either the phosphorylation levels of BRI3 and the BRI3:APP complex formation should be addressed in AD which could potentially provide novel and important insights on the pathology mechanisms.

IV.4. CONCLUDING REMARKS

The work presented in this thesis provides important novel insights into the biological properties of BRI2 and BRI3 proteins. Moreover, it takes advantage of the identification of novel BRI2 and BRI3 containing protein complexes to uncover putative roles and the underlying mechanisms in which these proteins may be involved.

In conclusion, this work resulted in:

- identification of both BRI2 and BRI3 as phosphoproteins;
- validation of BRI2 and BRI3 as novel PP1 interacting proteins;
- identification of BRI2 phosphorylation as a regulatory mechanism of its proteolytic processing;
- uncovering the BRI2 neuritogenic role and its regulation by phosphorylation;
- uncovering novel biological roles and the underlying mechanisms for BRI2 and BRI3 proteins.

The identification of protein phosphorylation as a regulatory mechanism of both BRI2 and BRI3 opens a new perspective in the study of their biological function, as well as their dysfunction which could be involved in the pathogenesis of specific neurodegenerative disorders. Moreover, our work suggests some novel putative roles for BRI2 and BRI3. Remarkably, the majority of biological processes associated with both proteins were similar (neurite outgrowth, synapse formation, synaptic signaling, and transmission) suggesting the existence of functional complementation of both proteins in the CNS. In fact, both are inhibitors of Aβ production by affecting APP processing, and the interaction of both proteins with PP1 and APP might underlie neurodegenerative diseases. Although the work here presented does not provide functional evidences for the novel proposed roles for BRI2 and BRI3, emerges as an important basis for future studies.

References

Agholme L., Lindström T., Kågedal K., Marcusson J., Hallbeck M. (2010) An in vitro model for neuroscience: differentiation of SH-SY5Y cells into cells with morphological and biochemical characteristics of mature neurons. *J. Alzheimers. Dis.* **20**, 1069–82.

Almeida C. G., Tampellini D., Takahashi R. H., Greengard P., Lin M. T., Snyder E. M., Gouras G. K. (2005) Beta-amyloid accumulation in APP mutant neurons reduces PSD-95 and GluR1 in synapses. *Neurobiol. Dis.* **20**, 187–198.

Béïque J.-C., Andrade R. (2003) PSD-95 regulates synaptic transmission and plasticity in rat cerebral cortex. *J. Physiol.* **546**, 859–67.

Campo M. Del, Hoozemans J. J. M., Dekkers L.-L., Rozemuller A. J., Korth C., Müller-Schiffmann A., Scheltens P., et al. (2014) BRI2-BRICHOS is increased in human amyloid plaques in early stages of Alzheimer's disease. *Neurobiol. Aging* **35**, 1596–604.

Choi S.-I., Vidal R., Frangione B., Levy E. (2004) Axonal transport of British and Danish amyloid peptides via secretory vesicles. *FASEB J.* **18**, 373–5.

Chung S.-H. (2009) Aberrant phosphorylation in the pathogenesis of Alzheimer's disease. *BMB Rep.* **42**, 467–74.

El-Husseini A. E., Schnell E., Chetkovich D. M., Nicoll R. A., Bredt D. S. (2000) PSD-95 involvement in maturation of excitatory synapses. *Science* **290**, 1364–8.

Esteves S. L. C., Korrodi-Gregório L., Cotrim C. Z., Kleeff P. J. M. van, Domingues S. C., Cruz e Silva O. A. B. da, Fardilha M., Cruz e Silva E. F. da (2013) Protein phosphatase 1γ isoforms linked interactions in the brain. *J. Mol. Neurosci.* **50**, 179–97.

Feyder M., Karlsson R.-M., Mathur P., Lyman M., Bock R., Momenan R., Munasinghe J., et al. (2010) Association of Mouse *Dlg4* (PSD-95) Gene Deletion and Human *DLG4* Gene Variation With Phenotypes Relevant to Autism Spectrum Disorders and Williams' Syndrome. *Am. J. Psychiatry* **167**, 1508–1517.

Garringer H. J., Sammeta N., Oblak A., Ghetti B., Vidal R. (2017) Amyloid and intracellular accumulation of BRI2. *Neurobiol. Aging* **52**, 90–97.

Ghiso J. A., Holton J., Miravalle L., Calero M., Lashley T., Vidal R., Houlden H., et al. (2001) Systemic amyloid deposits in familial British dementia. *J. Biol. Chem.* **276**, 43909–14.

Gong Y., Wu J., Qiang H., Liu B., Chi Z., Chen T., Yin B., Peng X., Yuan J. (2008) BRI3 associates with SCG10 and attenuates NGF-induced neurite outgrowth in PC12 cells. *BMB Rep.* **41**, 287–93.

Hoe H.-S., Fu Z., Makarova A., Lee J.-Y., Lu C., Feng L., Pajoohesh-Ganji A., et al. (2009) The Effects of Amyloid Precursor Protein on Postsynaptic Composition and Activity. *J. Biol. Chem.* **284**, 8495–8506.

Isaac J. T. R., Ashby M. C., McBain C. J., Biagini G., Agnati L. F., Muller R. U., Roder J. C., et al. (2007) The role of the GluR2 subunit in AMPA receptor function and synaptic plasticity. *Neuron* **54**, 859–71.

Kornau H. C., Schenker L. T., Kennedy M. B., Seeburg P. H. (1995) Domain interaction between NMDA receptor subunits and the postsynaptic density protein PSD-95. *Science* **269**, 1737–40.

Martin L., Fluhrer R., Haass C. (2009) Substrate requirements for SPPL2b-dependent regulated intramembrane proteolysis. *J. Biol. Chem.* **284**, 5662–70.

Matsuda S., Matsuda Y., D'Adamio L. (2009) BRI3 inhibits amyloid precursor protein processing in a mechanistically distinct manner from its homologue dementia gene BRI2. *J. Biol. Chem.* **284**, 15815–25.

Mentrup T., Häsler R., Fluhrer R., Saftig P., Schröder B. (2015) A Cell-Based Assay Reveals Nuclear Translocation of Intracellular Domains Released by SPPL Proteases. *Traffic* **16**, 871–92.

Niethammer M., Kim E., Sheng M. (1996) Interaction between the C terminus of NMDA receptor subunits and multiple members of the PSD-95 family of membrane-associated guanylate kinases. *J. Neurosci.* **16**, 2157–63.

Oliveira J. M., Henriques A. G., Martins F., Rebelo S., Cruz E Silva O. A. B. da (2015) Amyloid-β Modulates Both AβPP and Tau Phosphorylation. *J. Alzheimers. Dis.*

Rahman A., Friedman D. S., Goldstein L. S. (1998) Two kinesin light chain genes in mice. Identification and characterization of the encoded proteins. *J. Biol. Chem.* **273**, 15395–403.

Rebelo S., Vieira S. I., Cruz E Silva E. F. da, Cruz E Silva O. A. B. da (2008) Monitoring "De Novo"APP synthesis by taking advantage of the reversible effect of cycloheximide. *Am. J. Alzheimers. Dis. Other Demen.* **23**, 602–8.

Rocha J. F. da, Cruz E Silva O. A. B. da, Vieira S. I. (2015) Analysis of the amyloid precursor protein role in neuritogenesis reveals a biphasic SH-SY5Y neuronal cell differentiation model. *J. Neurochem.* **134**, 288–301.

Snyder E. M., Nong Y., Almeida C. G., Paul S., Moran T., Choi E. Y., Nairn A. C., et al. (2005) Regulation of NMDA receptor trafficking by amyloid-β. *Nat. Neurosci.* **8**, 1051–1058.

Spires T. L., Meyer-Luehmann M., Stern E. A., McLean P. J., Skoch J., Nguyen P. T., Bacskai B. J., Hyman B. T. (2005) Dendritic Spine Abnormalities in Amyloid Precursor Protein Transgenic Mice Demonstrated by Gene Transfer and Intravital Multiphoton Microscopy. *J. Neurosci.* **25**, 7278–7287.

Tamayev R., Giliberto L., Li W., d'Abramo C., Arancio O., Vidal R., D'Adamio L. (2010a) Memory deficits due to familial British dementia BRI2 mutation are caused by loss of BRI2 function rather than amyloidosis. *J. Neurosci.* **30**, 14915–24.

Tamayev R., Matsuda S., Fà M., Arancio O., D'Adamio L. (2010b) Danish dementia mice suggest that loss of function and not the amyloid cascade causes synaptic plasticity and memory deficits. *Proc. Natl. Acad. Sci. U. S. A.* **107**, 20822–7.

Tomidokoro Y., Lashley T., Rostagno A., Neubert T. A., Bojsen-Møller M., Braendgaard H., Plant G., et al. (2005) Familial Danish dementia: co-existence of Danish and Alzheimer amyloid subunits (ADan AND A{beta}) in the absence of compact plaques. *J. Biol. Chem.* **280**, 36883–94.

Tsachaki M., Ghiso J., Efthimiopoulos S. (2008) BRI2 as a central protein involved in neurodegeneration. *Biotechnol. J.* **3**, 1548–54.

Tsachaki M., Ghiso J., Rostagno A., Efthimiopoulos S. (2010) BRI2 homodimerizes with the involvement of intermolecular disulfide bonds. *Neurobiol. Aging* **31**, 88–98.

Tsachaki M., Serlidaki D., Fetani A., Zarkou V., Rozani I., Ghiso J., Efthimiopoulos S. (2011) Glycosylation of BRI2 on asparagine 170 is involved in its trafficking to the cell surface but not in its processing by furin or ADAM10. *Glycobiology* **21**, 1382–8.

Vidal R., Frangione B., Rostagno A., Mead S., Révész T., Plant G., Ghiso J. (1999) A stop-codon mutation in the BRI gene associated with familial British dementia. *Nature* **399**, 776–81.

Vidal R., Revesz T., Rostagno A., Kim E., Holton J. L., Bek T., Bojsen-Møller M., et al. (2000) A decamer duplication in the 3' region of the BRI gene originates an amyloid peptide that is associated with dementia in a Danish kindred. *Proc. Natl. Acad. Sci. U. S. A.* **97**, 4920–5.

Vitale M., Renzone G., Matsuda S., Scaloni A., D'Adamio L., Zambrano N. (2012) Proteomic characterization of a mouse model of familial Danish dementia. *J. Biomed. Biotechnol.* **2012**, 728178.

Xia C., Rahman A., Yang Z., Goldstein L. S. B. (1998) Chromosomal Localization Reveals Three Kinesin Heavy Chain Genes in Mouse. *Genomics* **52**, 209–213.

Yoshida T., Kato K., Yokoi K., Oguri M., Watanabe S., Metoki N., Yoshida H., et al. (2010) Association of genetic variants with hemorrhagic stroke in Japanese individuals. *Int. J. Mol. Med.* **25**, 649–56.